An Experimental Investigation of the Maximum Load Limit of Boosted HCCI Combustion in a Gasoline Engine with Negative Valve Overlap

by

Stefan Klinkert

A dissertation submitted in partial fulfillment
of the requirements for the degree of
Doctor of Philosophy
(Mechanical Engineering)
in The University of Michigan
2014

Doctoral Committee:

Adjunct Professor Dionissios N. Assanis, Co-Chair
Professor Volker Sick, Co-Chair
Professor André L. Boehman
Associate Research Scientist Stanislav V. Boháč
Professor James F. Driscoll
Research Scientist George A. Lavoie

To my Parents,
Werner and Lilo

Acknowledgments

The last seven years of graduate studies at the University of Michigan have been a marked experience for me and were characterized by the interaction with many intelligent, knowledgeable and special people. I cannot possibly list all people, who deserve recognition, but I am thankful to each and every one of them. Those that I mention have had an especially important role in the completion of this work, which has been a true team effort, and I could not have done it without selfless contributions of many other individuals.

First, I would like to sincerely thank Prof. Dennis Assanis, who gave me the opportunity to join his research group and work on an exciting dissertation project. His devotion to his students, his encouragement and positive attitude throughout my studies have had a lasting impact on me. I am very grateful to Prof. Volker Sick for joining the dissertation committee as a co-chair and taking over the managerial part of the project, after Prof. Assanis left, and his genuine interest in my work since then. I am thankful to Prof. André Boehman, who joined my doctoral committee recently but provided very insightful suggestions since then. I would like to thank Prof. James Driscoll serving as a cognate member on my committee for providing very useful input and an important perspective from outside the department.

Dr. Stani Boháč provided indispensable guidance as my first direct research adviser during my first few years in graduate school, always had a genuine interest in my work and provided valuable suggestions. I am extremely fortunate being able to have worked with Dr. George Lavoie closely during the very important last few years of my dissertation, for he has been a great research adviser and mentor, who always provided encouragement, made time for discussions, and taught me how to become a true scientist. His contributions to this work are invaluable and greatly appreciated.

I would like to thank General Motors (GM) for funding this research and providing the equipment for this unique collaborative research effort. All the people at GM have provided valuable feedback on a monthly basis throughout the past four years. I am especially thankful to Mr. Paul Najt and Drs. Nicole Wermuth and Orgun Güralp, who have taken a directing and guiding role in this research project. I would also like to acknowledge the instructive technical discussions with Drs. Hanho Yun, Seunghwan Keum and Ronald Grover.

During the first two years of my dissertation project, I had the privilege to work with Dr. Jiří Vávra, a visiting research scholar from Czech Technical University of Prague, who contributed enormously by sharing his technical experience, assisting with the upgrade of the engine air system, and also through his mentoring and friendship. Dr. Aris Babajimopoulos provided guidance and showed genuine interest not only in the modeling but also experimental aspects of the project while involved. I would also like to acknowledge Prof. Zoran Filipi, Dr. Jason Martz and Mr. John Hoard for their interest in my work and encouragement throughout the years.

Sotirios Mamalis had a pivotal role as a project collaborator and friend, when I started my doctoral work on the GM project, as he always provided support, gave useful feedback and shared his knowledge with me. I am also thankful to Vasileios Triantopoulos, who contributed significantly with the upgrade of the test cell over a period of more than six months. I am also thankful to Eric Bumbalough, who helped with the redesign and upgrade of the test cell, for his contributions. I am also grateful to Luke Hagen for helping with experimental runs and keeping up with the test cell. Laura and Samuel Olesky as well as Peter Andruskiewicz are acknowledged for their help in getting me acquainted with the test cell after I joined the GM project. I would like to thank Elliott Ortiz-Soto and Robert Middleton for developing the heat release tool used in this work. I would like to acknowledge Mark Hoffman, Joshua Lacey and Benjamin Lawler for many insightful discussions.

The University of Michigan staff also contributed to this work. I am grateful to Messrs. William Kirkpatrick and Kent Pruss for their help and support of this work by manufacturing parts in the machine shop and many useful technical discussions. I would also like to thank Mesdames Susan Clair, Laurie Stoianowski, Melissa McGeorge and Kathie Wolney for all the crucial managerial work that they do behind the scenes facilitating a productive work environment for students and faculty.

I would like to thank all my colleagues in the W.E. Lay Automotive Laboratory, who all had contributed in some way. I am thankful to my lab friends over the past seven years, in particular, Sotirios Mamalis, Janardhan Kodavasal, Mehdi Abarham, Prasad Shingne, Ashwin Salvi and Michael Smith. I would like to thank my friend Bud Collins for proof-reading this dissertation document, his interest in my work and mentoring me. I am truly thankful to all of my friends in the United States and elsewhere in the world for always supporting me and spending good times.

Finally, I would like to thank my family, especially my parents, Werner and Lilo, who always believed in me, gave me freedom, encouraged me and provided me with a good education. Last but not least, I would like to thank my loving wife and best friend, Karen, for supporting and caring for me, especially during the last few years.

Table of Contents

List of Tables

Table

List of Figures

Figure

List of Abbreviations

γ	ratio of specific heat capacities
η_{comb}	combustion efficiency
η_{gross}	gross indicated efficiency
η_{net}	net indicated efficiency
η_{th}	thermal efficiency
τ_{ign}	ignition delay time
Φ	fuel-to-air equivalence ratio
Φ'	fuel-to-charge equivalence ratio
Φ_{FO}	fuel-to-oxygen equivalence ratio
χ_{O2}	oxygen mole fraction
BDC	bottom dead center
BMEP	brake mean effective pressure
CAFE	corporate average fuel economy
c_p	constant pressure specific heat capacity
c_v	constant volume specific heat capacity
CA	crank angle
CA10-90	burn duration, in crank angle degrees
CA50	combustion phasing, crank angle at 50 % MFB, in cad aTDC

CAD	crank angle degree
CI	compression ignition
CO	carbon monoxide
CO_2	carbon dioxide
COV	coefficient of variation
CR	compression ratio
DAQ	data acquisition (system)
DI	direct injection
dP	pressure difference (between exhaust and intake runner)
E_A	activation energy
EGR	exhaust gas recirculation
eEGR	external EGR
iEGR	internal EGR
EOC	end of combustion
EOI	end of injection
EVC	exhaust valve closing
EVO	exhaust valve opening
exh	exhaust
FID	flame ionization detector
GDI	gasoline direct injection
H_2O	water
HC	hydrocarbon emissions
HCCI	homogeneous charge compression ignition
HS	high-speed

IC	internal combustion
$IMEP_g$	gross indicated mean effective pressure
$IMEP_n$	net indicated mean effective pressure
int	intake
$ISFC_g$	gross indicated specific fuel consumption
$ISFC_n$	net indicated specific fuel consumption
IVC	intake valve closing
IVO	intake valve opening
LS	low-speed
LTHR	low temperature heat release
MON	motor octane number
m_{air}	mass of air in-cylinder
m_{eEGR}	mass of eEGR in-cylinder
m_{fuel}	mass of fuel in-cylinder
m_{iEGR}	mass of iEGR in-cylinder
m_{tot}	total mass in-cylinder
MFB	mass fraction burned
MMCD	multi-mode combustion diagram
mpg	miles per gallon
N_2	nitrogen
NDIR	non-dispersive infra-red
NO_x	oxides of nitrogen
NVO	negative valve overlap
O_2	oxygen

OTE	overall turbocharger efficiency
P_{exh}	exhaust runner pressure
PFI	port fuel injection
P	cylinder pressure
PFI	port fuel injection
P_{int}	intake runner pressure
PM	particulate matter
PRF	primary reference fuel
PRR	pressure rise rate
PVO	positive valve overlap
$Q_{hr,ch}$	gross chemical heat release
Q_{wall}	wall heat transfer
R	mixture gas constant
RCCI	reactivity controlled compression ignition
RGF	residual gas fraction
RI	ringing intensity
RoHR	rate of heat release
RON	research octane number
RTD	resistance temperature detector
SACI	spark assisted compression ignition
SI	spark ignition
SOC	start of combustion
SOI	start of injection
TC	turbocharger

THC	total hydrocarbon emissions
T	average (in-cylinder) temperature
T_{IVC}	average in-cylinder temperature at intake valve closing
T_{TDC}	average in-cylinder temperature at top dead center
TDC	top dead center
TDC_f	top dead center firing
TDC_{ge}	top dead center during gas exchange
aTDC	after top dead center
bTDC	before top dead center
TWC	three-way catalyst
x_b	burned mass fraction
X_{EGR}	mole fraction EGR
X_{CSP}	mole fraction of stoichiometric combustion products
V	cylinder volume
VCR	variable compression ratio
VGT	variable geometry turbocharger
VVA	variable valve actuation

Abstract

Use of homogeneous charge compression ignition (HCCI) combustion mode in engines offers the potential to simultaneously achieve high efficiency and low emissions. Implementation and practical use of HCCI combustion, however, remain a challenge due to the limited operating load range. Managing the timing and duration of the combustion event, so that it is neither too early nor too late, neither too fast nor too slow, causing knock or misfire respectively, is difficult and represents a major obstacle to achieving high loads.

Most studies on high load extension of HCCI have been done on engines with conventional positive valve overlap (PVO) strategies, which use a heater to control intake temperature and adjust combustion timing. From a practical standpoint, however, this is not preferred, because of the additional energy required by the heater, slow response time and inadequate authority over combustion timing. Although there has been work on engines employing a more practical negative valve overlap (NVO) strategy, which controls charge temperature by varying the retained amount of hot internal residual gas, most of these studies were confined to a limited boost pressure range and/ or did not explore and isolate the effects of individual thermo-physical parameters on combustion and the maximum load limit.

This research work is unique in that a practical yet highly flexible NVO engine with fixed compression ratio, allowing for independent control of intake boost pressure, charge temperature and composition, thermal/ compositional stratification (NVO) and exhaust back-pressure, was used to independently investigate the effects of these variables on burn duration and combustion phasing limits. Results showed that maximum achievable loads for the NVO engine were less than those obtained by previous workers on a boosted PVO engine due to less efficient breathing, less stable combustion, which limits the achievable combustion phasing retard, and lower maximum allowable peak cylinder pressure. Lower engine speed enabled higher maximum load due to shorter crank-angle burn durations, facilitating later combustion phasing, and higher allowable peak pressure rise rates. Employing external EGR to partially replace air led to an increase in maximum load due to its retarding effect on ignition alleviating the constraint of limited cam-phasing authority. Similarly, lower intake temperature and exhaust back-pressure enabled higher maximum load.

Detailed studies of burn rates showed minimal effects of intake boost pressure and moderate effects of composition. In particular, replacing air with eEGR, thus decreasing in-cylinder oxygen concentration, led to a moderate increase of burn duration especially during the early heat release. Increase in boost pressure caused a minimal shortening of burn duration, but pressure rise rates and knock were unaffected.

Additional studies of knock and combustion stability limits showed that internal EGR has a negative effect on the combustion stability limit, because of increased cycle-to-cycle feedback, yet it had a positive effect on the knock limit by decreasing maximum pressure rise rates due to increased thermal stratification. Partially replacing air with external EGR led to an extension of the viable combustion phasing window, because of an increase in heat capacity moderately slowing down combustion rates. Boost pressure had no direct effect on either of the combustion phasing limits.

This research provides new insights into how boost pressure and other operating parameters in a NVO HCCI engine impact the maximum attainable load and combustion phasing limits. The results suggest that the maximum load is more dependent on the combustion stability limit and overall engine constraints, such as maximum allowable peak cylinder pressure and limited cam-phasing authority, than on burn rates.

Chapter 1
Introduction

This chapter presents the research topic of this dissertation by motivating the need for further research in the area of advanced internal combustion engines, reviewing the fundamentals of homogeneous charge compression ignition (HCCI) combustion and addressing its merits and challenges. Consequently, various approaches to extend the limited maximum load capability of HCCI combustion are reviewed to identify gaps within the literature and discuss benefits and shortcomings of previous works. Recent experiments involving these approaches are summarized and current challenges presented. Finally, the objectives for this dissertation are stated and an overview of its organization is given.

1.1 Motivation for Research on Advanced IC Engines

1.1.1 Increased Energy Consumption and Limited Resources

World-wide demand for energy has increased and will continue to increase as emerging countries including China, India, Brazil and Russia are about to join the established industrialized nations. High energy use characteristic of industrialized regions in the world such as the United States, Canada, Western Europe and Japan is directly related to economic prosperity, longer life expectancy and an improved quality of life [1]. A five-fold increase in world energy consumption over the past 60 years was accompanied by an increase in the world population from 2.5 billion in 1950 to 7 billion today. Since the middle of the twentieth century, as the US economy flourished and Europe and Japan rebuilt their economies, these nations required energy in proportions larger than their population growth. Whereas population in the industrialized countries has been stabilizing, emerging countries, and especially impoverished third world countries with high fertility rates, are expected to largely contribute to a projected increase of the world population from 7 billion today to 9 billion in 2050 [2].

Given finite fossil energy resources available, an increasing world population will make it even more challenging for leaders of all countries to make a decision in the interest of its people, as they have to carefully balance various national interests including economic progress, autonomy, peace and many others. Achieving and maintaining national energy security has become a decisive factor in the policies of many industrialized nations to preserve the economic status-quo. The United States (US) had been able to match their own energy needs until the 1970s, but since then increasingly larger amounts of energy especially petroleum, which is primarily used by the transportation sector, had to be imported. This has prompted the current US administration under President Obama to pursue the goal of energy independence within the next 10 years [3].

1.1.2 Climate and Environmental Concerns

Environmental impacts and in particular climate change, as a result of combustion of fossil fuels, which are still the back-bone of today's energy production grid, have been the subject of serious debate in recent years. By now, there is irrefutable evidence that the increase in atmospheric carbon dioxide (CO_2) concentrations is of anthropogenic nature. CO_2 is not only the most prominent product of combustion but also exhibits a pronounced green-house potential, which significantly alters the radiation balance of the atmosphere and leads to an increase of the average temperature on Earth. More severe weather conditions including raising water levels, floods, droughts and storms can be the consequences and occur more frequently as the CO_2 level increases [4]. CO_2 production is directly related to the amount of fossil fuel burned and also dependents on the type of fuel used, where natural gas performs better than petroleum, which in turn performs better than coal. Replacing fossil fuels with renewable energy sources in conjunction with higher efficiency energy conversion devices can alleviate the situation.

In an effort to stabilize atmospheric CO_2, currently at 400 ppm, or at least decrease the rate of increase, several countries have set goals and devised policies on the implementation of rules. The European Union (EU) has imposed a maximum allowable CO_2 amount per km traveled - 130 g/km by 2015 and 95 g/km by 2025 - that is to be phased in gradually [5]. The US have chosen a similar route through the Clean Air Act enacted by the current administration that sets corporate average fuel economy values of 34.1 mpg for 2016 and 54.5 mpg in 2025 [6]. These are steps in the right direction as they foster increased effort for developing more efficient technologies and create research opportunities for universities, government laboratories and industry.

While imposing more stringent CO_2 emission and fuel economy standards mainly

address the issue of climate and global warming, the challenge of keeping environmental pollution, in particular air pollution, in check remains. This is exacerbated by the fact that urban environments are becoming increasingly more popular and attractive as people move from the countryside to cities. Currently, about 3.5 billion people live in urban areas and this number is expected to increase to 5.3 billion by 2050. This trend toward urbanization entails several implications on transportation system modality and energy requirements [7]. In particular, legislation needs to account for these changes by adjusting emission standards for power plants and automobiles. Recently, US CO_2 emissions from power plants have decreased because of a progressive switch from coal to natural gas.

1.1.3 Success Story of the Automobile and the IC Engine

Since the invention of the first four-stoke engine by Nicolaus A. Otto in 1887 [8] and the first automobile by Carl Benz in 1886 [9], there has been a lot of progress in terms of the development of the technology over the years. It was not until 1908, when the very first Model-T, to be followed by millions more, left Henry Ford's factory, that the automobile could become affordable and available to many people in Europe and North America. Now there are approximately 250 million automobiles on American roads and one billion world-wide. Along with this growth, the automobile brought many great societal advances but perhaps its greatest contribution has been the freedom of personal mobility [10].

1.1.4 Advanced IC Engines as Part of the Solution

Having stated the incentives for less energy consumption per capita and more efficient automobiles in the preceding sub-sections, there are various potential avenues. The increasingly more stringent CO_2 and mpg regulations in the EU and the US have already sparked research in search of more efficient powertrain technologies and development and implementation of advanced powertrain technology. To maximize chance of success, a diverse range of technologies are being considered ranging from improved advanced internal combustion (IC) engines, hybrid powertrain architectures, electrified vehicles to fuel cells that use hydrogen as energy storage medium.

The IC engine has evolved over more than a century and in terms of efficiency improvements, for a variety of reasons, there is still no end in sight. It can be run off a myriad of fuels, most commonly liquid hydrocarbons, which have an inherently high energy density allowing for hundreds of miles to be traveled without need to refuel. Moreover, infrastructure for liquid fuels is already in place. Due to their long history of more than a hundred years, IC

engines today have reached a very high level of maturity and are a well proven technology available at relatively low cost thanks to mass production and optimization of manufacturing processes. Although fuels cells promise even higher efficiency and no tail-pipe emissions, the technology is still very expensive and the storage question of hydrogen as a fuel including infrastructure has not been fully clarified yet. Similarly with electric vehicles, despite a lot of progress has been made on development of batteries in recent years, a few key challenges need to be resolved before adoption of this technology in a sustainable manner at large scale becomes possible. The current electric grid cannot handle millions of electric vehicles, so it needs to be modified and a transition toward truly renewable power generation sources needs to occur.

In the near to mid-term future, most likely, a myriad of different powertrain technologies will evolve concurrently and we will witness a gradual transition going from the IC engine, hybridization and electric vehicles to fuels cells eventually. However, currently and in the near term future, in particular when having to meet EU 2015 and CAFE 2016 standards, highly advanced IC engines will play a pivotal role. Homogeneous charge compression ignition (HCCI) as a prominent example of modern low temperature combustion modes shows great promise and might facilitate a further leap in terms of efficiency improvement.

1.2 HCCI Background

1.2.1 Fundamentals

Homogeneous charge compression ignition (HCCI) is an advanced combustion mode, which has the potential to achieve high efficiency as a compression ignition (CI) engine and low emissions as a spark ignition (SI) engine [11]. As a low temperature combustion mode, HCCI uses a highly dilute and homogeneous fuel-air-mixture that undergoes a global auto-ignition event. A modern conventional SI engine can be operated in HCCI mode with minimal engine hardware modifications.

The origins of HCCI date back to the late 1970s. In 1979, Onishi et al. were the first to report running a two-stroke engine, whereby a fuel-air-mixture was brought to ignition without a spark simply by compression [12]. In the same year, Noguchi et al. showed HCCI combustion in a two-stroke opposed piston engine [13]. In 1983, Najt and Foster demonstrated HCCI combustion on a four-stroke engine suggesting that HCCI is predominantly controlled by chemical kinetics [14]. Thring reported operating a four-stroke engine with exhaust gas recirculation (EGR) over a wider range of loads in 1989

[15]. Starting in the 1990s, research on HCCI was intensified, and especially since 2000, extensive amounts of research have been done yielding a greater understanding of the HCCI combustion process.

Contrasting HCCI combustion with SI and CI combustion facilitates drawing a direct comparison between this novel and the two important and distinct conventional combustion modes. While HCCI exhibits features of both SI and CI combustion, it is unique in that combustion onset is not triggered through a spark discharge or fuel injection event, but instead solely relies on chemical kinetics triggering auto-ignition. The properties of the fuel-air-mixture and its thermo-kinetic state around top dead center (TDC) determine the onset of combustion.

SI combustion is characterized by a flame propagating through a premixed fuel-air-mixture, whereas CI combustion can be best described by mixing-controlled burning of fuel and air, after fuel injection and combustion onset have occurred. Because of the presence of locally very hot reaction zones, specifically across the flame fronts, both SI and CI engines emit relatively high levels of nitric oxide and nitrogen dioxide emissions, together commonly referred to as NO_X. Moreover, the heterogeneous nature of the fuel-air-mixture charge preparation process in a CI engine leads to locally rich pockets, despite a globally lean composition, that give rise to the formation of considerable amounts of particulate matter (PM) in these fuel rich regions [16].

HCCI combustion, in contrast to SI or CI combustion, involves no flame, that develops and propagates, instead imaging studies have revealed that the fuel-air-mixture undergoes a sequential auto-ignition process [17, 18, 19, 20]. During this staged auto-ignition event, combustion occurs rapidly, where burned gas originating from the portion of the mixture that burned first compresses the remaining mixture, and therefore, leads to an auto-ignition cascade [21]. Typically, HCCI combustion is completed within 10-15 cad, which is much faster than in a conventional SI engine. HCCI engines operate at compression ratio (CR) values intermediate to those of SI (8-14) and CI (14-24) engines i.e. CR $\sim$ 10-18. When HCCI combustion is phased correctly, CA50 $\sim$ 5-10 cad aTDC, it generally exhibits very low cyclic variability relative to SI combustion.

1.2.2 Merits and Some Drawbacks

Based on the discussion in sub-section 1.2.1, the merits and some of the challenges of HCCI engines can now be stated and discussed. From a thermodynamic point of view, a greater compression ratio (CR) and a highly dilute fuel-air-mixture, characterized by a large value of the ratio of specific heats, γ, each facilitate high thermal efficiency, η_{th}, as can be seen

from the equation for the efficiency of the ideal Otto cycle in equation (1.1).

$$\eta_{th} = 1 - \frac{1}{CR^{\gamma-1}} \tag{1.1}$$

As mentioned before, the burn duration during HCCI combustion is significantly shorter than that during SI combustion i.e. CA10-90 $\sim$ 10-15 cad compared to CA10-90 $\sim$ 40-90 cad, which facilitates combustion to be phased closer to TDC. This ensures maximizing the expansion ratio and aides indicated thermal efficiency. From an ideal cycle point of view, a HCCI engine resembles the ideal constant volume process more closely than a SI engine thus facilitating higher η_{th}. Compared to SI engines, HCCI engines are generally operated unthrottled, which entails decreased pumping work and an increase in net indicated efficiency, η_{net}. Since rich zones are absent in HCCI combustion, due to a homogeneous fuel-air-mixture, particulate matter (PM) and soot emissions tend to be very low. Another benefit of HCCI, related to emissions, stems from its high dilution levels, which lead to peak in-cylinder temperatures that usually are below the NO_X formation threshold of 1900 K.

Despite many benefits related to improved indicated efficiency and lower emissions of pollutants, notably PM and NO_X , HCCI also has its own specific requirements and some shortcomings, of which a few will be mentioned here, but certain key drawbacks will be covered in greater detail in section 1.3. HCCI necessitates a well-mixed fuel-air-mixture, which typically can be achieved using modern high pressure gasoline direct injection. More importantly, HCCI requires the fuel-air-mixture to have a certain minimal amount of thermal energy to facilitate auto-ignition around TDC. HCCI operation is only possible for a limited speed and load range. If peak in-cylinder temperatures are below 1300-1400 K during light load operation, combustion efficiency may decrease substantially eventually leading to a partial burn or incomplete burn that is a misfire. Moreover, higher levels of carbon monoxide (CO) and hydrocarbons (HC), originating from near-wall regions with low temperature and/ or outgassing from crevices, may not be oxidized, because post-combustion in-cylinder temperatures are too low for completion of combustion. At higher loads, it is difficult to keep heat release rates low enough to avoid harsh combustion and objectionable knock. Under certain high load conditions, NO_X emissions can increase to a level that may deem a de-NO_X aftertreatment device necessary, unless EGR is used to attain a stoichiometric composition, $\Phi \sim 1.0$, facilitating use of a conventional three-way catalyst (TWC).

1.2.3 Enabling Technologies

HCCI combustion requires appropriate thermodynamic and chemical in-cylinder conditions close to TDC to facilitate auto-ignition with proper combustion phasing. Moreover, the fuel-air-mixture needs to be adequately dilute to keep combustion rates and peak in-cylinder temperature low enough to avoid objectionable knock and limit NO_X formation thus not requiring a three-way catalyst (TWC) to meet emission standards. This section will describe and discuss some of the most common enabling technologies, which facilitate HCCI combustion including variable valve actuation, exhaust gas recirculation, intake charge boosting and direct injection.

Variable Valve Actuation

HCCI combustion requires a higher TDC temperature than those typically obtained in conventional SI and CI engines, and this can be achieved with intake charge heating, whereby two different methods are commonly used: external heating and internal heating. In case of the external heating method, an external heater provides above ambient intake air/ EGR temperature thus increasing the in-cylinder temperature at the end of compression. The internal heating method relies on manipulating the initial mixture composition and temperature at intake valve closing (IVC) with the same result regarding TDC temperature. The latter method usually involves retention of a portion of burned residual gas [22]. Both methods are effective, however, the former one requires an external heater that requires energy input, unless it works in conjunction with a smart waste heat recovery device. In either case, the energy balance is negatively affected or system complexity greatly increases. The latter one offers the benefit of being able to make fast adjustments almost on a cyclic base, which is especially useful during transients but also facilitates maintaining stable combustion at steady state operating condition near the stability limit.

Being able to effectively manipulate the residual gas fraction (RGF), also referred to as internal EGR (iEGR), thus composition and temperature at intake valve closing (IVC), is important and variable valve actuation (VVA) is a key enabler making this possible and also providing some form of authority over combustion phasing in a HCCI engine. By now, VVA is a proven and well established technology, that is robust, readily available at low enough cost, and that has made its way into production vehicles over the past $\sim$ 10 years. VVA systems consisting of two separate cam profiles can be used to realize a system that is capable of transitioning between a high RGF HCCI enabling operating strategy and a conventional SI valve strategy.

Two strategies that have received a lot of attention, within the context of facilitating HCCI combustion, are the recompression and rebreathing strategies. A recompression strategy as employed by Milovanovic et al. is characterized by an early exhaust valve

closing (EVC) event facilitating retention of considerable amount of burned gas in-cylinder [23]. As a result, the retained hot burned gas (RGF/ iEGR) will be blended with incoming fresh charge entering the cylinder after intake valve opening (IVO). Typically, EVC and IVO are phased symmetrically around gas exchange TDC to minimize losses due to pumping. The recompression strategy is also referred to as negative valve overlap (NVO) strategy. An alternative to the recompression is the rebreathing strategy, where a second exhaust valve event of shorter duration occurs during charge induction process while the intake valves are open. This allows re-induction of some of the hot burned gas from the exhaust port. While both strategies are effective, the rebreathing strategy has been found to allow slightly higher load and improved efficiency, however, it is more limited for the low load range [24]. Babajimpopoulos et al. investigated the benefits associated with each strategy [25, 26]. The recompression strategy is commonly the preferred choice.

Yet another valve strategy that has been used by some researchers is a conventional valve strategy using full duration and height valve lifts, which is referred to as positive valve overlap (PVO) strategy. The name is inferred form the fact that EVC occurs slightly after IVO [27, 28, 29]. In contrast to both RGF/ iEGR retention strategies described before, the PVO strategy can be useful at achieving HCCI combustion and allowing certain authority over combustion timing by adjusting the back-pressure, thus manipulating RGF as shown by Mamalis et al. [30]. Using a NVO versus PVO strategy may limit the amount of fresh incoming charge, thus potentially affect the maximum fueling rate and maximum attainable load. If both NVO and PVO strategies are sought to be implemented in the same engine, a cam shaft with two different cam lobes and mechanical mechanisms to switch between the two profiles are will be required, and technologies capable of this are already in the market place.

Exhaust Gas Recirculation - Diluent Composition

Exhaust gas recirculation (EGR) is a well established technique facilitating control over ignition and combustion phasing, and affecting combustion performance, which has been widely used among CI engines for the past $\sim$ 10 years. EGR was also adopted in SI engines in recent years. External EGR (eEGR) refers to a portion of exhaust gas from the tailpipe that is fed back, possibly cooled in a heat-exchanger, into the intake system of the engine, whereby internal EGR (iEGR) refers to internally retained hot burned gas. When the term EGR is used, this includes iEGR and eEGR. Use of either eEGR or iEGR facilitates changing of the charge composition and charge mixture properties. The thermodynamic and chemical properties of EGR are substantially different than this of air, which is commonly the diluent of choice in any conventional combustion engine. EGR is composed of considerable amounts of complete combustion products, CO_2 and H_2O , potentially a large variety of

products of incomplete combustion, CO and different hydrocarbons referred to as THC, and trace species including NO_X , in addition to the regular air constituents N_2 and O_2.

EGR as a diluent has the potential to significantly alter and affect combustion characteristics including ignition timing, burn rates, emissions, combustion and engine thermal efficiencies. There have been numerous studies in an attempt to understand the impact of EGR as a diluent on the HCCI combustion process [31, 32, 33, 34, 35, 36, 37, 38, 39, 40]. It was found to alleviate the intake temperature requirement of a high load HCCI engine [31, 29]. EGR was also found to be useful in extending the maximum load of a HCCI engine [29]. It is not entirely clear whether the effect of EGR is primarily a thermal one related to different thermodynamic properties i.e. higher specific heat capacity, c_p, thus lower end of compression temperature, which could lead to later combustion phasing, or a chemical one that is kinetics are efficiently modified to affect combustion.

As part of his computational study in 2002 investigating the effect of EGR on heat release rates, Dec found that EGR led to slower reaction rates likely due to changes in thermodynamic properties i.e. higher heat capacity and lower O_2 concentration. He concluded that the largest effect of EGR is a reduction of in-cylinder temperature at the end of compression as a result of different thermodynamic properties. Both the thermodynamic and chemical effect were estimated to have a significant impact on burn rates i.e. burn rates could change by a factor of 2-3 depending on the conditions. Dec also indicated that there is a strong coupling between conditions at ignition and burn rates [41].

In an experimental study in 2003, Olsson et al. also investigated the effect of EGR on various combustion characteristics. They concluded that emissions of CO, THC, and NO_X were generally lower with EGR hence yielding a higher combustion efficiency. They also noted a decrease in thermal efficiency due to changes in properties. The effect of EGR on ignition was also stated in that higher intake temperatures were required. Although burn duration was expected to slow down with EGR, this could not be observed [42].

Cairns and Blaxill explored the effect of cold eEGR addition to extend the maximum load in a practical NVO HCCI engine, and found that EGR facilitated retarding of ignition and combustion phasing, and that longer burn durations resulting in lower pressure rise rates could be achieved [43]. Moreover, they found that engine efficiency increased and THC emissions decreased. Most importantly, they stated that the achievable load could be increased by 20-65 % with eEGR addition. In another study on a turbocharged NVO engine, Cairns and Blaxill also reported that a combination of eEGR and iEGR in a boosted HCCI engine can be used to extend the maximum load limit relative to naturally aspirated operation [44]. They also found that EGR improved combustion stability.

In another experimental study in 2009, Dec et al. attempted to isolate the effect of

EGR from other combustion parameters, e.g. combustion phasing, CA50, and found that peak pressure rise rates decrease with EGR addition despite the fact that fueling rate was increased to maintain load. They found a 2 % loss in thermal efficiency and higher peak in-cylinder temperature and NO_X emissions [33]. It was shown that EGR addition did not change burn rates significantly when combustion phasing was matched.

Sjoberg et al. explored how boost pressure and EGR can be used to manage low temperature heat lease (LTHR) in HCCI combustion, and found that modification of the EGR level can be used as a means to control combustion phasing, especially when a reactive fuel is used [31]. Although there seems to be agreement in the literature that EGR addition tends to slow down burn rates, so far there has not been any work done to isolate the effects of EGR in conjunction with intake boost pressure on burn rates under controlled conditions i.e. with fixed CA50.

Intake Charge Boosting

Intake boosting is a promising technique with the potential to dramatically increase the maximum load capability of a HCCI engine and also to improve its efficiency. Using elevated intake or boost pressure can facilitate an increase of the overall charge dilution and affect combustion characteristics through chemical effects associated with increased pressure. A high level of charge dilution results in a larger amount of inducted air mass, which helps to reduce pressure rise rates for a given fueling rate. With the same pressure rise rate or knock constraint, more fuel can be injected and therefore the maximum load limit extended via boosting.

Christensen et al. converted a Diesel engine for HCCI operation in 1998, and showed that a higher load and a small decrease in emissions, notably NO_X and THC, could be accomplished with intake boosting. They also observed an increase in combustion efficiency and longer burn duration with increasing boost pressure [27]. Hyvonen et al. studying a supercharged VCR engine found that boosting can extend the operation range and decrease the burn rate, which leads to a decrease in knock. Yap et al. showed in 2005 that they were able to cover 75 % of the maximum load of a naturally aspirated SI engine with an intake pressure of P_{int}=1.4 bar [45].

A study by Cairns and Blaxill on a boosted 4-cylinder engine showed that the maximum load could be increased and heat release rates decreased. They showed that most high load points on the federal driving cycle could be attained yielding with a 12 % fuel economy improvement and that dilution poses a limit on the maximum load [44]. Johannson et al. found that boosting led to increased thermal efficiency compared to naturally aspirated operation, but that it dropped significantly as soon as combustion phasing was retarded [46].

The equipment providing the boost pressure needs to be appropriately sized and matched

to the needs of a HCCI engine to facilitate decent engine and system level efficiency. Olsson et al. found that the turbocharger needed to be smaller in case of a boosted HCCI engine compared to a conventional SI engine and identified increased pumping work due to high exhaust back-pressure as the main problem [28]. They suggested that a more flexible turbocharger system possibly including a variable geometry turbine (VGT) could be effective at lowering the exhaust back-pressure by leveraging most from a relatively low exhaust enthalpy. However, using s small and designated turbine for HCCI only could potentially hinder SI operation and mode switches with same equipment [47].

A modeling study by Mamalis et al. in 2010 compared different boosting strategies i.e. supercharging versus turbocharging, and found that while supercharging provided better combustion phasing control, turbocharging resulted in higher efficiency [48]. A two-stage turbocharger would allow even higher load but result in lower efficiency due to even higher back-pressure and a greater pumping penalty. Another modeling study by Shingne et al. on turbocharger matching for 4 cylinder boosted HCCI engine confirmed some of the findings by Mamalis i.e. a smaller turbocharger was required for a HCCI engine relative to a SI engine. A maximum $IMEP_n$ of 12 bar could be attained with a 2-stage turbocharger although at the expense of a high pumping penalty [49]. A follow-up modeling study by Mamalis et al. investigating the potential of switching from NVO to PVO valve strategy, revealed that the PVO strategy offered significant efficiency improvements at higher loads i.e. in the 5-12 bar $IMEP_n$ range. The key conclusion of that study was that external charge heating was more efficient than internal heating [30].

Direct Injection

A relatively high compression ratio (CR), in addition to intake air heating, aids the implementation of HCCI combustion, because it facilitates achieving the required TDC temperature for auto-ignition to occur. Since a future HCCI engine, most likely, will be a multi-mode engine, which operates in SI mode for high loads, knock mitigation will be challenge with a high CR engine especially during high load SI operation. Direct injection (DI), which benefits from a significant charge cooling effect due to the vaporization of the fuel, represents a powerful means to improve the knock resistance of a high CR engine. Mitsubishi was among the first to introduce DI in SI engines in the 1990 [50].

Direct injection offers a variety of additional opportunities, especially within the context of HCCI engines, to improve combustion phasing control, extend the high and low load limit, and improve combustion stability. Whitaker et al. used a dual fuel strategy, directly injecting an alcohol-based fuel, to mitigate knock under high load boosted conditions [51]. Reactivity controlled compression ignition (RCCI) employs a similar strategy to extend the maximum load capability of a HCCI engine equipped with DI [52]. Whereas the majority of the fuel

is premixed before entering the cylinder, via port fuel injection (PFI), a small fraction of a more reactive fuel is direct-injected during the compression stroke. Manipulating the ratio of the amounts of fuel between PFI and DI as well as the DI timing provide additional degrees of freedom to control combustion. Even with a pure DI engine without PFI, injection timing can be modified so as to affect combustion phasing and other characteristics as was demonstrated in a study by Li et al., who showed that earlier injection timing yielded faster and more stable combustion, with low CO and THC but higher NO_X emissions [53]. Fuel injection during the recompression part of the cycle in a NVO engine can lead to partial fuel reforming, which was found to be useful for extending the low load capability of HCCI combustion [54, 55].

HCCI research has been done on a variety of different engines, some of which employ direct injection and some of which use port fuel injection. The charge preparation process could potentially have a significant impact on HCCI combustion and was part of an extensive 3-D modeling study by Kodavasal, where he investigated the effects of these two strategies on HCCI combustion [56]. In both cases, a NVO valve strategy was adopted, start of injection was at 330 cad bTDC in the DI case, and the fuel-air-mixture of the incoming charge in the PFI case was assumed to be perfectly homogeneous. Despite more compositional stratification in the DI case, burn duration for DI and PFI were fairly similar. Spray cooling by injection into hot residual in the DI case yielded a lower maximum temperature, while additional intake air heating required to match CA10 in the DI case resulted in a higher minimum temperature. The reduced thermal width thus less thermal stratification in the DI case is believed to offset most of the benefits of a more favorable compositional stratification. NO_X emissions were found to be one order of magnitude higher in the DI case compared to the PFI case.

1.3 Key Challenges of HCCI Combustion

1.3.1 Combustion Phasing Control

Control of combustion phasing in a HCCI engine is a challenge, because, this combustion mode does not rely on an external trigger for combustion unlike SI and CI engines. The fact that HCCI is enabled and controlled by chemical kinetics and history of in-cylinder temperature, cylinder pressure, charge composition, and thermal/ compositional stratification implies that the in-cylinder condition at intake valve closing (IVC) is of critical importance to the final TDC state [57]. Although charge mixing and heat transfer occurring during

compression may affect the final state to some extent, any means possible to facilitate the appropriate conditions at combustion onset and during the entire burning of the mixture are critical.

Depending on the end-of-compression pressure, mixture composition and homogeneity, an average in-cylinder TDC temperature $\sim$ 900-1100 K is required to facilitate ignition and HCCI combustion with proper phasing. Various methods including intake air heating, retention of hot burned gas or adjustment of CR can be used to accomplish this, but each of these has its own benefits and drawbacks.

Sjoberg and Dec investigated how intake air heating, modifying intake temperature, can be used to control combustion phasings and found that a clear relationship existed [58]. Due to the slow response time of the heater, however, retention of hot burned gas is the preferred method from a practical point of view, because transients can be addressed better in this way. Hot burned gas can be retained in or introduced into the cylinder either via a recompression or rebreathing valve strategy [59, 60]. The recompression strategy is adopted most often, whereby early exhaust valve closing (EVC) allows a larger amount of hot burned residual gas to be trapped in-cylinder resulting in a higher IVC thus TDC temperature [61]. EVC timing was found to be most effective in modifying ignition timing [60]. Although intake valve opening (IVO) is less important regarding the amount of trapped hot residual, symmetric NVO is often used to minimize pumping work in a NVO engine [62, 63, 23].

Hyvonen et al. investigated the potential of mechanically modulating compression ratio in a variable compression ratio (VCR) engine to control combustion phasing in a HCCI engine [64, 65]. Their system also included an intake air heater that could be bypassed and adjusting the portions of the flow that pass through the heater and bypass, they would use this to start-up the engine offering fast control. But they also reported that after start-up, they could successfully control combustion phasing solely relying on the VCR mechanism. Having a VCR mechanism in an engine is currently not standard and entails additional cost and potential difficulties associated with the complexity of the technology.

Heat release and burn rates are closely related to combustion phasing (CA50) that is as combustion occurs earlier in the cycle and heat release rates are higher. Both higher and earlier heat release leads to higher in-cylinder temperatures and pressures, and also pressure rise rates thus knock [66]. Exceedingly early combustion can result in a significant portion of the charge burning before TDC, which yields excessive knock, increased heat transfer and may even decrease work output and engine thermal efficiency. Too late ignition and therefore combustion phasing can result in highly unstable combustion, where few cycles do not complete combustion or misfire occur [67]. The following sections will discuss these combustion phasing limits and how they are affected in more detail.

1.3.2 Combustion Phasing Limits

Although HCCI combustion is highly stable and exhibits low cyclic variability when correctly phased, the viable operating window is fairly narrow and limited by knock and high combustion variability (unstable combustion) for too early and late combustion phasing respectively. These two limits are very important as they govern the maximum achievable load of a HCCI engine, which typically limited to $\sim$ 4 bar $IMEP_g$ on a single-cylinder engine or $\sim$ 3 bar BMEP on a practical multi-cylinder engine. Each of these two important limits is discussed in more detail in the following.

Knock in an HCCI engine is caused by elevated gas temperatures that lead to bulk auto-ignition of the fuel-air mixture early in the cycle close to or before TDC [66]. Whereas knock observed during conventional SI combustion is usually limited to a to a small portion of the combustion chamber, also referred to as the end-gas, knock in HCCI combustion mode is not bound to a specific region, but occurs throughout the combustion chamber, hence it is referred to as volumetric or HCCI knock [68]. Potential consequences of HCCI knock are audible ringing sound emitted from the engine structure on the one hand, and high mechanical and thermal stresses of key engine components on the other hand.

The rapid auto-ignition events in a HCCI engine lead to in-cylinder pressure oscillations resulting in pressure waves propagating though the combustion chamber [66, 69, 70]. When these pressure waves impact on or are reflected by a wall, standing waves inside the combustion chamber form with certain resonant modes prevailing based on the combustion chamber geometry. The pressure oscillations can also excite the engine structure and cause it to vibrate. The resulting noise emission to the ambiance can be audible and recognized as a ringing sound, which may be considered objectionable and prompt for strategies to mitigate or decrease the ringing to be pursued [71]. Beside the acoustic problem, severe pressure oscillations and high rates of pressure rise associated with knock may result in excessive mechanical and thermal stress of key engine components. For instance, knock is also known to increase heat transfer from the working fluid to the combustion boundaries including pent-roof, liner and especially the piston [72, 73]. Excessive heat transfer may not only lead to a decrease in thermal efficiency of the engine, but, maybe more importantly, it can also lead to premature and severe engine damage.

Although HCCI combustion near optimal combustion phasing is a very stable combustion mode exhibiting relatively less cyclic variability [74], late combustion phasing (CA50) is characterized by high cyclic variability, which can eventually lead to partial or complete misfire. Note, that this limit occurs already for CA50 $\sim$ 10-12 cad aTDC for naturally aspirated operation.

Since HCCI operation in a NVO engine relies on the retention of significant amounts of

hot residual (iEGR), this is considered a major reason for this high combustion variability near the stability limit. A cycle with late combustion phasing, a partial misfire, leaves a large amount of unburned fuel or intermediate combustion products left, which increases the overall fuel-to-charge ratio of the next cycle and enhances reactivity. Therefore a late cycle is oftentimes followed by an early cycle and there is a naturally tendency of bi-modal combustion instability. Hellstrom et al. pointed out this behavior and noticed a strong link through unburned fuel and residual temperature that is propagated and affects the following cycle, which he refers to as dynamic coupling in a high RGF engine [75].

Sjoberg and Dec comparing late-cycle auto-ignition stability of gasoline and two-stage ignition (PRF) fuel found that combustion variability increased as CA50 is retarded for both fuels [76]. However, the more reactive PRF 80 fuel exhibited lower combustion variability than the gasoline fuel. The higher relative magnitude of random in-cylinder temperature fluctuations and less temperature rise rate prior to run-away (ignition) in case of gasoline were considered to be the main reasons for higher combustion variability. A cycle with partial burn yielding a higher effective Φ' in the next cycle enhances the reactivity relatively much more in case of the less reactive gasoline fuel compared to PRF80. Sjoberg and Dec also considered that the RGF/ iEGR was a major contributing factor to combustion instability, although their PVO engine inherently used a magnitude of order lower RGF/ iEGR value than a NVO engine.

When fueling rate and load is increased, the viable operating window in terms of combustion phasing (CA50) becomes even more narrow. This and the connection of both knock and combustion phasing limits within the context of maximum load extension are discussed in more detail in the following section.

1.3.3 Limited Maximum Load Capability

The ringing or knock and combustion variability or stability limits, which are associated with early or late combustion phasing, result in narrow operating range for HCCI combustion. In particular, as load is increased, peak pressure rise rates and peak pressures increase, which requires further combustion phasing retard to keep knock in check and comply with the imposed ringing limit [42]. During this process of increasing fueling rate and load, ringing and stability limit finally converge to a small combustion timing window or almost a single point representing the maximum load limit for HCCI combustion, as can be seen in Figure 1.1 [67]. Slight changes beyond this limit can lead to in-cylinder changes that in turn can have dramatic effects on combustion leading to excessive knock, misfire or both [29]. The maximum load for a naturally aspirated HCCI is $\sim$ 4 bar $IMEP_g$ but at this condition burned

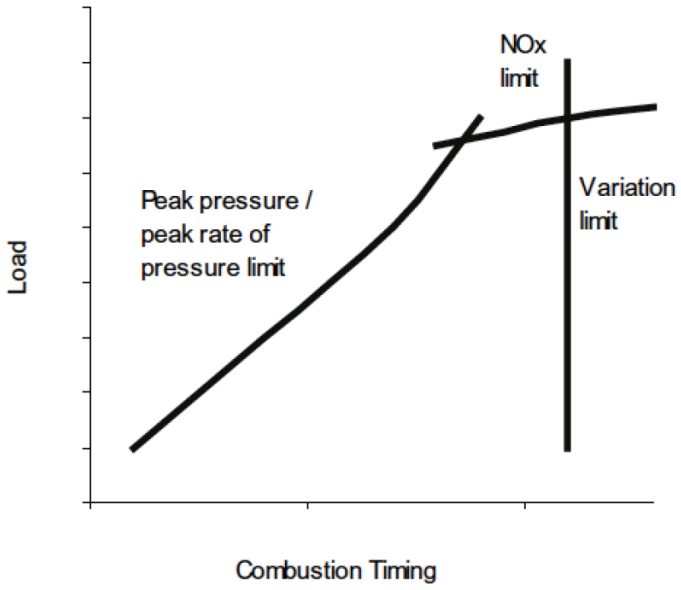

Figure 1.1 Limits of HCCI combustion: pressure rise rate (knock), NO_X emissions, and combustion variability (stability) as shown by Olsson [67]

gas temperature are high enough to allow for significant NO_X formation [29, 77, 78, 62].

Combustion phasing retard only enables increasing burn duration and decreasing maximum pressure rise rates to a certain extent [79]. Because this strategy has its own limitations, namely the combustion variability limit, there is a need to extend the operating range of HCCI combustion to fully benefit from its high efficiency over a wider load range [80]. A variety of different strategies have been considered for extending the maximum load capability of a HCCI engine. These strategies including thermal stratification [79], charge stratification [81], eEGR addition [33], spark-assisted compression ignition (SACI) [82, 77, 83], and boosting [29, 47, 84] will be discussed in the following.

Sjoberg et al. investigated the effect of thermal stratification on the rate of heat release and found that burn duration slightly increased i.e. by $\sim$ 1 cad, when coolant temperature was decreased by $\sim$ 50 °C due to increased thermal stratification. Consequently, ringing intensity decreased by $\sim$ 15 %, however, thermal efficiency decreased slightly, primarily due to increased heat losses [79].

Aroonsrisopon et al. studied the effect of compositional stratification, induced by late injection timing during the compression stroke, and reported a moderate i.e. $\sim$ 10 % improvement due the increased thermal and especially compositional stratficiation [81]. Another study also found that burn duration could be extended with later fuel injection thus partial fuel stratification, but at the expense of increased particulate matter (PM) emissions as a result of significant compositional inhomogeneities thus locally rich zones [85].

The effect of cooled external EGR (eEGR) on combustion was studied by Dec, and he found that burn rates could be lowered primarily due to the changes in thermodynamic properties i.e. higher specific heat capacity in the case of eEGR [41]. The main effect was a decrease of the end-of-compression temperature and consequently a later CA50. However, when CA50 was held constant, the eEGR effect was relative small, as was shown by Olsson as well [42]. Combustion phasing retard generally is helpful in achieving higher maximum loads with a given knock constraint, and this technique has been utilized too in conjunction with intake boosting to dramatically increase the load [29].

Spark-assisted compression ignition (SACI) is a hybrid combustion mode combining features of SI combustion and HCCI combustion. The spark is turned on and a flame kernel initiated so that a flame can development and propagate through the combustion chamber. The compression heating of the unburned gas eventually triggers auto-ignition in this portion of the mixture, so that pure HCCI-type auto-ignition combustion takes over. SACI enables higher loads than HCCI, because pressure rise rates and knock are attenuated, which in turn facilitates higher fueling rates [82, 77, 83]. However, SACI also has some shortcoming including slightly lower thermal efficiency, possibly high NO_X emissions, and more deleterious knock. Addressing the NO_X emissions might require either a de-NO_X -catalyst or stoichiometric engine operation, using lots of eEGR, and a three-way catalyst, which represent a burden. Knock in SACI combustion mode can be especially problematic as shown by Vavra et al. [68].

Given all these options, each with its limitation, and acknowledging the fact that downsized SI engines employing turbo-charging equipment have become a reality in the last few years, boosting appears to be the most practical approach to increase the maximum load capability of a naturally aspirated HCCI engine. The following section, therefore, will address boosting and a few other related aspects that affect combustion and combustion phasing limits.

1.4 Boosting for High Loads

1.4.1 Benefits of Boosted HCCI

Boosting that is increasing the intake pressure above ambient is a promising pathway to extend the load range of a HCCI engine, because a lot of the necessary technology now has become readily available. Given its limited operating range, a naturally aspirated HCCI engine is almost uncompetitive compared to progress that has happened to downsized and

turbo-charged SI engines. The noise, vibration and harshness issue can only partially be addressed by retarding combustion phasing, because ultimately both knock and combustion variability limits merge.

Boosting, when fueling rate is kept constant, can be used to significantly increase the mixture dilution resulting in lower pressure rise rates, which in turn enable higher fueling rates so that the load can be increased while still complying with the knock limit. Increased intake boost pressure, P_{int}, also leads to enhanced reactivity of the mixture, which results in more advanced combustion phasing and higher pressure rise rates [31, 86]. However, the chemical effect of promoting earlier ignition and faster combustion, thus more knocking, is outweighed by the benefits of increased dilution. In addition, the TDC state can be modified in such a way that combustion does not occur earlier but rather later. In fact, increased boost pressure is shown to enable later CA50, which implies that the combustion variability limit could be potentially further retarded.

Recently, Lavoie et al. conducted a fundamental modeling study exploring the potential of boosting within the context of advanced combustion modes including HCCI etc. and explaining the specific benefits due to different effects [87]. The results show that increased dilution provided by increased intake pressure yielded higher gross efficiency due to improved thermodynamic properties and a reduced peak cylinder temperature. Increasing the load, Φ, generally resulted in improved brake efficiency because of reduced relative friction losses. Higher intake pressure also resulted in a decrease of relative heat losses, because the Nusselt Number only scales with the power of 0.7 with the Reynolds number, where the latter one increases according to pressure. The study, employing an ideal turbocharger model, also indicated that higher turbocharger efficiency yielded improved dilution and hence higher loads. Some of the shortcomings of this study, however, were that a constant burn duration was imposed, which does not necessarily correctly reflect potential effects of composition and boost pressure, and that for the conditions shows in Figure 1.2 no back-pressure or pressure differential was applied i.e. $dP=P_{exh}-P_{int}$, which is unrealistic.

There has been a lot of work on boosted HCCI combustion in an attempt to extend the maximum load capability of HCCI combustion. In 1998, Christensen et al. reported that boosting can be successfully used to extend the maximum load/ IMEP [27]. In order to address the resulting advanced combustion phasing, researchers looked at other fuels than gasoline, including natural gas and ethanol, to avoid this potential limiting aspect. Later, the same group used pilot injection and eEGR to further extend the maximum load to $\sim$ 16 bar IMEP with P_{int}=2.5 bar [88]. Olsson et al. achieved a BMEP of $\sim$16 bar with P_{int}= 3 bar [28].

In 2010, Dec and Yang demonstrated that boosting in conjunction with eEGR can be

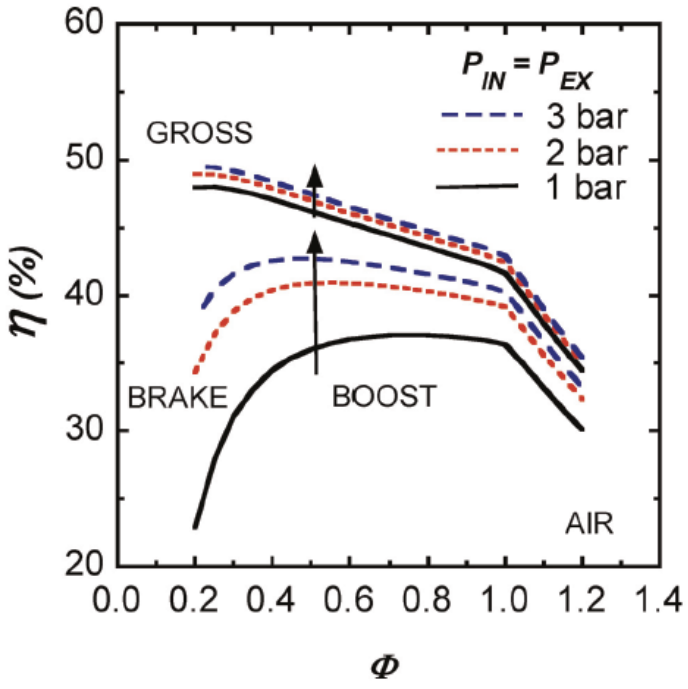

Figure 1.2 Gross and brake efficiencies as function of fuel-to-air equivalence ratio for various intake boost pressures: the effect of reduced relative heat transfer and friction losses assuming an ideal boosting device (no back-pressure) as shown by Lavoie [87]

used to achieve a high load with conventional gasoline fuel i.e. they attained an $IMEP_g$ of $\sim$ 16.3 bar with P_{int}=3.25 bar. [29]. External EGR (eEGR) addition was necessary to keep TDC temperatures low enough to facilitate sufficient combustion phasing retard to meet knock/ ringing constraints. Without eEGR, load could not be extended beyond P_{int}=1.8 bar, because combustion could not be further retarded. Saxena et al. studied in more detail the limiting factors of boosted HCCI combustion in a multi-cylinder engine and achieved a maximum $IMEP_g$ of $\sim$ 9 bar [89, 90].

As mentioned before, NVO valve strategy is the preferred choice when considering practical implementation of HCCI combustion in an engine and the research reviewed so far was performed on engines with a conventional PVO valve strategy. Yap et al. applied intake charge boosting to a HCCI engine using residual gas trapping, and they reported a substantial increase in the maximum load without requiring an auxiliary heater. They noticed an increase in fuel consumption due to increased pumping work and lower combustion efficiency. Ultimately, the maximum allowable peak cylinder pressure of the engine was the factor limiting maximum load [45]. In a later study on the effect of intake valve timing, the same group found that non-optimal timing can lead to a lower effective compression ratio, which would require adjustments in fueling, thus decreasing the total dilution level and

diminishing some of the benefits of boosting [91]. Xu et al. also investigated a NVO engine and reported similar findings. In addition, they noticed that the breathing capability was significantly compromised due to reduced valve lift and duration [92]. Martins and Zhao reported that emissions, especially NO_X and CO, substantially decreased with boosting, but they also found limitations in the gas exchange process, especially at higher engine speeds [93].

The role of the diluents, air versus eEGR, with respect to the knock and later also the stability limit was studied by Wildman et al. They found that eEGR helps to decrease the maximum pressure rise rate, however, it would not enable higher load unless reaction times could be slowed down [94]. In a follow-up study, Scaringe et al. found that dilution with cooled eEGR shifted both the knock and stability limit so that at higher load would be feasible. However, they did not find any dependence on boost pressure and reported that the stability limit is not sensitive to stratification (NVO) [95]. Szybist et al. were able to increase load in a NVO engine up to 6 bar IMEP/textsubscriptn at P_{int}=1.9 bar achieving 41 % peak efficiency. They found that increasing P_{int} and eEGR each retarded combustion phasing, and that the sensitivity to NVO increases with increasing P_{int} and load, so that fueling rate may be more suitable to fine-tune combustion phasing. They also identified that the RI metric might significantly underestimate engine noise under boosted conditions [96].

Previous research has shown that boosting in general is effective at increasing the maximum load range of a HCCI engine, however, there are certain limitations and ambiguities, especially related to the NVO engine and the effect of the diluent on combustion phasing, burn duration and the maximum load limit. PVO engines demonstrated very high loads but oftentimes the setups were either of a laboratory-style i.e. not accounting for back-pressure resulting from an actual turbocharger [29], or they were closer to a production engine, in which case it is difficult to separate and isolate various effects. Some of the findings seem to contradict each other, which is a key motivation for this research i.e. to study the effects of various engine operating and fundamental thermo-physical parameters on combustion in a NVO HCCI engine.

1.4.2 Limitations of NVO - NVO vs. PVO

From the preceding sections it has become clear that NVO is more suitable for implementing HCCI combustion from a practical point of view, however the maximum achievable load seems to be significantly lower than that of a PVO engine. While Dec and Yang were able to demonstrate loads above 16 bar $IMEP_g$ experimentally, Mamalis et al. showed in a modeling study that a NVO engine can achieve a similarly high load i.e. a maximum $IMEP_n$ of 17 bar

at P_{int}=3 bar was achieved, while the maximum cylinder pressure was 145 bar [97]. The fact that all experimental research never reported maximum loads exceeding 10 bar $IMEP_g$ thus not getting close to the results shown by Dec and Yang has prompted the questions: what causes the difference between a NVO and PVO engine, and what prevents a NVO engine from achieving the load of a PVO engine? Since many parameters are different between the PVO engine used by Dec and Yang and various other NVO engines, including engine size, compression ratio, engine speed, valve strategy, and the turbocharging device, it is important to understand which of these and how exactly they limit the maximum load output of a NVO engine.

A key difference between NVO and PVO engines is that the former one uses significant amounts of iEGR/ RGF ($\sim$ 30-45 %), whereas the latter one usually has much less iEGR/ RGF ($\sim$ 4-6 %). Although overall composition may be the same for both engines, the EGR may either be well mixed when entering through the intake valve or considerably less mixed when it is internally retained from the previous cycle. Using an optically accessible engine, Rothamer et al. quantified thermal and compositional stratification for a conventional PVO and NVO strategy [98]. They found that the NVO strategy yielded a much higher level of in-cylinder thermal and compositional stratification due to incomplete mixing of the residual gas with the fresh charge. Moreover, they noticed that temperature in zones with higher RGF concentration was higher, and that auto-ignition would start there. A recent 3-D computational study by Kodavasal investigating the difference between NVO and PVO charge preparation confirmed that thermal and compositional stratification increase with NVO strategy [56]. Moreover, he isolated these two effects and concluded that thermal stratification, owing to non-homogeneous distribution of iEGR, is almost exclusively responsible for a longer burn duration.

Another modeling study only investigating thermal stratification found that an increased thermal width increased the time between ignition of different zones thus yielding longer burn duration [99]. Lawler investigated the effect of various parameters on thermal stratification using a novel methodology that back-calculates temperature distribution from the heat release curve assuming that sequential auto-ignition of the charges is not kinetically limited [100]. In his study he found that PVO operation yielded a more narrow temperature distribution thus shorter burn duration. Generally, slower burn rates thus longer burn duration results in a decrease in pressure rise rate, which acts to reduce knock. From that point of view, NVO seems to be attractive and potentially useful for extending the maximum load limit but the effect on combustion stability is not entirely clear.

Olesky et al. compared intake air heating and NVO as charge heating methods in a NVO engine [101]. In case of intake heating, NVO was held constant, whereas in case of NVO,

intake temperature was fixed, and NVO was varied. The results indicated that NVO charge heating method led to increased COV of $IMEP_n$ values toward later CA50. Introduction of cycle-to-cycle feedback via iEGR is considered to be a primary reason that causes high combustion variability and instability in a NVO engine. Sjoberg et al. argued that any change in charge temperature at TDC can result lead to cyclic variability, and that changes in heat transfer and stratification can affect this as well[79]. In general, if a larger amount of iEGR is retained, ignition becomes more affected by residual than inlet conditions, which are more easily controlled, and this is especially the case for operation near combustion stability limit [61].

The NVO valve strategy appears to be advantageous in regards to the knock limit, because increased thermal stratification may result in slower burn rates, which could be used to extend the load range. However, combustion variability may be negatively affected, and it is not clear what the next effect on the maximum load range is. Moreover, other fundamental thermo-physical parameters such as boost pressure and composition are not necessarily constant and may also play a role. Hence, there is a need to more carefully investigate how engine operating parameters affect fundamental thermo-physical parameters such as temperature, pressure, composition and stratification, and then understand how those thermo-physical parameters affect burn rates, knock and combustion phasing limits.

1.4.3 Factors Affecting Ignition and Burn Duration

The onset of HCCI combustion is triggered by chemical kinetics and auto-ignition of presumably the hottest portion of the charge initiating the combustion process. It is not entirely clear what determines combustion rates i.e. whether it is thermal gradients, chemical kinetics or both. Although a longer burn duration appears to be advantageous from a knock point of view, it is not clear if a slower burn rate potentially affects combustion stability in a negative way thus reducing the potential of combustion phasing retard. The effect of boost pressure and other fundamental thermo-physical parameters on combustion and especially combustion phasing limits within the context of a gasoline-fueled NVO HCCI engine is still not clear.

The auto-ignition integral concept introduced by Livengood and Wu is a powerful tool that has been extensively and quite successfully used within the HCCI community [102]. It facilitates using ignition data from a very controlled combustion system e.g. a rapid compression machine within the context of a reciprocating internal combustion engine. The

ignition delay is usually given in Arrhenius form

$$\tau = A \cdot P^{-a} \cdot exp(\frac{E_A}{R \cdot T}) \tag{1.2}$$

where A is a pre-exponential factor, that can be a function of composition and temperature, P is the cylinder pressure, T is the in-cylinder temperature, E_A is the activation energy, R is the universal gas constant, and a is the reaction order. The ignition time, t_{ign}, is defined as the time, when the auto-ignition integral reaches a value of 1:

$$\int_0^{t_{ign}} \frac{1}{\tau} d\tau = 1 \tag{1.3}$$

There have been numerous research, both computation and experimental, quantifying auto-ignition delays for different hydrocarbon fuels, temperatures and pressures [103, 104, 105, 106, 107, 108]. Generally, single-component fuels or surrogates are used, especially for modeling purposes, to limit the computation cost. The ignition delay expression suggested by He et al., which was developed based on experiments with iso-octane, is commonly used for estimating auto-ignition in a gasoline HCCI engine [108]. It is given as

$$\tau_{ign} = 1.3 \cdot 10^{-4} \cdot P^{-1.05} \cdot \Phi_{FO}^{-0.77} \cdot \chi_{O_2}^{-1.41} \cdot exp(33,700/(R \cdot T)) \tag{1.4}$$

where P is the chamber pressure (atm), T is the chamber temperature (K), Φ_{FO} is the fuel-to-oxygen equivalence ratio, χ_{O2} is the oxygen mole fraction (%), R is the universal gas constant (cal/mol K), and τ is the ignition delay time (ms). This expression shows weak dependency of pressure. Kodavasal carried out a sensitivity analysis based on nominal ignition conditions in a HCCI engine i.e. at 10 cad bTDC, T=1050 K, Φ_{FO}=0.5 and χ_{O2}=15 %, which provides a better intuition for how much impact each factor has relative to another one on the ignition delay[56]:

$$\Delta T = 50K \equiv \Delta\Phi_{FO} = 0.5 \equiv \Delta\chi_{O2} = 8\% \tag{1.5}$$

Pressure is the least important factor in this expression. However, it is known that iso-octane, and even more so, gasoline, exhibit some NTC behavior. Goldsborough proposed a more complex expression that can capture a wider range of conditions including some of the high pressure low temperature effects [109].

Most of the ignition delay data is obtained from very controlled experiments e.g. rapid compression machine or shock-tube, and most simulations also use ideal assumptions that is no heat loss and uniform mixture. Whereas the ignition integral in conjunction with the ignition delay expression can be used fairly reliably to estimate auto-ignition, it is not

straight forward to infer combustion and burn duration based on that, because the real engine is much more complex. Thermal and compositional stratification are present, and the effect of these as well as composition on combustion has not been adequately studied within the context of a boosted NVO HCCI engine. Burn duration is directly related to knock and it may also have a significant impact on combustion stability, both of which affect the maximum load limit. This is the motivation for this thesis and the objectives are stated in the next section.

1.5 Research Objectives and Document Organization

1.5.1 Research Objectives

The main objective of this doctoral research work is to draw insights into the fundamental mechanisms limiting the maximum load capability of boosted HCCI combustion in a gasoline-fueled NVO engine, which encompasses the following aspects:

- Demonstrate how engine operating parameters affect thermo-physical state of fuel-air-EGR mixture required to initiate combustion and explore the role of engine hardware constraints within the context of maximum load limit.
- Understand how two key fundamental thermo-physical parameters, boost pressure and charge composition, impact burn duration and other combustion characteristics.
- Investigate fundamentals of knock and combustion variability limits and explore how they are affected by boost pressure, composition and thermal/ compositional stratification via NVO.

A second objective is to verify, whether or not the framework of a staged auto-ignition cascade for HCCI combustion with all its implications is valid under boosted conditions. The third and last objective is, based on the findings, to answer the first objective, to recommend an advantageous engine operating strategy to achieve high load HCCI combustion under practical system considerations.

Some key research questions to be answered are:

- How are burn duration and combustion phasing limits affected by thermo-physical state (boost pressure and eEGR) and thermal/ compositional stratification introduced via iEGR/ NVO?
- Why can the SNL PVO engine attain a higher maximum load than the UM NVO engine?
- Are there any specific engine parameters that can be adjusted to achieve higher maximum load and improve efficiency of a NVO HCCI engine?

In order to accomplish the aforementioned objectives, it is necessary to leverage all the flexibility, which the state-of-the-art single-cylinder research engine used for this research offers, including independent control over all key variables that affect combustion in a NVO engine setting. The effects of engine operating parameters such as intake temperature, composition (eEGR vs. air), intake pressure and exhaust back-pressure on thermo-physical variables are explored. Burn rates and combustion phasing limits are analyzed in terms of these fundamental thermo-physical variables. Finally, to explore the potential benefit of switching from NVO to PVO operation, a parametric study using a 1-D engine simulation tool is performed that provides additional insight into the phenomena that enable higher loads with PVO.

1.5.2 Document Organization

The remainder of this dissertation is organized as follows:

- Chapter 2 gives an overview of the experimental engine setup used for this doctoral work, which required significant upgrading and modifications at the beginning of this research. The heat release analysis tool used for data analysis and key combustion constraints, which are imposed during the experiments, are explained. GT Power as 1-D engine simulation tool, leveraged for part of this research, is outlined. Lastly, this chapter concludes with a discussion on experimental and simulation uncertainty.
- Chapter 3 investigates the effects of charge dilution, intake temperature, turbocharger efficiency, and engine speed as a function of intake boost pressure on the maximum

load limit of this NVO engine. For each intake pressure, the maximum load point, where knock and combustion variability limits occur simultaneously, is reached by successively increasing fueling rate and retarding combustion phasing. NVO is used as a control knob for all these maximum load sweep experiments. A parametric modeling study with GT Power is performed to identify key enablers that are responsible for a higher maximum achievable load of another well documented PVO engine relative to the NVO engine used in this work.

- Chapter 4 explores and isolates the effects of boost pressure and charge composition on burn rates in a NVO HCCI engine. This chapter is the most fundamental one of this doctoral work and the experiments performed, to isolate both of these two fundamental thermo-physical parameters in a rigorous and effective way, require the full level of flexibility of this NVO engine. Overall fuel-to-charge ratio, combustion phasing and NVO were held constant to minimize any potential bias, and intake temperature was used to compensate for changes in combustion phasing with increasing amounts of EGR.
- Chapter 5 analyzes and quantifies how boost pressure, charge composition and thermal/ compositional stratification via NVO impact both the knock and combustion variability limit during boosted HCCI operation. This chapter links findings about burn duration from the previous chapter to the knock limit and connects the fundamental aspects with the high load limit of a practical NVO engine. Careful combustion phasing sweeps via intake temperature adjustments were performed so as to keep as many other parameters as possible constant. Two different ringing intensity metrics are compared and explanations for different limit behavior suggested.
- Finally, chapter 6 presents summaries of key findings and conclusions drawn from the results. Contributions that follow are stated as well as recommendations for future work given.

Chapter 2

Experimental Setup, Analytical Methods and Simulation Tool

This chapter introduces the boosted single-cylinder research engine used for this work. The high degree of flexibility of this engine setup is crucial and allows for controlled experiments to be designed and performed to achieve the goal of this research. Important engine hardware, instrumentation and the heat release analysis tool including error analysis are described. Finally, the 1-D engine simulation software, GT Power, and the model developed using it to supplement this work are presented.

2.1 Experimental Setup

2.1.1 Engine Hardware

The boosted single-cylinder research engine used in this research was provided by General Motors RD and employs a Ricardo Hydra crankcase. Flexible valve timing is facilitated via hydraulically actuated cam phasers on intake and exhaust side, which allows for retention of appreciable amounts of internal EGR (iEGR) to facilitate HCCI combustion. The engine also includes an external EGR loop allowing for external EGR (eEGR) to be redirected into the intake. eEGR is assumed to be well mixed and considered homogeneous in contrast to iEGR. The schematic in Figure 2.1 shows the air path and key components of this engine.

The engine has a compression ratio of 12.4:1, which is higher than what is commonly used for spark-ignition engines. This facilitates implementation of HCCI combustion, which requires elevated in-cylinder gas temperature and pressure close to TDC for the mixture to auto-ignite. The combustion chamber design is a conventional pent-roof and the piston has a bowl asymmetrically located in the wedge-shaped piston crown. These and all other relevant engine geometry are listed in Table 2.1.

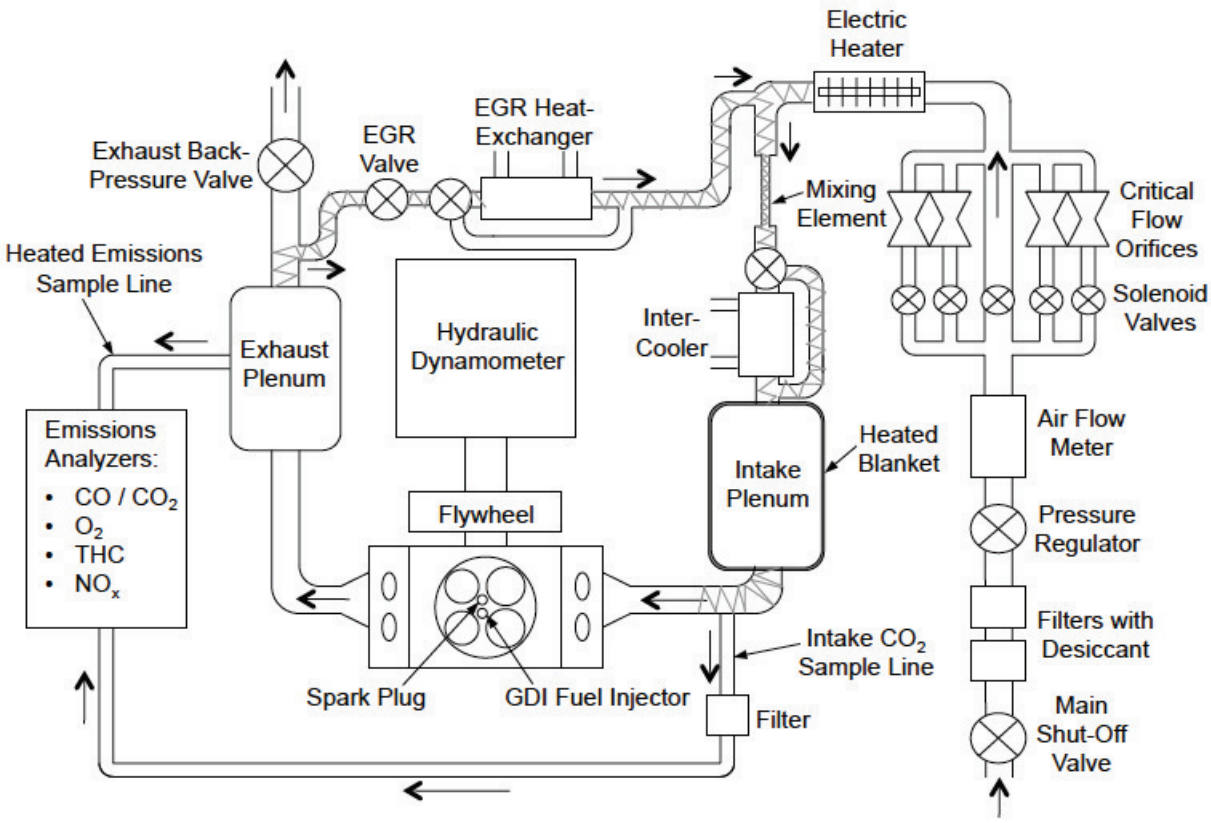

Figure 2.1 Boosted engine schematic

Table 2.1 Boosted engine specifications

Parameter	Value	Unit
Displacement volume	550	cm^3
Number of cylinders	1	-
Bore	86.0	mm
Stroke	94.6	mm
Connecting rod length	152.2	mm
Piston pin offset	0.8	mm
Compression ratio	12.4:1	-
Number of valves	4	-
Piston shape	asymmetrical bowl-in-wedge	-
Head design	pent-roof	-

Table 2.2 Valve system specifications

Parameter	Value	Unit
Operating principle	hydraulic	-
Number of valves	4	-
Maximum lift	4	mm
Duration	120	cad
Valve lash	0.1	mm
EVC @ 0.1 mm lift (parked position)	36	cad bTDC
IVO @ 0.1 mm lift (parked position)	89	cad aTDC
NVO range (symmetric)	72-178	cad

As this type of single-cylinder research engine does not contain any ancillary devices of a multi-cylinder engine, external pumps and heaters are used for both oil and coolant temperature control. The torque produced by the engine is absorbed by a hydraulic steady-state dynamometer from Electro-Mechanical Associates allowing engine speed control. The engine crankshaft is mechanically connected to a hydraulic motor, which is connected to a pump via hydraulic lines. A Hall effect sensor is used to measure engine speed.

2.1.2 Variable Valve System

The valve system in this engine allows employment of a recompression strategy via negative valve overlap (NVO) to retain appreciable amount of hot iEGR and facilitate auto-ignition. The valve system consists of two hydraulically actuated cam phasers for each intake and exhaust cam and allows for independent control over intake and exhaust valve timing. In particular, each cam can be moved within a 60 cam angle degree window from its parked position so that a total symmetric NVO range of 74-178 cad can be covered (see Figure 2.2). Note that since the valve system uses fixed duration cams IVC shifts as NVO is varied i.e. from 157 to 209 cad aTDC. Generally, symmetric NVO is preferred to minimize pumping losses. Given everything else remains constant (dP, fueling etc.) an increase in NVO leads to increase in iEGR fraction, which advances combustion phasing. A similar effect can be attained by changing intake temperature, but response time is considerably slower, hence using NVO to adjust combustion phasing is the preferred method. Table 2.2 provides details about the valve system.

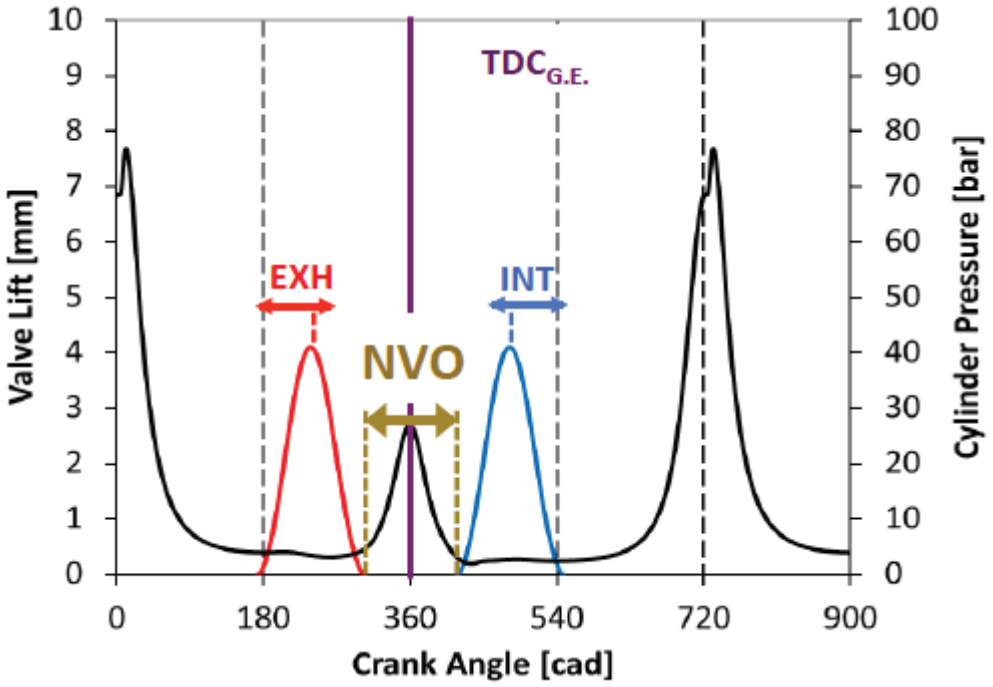

Figure 2.2 Valve profiles and cylinder pressure trace for recompression (NVO) valve strategy

2.1.3 Fuel System

Fuel is injected directly into the cylinder with a Bosch solenoid-actuated 8-hole fuel injector, which is centrally mounted between intake and exhaust valves and adjacent to the spark plug. The fuel delivery pressure is held constant at 100 bar by means of a bladder-type accumulator that is pressurized with gaseous nitrogen from a gas cylinder equipped with a two-stage pressure regulator. Fuel flow rate is measured with a piston-type positive displacement flow meter. Although the system is capable of multiple injections, only one injection per cycle is performed. End of injection timing is fixed at 330 cad b TDC$_f$for all experiments to allow for enough time for fuel evaporation, mixing and homogenization of the fuel-air-mixture to occur. The fuel used for all experiments is a 87-octane research-grade gasoline and its properties are listed in Table 2.3.

2.1.4 Upgrade for Boosting Capability

At the beginning of this research, the air handling system was upgraded substantially to allow for boosted engine operation and to be able to simulate a turbo-/super-charger. The objectives of the redesign process were to conceive a highly flexible system capable of

Table 2.3 Fuel specifications

Parameter	Value	Unit
Research octane number (RON)	91.1	-
Motor octane number (MON)	83.0	-
Anti-knock index (R+M)/2	87.1	-
Aromatics	26.1	vol. %
Olefins	8.6	vol. %
Saturates	65.3	vol. %
Carbon	86.37	wt. %
Hydrogen	13.63	wt. %
Oxygen	0.0	wt. %
H/C atomic ratio	1.8803	-
Stoichiometric air-fuel ratio	14.52	-
Lower heating value	43.129	MJ/kg
Density	0.74	g/ml
Reid vapor pressure	62.5	kPa

Table 2.4 Air handling system design requirements

Parameter	Value	Unit
Intake temperature	40-200	°C
Intake pressure	1-3	bar_{abs}
Exhaust pressure	1-5	bar_{abs}
External EGR	0-50	%
Air mass flow	4-50	g/s

independent control of intake pressure, temperature and composition, a system with reduced runner wave dynamics accounting for higher mass flow rates during boosted operation and a high level of safety. A key constraint of the design of the air system was to accommodate a potential misfire through combustion of raw fuel in the exhaust runner or plenum and still be able to contain it. Table 2.4 shows important design requirements of the system during normal operation. The redesign and upgrade of the engine for boosted operation was a real team effort. Bumbalough described the different stages of the process in more detail[110].

The following key components were added to the system or significantly modified as part of the upgrade:

- Thermal air mass flow meter

- Intake air heater
- Intercooler
- Intake and exhaust plenums
- Heated blanket around intake plenum
- Intake and exhaust runners
- EGR heat-exchanger and EGR valve
- Heat tapes along sections of air/ EGR path
- Back-pressure valve

2.1.5 Air Handling System

Following the air path in shown in Figure 2.1 the key components are described in this paragraph. Compressed building shop air is filtered, dried and the incoming pressure is regulated down to attain the desired target intake pressure measured in the intake runner. An array of critical flow orifices and a thermal mass flow meter (Fox Instruments FT2) are used to measure the air mass flow rate into the engine. A 12 kW electrical heater (Farnham HT-200) is used to preheat the incoming air and exhaust gas (eEGR) from the EGR loop. The air-eEGR mixture then passes through an intercooler, which is a liquid-to-liquid shell-type heat exchanger supplied by Ford. In case an intake temperature slightly lower than test cell ambiance is required, this intercooler cooled with city-water can be used. Alternatively, the intercooler can be bypassed.

The intake and exhaust plenum are large pressure vessels to allow for decreased wave dynamics in the intake and exhaust runner. Each plenum has a volume that is 75 times the size of the engine displacement volume i.e. 42 Liters. The were designed to be able to withstand combustion of a stoichiometric mixture at typical exhaust gas temperatures, and due to the requirements that were made of stainless steal. Each plenum has a two-stage safety mechanism to vent off pressure buildup. The intake plenum is wrapped with a well-insulating 5 kW heated blanket that was custom-made to fit the plenum. When the plenum pressure reaches a value of 1 bar above the design value, a blow-off valve opens to release excess pressure. In the event of an explosion, a large rupture disk allows for fast pressure discharge.

Intake and exhaust runner are cast and made of stainless steel. They were designed

short and with large cross-sectional area to minimize pressure oscillations due to runner wave dynamics. The exhaust or back-pressure of the engine is adjusted by manipulating the position of an electrically actuated globe valve (Koei Industries Nucom-Z). A similar globe valve is used in the EGR line for adjusting the EGR rate. Typically, the EGR rate is fine-tuned by slight modification of the back-pressure with respect to the intake pressure. The temperature of the EGR heat-exchanger is kept at engine coolant temperature level of 90 °C. All piping downstream of the intake air heater until the intake plenum and the entire EGR loop from the exhaust plenum to where it joins the intake air path has been wrapped with electric resistant type heat tape. The wall temperature of the piping is kept constant at 60 °C through PID bench-top temperature controllers. This is done to prevent the heated air exiting the intake air heater from cooling down by the time it reaches the engine intake, and also to prevent condensation of water and exhaust species when operating the engine with eEGR.

2.1.6 Optimizing Thermal Response for Full Control over Intake Conditions

Full independent control over intake conditions including pressure, temperature and composition was crucial, and the upgrade of the air handling system for boosting capability imperative to perform the required experiments in this dissertation. As a result of the upgrade of the air handling systems, and as described as in section 2.1.4, several components with high mass and thermal inertia were added. It was found that the heat up of the system was very slow initially and prevented the intake runner gas temperature from reaching 200 °C within reasonable time. As potential reasons for the slow thermal response of the intake plenum and runner, several points were considered.

- Long piping between air intake heater and plenum
- Air intake heater only on for short periods of time
- Significant temperature drop from intake plenum to runner

The intake air heater originally was mounted approximately 10 feet upstream in the air path with respect to the intake plenum and runner and the long piping section in between was not insulated or wrapped with heat tapes. The long distance between air intake heater and plenum was problematic but also partially needed for two reasons. First, an intercooler had to be positioned in between air intake heater and plenum, and second, it was not desirable to

have the eEGR flow pass through the air intake heater, because of long-term deposition of soot potentially impairing the effectiveness of the heater, and also because the hot electric heating wires may alter the chemical composition of eEGR through potential reactions of eEGR constituents. Due to the nature of the Teflon-based threat sealant used in the piping, the heater gas exit temperature had to be limited to about 250°C due keep the system leak-free. This in turn meant that the heater would not operate at its full potential, as it can tolerate exit temperatures of 650 °C and operate at higher mass flow rates. Lastly, and maybe most importantly, a significant temperature drop along the air flow path between air intake heater and plenum as well as plenum and runner could be observed resulting in system warm-up times of several hours to attain 200 degrees C intake runner gas temperature.

In the following, based on the observations made and measurements taken during the warm-up experiments, it was deemed necessary to re-evaluate the intake side of the air handling system and identify causes and remedies to this problem of exceedingly slow thermal response and not being able to attain and control target intake runner gas temperature to the extent needed. A one-dimensional finite-difference model, discretizing along the flow direction in the air path system and capturing gas and metal wall temperature of the piping, was created using basic heat transfer and energy conservation expressions. After tuning a few adjustable parameters, the wall and gas temperature profile evolution could be generated that was in nice agreement with the experimental measurements during warm-up. The results have shown that the large thermal masses of piping lead to large amounts of heat losses to the ambiance via natural convection, and that the large diameter of the plenum induces a low Reynolds number flow, which does not have a great heat transfer coefficient. In other words, it is difficult and ineffective to heat up air in the intake plenum due to the low heat transfer coefficient, however, because it is so bulky, including the relatively large diameter piping section between plenum and runner, it still allows for enough heat loss if the walls are not kept at the same temperature as the gas flowing through the pipes and plenum.

Based on the results of the simulations and lessons learned, several key modifications to the air handling system were made. First, it is imperative to keep all pipe wall temperatures at the desired intake runner gas temperature, which requires use of electric resistant-type heat tapes and appropriately thick heavy-duty fiberglass pipe insulation on all piping sections downstream of the air intake heater and including eEGR loop. The large diameter section downstream of the intake plenum was fitted with a custom-made heated blanket manufactured by the same company as the intake plenum heated blanket. Second, to increase the effectiveness of the air intake heater, the heater was moved closer to the air-eEGR-mixing junction so that its distance to the intake plenum could be decreased from 10 to 6 feet. Third, also to increase the effectiveness of the air intake heater, the pipe sealant used throughout

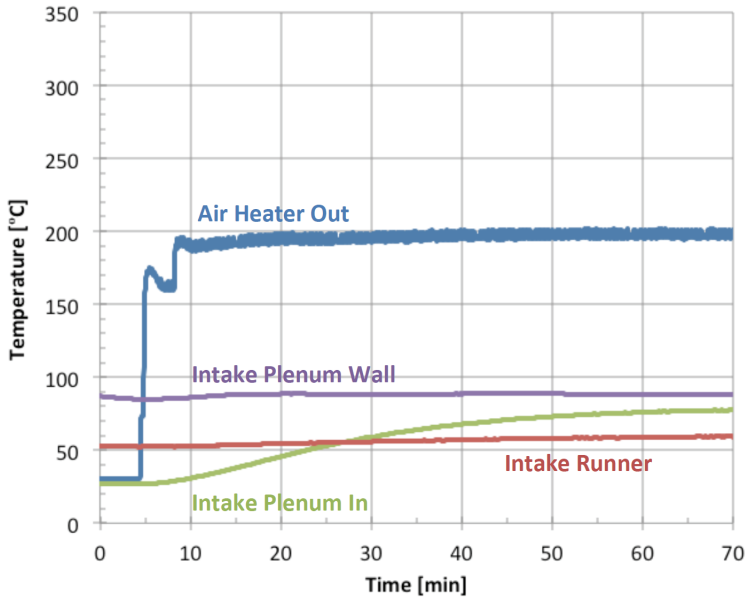

Figure 2.3 Temperature profile evolution (before making modifications)

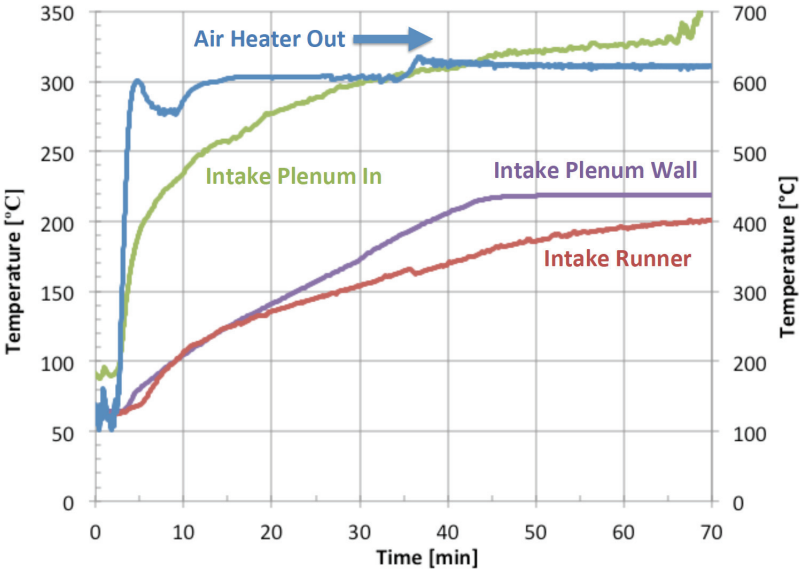

Figure 2.4 Temperature profile evolution (after making modifications)

the intake portion of the air handling system was replaced by a high-temperature-type that allowed leverage of the maximum allowed heater exit gas temperature of 650 °C, improving its duty cycle and practical use.

Figures 2.3 and 2.4 show the warm-up temperature traces before and after making the aforementioned modifications to the system. It is clear, that in the end, the adjustments performed were successful yielding a dramatically shorter warm-up time i.e. only requiring

40 minutes to reach 200 °C and much better controllability of the intake runner air temperature via the air intake heater for fine-tuning. It was also found that the air intake heater now actively aids heating up the massive intake plenum allowing it to reach its desired temperature faster than it would if heating by itself.

Based on the experience made working on the boosting upgrade of this single-cylinder research engine, for similar applications in the future, it can be recommended to have the main air heater as close as possible to the intake plenum. Ideally it may be located inside the plenum or even downstream of it. Alternatively, an auxiliary heater between intake plenum and runner would enhance controllability of the intake air temperature even more. The potential concern about conversion of unburned HC species or soot deposition in the heater could be accommodated by using a slightly different style of heater that does not require extremely hot electric wires, but using one that works more indirectly e.g. heating up a fin-type surface made of highly conductive material inside the plenum.

2.1.7 Engine Control and Data Acquisition

Engine Control

The engine controller was implemented using National Instruments hardware and a digital output module provided by Drivven Inc. in addition to other input and output modules supplied by National Instruments. The Drivven module was accompanied by a piece of software that was used to implement the engine controller software within National Instruments LabView. The in-house developed engine controller program allows for control over spark dwell, spark timing, fuel injection timing and duration. Spark is only used to start up the engine and to transition into HCCI mode upon which the spark is turned off. The spark plug is fired by a MoTeC M DEN-580 inductive smart coil. Injection timing is kept constant with end of injection (EOI) fixed at 330 cad b TDC_f for all experiments. The engine controller sends a 5 V pulse signal to a Bosch injector driver module. Andruskiewicz documented these and other features of the experimental setup prior to the upgrade in detail [111].

Low Speed Data Acquisition

The low-speed data acquisition (LS DAQ) system is based on National Instruments hardware and LabView software. The latter was used to develop a versatile LS DAQ environment that allows tracking of all important time-based signals. These signals include temperatures such as coolant, oil and gas temperatures, various flow rates and other analog signals. Platinum based class A resistance temperature detectors (RTD) are used for measuring intake gas temperatures due to their high level of accuracy. For measurements

of exhaust gas, coolant and oil temperatures, K-type thermocouples are used and deemed sufficient.

High Speed Data Acquisition

For each data point recorded, the cylinder pressure is sampled at 0.1 cad resolution for 200 consecutive cycles using a Kistler model 6125A piezo-electric pressure transducer. The cylinder pressure transducer is installed between intake and exhaust valves close to where the pent-roof transitions into the wall and it is protected from direct exposure with the hot combustion chamber gases with a perforated flame shield. The flame shield improves the thermal characteristics of the sensor and allows for higher quality measurements [112].

Due to the nature of the measurement, which is a dynamic measurement of pressure versus time, it needs to be referenced or pegged once per cycle to obtain an absolute value. A piezo-resistive absolute pressure sensor (Kistler model 4007B) mounted close to the intake port in the intake runner is used for pegging. Due to the dynamic nature of intake pressure, the pressure value is averaged over a +/- 5 cad window 10 cad before intake valve closing (IVC) for each cycle, because at this location mass flow into the cylinder is minimal and intake and cylinder pressure should be in equilibrium. The exhaust pressure is measured with a dynamic piezo-resistive pressure sensor (Kistler 4045A) located in the exhaust runner. This sensor is mounted in a water-cooled switching adapter, which prevents it from over-exposure to high exhaust temperature over extended periods of time. All three pressure signals are recorded by an AVL high-speed combustion analysis system (Indiset 642). An AVL crank angle encoder model 365C is used for synchronization with the engine crankshaft during operation.

2.1.8 Emissions Sampling

A Bosch LA4 wide-ranger oxygen sensor mounted in the exhaust runner is used primarily to determine and monitor the fuel-to-air equivalence ratio. Exhaust constituents are measured with a Horiba MEXA 7500-DEGR emissions analysis system. Exhaust gases are sampled from the center of the exhaust plenum through a perforated tube and transferred to the individual emission analyzers after passing through various heated filters and lines. The individual analyzers and their operating principle are outlined in the following paragraphs.

The emissions analysis system comprises two combined CO/ CO_2 analyzers, one for measuring both constituents in the exhaust stream, and one for measuring CO_2 exclusively in the intake runner to determine EGR rate, which is defined as the ratio of intake and exhaust runner volumetric CO_2 fractions. Both constituents, CO and CO_2 , absorb significant amounts of energy of light in the infra-red spectrum due to their molecular structure. This

Table 2.5 Emissions analyzers and measuring principle

Exhaust constituent	Analyzer operating principle
CO/ CO_2	non-dispersive infra-red (NDIR)
THC	flame ionization detector (FID)
O_2	para-magnetic
NO_X	chemiluminescence

feature is used by the non-dispersive infra-red (NDIR) analyzer, which infers the gas concentration by relating the amount of absorption in a chamber with the test gas to the amount absorbed by a reference gas in another chamber. THC emissions are measured with a flame ionization (FID) detector. The FID detects ions generated through combustion of organic molecules in a hydrogen flame. The response factor of the FID is closely related to the number of carbon atoms in the THC molecule. Both CO and THC are important exhaust species in HCCI exhaust because they determine the engine combustion efficiency.

Significant amounts of NO_X emissions usually are only produced when peak cylinder temperatures are above 1900 K. This is the case for high load naturally aspirated HCCI operation, but typically much less problematic during boosted operation because of increased dilution levels i.e. lower fuel-to-charge equivalence ratio. The chemiluminescence analyzer used to measure NO_X utilizes ozone to oxidize NO to NO_2 upon which light is released, whose intensity correlates to the NO concentration. Any NO_2 in the exhaust is internally catalytically converted to NO prior to passing through the ozone stage, so that both NO and NO_2 commonly referred to as NO_X are measured. Lastly, O_2 is measured with a para-magnetic analyzer that takes advantage of the fact that O_2 has a much higher magnetic susceptibility than most other gases. Table 2.5 summarizes the operating principle for each analyzer.

Fuel-to-air equivalence ratio or lambda is calculated from emissions as well using Brettschneider's equation [113].

2.2 Heat Release Analysis

2.2.1 Overview

To understand how the combustion process is affected by engine operating and control parameters, it is necessary to carry out heat release analysis of the experimentally measured cylinder pressure data. Important outputs of the heat release analysis that facilitate analysis

and evaluation of combustion include heat release profile, mass fraction burned (MFB), and average in-cylinder gas temperature. This section describes the methods used in the in-house heat release analysis tool developed by Ortiz-Soto and how it was implemented and used to analyze experimental data in this work [114, 115].

2.2.2 First Law Approach

The first Law of Thermodynamics is implemented in the heat release tool to calculate the heat release profile [116], where the gross chemical heat release rate ($dQ_{hr,ch}/dt$) is given by:

$$\frac{dQ_{hr,ch}}{dt} = mc_v\frac{dT}{dt} + P\frac{dV}{dt} + \dot{Q}_{wall} \tag{2.1}$$

In (2.1), m, c_v, T, are estimated mass, constant volume specific heat and mean bulk gas temperature respectively, P is the measured and processed cylinder pressure and V is the instantaneous cylinder volume calculated from the engine geometry using the crank-slider equation. $dQ_{hr,ch}/dt$ equals the net apparent heat release rate ($dQ_{hr,net}/dt$) plus losses through wall heat transfer ($\dot{Q}_{wall}$). The first and second term on the right hand side in (2.1) are the change in sensible internal energy and piston work respectively.

The burned mass fraction x_b is calculated by normalizing $dQ_{hr,ch}/dt$ with respect to the the cumulative value of it between start and end of combustion, where start and end of combustion are defined as the crank angle location where the minimum and maximum in $dQ_{hr,ch}/dt$ occur respectively. The rate of heat release (RoHR) is obtained by numerical differentiation of the cumulative gross heat release $Q_{hr,ch}$ with respect to crank angle.

The mean bulk gas temperature, T, is required to estimate thermodynamic properties for heat release calculation and is computed from the ideal gas state equation:

$$T = \frac{PV}{mR} \tag{2.2}$$

In (2.2), P and V are the instantaneous cylinder pressure and volume respectively, while m is the total trapped mass. The specific gas constant, R, depends on the mean composition of the charge in-cylinder and varies throughout the combustion process as reactants are undergo combustion and form products. R is a function of average in-cylinder composition that undergoes changes during combustion process as reactants go to products. Due to the interdependence of T, R and x_b, the heat release analysis needs to follow an iterative solving process to determine mixture properties. In-cylinder composition and mass estimation are further discussed in sections 2.2.5 and 2.2.6 respectively.

2.2.3 Cylinder Pressure Filtering and Pegging

Although great care is taken in acquiring the high-speed crank-angle resolved cylinder pressure measurements, there can be noise in the signal and this can represent a problem, in particular, because numerical derivatives are computed to obtain ROHR for example. Therefore, it is necessary and common practice to filter the cylinder pressure data to eliminate undesirable, mostly high frequency, noise. The heat release tool employed uses a second-order Butterworth digital low pass filter. A cut-off frequency value of 2.5 kHz was chosen for all data sets in this research, because it offers the right trade-off between smoothing the heat release traces while still keeping important combustion features.

Cylinder pressure is measured on a relative basis using a piezo-electric pressure transducer, hence accurate referencing or pegging of the cylinder pressure is critical. Pegging relies on the instantaneous pressure referencing to an absolute sensor in either intake or exhaust runner close to the port. For this work, a Kistler 4007B piezo-resistive absolute pressure sensor mounted in the intake runner close to the intake port was used. Pegging occurs shortly before IVC when the intake valves are still open but already closing and flow into the cylinder is low, so that in-cylinder and intake runner pressure are approximately in equilibrium. Since IVC changes depending on the amount of NVO commanded, pegging location is fixed relative to IVC and always occurs 10 cad before IVC, where an averaging window of +/- 5 cad is used. The pressure offset value is then applied to the whole in-cylinder pressure trace, which is shifted accordingly. This is done for each individual one out of the total of 200 recorded cycles for each data point. Since the combined linearity and hysteresis errors of the intake sensor are less than 0.3% , significant error in pressure offset due to the method may be larger than the intrinsic measuring device error.

2.2.4 Average vs. Cyclic Analysis

All experiments in this thesis were done under steady-state conditions and 200 consecutive cycles of cylinder pressure data were recorded to obtain statistically significant results.

Instead of averaging all individual cyclic pressure traces and then processing the ensemble average pressure trace, the heat release analysis tool performs heat release analysis of the filtered pressure trace of each individual of all 200 cycles. Averaging for output quantities, if desired, is done afterwards. The benefit of this method is that the ensemble average pressure trace may not be an accurate representation of the actual combustion behavior, especially when operating the engine near the combustion variability limit as was done for results in chapters 3 and 5. For example, having one early fast burning cycle with

early CA50 and high pressure rise rate and having a few cycles burning more slowly with later CA50 and lower pressure rise rate, the ensemble average pressure trace would smear out the characteristics of all cycles but in particular the early fast burning one.

Therefore, for all data documented in this thesis, cylinder pressure, average bulk gas temperature, rate of heat release and mass fraction burned curves have been averaged from the processed 200 cycles. Quantities like CA50, ringing intensity, peak temperature etc. were all calculated on a cyclic basis and then averaged over all 200 cycles.

2.2.5 Mixture Properties Estimation

Proper treatment of gas properties is crucial for obtaining reasonable estimates of trapped masses. temperature and heat release profile. (2.1) can be written in a slightly different form using the ideal gas law [116]:

$$\frac{dQ_{hr,ch}}{dt} = \frac{\gamma}{\gamma-1}P\frac{dV}{dt} + \frac{1}{\gamma-1}V\frac{dP}{dt} + \dot{Q}_{wall} \tag{2.3}$$

From (2.3) it becomes apparent that the ratio of specific heats, γ, is a key parameter that is a function of temperature and composition itself. No matter if looking at c_v in (2.1) or γ in (2.3), thermodynamic properties enter the heat release calculation and the interdependence between them and temperature and burned mass fraction profile require iterative solving.

To determine mixture properties as a function of crank angle throughout the combustion process, complete conversion of reactants to complete combustion products (CO_2, H_2O, N_2, and O_2) is assumed. Ortiz-Soto has shown that this assumption gives results almost identical to a far more complex 15-species equilibrium model for lean and stoichiometric fuel-air mixtures [115]. The gas mixture properties routine used for estimation of γ is based on thermodynamic data from the JANAF tables and Burcat's database and includes an equilibrium model [117, 118]. It also allows for multi-component fuels including gasoline surrogates. Based on the molecular weight and atomic H/C ratio of the fuel, a gasoline surrogate can be created to match these values.

The mean gas composition is assumed to be a mixture of unburned and burned gases that are each weighted according to the corresponding mass fractions $1-x_b$ and x_b respectively. The instantaneous mass fraction of each individual species is given by (2.4),

$$Y^k = (1-x_b)\cdot Y_u^k + x_b \cdot Y_b^k \tag{2.4}$$

where Y^k is the mass fraction of the k^{th} species. The unburned species Y_u^k is a mixture of fresh reactants, with mass fraction $1-EGR$, determined from measured fuel-to-air

equivalence ratio Φ, and combustion products, with mass fraction EGR , determined from the estimated burned gas mass fraction (EGR), and its mass fraction is given by:

$$Y_u^k = (1 - EGR) \cdot Y_{reac}^k + EGR \cdot Y_{EGR}^k \tag{2.5}$$

The composition of the EGR mixture (Y_{EGR}^k) in (2.5) is assumed to be composed of complete combustion products (Y_{prod}^k) and fresh reactants (Y_{react}^k) weighted by the cycle combustion efficiency (η_{comb}):

$$Y_{EGR}^k = (1 - \eta_{comb}) \cdot Y_{reac}^k + \eta_{comb} \cdot Y_{prod}^k \tag{2.6}$$

Although the assumption of conversion to complete combustion products does account for the individual species measured by the emissions analysis system, the error in the estimated mixture properties as a result of that is considered minor and negligible.

2.2.6 Residual Mass Estimation

Accurate estimation of the trapped in-cylinder mass is critical when calculating quantities such as mean in-cylinder gas temperature, mixture properties and overall energy balance. The total mass trapped in-cylinder at IVC comprising fuel, air, external EGR (eEGR) and internal EGR (iEGR) is given by

$$m_{tot} = m_{fuel} + m_{air} + m_{eEGR} + m_{iEGR} \tag{2.7}$$

where m_{fuel} is the mass of injected fuel, m_{air} is the mass of inducted fresh air, m_{eEGR} is the mass of external EGR introduced through the EGR loop with the intake flow and m_{iEGR} is the mass of internally trapped EGR or residual retained from the previous cycle.

Redundant methods to measure the air flow rate and to computer the air-fuel ratio are used in this engine setup. The fuel mass flow is directly metered and the air mass flow is metered independently using two measuring devices, namely a calorific flow meter and a set of critical flow orifices. From one of the two air flow and the fuel flow measurements, the air-fuel ratio can be calculated directly. Alternatively, by employing either the fuel or the air mass flow measurement in conjunction with a measurement of the air-fuel ratio, the other quantity can be computed as well. There are two air-fuel ratio measuring systems in place, first, the emissions analysis system, and second, the Bosch LA4 wide-range oxygen sensor. In case of the emissions analysis system, emission measurements in conjunction with atomic balances of oxygen and carbon are used to compute the air-fuel ratio [119].

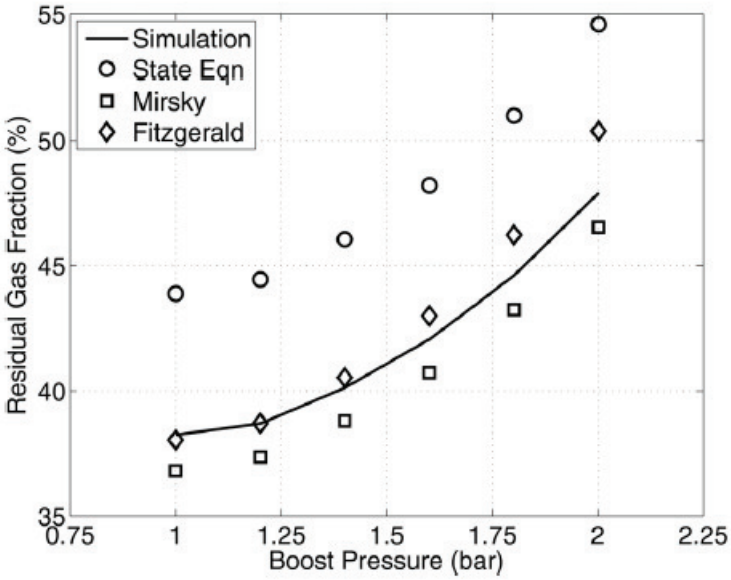

Figure 2.5 Evaluation of three different RGF estimation methods at boosted conditions [114]

Brettschenider's formula also falls in this category, but it incorporates different elements to be balanced and can be considered more robust [113].

Although generally there is good agreement between the different measurement techniques for fuel flow, air flow and air-fuel ratio, due to the higher accuracy the fuel mass flow rate in conjunction with the measured air-fuel ratio from the emissions using Brettschneider's formula is used throughout this thesis. The volumetric fraction of external EGR (eEGR) in the intake runner is obtained from CO_2measurements in the intake and exhaust runner. The eEGR mass is computed from volumetric fraction of EGR in the intake runner and the total incoming mass flow.

One of the major uncertainties in the trapped mass calculation arises from the residual mass estimation (iEGR), and this can be especially problematic for combustion modes that employ large amounts of NVO. In HCCI combustion, the internal EGR or residual gas fraction (RGF) can be as high as 45 % of the total in-cylinder mass. In this work, the RGF estimation method developed by Yun and Mirsky [120] was used because of its robustness and consistency of results even under boosted operating conditions when compared to other methods. Other methods that are also implemented in the heat release tool include the State Equation method [114] and the method by Fitzgerald et al. [121].

In this heat release analysis method of residual gas fraction (RGF) estimation developed by Yun and Mirsky is used, [120]. Although there are other method e.g. State equation method and Fitzgerald method [121, 122], Yun and Mirsky method is chosen, because it

provides more consistent results especially when a intake boost pressure sweep. Ortiz-Soto compared various method and found that Yun and Mirsky shows most consistent agreement with 1-D-GT Power gas dynamics calculations [114]. Ortiz-Soto et al. compared various RGF estimation methods with one-dimensional GT Power gas dynamic simulation results [114], and concluded that the method by Yun and Mirsky yields most consistent results, especially when intake boost pressure is varied as can be seen in Figure 2.5. The State Equation method is the simplest method but over-predicts RGF significantly, while the Fitzgerald method is the most complex one and delivers very good agreement at naturally aspirated conditions but lacks consistency as it increasingly over-predicts RGF for higher boost pressures.

The method by Yun and Mirsky falls in between the other two methods in terms of complexity, but it stands out because of very consistent results with changing boost pressure. The method according to Yun and Mirsky assumes that the combustion products remaining in the cylinder undergo an isentropic process during the exhaust period. models an isentropic blow-down process at EVO:

$$m_{iEGR} = m_{EVC} = m_{EVO}(\frac{V_{EVC}}{V_{EVO}})(\frac{P_{EVC}}{P_{EVO}})^{\frac{1}{\gamma}} \tag{2.8}$$

Note that the mass at EVO, m_{EVO}, equals the total mass, m_{tot}, whereas the mass at EVC, m_{EVC}, equals the iEGR mass, m_{iEGR}. In equation (2.8), the mean of the ratio of specific heats, γ, is estimated by taking the average temperatures at EVO and EVC, which are obtained by applying the Ideal gas Law at EVO and EVC:

$$T_{EVO} = \frac{P_{EVO}V_{EVO}}{m_{EVO}R} \tag{2.9}$$

$$T_{EVC} = \frac{P_{EVC}V_{EVC}}{m_{EVC}R} \tag{2.10}$$

It is clear that besides the assumption and measurement errors, the only approximation made is for γ. The fact that equation (2.8) includes ratios of pressures and volumes makes it intuitively comprehensible that the method is robust for measurement errors, as those would directionally cancel each other out. This can be seen in Figure 2.6.

Once the mass at EVC, m_{iEGR}, has been computed, the internal residual gas fraction (RGF) or iEGR and total EGR fraction (internal + external) can be determined. The total EGR fraction is calculated as:

$$EGR = \frac{m_{iEGR} + m_{eEGR}}{m_{tot}} \tag{2.11}$$

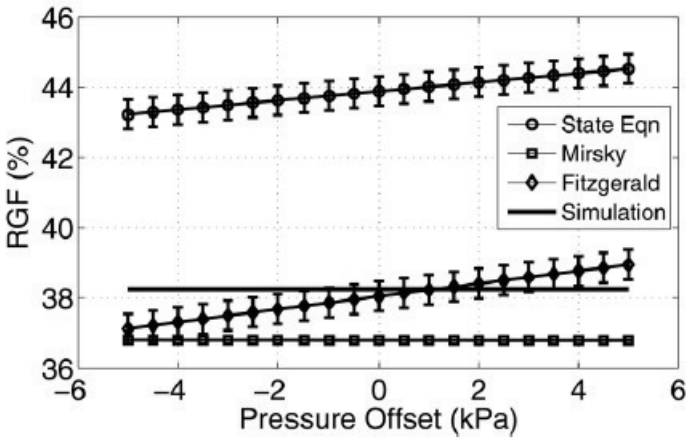

Figure 2.6 Sensitivity analysis of RGF estimation methods

2.2.7 Combustion Efficiency

The tailpipe combustion efficiency is computed from exhaust emission measurements using the equations presented by Stivender [119]. Comparing HCCI engine experiments and cycle simulations employing a re-breathing strategy, Chang found that the steady state burned fuel mass was always higher in the simulation than what the experimental measurements suggested, and consequently proposed a correction based on the total EGR fraction[123]. The total amount of burned, $m_{fuel,burned}$, from an in-cylinder analysis is given by:

$$m_{fuel,burned} = [m_{fuel} + (1 - \eta_{comb,cyl}) \cdot m_{fuel} \cdot EGR] \cdot \eta_{comb,cyl} \tag{2.12}$$

In (2.12), the first term represents the fuel directly injected into the cylinder, while the second term in square parentheses represents the unburned portion of the fuel re-introduced through EGR accounting for both iEGR and eEGR. The total amount of burned fuel, $m_{fuel,burned}$, also equals the amount of fuel injected multiplied by the combustion efficiency based on tailpipe emission measurements, $\eta_{comb,exh}$:

$$m_{fuel,burned} = m_{fuel} \cdot \eta_{comb,exh} \tag{2.13}$$

Equating (2.12) and (2.13) and solving for the in-cylinder combustion efficiency, $\eta_{comb,cyl}$, yields

$$\eta_{comb,cyl} = \frac{(EGR+1) - \sqrt{(EGR+1)^2 - 4 \cdot EGR \cdot \eta_{comb,exh}}}{2 \cdot EGR} \tag{2.14}$$

where $\eta_{comb,cyl}$ is always lower than $\eta_{comb,exh}$ due to the fact that some of the fuel

mass in-cylinder does not burn to completion and is re-inducted to be burned again in the next cycle. Introducing the total mass of fuel, $m_{fuel,tot}$, being the sum of the mass of fuel injected, m_{fuel}, and the mass of unburned fuel retained from residual, $m_{fuel,res}$, the following relationship can be derived clarifying the previously stated notion that $\eta_{comb,cyl}$ is lower than $\eta_{comb,exh}$:

$$(m_{fuel} + m_{fuel,res}) \cdot \eta_{comb,cyl} = m_{fuel} \cdot \eta_{comb,exh} \tag{2.15}$$

2.2.8 Heat Transfer Estimation

Calculating the gross heat release from the cylinder pressure data requires the wall heat transfer loss to be estimated over the heat release analysis range. Since the wall heat transfer loss is typically not measured in engine experiments and temperature distribution may be spatially non-homogeneous, global heat transfer correlations are used. The total wall heat transfer loss is the sum of the individual contributions from the cylinder head, liner and piston:

$$\dot{Q}_{wall} = \sum h \cdot A_i \cdot (T - T_i) \tag{2.16}$$

The subscript in equation (2.16) denotes the various combustion chamber boundary regions. While the head area, A_{head}, and the piston area, A_{pist}, are constant for a given engine geometry, the liner area, A_{liner}, is computed using the crank-slider expression. The wall temperatures for each region, T_i, are all prescribed as constant 450 K for all experiments in this thesis, because no wall temperature measurement has been performed. The mean bulk gas temperature T is calculated on a crank-angle basis throughout the cycle.

The global convective heat transfer coefficient, h (W/m^2), is a function of the instantaneous pressure, temperature, cylinder volume, and operating conditions. Most global heat transfer correlations found in the literature are originally derived from the Reynolds Analogy and are functions of temperature, pressure and mean piston speed as well as some length scale. The heat transfer correlation used in this work is based on the commonly used Woschni correlation [124]

$$h = 3.26 \cdot B^{-0.2} \cdot P^{0.8} \cdot T^{-0.55} \cdot w^{0.8} \tag{2.17}$$

where $B(m)$ is the engine bore, $P(kPa)$ is the cylinder pressure, $T(K)$ is the mean bulk gas temperature, and $w(m/s)$ is the characteristic gas velocity calculated from the following

expression:

$$w = C_1 \cdot \bar{S}_P + C_2 \cdot (\frac{T_r}{P_r V_r}) \cdot (P - P_{mot}) \tag{2.18}$$

The characteristic gas velocity is proportional to the mean piston speed, $\bar{S}_P(m/s)$, and a pressure velocity given by the difference between firing and motoring pressure (P_{mot}) scaled by the displacement volume, $V_d(m^3)$, and the temperature (T_r), pressure (P_r) and volume (V_r) at some referencer condition e.g. intake valve closing (IVC). The first term on the right hand side in (2.18) affects the in-cylinder flow motion, whereas the second term on the right hand side is a flame enhancement term accounting for heat transfer enhancements due to flame-induced convection [124]. As suggested by Woschni, the constants used in (2.18) are $C_1 = 2.28$ and $C_2 = 3.24 \times 10^{-3}$ for the closed portion of the cycle [124].

As first suggested by Chang et al. [125], the traditional Woschni correlation was slightly modified, due to the absence of a propagating flame in a purely auto-igniting homogeneous fuel-air mixture, in that the flame enhancement term in (2.18) is decreased by a factor of $1/6$. Chang et al. found that this adjustment was necessary to be able to match the experimentally measured heat fluxes in a HCCI engine [125]. Using this modified Woschni correlation yields the smallest error regarding energy closure (below 3 %) of the total heat released, confirming its appropriateness for HCCI combustion.

Beside the standard Woschni and modified Woschni correlation, there are other heat transfer correlations available that were considered as well [126, 124, 127, 128, 125]. The applicability of various correlations to advanced combustion modes including HCCI has been the subject of numerous studies [129, 130, 131]. Without having instantaneous heat flux and temperature measurements available or new correlations specifically developed for the conditions, the existing models with the adjustment described is the best option available.

2.3 Combustion Constraints

2.3.1 Overview

The multi-mode combustion diagram (MMCD) developed by Lavoie et al. is a good conceptual representation of different combustion modes, including HCCI, and the boundaries associated with each combustion mode, graphically shown in terms of the burned gas temperature as a function of the unburned gas temperature near TDC [132]. It

is based on a modeling study, using iso-octane and air mixture, and assumes an adiabatic compression from IVC to TDC. The unburned temperature at end of compression depends on the compression ratio and mixture properties at IVC, including pressure, temperature and composition. The fuel-to-charge ratio, ϕ', is given by

$$\phi' = \frac{\frac{F}{A+R}}{(\frac{F}{A})_{st}} = \frac{\phi \cdot (1 - RGF)}{1 + RGF \cdot \phi \cdot (\frac{F}{A})_{st}} \approx \phi \cdot (1 - RGF) \tag{2.19}$$

where F, A, and R are the masses of fuel, air and residual respectively. ϕ is the fuel-to-air ratio, *st* refers to stoichiometric mixture and RGF is the sum of iEGR and eEGR. ϕ' is a measure of the specific energy content of the charge and correlates well with $IMEP_g$. If ϕ equals to 1, ϕ' is a measure of the amount of dilution with EGR, where a lower value of ϕ' corresponds to a more EGR-dilute mixture. For a purely air-dilute case, ϕ' equals ϕ. T_b is calculated from T_u and ϕ' using the assumption of adiabatic combustion and invoking constant pressure equilibrium calculations with a TDC pressure equal to 40 bar.

The lines for auto-ignition, that is for early phased HCCI combustion, corresponding to the ringing limit, and for late phased HCCI, corresponding to the combustion variability limit, are derived employing the ignition delay expression by He et al. and using a 10 cad combustion phasing interval near TDC [108]. In case of naturally aspirated HCCI combustion, unburned temperatures usually are around 1000 K near the ringing and combustion variability limits, but they may be slightly lower for boosted conditions.

Figure 2.7 shows various combustion regimes and it can be seen how the HCCI region is bounded by the knock and combustion variability limit allowing only a narrow window of unburned temperatures. It also becomes apparent that the allowable window in terms of burned gas temperature is constrained as well, namely by the bulk gas quenching limit for low T_b and excessive NO_Xemissions for high T_b. The following sub-sections 2.3.2 through 2.3.2 discuss the various boundaries limiting HCCI operation and the metrics that are used to quantitatively characterize each of them.

2.3.2 Knock Limit: Ringing Intensity

There are different methods to characterize and metrics to quantify knock, and here in this work two methods originally proposed by Eng [66] and later independently validated by Vavra et al. [68] are used. Eng showed a good correlation for HCCI between a high pass method derived from fundamental acoustic equations and a low pass method based on an empirical correlation [66]. Vavra studied the applicability of various knock detection methods for different combustion modes and concluded that the two methods proposed by

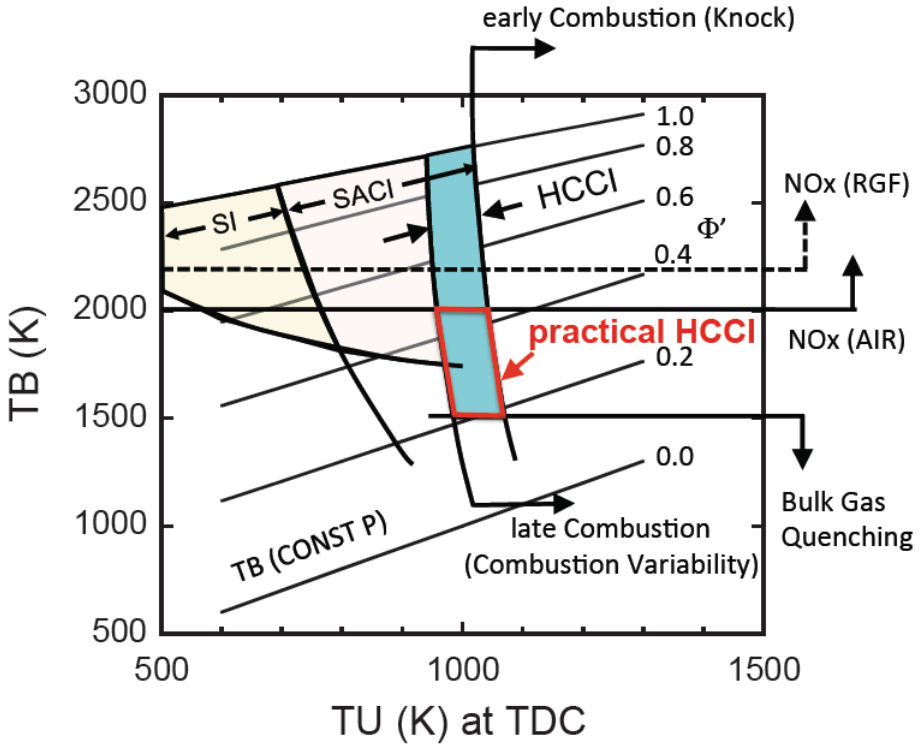

Figure 2.7 Multi-mode combustion diagram [132]

Eng yield good agreement for HCCI combustion [68]. These methods are described in the following:

According to Eng [66], the excitation of the engine structure is due to the first waves of pressure oscillations and proportional to the acoustic intensity of these waves, which can be expressed as

$$I = \frac{1}{2\gamma} \cdot \frac{[\Delta P]^2}{P} \cdot \sqrt{\gamma R T_{max}} \tag{2.20}$$

where γ is the ratio of specific heats, ΔP is the pressure fluctuation amplitude, P is the pressure, R is the gas constant, and T is the temperature. Eng termed this quantity ringing intensity, but in this work the term high-pass ringing intensity suggested by Vavra et al. is adopted, because a high-pass filter is applied on the measured pressure trace as input. For every cycle a Butterworth second order Butterworth filter with cut-off frequency of 2.5 kHz is applied to the raw pressure trace. The maximum peak-to-peak amptitude of the filtered pressure trace, $_{max}$, is used in equation (2.20). Moreover, the peak cylinder pressure, P_{max}, and the peak temperature, T_{max}, are substituted into equation (2.20) to yield the high-pass

ringing intensity RI_{HP}:

$$RI_{HP} = \frac{1}{2\gamma} \cdot \frac{[\Delta P_{max}]^2}{P_{max}} \cdot \sqrt{\gamma R T_{max}} \tag{2.21}$$

Eng suggested another widely accepted metric to quantify HCCI knock based on a low-pass filtered pressure trace that shows very good agreement with the high-pass method. He calls this metric based on an empirical correlation ringing index, but in this work it is referred to as low-pass ringing intensity. The low pass ringing intensity is given as

$$RI_{LP} = \frac{1}{2\gamma} \cdot \frac{[0.05 \cdot (\frac{dP}{dt})_{max}]^2}{P_{max}} \cdot \sqrt{\gamma R T_{max}} \tag{2.22}$$

where $(dP/dt)_{max}$ and $_{max}$ are the maximum rate of pressure rise and peak pressure respectively. β is a correlation coefficient, which has a fixed value for a given engine geometry. Eng suggests a value of $\beta = 0.05\ ms$ for light-duty HCCI engines to be used. The main advantage of equation (2.22) over equation (2.21) is that it can be easily used to quantify HCCI knock in a simulation, which usually does not capture any high frequency pressure oscillations.

A third method to evaluate HCCI knock in this work, applied to a sub-set of the experimental data used in this work, is the combustion noise as measured with an AVL 450 combustion noise meter. The combustion noise measurement is a simple filtering technique developed for the measurement of the noise radiated by engine surfaces in response to combustion excitation [133]. This technique was especially important and used when the compression ignition direct injection (CIDI) technology was implemented into passenger vehicles in the 1980s. A fast Fourier transformation (FFT) is applied to the cylinder pressure signal followed by two filters in series, first, a U-filter that emulates the attenuation by the engine mass, and second, an A-filter that emulates the noise reception by the human ear. The root mean square (RMS) value is calculated and the result is scaled and reported in decibels [134].

For these experiments a RI_{LP} = 5.0 MW/m^2 is considered limit. This is what is implemented in HS DAQ and monitored during experimental runs.

2.3.3 Combustion Variability Limit: COV of $IMEP_g$

Section 2.2.4 already eluded to the importance of processing each cycle of the ensemble individually and to average the results instead of processing an averaged pressure trace with the heat release analysis. Although HCCI combustion near optimal combustion phasing is

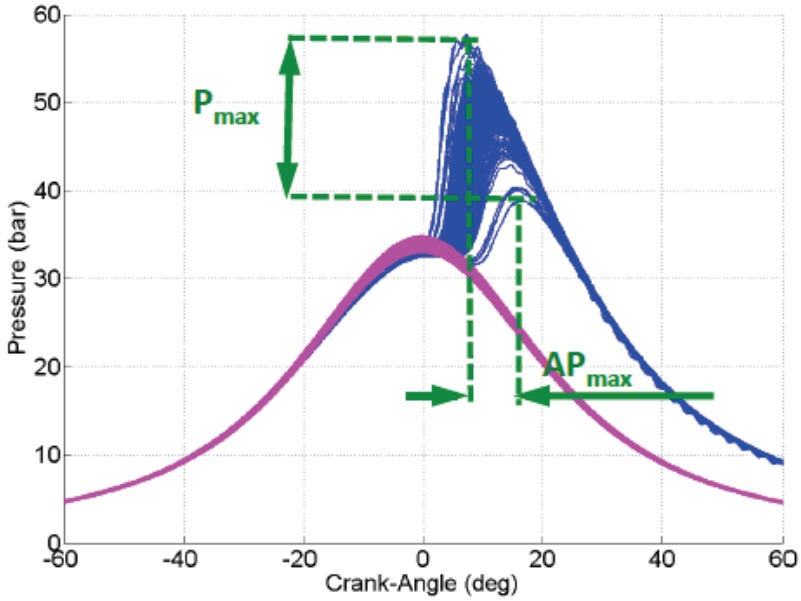

Figure 2.8 Operation near combustion variability limit

a very stable combustion mode exhibiting relatively less cyclic variability [74], it is still important to consider all cycles and account for the statistics, especially for operation near the combustion variability limit.

Figure 2.8 shows an example of a HCCI data point collected near the combustion variability limit, and it is clear that the spread in peak pressure, its location and other parameters that are dependent on the actual pressure trace will vary dramatically. Since HCCI operation in a NVO engine relies on retention of significant amounts of hot residual (iEGR), there is a naturally tendency to exacerbate bi-modal unstable behavior near the stability limit. This is because a cycle with late combustion phasing and partial misfire, hence a large amount of the unburned fuel fraction left is retained and added to the fuel injected in the next cycle, which leads to a relatively rich mixture and early combustion phasing in the next cycle. Hellstrom et al. pointed out to this behavior and noticed a strong link through unburned fuel and residual temperature that is propagated and affect the following cycle [75].

In this work, combustion variability is quantified using the coefficient of variance (COV) of IMEPg over 200 consecutive cycles. A value of 3-5 % is considered typical of HCCI operation near the combustion variability limit, whereas values above are usually not feasible, because engine operation would not be possible for an extended period of time due to heavy

knock and finally misfire.

$$COV_{IMEP_g} = \frac{\sigma_{IMEP_g}}{\mu_{IMEP_g}} \tag{2.23}$$

2.3.4 Emissions: Peak in-Cylinder Temperature

As can be seen from Figure 2.7 in section 2.3.1, the HCCI operating region that is accessible in practical terms is bound by excessive NO_X emissions and bulk gas quenching at the top (high T_b) and bottom (low T_b) respectively. These limits arise from the maximum burned gas temperature during combustion. On the one hand, if T_b exceeds 1900-2000 K in a purely air-dilute case without RGF, the threshold for significant NO_X formation is trespassed. The threshold may shift to somewhat higher T_b depending on the amount of RGF in the mixture. On the other hand, if T_b is below 1400-1500 K, bulk gas quenching can occur, that is combustion does not complete throughout the chamber and, in particular, reactants in regions closer to the cooler walls may not fully convert. In either case, the burned gas temperature, at which this occurs, is directly related to ϕ', as it is the ratio of fuel-to-charge that mainly dictates how much heat is liberated during combustion leading to a certain temperature rise, hence burned gas temperature. From Figure 2.7, it is clear that a range of $\phi' = 0.2 - 0.45$ seems permissible.

Aceves et al. found that as a result of too low temperature, first, CO may not convert to CO_2, and then, even fuel may not be broken down further into intermediate combustion products, which results in a gradual transition from the wall to the core with unburned fuels, intermediate combustion products, then CO and finally complete combustion products prevailing [135]. This is shown in Figure 2.9, and note that as ϕ decreases these regions, where high CO and THC prevail, extend further into the bulk. A value of $\phi = 0.2$ can be seen as a threshold, beyond which excessive CO and THC emissions result.

The practical NO_X limit for lean HCCI operation, to comply with US passenger car emissions regulations, is EI_{NO_x} = 1 g/kg fuel [29, 132]. Although there are de-NO_X aftertreatment devices available that work under lean conditions, their use entails additional cost and requires extra hardware that needs to be packaged, hence this option is not considered and the EI_{NO_x} = 1 g/kg constraint used for this work. For CO and THC emissions, no sharp limit is imposed in this work, because a conventional oxidation catalyst can almost achieve 100 % conversion efficiency, provided exhaust gas temperatures are above 200 °C and it is lit up. Excessive CO and THC emissions lead to low combustion efficiency, which is undesirable as it compromises the overall performance and benefits of HCCI operation.

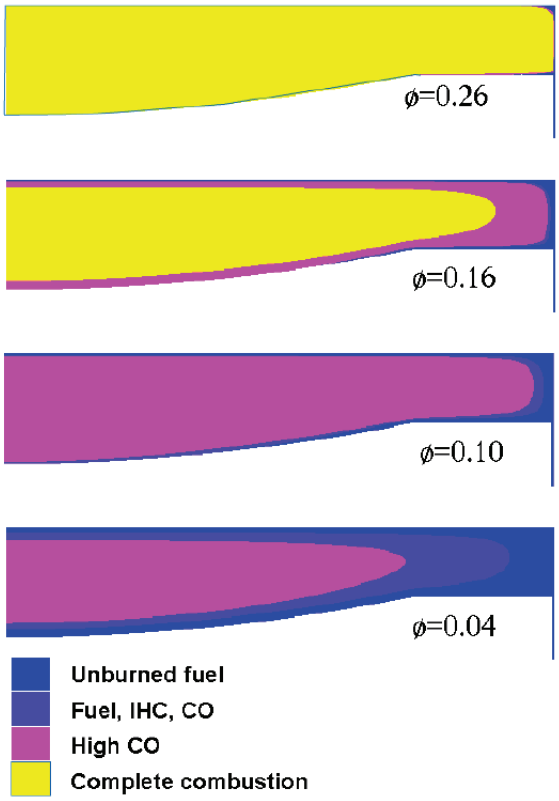

Figure 2.9 Geometrical distribution of masses [135]

2.4 1-D Engine Simulation Approach

2.4.1 GT Power Model

GT Power is part of the commercial software package GT Suite distributed by Gamma Technologies, Inc., which is an engine cycle simulation tool capable of steady-state and transient simulations [136]. An object-oriented code design makes building of models easy. The software tool allows managing of object libraries as well as editing and executing them. It has a powerful post-processing tool built in and is well suited for analysis of powertrain systems. GT Power benefits from a user-friendly graphical user interface and offers a good compromise between high fidelity results and reasonable computational cost. That being said, GT Power inherently runs much faster than any 3-D CFD software without loosing much information as far as the breathing process of the engine is concerned, hence it can be deemed sufficient for a vast number of modeling studies.

The simulation is based on one-dimensional (1-D) gas dynamics, representing fluid flow, mechanical and heat transfer processes through pipes, valves, ports, cylinders and

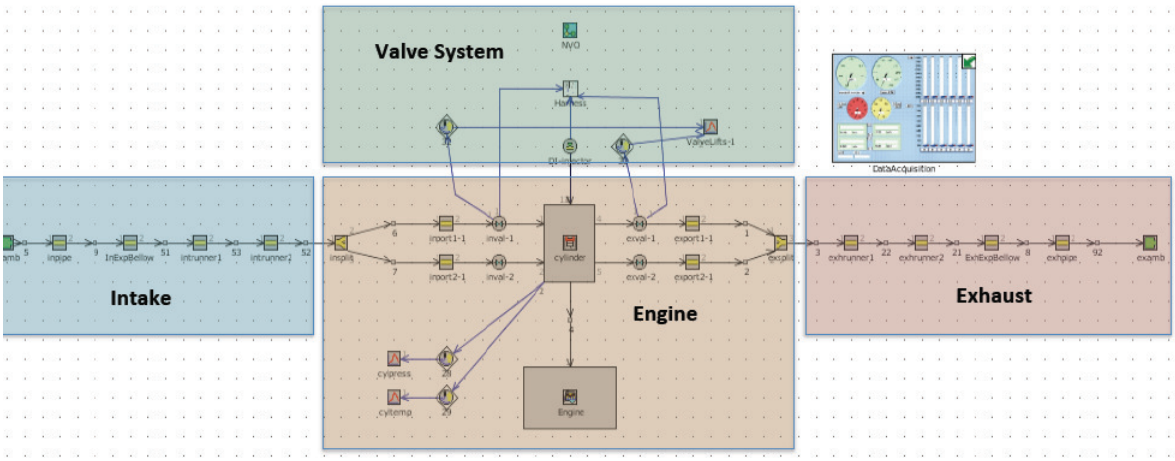

Figure 2.10 Boosted engine model in GT Power

other components of engine systems such as turbochargers and intercoolers that can be represented as sub-models. The Fortran based solver solves 1-D conservation equations for mass, momentum and energy to predict the flow rates in the intake and exhaust system. In-cylinder modeling of combustion, pressure, heat transfer and work to cylinders is modeled as well using appropriate thermodynamic equations. Orifices, valves and flow contractions are modeled by imposing laws prescribing flow losses or specifying discharge coefficients.

The single-cylinder model used in this research is from Mamalis [137] and has been modified with respect to a few aspects. First, careful measurements of intake and exhaust systems have been taken from the experimental setup in the laboratory exactly replicating diameters and lengths of individual elements. Second, intake system wall temperatures were imposed to eliminate any need to deal with uncertainty of modeling heat transfer in the intake section. Wall temperatures of the entire intake section and the incoming gas temperature in the model were all set equal to the experimentally measured gas temperature in the intake runner. Similarly, a generic parameter is imposed for the temperature of the head, liner and piston (see section 2.4.3). Third, the proper level of discretization for the individual elements has been verified. For GT Power to provide reasonable results, it is important to follow instructions for choosing right spatial and temporal discretization. In addition to the engine geometry information in Table 2.1, General Motors also provided, more detailed geometric information about valves and ports, which are listed in Table 2.6. Figure 2.10 shows the actual model used for this work with the different sections highlighted in colors.

Table 2.6 Cylinder head geometry

Parameter	Value	Unit
Intake flow split	38.0	cm^3
Intake port length	56.0	mm
Intake port diameter	30.6	mm
Intake valve diameter	35.5	mm
Exhaust valve diameter	30.0	mm
Exhaust port diameter	23.6	mm
Exhaust port length	50.0	mm
Exhaust flow split	14.0	cm^3

2.4.2 Wiebe Burn Profiles

A significant modification to the original single-cylinder model of the boosted HCCI engine, as received from Mamalis, was to use a non-predictive combustion model to replace the predictive burn model implemented. The previous burn model was based on a correlation, which had been developed at the University of Michigan [138] and used in numerous works to follow [48, 97, 30, 137]. Moving from a predictive to a non-predictive model allows to more specifically isolate thermodynamic and breathing-related effects, because combustion known from experimental measurements.

A simple single-stage Wiebe burn profile was chosen and imposed with the goal of matching the center of combustion, CA50, and burn duration, CA10-90, determined from experimental measurements and post-processing using the heat release tool described in section 2.2. The Wiebe function in its most general form is defined as [139]

$$x_b = 1 - \exp\left[-a\left(\frac{\theta - \theta_0}{\Delta\theta}\right)^{(m+1)}\right] \tag{2.24}$$

where θ_0 is the crank angle at the start of combustion (CA00), and m is an adjustable parameter that fixes the shape of the burn profile, also referred to as Wiebe exponent. Equation (2.24) is a very generic expression that is it contains two adjustable constants that determine combustion duration, $\Delta\theta$ and a. CA10-90 was imposed for combustion duration $\Delta\theta$, but other values could, in principle, be used as well. Substituting values for the specific burn fractions, $x_b = 0.1$ and $x_b = 0.9$ for CA10 (θ_{10}) and CA90 (θ_{90}) respectively, in (2.24) and using $\Delta\theta = \Delta\theta_{10-90} = \theta_{90} - \theta_{10}$, yields:

$$a = a_{10-90} = \left[\left\{ln\left(\frac{1}{1-0.9}\right)\right\}^{1/(m+1)} - \left\{ln\left(\frac{1}{1-0.1}\right)\right\}^{1/(m+1)}\right]^{m+1} \tag{2.25}$$

At this point, the start of combustion still shows up as the anchor location for the Wiebe function. Since θ_0 is hard to discern from experimental rate of heat release traces, it is more convenient to use the center of combustion CA50 (θ_{50}) instead. Therefore, substituting appropriate values for the specific burn fraction, $x_b = 0.5$ for CA50 (θ_{50}), in (2.24) and rearranging yields the following expression for θ_0:

$$\theta_0 = \theta_{50} - \Delta\theta_{10-90} \cdot (\frac{ln(2)}{a})^{1/(m+1)} \tag{2.26}$$

Now substituting both (2.25) and (2.26) into equation (2.24) results in a form of the Wiebe function that allows to compute the mass fraction burned, x_b, as a function of CA50 and CA10-90, two commonly used and easily measurable metrics, and the Wiebe exponent, m, as a parameter. GT Power is very flexible and already set up to accept the input parameters in this way. A Wiebe exponent of $m = 2$ was used for all GT Power studies conducted and results presented in chapter 3.

2.4.3 Heat Transfer

Heat transfer is implemented in this GT Power model via a user sub-routine that exactly uses the equations and expressions outlined in section 2.2.8. Note that a multiplier of $1/6$ is applied during the closed portions of the cycle, including compression and expansion as well as the recompression part of the cycle. During the open portions of the cycle this multiplier is set back to 1, since the conventional Woschni heat transfer correlation is well suited to capture heat transfer during the gas exchange process.

In contrast to the processing of the experimental data in section 2.2 not a fixed wall temperature of 450 K was chosen, but instead a wall temperature as a function of engine load and speed, was used for the GT Power simulation study. Although the effect is minor, it gives a little more accuracy as the GT Power simulation is applied for a maximum load sweep covering a wide range of boost pressures and engine loads. The idea is that wall temperature increases as engine load and heat dissipated in the engine increase. The following correlations (from General Motors), generated by fitting experimentally measured wall temperature data over a range of conditions i.e. different fueling rates at 2000 rpm, was used for head and piston wall temperatures

$$T_{head} = 3.21 \cdot m_{fuel} + 376.3 \tag{2.27}$$

$$T_{piston} = 4.91 \cdot m_{fuel} + 374.8 \tag{2.28}$$

where m_{fuel} is the fueling rate in mg/cycle and the temperatures are in K. Note that, since there has not been any correlation available, the liner temperature was set equal to the head temperature.

2.5 Error and Uncertainty Analysis

2.5.1 Overview

Experimental data is inherently subject to uncertainty, which can be related to measurement errors and varying conditions. Measurement errors can be divided into two components: random error and systematic error. While random error can be minimized by using appropriate and carefully calibrated measurement instruments, systematic errors are difficult to identify and remedy. Variability of the experiment itself or the environment may affect measurements over time e.g. a day of engine testing, and can be best addressed by following strict and careful test procedures.

Random error is always present in a measurement and a result of inherently unpredictable fluctuations in the readings of an instrument or interpretation of the instrument reading. It appears as discrepancy in results of the same repeated measurement. This error can be decreased by using accurate measuring instruments that are properly calibrated and conditioned for the measuring purpose. If experimental and ambient conditions are stable, repeating the experimental condition, taking multiple measurements, and then averaging them, can help decrease the uncertainty and quantify unavoidable fluctuations inherent to the instrument or measuring process.

Systematic error or bias error refers to the presence of bias in a measurement, which means that there is a consistent offset between the actual experimental value to be measured and the measurement of it. Sources for systematic errors are imperfect calibration of measuring instruments, changes in the environment that interfere with the measurement process, or incorrect methods of observation and incorrect assumptions. Systematic error cannot be discovered through repeated measurements and decreased by taking multiple measurements followed by averaging, because it is not random.

Variability of conditions over time, be it the measurement itself, a process affecting the measuring device or the environment interacting with the measurement, is sometimes unavoidable, so at best, steps to minimize this can be taken and the remaining variability can be characterized and quantified through repeated sanity checks and repeatability measurements. In this thesis, an effort has been made to ensure repeatable conditions

both during the course of a measurement sweep in a day and also in between measurements taken on different days. Specific baseline conditions before and after conducting experiments have been done frequently and regularly.

This sub-chapter deals with measurement uncertainty of the experimental data itself, uncertainty related to the heat release tool used for post-processing, and the simulation tool, GT Power, used in this thesis. Section 2.5.2 addresses inaccuracies inherent to various key measurement devices, section 2.5.3 deals with the propagation of systematic errors through the heat release analysis tool and identifies sensitivities of various important output quantities to potential bias error in input quantities, and section 2.5.4 summarizes the observed variability of the engine setup based on multiple baseline points taken in consecutive days that were analyzed. Finally, section 2.5.5 addresses systematic or bias error associated with the simulation tool and modeling incorporated in it.

2.5.2 Measurement Instrument Errors

The focus in this section lies on measurement instrument and method uncertainty, hence a slightly different view and division of uncertainty than what was presented in section 2.5.1, dividing measurement error into a random and systematic component, seems more appropriate. The overall uncertainty is considered composed of instrument uncertainty, measurement variation, and condition variation. This section deals with the first two components, instrument uncertainty and measurement variation, whereas the third component is what what was referred to as variability or repeatability before, and addressed separately in section 2.5.4.

Instrument uncertainty is the capability of an instrument including its measuring principle to accurately measure a physical phenomenon. It is fundamental to measurement device and can only be minimized by appropriate selection of the measurement method and instrument. Measurement variation is the variation of recorded values across a test, and can be viewed as a measure of relative stability of the test system and operating conditions. Unless noted otherwise, measurement uncertainty is presented at 95 % confidence interval representing two standard deviations ($\pm 2\sigma$) of measurement variation in this work.

The overall uncertainty of a given result is the combination of measurement uncertainty and instrument uncertainty. By using of the root mean square (RMS) method, these two separate uncertainties can be combined into one overall uncertainty [140] as

$$U_x = \sqrt{\sum_{i=1}^{n} (e_x)^2} \tag{2.29}$$

where U_x is overall combined uncertainty and e_x is the elemental uncertainty.

Some reported parameters, in particular emissions, air-fuel-ratio etc. are calculated using several individual measurements, where each measurements has its own unique uncertainty. The uncertainty of the final end parameter is computed using sequential perturbation. With the sequential perturbation method, the uncertainty of each measurement is calculated and then combined using the RMS method. The following equation shows how to determine the uncertainty of a calculated parameter F as a function of other measured parameters $a_1 \ldots a_n$ [140]:

$$U = \sqrt{\sum_{i=1}^{n} \left(\frac{|F(a_i+u_i)-F(a_i)| + |F(a_i-u_i)-F(a_i)|}{2}\right)^2} \tag{2.30}$$

In equation (2.30), F is a function of measured parameters, $F = F(a_1, a_2, \ldots a_n$, U is the overall uncertainty of the function F, a_i are the measured parameter used in calculation of F, and u_i is the related total uncertainty of each parameter a_i.

Accurate cylinder pressure and intake pressure measurements are especially important, because they are very important inputs to the heat release analysis calculation. The individual uncertainties for each sensor are linearity (calibration uncertainty), thermal drift (variation in measurement accuracy due to thermal condition e.g. thermal shock) and hysteresis (non-linear behavior when pressure decreases after increasing). Note, that although the pressure transducers are very precisely manufactured devices, the full scale (F.S.) measuring range, especially of the cylinder pressure sensor, is very large, hence despite low values for linearity, the overall uncertainty can be relatively much bigger. Table 2.7 shows the individual uncertainties of the pressure transducers that are combined into an overall uncertainty using the RMS method.

The uncertainty of the individual gaseous emissions measurement is a combination of instrument uncertainty and measurement variation. Instrument uncertainty is the combination of uncertainties for a given analyzer: resolution, sensitivity (calibration uncertainty), repeatability (variation in measurement accuracy over one day/ test), and drift (day-to-day change in measurement accuracy). The overall uncertainty is the combination of the combined instrument uncertainty and uncertainty of span gas. The various individual uncertainties are combined using the RSS method to yield an overall instrument uncertainty (see Table 2.8).

Uncertainties of other low-speed measurements including combustion noise meter, temperature sensors, engine speed, fuel flow and air flow are listed in Table 2.9.

Table 2.7 Instrument uncertainty of pressure transducers

Sensor	Model	Linearity	Thermal drift	Hysteresis	F.S. range	Overall
-	-	%FS	%FS	%FS	bar	bar
Cylinder	6125A	0.4	1.0	n/a	0 - 250	1.62
Intake	4007B	0.2	1.0	0.5	0 - 5	0.05
Exhaust	4045A	0.3	1.0	n/a	0 - 5	0.05

Table 2.8 Instrument uncertainty of emissions analysis system

Species	Range	Res.	Sens.	Repeat.	Drift	F.S. range	Span gas	Overall
-	-	%FS	%FS	%FS	%FS	ppm	%FS	ppm
CO	low	1.0	1.0	0.5	1.0	5000	2.0	134.6
CO	high	1.0	1.0	0.5	1.0	20000	2.0	538.5
CO_2	-	1.0	1.0	0.5	1.0	150000	2.0	4038.9
O_2	-	2.0	1.0	0.5	1.0	150000	2.0	4802.3
THC_{C1}	low	1.0	1.0	0.5	1.0	1800	2.0	48.5
THC_{C1}	high	1.0	1.0	0.5	1.0	9000	2.0	242.3
NO_X	low	2.0	1.0	0.5	1.0	100	2.0	3.2
NO_X	high	2.0	1.0	0.5	1.0	2500	2.0	80.0

2.5.3 Sensitivity Study on Error Propagation Through Heat Release Analysis

Although great care was taken in choosing, setting up and calibrating measurement instruments, and conducting experiments under stable and repeatable conditions, all measurements still have a certain level of uncertainty associated with them as pointed out in section 2.5.2. The heat release tool explained in section 2.2 uses several experimental inputs and computes output parameters, which are important and used for analysis of combustion

Table 2.9 Instrument uncertainty of other variables measured from the engine

Measurement	Uncertainty	Unit
Combustion noise	1	dB
Thermocouple	2.2	K
RTD	0.8	K
Speed	5	rpm
Fuel flow	2.5	mg/s
Air flow	0.4	g/s

phenomena and drawing conclusion. The goal of this section is to evaluate how uncertainty in various input parameters to the heat release tool affect output results, which are used extensively for analysis purpose in chapters 3 through 5.

Ortiz-Soto assessed the heat release analysis tool used in this thesis against a series of closed-cycle high fidelity engine simulations for advanced combustion modes, including HCCI, using the KIVA-3V CFD code, and concluded that the standard heat release analysis could be extended with reasonable confidence to estimate quantities of interest in advanced combustion engines [141]. Knowing that processing input data with the heat release analysis tool involves several computations, which are highly non-linear by nature, and that input data naturally has some uncertainty, it is critical to understand and quantify how and to what extent potential errors in the input parameters affect heat release results. Ortiz-Soto also conducted an extensive sensitivity study of the heat release tool regarding the propagation of systematic errors from the input data [141]. In particular, he characterized how various important output parameters varied in absolute or relative terms in response to a given perturbation of a single input parameter. Key output parameters included maximum pressure, P_{max}, net IMEP, maximum rate of pressure rise, $(dP/d\theta)_{max}$, residual gas fraction, RGF, combustion phasing, CA50, burn duration, CA10-90, maximum peak temperature, T_{max}, ringing intensity, R.I., maximum rate of heat release, $RoHR_{max}$, etc.

One general and important criterion that allows to assess the overall confidence one can have in the results of the heat release analysis is the quality of energy closure. Significant errors in input parameters, measurements, assumptions or methods will directly affect the total chemical heat released, $Q_{hr,ch}$, computed at end of combustion (EOC). The energy balance is calculated from the ratio of the gross chemical heat release at EOC to the expected fuel energy released and given by

$$EnergyBalance = \frac{Q_{hr,ch}(EOC)}{\eta_{comb} \cdot m_{fuel} \cdot Q_{LHV}} \tag{2.31}$$

where η_{comb} is the in-cylinder combustion efficiency, m_{fuel} is the total amount of fuel in-cylinder and Q_{LHV} is the lower heating value of the fuel. For all data shown in this thesis, the energy balance ratio calculated with Equation (2.31) is always within ± 4 % of 1.0.

In the following, results of the sensitivity analysis is presented, first according to engine geometry and pre-conditioning, then according to system masses, combustion efficiency and heat transfer, and finally, according to analysis method chosen in the heat release tool, in this case energy closure.

Effect of Engine Geometry and Pre-Conditioning Parameters

Various engine geometry and pre-conditioning parameters including the compression

ratio (CR), thermodynamic loss angle, cylinder pressure reference and filter cut-off frequency affect the heat release analysis and output calculated from it. Although a nominal value of CR=12.4 is specified, this value is subject to uncertainty due to e.g. manufacturing tolerances, effective gasket thickness when assembled, and effective crevice volume. Although CR is a difficult parameter to measure, an effort was made to determine the actual TDC volume with oil metered from a burette, but even this process involves some uncertainty. A TDC offset parameter within the heat release code allows to account for uncertainty in the thermodynamic loss angle and crank angle encoder measurement. The low-pass filter cut-off frequency is another crucial parameter that can be adjusted.

CR varied by $\pm$ 0.25 from 12.4 has a large effect on burn duration, as CA10-90 increases 16 % % for CR = 12.4 + 0.25 and decreases 1 % % for CR = 12.4 - 0.25. The effect is asymmetric and the relative change is much larger for higher CR. The maximum rate of heat release, $RoHR_{max}$, decreases $\pm$ 2.25 % for CR = 12.4 + 0.25, but only increases $\pm$ 0.45 % for CR = 12.4 - 0.25. Moreover, a larger value of CR yields a more retarded start of combustion timing i.e. + 2.26 cad.

A TDC probe to quantify the actual thermodynamic loss angle has not been used. Beside uncertainty in the estimate of the thermodynamic loss angle, there could also be small slippage of the crank angle encoder potentially affecting the true crank angle measurement, although this is unlikely, as it was checked regularly before every experiment. Changing the TDC offset parameter by $\pm$ 0.2 cad yields a very noticeable change in the calculation of IMEP, which increases or decreases by 4.4 % for a $\pm$ 0.2 cad respectively.

There is some residual uncertainty with the method of cylinder pressure referencing and choosing the location for pegging assuming no flow and pressure drop between intake and cylinder at this crank angle. A change of $\pm$ 10 kPa has a rather large impact on RGF fraction estimation, which increase by 3.9 % for a + 10 kPa change and decreases by 4.1 % for a - 10 kPa change in reference pressure. This also has a significant effect on the in-cylinder temperature results. Note though, that Ortiz-Soto used the Fitzgerald and not the Yun and Mirsky method to determine RGF, where the latter is much less sensitive of incorrect pressure inputs as shown in 2.6, hence this particular uncertainty should be less of a concern for this work.

The filter cut-off frequency, varied by $\pm$ 1.5 kHz from 3.5 kHz, does not have a large effect on most results, however, all rate-based results are highly sensitive to it, especially if the cut-off frequency is lowered, in which case for example the maximum rate of heat release, $RoHR_{max}$, increases by 1.7 % for a frequency of 3.5 + 1.5 kHz and decreases 8.4 % for a frequency of 3.5 - 1.5 kHz respectively. Similar results are found for the maximum rate of pressure rise and the ringing intensity.

System Masses, Combustion Efficiency and Heat Transfer

Trapped in-cylinder masses are not measured, so models are used and simplifying assumptions made. In addition, limited accuracy of air and fuel mass flow measurements means that there is uncertainty in any estimate for mass trapped in-cylinder at IVC, and this applies to fuel, air and residual trapped. A $\pm$ 10 % variation is applied for each mass. For example, a $\pm$ 10 % change in RGF yields high sensitivities for the total trapped mass, which may increase by 5-6 %. This error is also reflected in the in-cylinder temperatures obtained, that rely on the total trapped mass estimate. A higher mass also encompasses a relative 80 % increase in CAS10-90 i.e. by 3-4 cad. CA50 is minimally affected, however, the shape of the burn curve is more sensitive especially at earlier and later crane angles due to a change in energy balance resulting from a change in mass, especially fuel mass. RoHR results are affected on the order of 7 - 9 %.

In-cylinder combustion efficiency is determined from exhaust emissions measurements are uncertainty in these measurements as well as in the fuel composition and property estimation used can affect combustion efficiency. The sensitivity analysis shows that a rather small effect, e.g. a $\pm$ 2 % in combustion efficiency only yields a corresponding $\pm$ 2 % change in in RoHR.

For the particular baseline condition used in this sensitivity analysis, heat transfer including wall temperature both only have a modes effect as a 40 % change in heat transfer did not encompass significant changes. Varying the wall temperature by $\pm$ 50 K shows minor sensitivity i.e. at most 1 %.

Analysis Method and Others

There are three different methods that the heat release tool can be run: analysis based on of mean cylinder pressure trace, analysis based on individual cycle (but properties are estimated and not computed for each cycle) and analysis based on individual cycle (and properties computed each cycle as well). Ortiz-Soto showed that there is very good agreement between both cyclic methods, but that the average method is not as accurate. For all data shown the third option is used.

Another potential uncertainty stems form the method of estimating mixture properties. The error in the method itself is considered small, when compared to the error introduced by uncertainty of not knowing the in-cylinder temperature, which is related to the RGF estimation.

Energy closure as described in earlier in this section and quantified as shown by (2.31) gives useful insight into the quality of the overall analysis. If the value deviates from 1.0, then that is an indication of certain errors or inadequacies. The heat release tool allows for energy closure to be forced on or off. In case energy closure if on, then heat transfer is multiplied

so that the overall energy balance yields a value of 1.0. This lumps all uncertainties into the heat transfer term. Under boosted conditions the actual energy release is noticeably larger than the expected heat release, which yields in multipliers smaller than 1.0 for the heat transfer to achieve energy closure. In the following, the results of energy closure turned on vs. kept off, and how it impacts important results is shown.

2.5.4 Variability in Measured Data

Even though great care was taken in setting up measurement instruments to minimize uncertainty, it is nearly impossible to eliminate all uncertainty and get true repeatability. Previous sections showed what these experimental instrument uncertainties are and how they propagate through the heat release analysis and manifest themselves in key output results. An alternative approach to dealing with residual uncertainty and variability is to quantify the amount of variability in various key parameters over the course of one or several days of testing by recording baseline conditions. This gives yet another perspective on how much the same nominal condition changes throughout the course of a typical experiment due to variability.

Most of the time, before beginning and after finishing an experiment, sometimes even in between, baseline conditions were recorded, which allowed to monitor the correct functioning of the engine and ensure full break-in and deposit conditioning. A fixed valve strategy with symmetric NVO of 140 cad, fixed intake and exhaust back-pressure (P_{int}=1.0 bar and P_{exh}=1.05 bar), and intake temperature (T_{int}=40 C) is used for the baseline condition. The peak motoring pressure for that baseline condition was monitored as an indicator that blow-by has not substantially changed. One standard deviation in peak motoring pressure recorded was recorded to be $\pm$ 1.2 % over more than 10 days spread out through 9 months of engine testing.

In this work, most experiments were performed over one day of testing to eliminate variation associated with day-to-day changes in ambient conditions, but it is still possible that conditions change during the course of one day of testing. For that reason baselined conditions were usually taken, both motored and fired, before and after each test. Table 2.10 shows the variability for the fired baseline condition over a few days including a total of 7 data points with 200 cycles each.

Table 2.10 Estimated variability in measured parameters of interest for baseline fired condition

Combustion parameter	Mean	Error (1σ)
$IMEP_g$ (kPa)	384	$\pm$0.7%
Peak pressure (bar)	41.8	$\pm$4.0%
Fueling rate (mg/s)	183.2	$\pm$0.5%
CA50 (cad aTDC)	7.0	$\pm$16%
CA10 (cad aTDC)	3.5	$\pm$18.5%
CA90 (cad aTDC)	13.4	$\pm$14%
Peak rate of heat release (J/cad)	54.2	$\pm$1.2%
Peak temperature (K)	1898	$\pm$1.9%
Exhaust temperature (°C)	347	$\pm$1.5%
Temperature at IVC (K)	512	$\pm$1.2%
EGR mass fraction (-)	0.42	$\pm$1.2%

2.5.5 Simulation Uncertainty

The 1-D engine simulation tool, GT Power, is devoid of random error and variability, and only accompanied by systematic errors. The sources of systematic error can be incomplete knowledge of the system and the physical processes that are modeled. For example, many processes in combustion engines are highly non-linear, which means that small uncertainty in input variables can be amplified largely.

GT Power has been specifically designed to model engine systems, in particular, to deal with the gas exchange process, combustion and heat transfer. To determine that gas exchange, it solves 1-D compressible flow equations [136]. In fact, GT Power solves conservation equations for mass, momentum and energy for every discretized element of the engine system using an explicit solver. Whereas GT Power is very good at modeling flow through various sections of smooth piping with gradual diameter changes, practical engine systems may have flow splits or junctions, discontinuous diameter changes and flow may pass through orifice restrictions, which needs to be modeled approximately. GT Power has been provided for to deal with that and has already several empirical expressions built in.

One specific example here that needs to be mentioned, because it directly related to and largely impacts the gas exchange process and determination of in-cylinder trapped masses, is the flow through the valves. Both the valve profiles and discharge coefficients given as function of valve lift are subject to some uncertainty, which unfortunately cannot be reported, because it has not been provided. However, it is very likely that General Motors RD obtained valve discharge coefficients from flow-bench measurements that are associated

with some experimental uncertainty. The cam lobes are manufactured to within a certain degree of accuracy to be within certain tolerance and is not necessarily identical to the nominal values. As a result, the overall uncertainty in determining the trapped mass and residual gas fraction (RGF) is approximated to be within $\pm$ 3.5 %.

Another specific example for modeling uncertainty is combustion, which is imposed based on the experimentally measured burn profiles using a simple single-stage Wiebe function. Replacing the predictive combustion model allows to remove uncertainty from not knowing combustion on the one hand, but on the other hand, the simple single-stage Wiebe function is only an approximation of the actual mass fraction burned profile from the experiment. In particular, matching CA10, CA50, CA90 and using a Wiebe exponent of 2.0 as was done for the matching, provided reasonable results from an efficiency point of view. However, using this approach, the peak pressure rise rates, hence ringing intensity values competed are not necessarily deemed accurate. In general, a certain error is introduced even for efficiency aspects, because of fitting the Wiebe curve through three points, which is not a perfect match of the experiment.

Again, as already mentioned in section 2.2.1, the heat transfer model used in the simulation is the identical to the one used for processing the experimental data with the heat release tool, i.e. standard Woschni but modified using a reduced multiplier of 1/6 for the pressure term, and is by itself subject to a high degree of uncertainty. This uncertainty stems from the fact that a global heat transfer coefficient is assumed, which does not account for spatial temperature variation in the gas but also of the wall. Locally, wall boundary layer may be quite different especially at higher boost pressures and depending on knock of engine, hence this should be kept in mind.

Lastly, there is room for interpretive errors that may occur when comparing experimental and modeling results, which is another potential uncertainty. The fact that experimental data and simulation results are close but could not be perfectly matched indicates that there is some unidentified systematic error in the model.

Chapter 3

Practical Limits of Boosted HCCI Operation in a NVO Engine

This chapter investigates various relevant operating parameters in a practical negative valve overlap (NVO) HCCI engine regarding their potential for high load extension through experiments, in which both the knock and combustion variability limits were simultaneously approached, while intake boost pressure and fueling rate, hence load, were gradually increased. In addition, a parametric modeling study is conducted to compare this engine to another well-known HCCI engine capable of even higher loads, and to identify specific parameters, that are different between the two engines, which are key enablers. This chapter summarizes the findings and sets the stage for further investigations.

3.1 Motivation

Based on the discussion in chapters 1 and 2, HCCI operation is limited by knock and combustion variability for advanced and late combustion phasing respectively, and these two limits merge toward the maximum load limit as fueling rate is increased, so that knock and combustion variability occur simultaneously. Knock is a result of rapid bulk gas auto-ignition causing by excessive pressure rise rates, and there has been consensus that knock characterized by ringing intensity is inversely related to burn duration (CA10-90). There have been different views evolved over time regarding HCCI combustion, in particular, understanding how and what drives the rapid combustion event. Whereas earlier studies by Najt and Foster [14] viewed HCCI combustion as a well-mixed reactor considering it to be mainly kinetically limited and proposed a global pseudo-kinetic expression to predict peak heat release rate, some more recent research has suggested that thermal and compositional spatial inhomogeneities are responsible for the progression of combustion [98, 142], which invokes the notion of a sequential auto-ignition cascade.

Since Christensen and Johansson demonstrated boosted HCCI operation for the first time[27], a lot of research has been done attempting to extend the maximum load limit of HCCI combustion using boost, most notably and recently, Dec and Yang demonstrated a maximum load beyond 16 bar IMEPg [29]. Many of the engine setups used in these research employ a conventional positive valve overlap (PVO) valve strategy [27, 29, 89, 90], which does not offer fast control and adjustment of combustion phasing within a few cycles, and are deemed impractical from the point of view of an original equipment manufacturer (OEM). Amongst those studies employing a more practical NVO engine, many either use a specific turbo charger or operate the engine without any exhaust back-pressure [44, 45, 46, 95]. Whereas, the former approach is most realistic, it does not allow independent investigation of the effect of the pressure differential (exhaust pressure greater than intake pressure) as a result of the turbo charger matching to the engine. The latter one allows more flexibility, in case a throttle in the exhaust stream is available, but specifically using this freedom to investigate the effect of pressure differential amongst others has not been done to date. Modeling studies by Mamalis et al. have shown that turbo charger matching is very important and needs to be accounted for in HCCI combustion due to the low exhaust gas enthalpy [48, 97].

The goal of this chapter is to explore the limits of a practical HCCI engine, boosted, and operated with negative valve overlap (NVO), and to understand how operating parameters such as eEGR addition, intake temperature, overall turbo-charger efficiency (OTE), and engine speed affect the maximum load limit. This can be realized taking advantage of the high degree of flexibility of the single-cylinder research engine used in this research. Engine hardware constraints such as limited cam phasing authority via NVO and maximum allowable peak cylinder pressure and their effects on the high load limit are also investigated. The experiments in this chapter seek to discern, whether or not changes in burn duration as a result from variation of operating parameters could facilitate the extension of the high load limit.

3.2 Experimental Investigation of Maximum Load Capability

3.2.1 Procedure

This experiment primarily focused on isolating the effects of eEGR addition, intake temperature, OTE and engine speed on the maximum load limit. Mapping the engine

Table 3.1 Experimental conditions during maximum load sweeps

Parameter	Value	Unit
Engine speed	2000	rpm
Fuel flow rate	11-32	mg/cycle
Fuel pressure	100	bar
Intake pressure	1.0-3.0	bar
Pressure differential (P_{exh}-P_{int})	0.5	bar
Intake charge temperature	90	°C
Negative valve overlap	74-110	cad
Coolant temperature	90	°C
Oil temperature	90	°C
Fuel injection timing	330	cad bTDC
External EGR	23-45	%

for all combinations of these parameters, that is varying combustion phasing for different fixed fueling rates for different fixed intake pressures, would represent too large a data set and be impractical. Moreover, since only the maximum load limit, that is constrained by knock and combustion variability limit simultaneously, is of interest, a more effective procedure was devised.

Starting under naturally aspirated conditions with ambient intake pressure, fueling rate is gradually increased and CA50 retarded, by decreasing NVO, until both knock limit (RI_{LP}=5 MW/m^2) and combustion variability limit (COV=3%) are simultaneously reached (see Figure 3.1). Once the maximum load limit is reached and operating conditions have stabilized (steady state), only one data point is recorded, which speeds up the process as the operating map can be traversed much more quickly compared to the full mapping approach. In this experiment, NVO still serves as independent control knob to adjust combustion phasing. This procedure is repeated, while intake pressure is increased in increments of 0.25 bar. The pressure differential is kept constant at 0.5 bar for all cases excluding the one, where overall turbocharger efficiency (OTE) is varied to investigate the effect of simulated OTE in section 3.2.4. Engine speed is held constant at 2000 rpm for all cases excluding the one, where engine speed is varied in section 3.2.5. This approach is much more effective than mapping the engine for all intake pressures and all possible combinations of other parameters. Table 3.1 shows experimental conditions for all experiments in this chapter. The following sections will look at the effect of one specific parameter at a time.

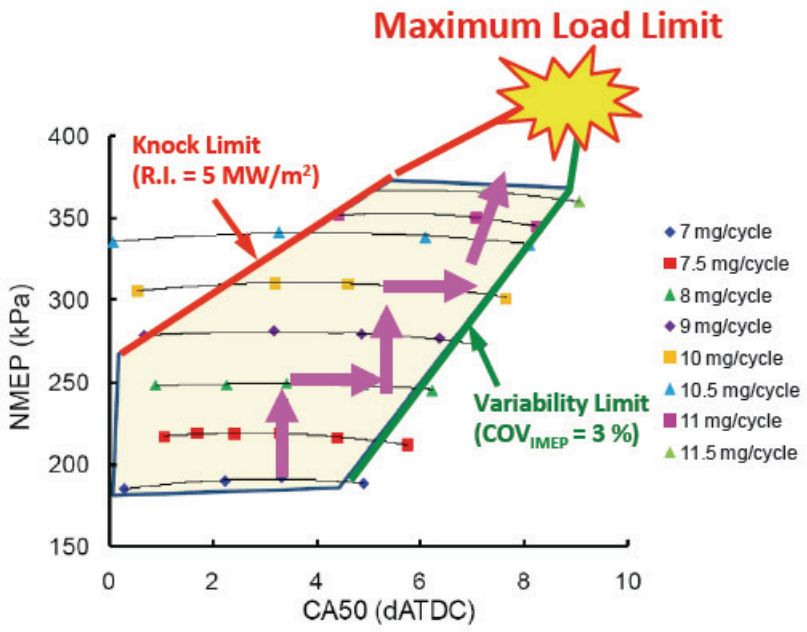

Figure 3.1 Experimental procedure for maximum load sweeps (adopted from [77])

3.2.2 Results: EGR Effect

In this section, the effect of the diluent on maximum attainable $IMEP_g$ as a function of P_{int} is considered. For that purpose, a case with external EGR (eEGR) addition is compared to a baseline case without eEGR addition. In both cases, internal EGR (iEGR) is present, because the UM NVO engine inherently traps a significant fraction of residual gas (RGF) or iEGR. The experimental procedure as described in section 3.1 is followed and the conditions listed in Table 3.1 are applied during the maximum load sweep experiments.

During both sweeps, intake charge temperature, T_{int}, is held constant at 90 °C, and NVO is used as adjustment knob for controlling combustion phasing (CA50), as can be seen in Figure 3.2. NVO decreases in both cases as P_{int} increases, and in particular, note that NVO for the case with eEGR addition is higher than the baseline case for a given P_{int}. As will be explained soon, this is related to the fact that for a similar or slightly more retarded CA50 with increasing P_{int}, a higher IVC temperature is required to maintain a certain ignition delay, which requires more hot iEGR to be trapped via a greater amount of NVO. EGR rate, measured as the ratio of CO_2 in the intake and exhaust runner, increases gradually for the eEGR addition case to keep the fuel-to-air equivalence ratio close to stoichiometry. In contrast, Φ decreases with increasing P_{int} in the case without eEGR, which indicates a leaning out the fuel-air mixture.

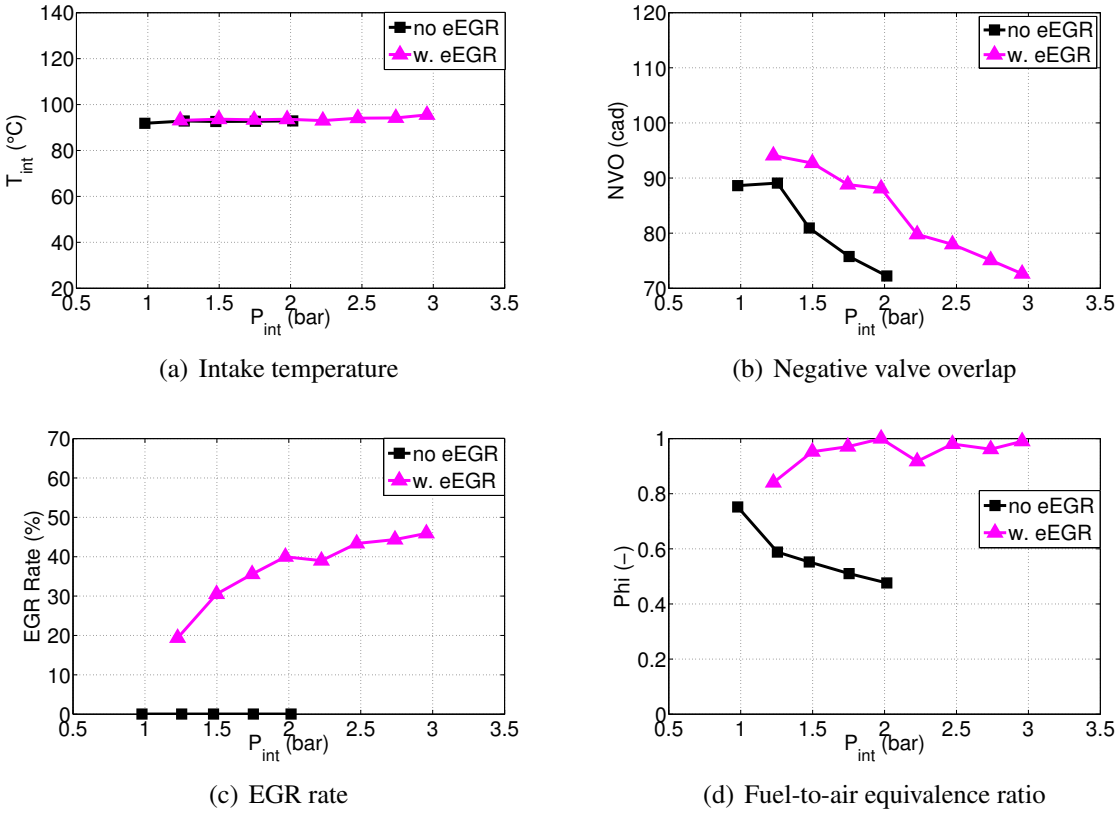

(a) Intake temperature

(b) Negative valve overlap

(c) EGR rate

(d) Fuel-to-air equivalence ratio

Figure 3.2 Boundary conditions as function of intake pressure during maximum load sweeps with different diluents

Adding eEGR to the intake air certainly is a high load enabler facilitating a relative increase in the maximum attainable $IMEP_g$ of 56 %. from 6.8 bar to 10.6 bar at a P_{int} of 2.0 bar and 3.0 bar respectively (see Figure 3.3). A secondary and much smaller benefit of eEGR addition is, that $IMEP_g$ increases on average by $\sim$ 3-4 % for a given P_{int} within the range of 1.25 bar to 2.0 bar. Figure 3.4 in conjunction with Figure 3.2 (b) can explain, why eEGR addition facilitates extension of the maximum load capability for this particular engine configuration. Note, that in either case, the UM NVO engine only allows a certain degree of cam phasing authority, namely a minimum value of NVO=74 cad. This engine hardware constraint together with the ignition delay expression shown in chapter 1.4.3 is what dictates the maximum load limit.

Through addition of eEGR, a portion of the incoming air is replaced by burned gas decreasing the in-cylinder oxygen concentration, χ_{O_2}, by $\sim$ 42 % from 17.3 % to 10 % and increasing the fuel-to-oxygen equivalence ratio, Φ_{FO}, by $\sim$ 95 % from 0.47 to 0.92 on average for the P_{int} considered respectively (see Figure 3.4). Whereas the former leads to a lengthening, the latter leads to a decrease of the ignition delay time. Based on the

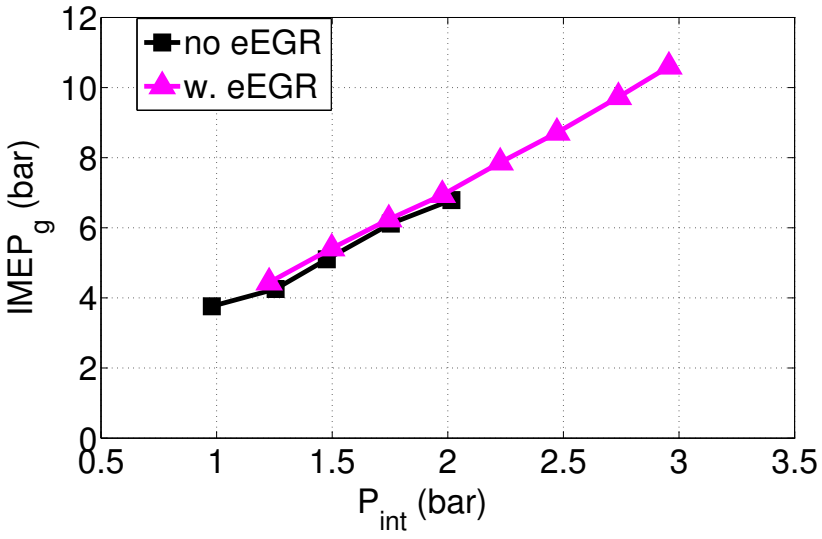

Figure 3.3 eEGR vs. air dilution: effect on maximum load limit

relative changes for each χ_{O_2} and Φ_{FO} and the fact that the χ_{O_2}-term in equation (1.4) has a higher sensitivity than the Φ_{FO}-term, that is an exponent of -1.41 compared to -0.77, this results in a longer ignition delay overall combining these two effects. According to Babajimopoulos et al. [143], there exists a direct relationship between ignition delay in time and crank-angle domain, which implies that, to maintain similar CA50 hence ignition delay time, in-cylinder temperature at TDC needs to be higher in the case with eEGR to compensate the net effect of the other two parameters. TDC pressure is not particularly important in this consideration, because it changes in a similar fashion for both cases, eEGR and air dilute, and also because sensitivity toward pressure is very low i.e. the exponent is almost unity. Higher TDC temperature is achieved by employing more NVO to trap a larger amount of hot iEGR.

Combustion phasing, including crank-angles for 5 %, 50 % and 90 % mass fraction burned (CA10, CA50, CA90), as depicted in Figure 3.5, reveals a few interesting insights. First, increased P_{int} facilitates later combustion phasing, as can be seen by later CA05, CA50 and CA90. In particular, CA50 can be retarded from $\sim$ 10 cad to $\sim$ 14 cad aTDC for P_{int}=1.0 bar and 3.0 bar respectively. Second, while CA50 and CA90 lines are almost indistinguishable between eEGR and air dilute cases, it appears that CA05-50 is $\sim$ 1 cad longer for the eEGR dilute case for all P_{int}. This hints at slightly longer burn duration in the case of eEGR and will be considered as subject of investigation at a later point in this thesis. Third and last, there is a slight trend toward longer CA05-90 i.e. from $\sim$ 11.5 cad to $\sim$ 14.5 cad aTDC by $\sim$ 3 cad, corresponding to a relative increase of $\sim$ 26 %, as P_{int} increases for

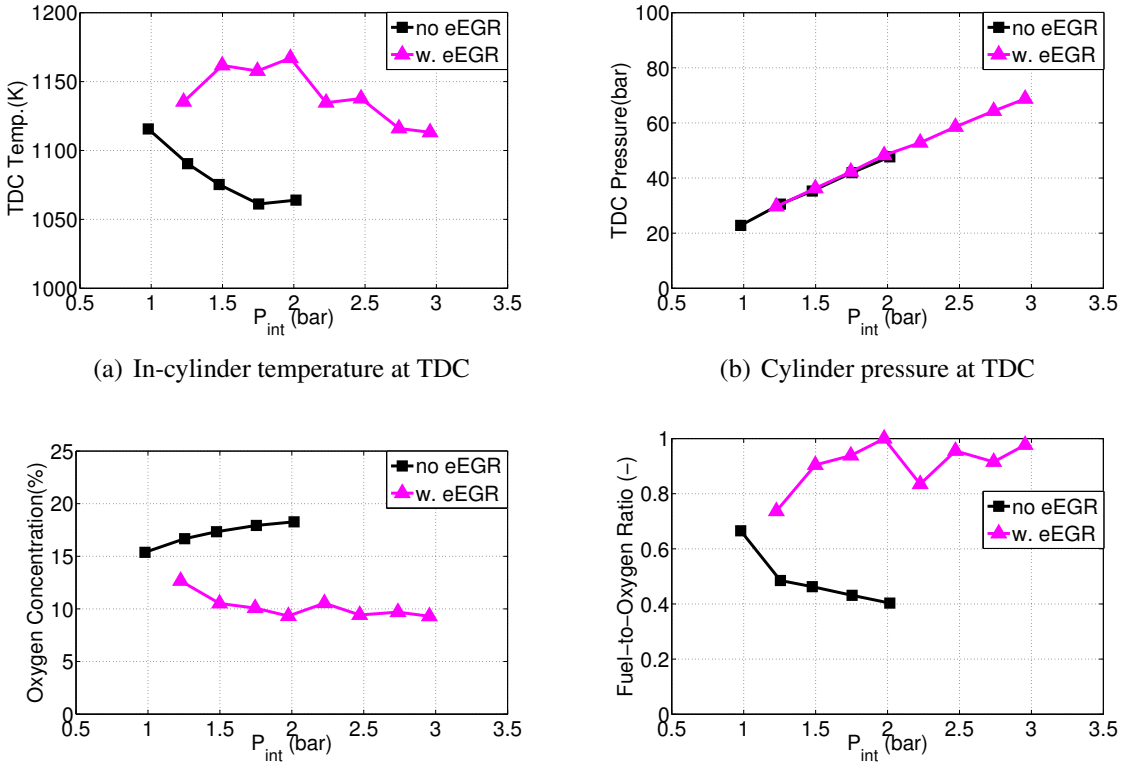

(a) In-cylinder temperature at TDC

(b) Cylinder pressure at TDC

(c) In-cylinder oxygen concentration

(d) Fuel-to-oxygen equivalence ratio

Figure 3.4 Boundary conditions as function of intake pressure during maximum load sweeps with different diluents

both eEGR and air dilute cases. This lengthening of the burn duration can be attributed simply to the effect of retarding CA50 by $\sim$ 4 cad, so that a larger portion of the mixture burns at a later crane angle after TDC, where the piston has already descended further and the resulting temperature increase due to the heat released from burning the fuel is somewhat counteracted by the effect of the piston namely a decrease in pressure and temperature. The fact that CA05-50 changes mostly and not CA50-90 hints at the importance of a staged auto-ignition cascade, where the first part of the burn is more susceptible to changes in conditions.

From the discussion about higher TDC temperature requirements in the case of eEGR addition, it has become clear that this is realized by using more NVO to retain a relatively larger portion of hot iEGR facilitating higher IVC thus TDC temperature, as can be seen in Figure 3.6. As a consequence of a lower charge density at IVC, volumetric efficiency, accounting for incoming air and eEGR, is lower in case of eEGR dilution. For eEGR and air dilute cases volumetric efficiency increases with P_{int} from 41.7 % to 51.4 % and from 42.6 % to 49.8 % corresponding to relative increases of $\sim$ 23 % and $\sim$ 17 % respectively, as a

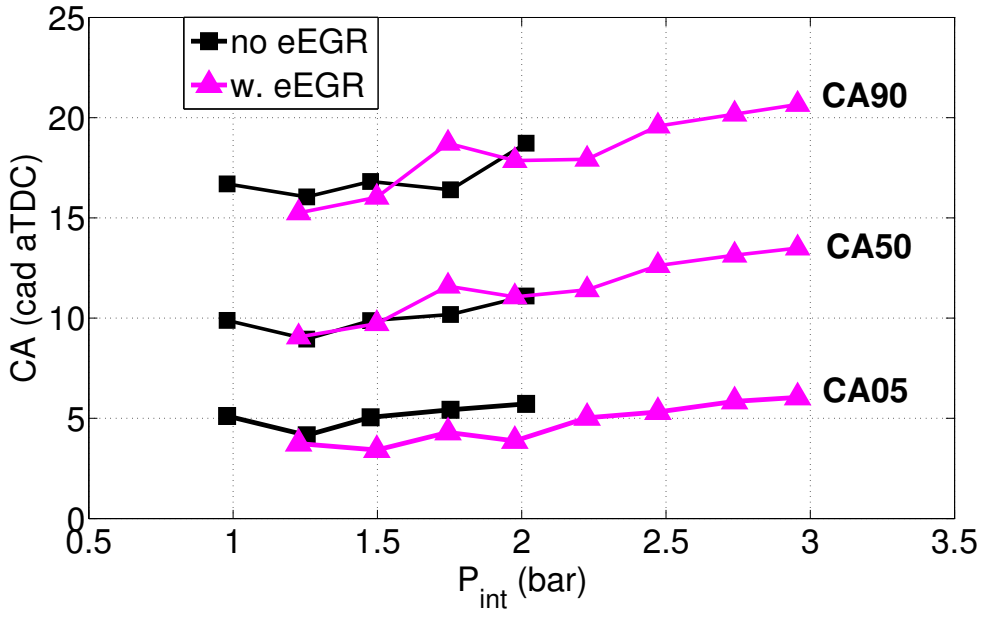

Figure 3.5 eEGR vs. air dilution: effect on combustion phasing and burn duration

result of using less NVO. Fuel-to-charge equivalence ratio, Φ', is higher in the case of eEGR dilution compared to air dilution, that is on average 0.43 as opposed to 0.38 corresponding to a relative increase $\sim$ 13 %, owing to the fact that CA05-50 is somewhat longer allowing for relatively more fuel to be injected. The net effect of lower volumetric efficiency and higher Φ' is that $IMEP_g$ increases by $\sim$ 3-4 %. Gross efficiency increases with increasing P_{int} for eEGR and air dilute cases, indicating the benefits of boosting, which are lower relative heat loss and a leaner mixture and higher ratio of specific heat capacities γ. Note, though, that the eEGR case shows lower gross efficiency values and drops off relative to air dilute case especially as P_{int} increases. This can be attributed mainly to lower γ and higher relative heat loss due to higher peak temperature.

The higher peak in-cylinder temperature, T_{max}, by $\sim$ 100 K in the case of eEGR dilution, is due to higher T_{IVC}, $\sim$ 40 K, and Φ' (see Figure 3.7). Despite the higher T_{max} for the eEGR case, $T_{max}\sim$ 2000 K versus 1900 K, NO_X emissions follow a similar trend in both cases, that is they decrease slightly for increasing P_{int}. Only for P_{int}=1.0 bar in the air dilute case, NO_Xexceeds the limit of 1.0 g per kg fuel. The reason that NO_X is still in check for the eEGR case with higher T_{max} is that O_2 concentration is significantly lower in eEGR case, so that the T_{max} threshold for NO_X formation increases. CO and THC emissions are lower for the eEGR dilute case compared to air dilute case yielding higher combustion efficiency i.e. 97.5 % versus 96.6 % corresponding to a $\sim$ 1 % relative increase. Reasons for that are the

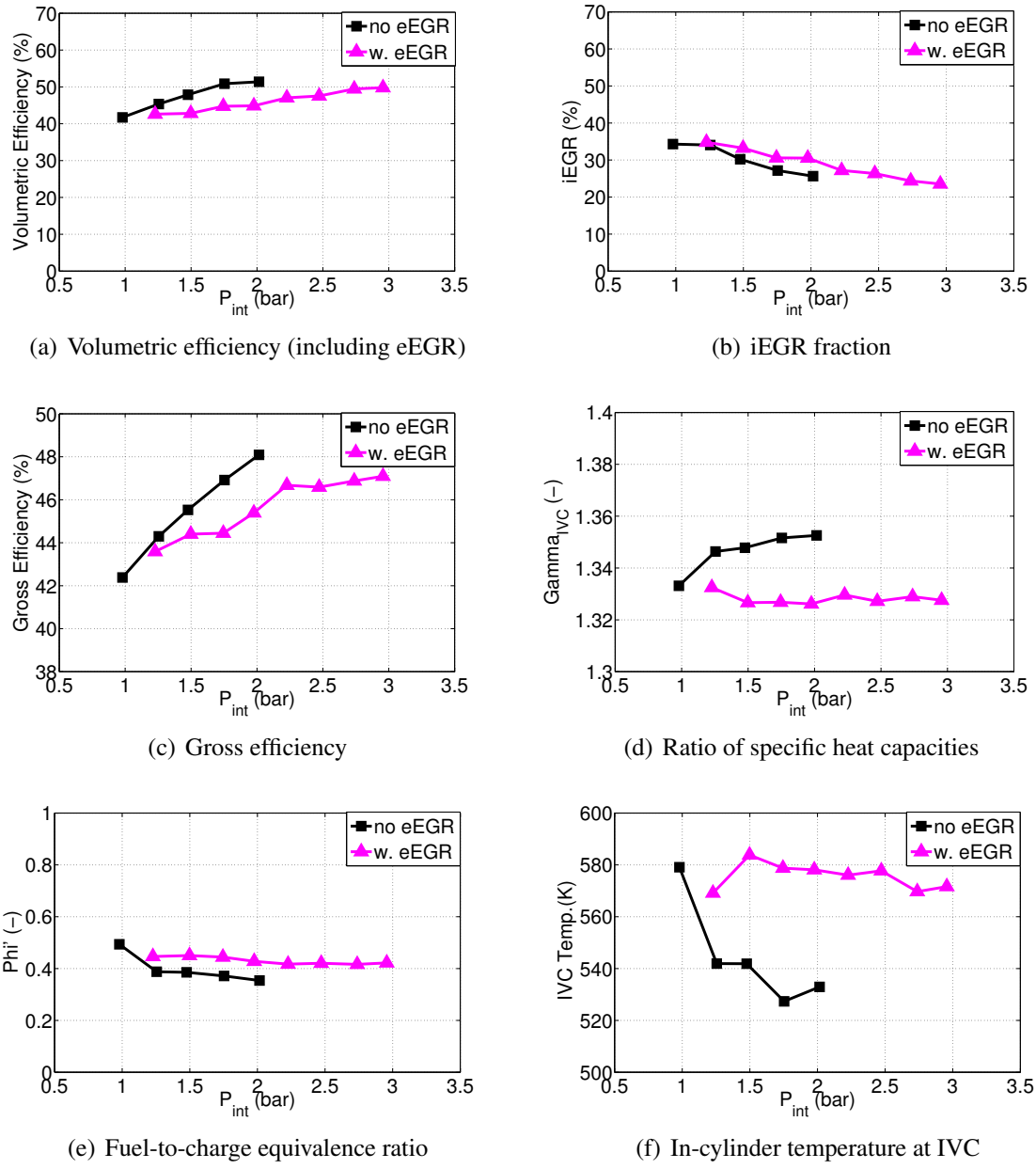

(a) Volumetric efficiency (including eEGR)

(b) iEGR fraction

(c) Gross efficiency

(d) Ratio of specific heat capacities

(e) Fuel-to-charge equivalence ratio

(f) In-cylinder temperature at IVC

Figure 3.6 Boundary conditions as function of intake pressure during maximum load sweeps with different diluents

fact that part of the charge in case of eEGR has a second chance to burn and also that T_{max} is higher for eEGR case enabling higher conversion efficiency of fuel in near-wall regions. CO emissions tend to increase with increasing P_{int}, which could be due to decreasing T_{max}. The same trend cannot be observed for THC, instead THC remain fairly insensitive to P_{int}, at most showing a slightly decreasing trend, indicating that most of the THC originate from crevice volume and not near-wall regions in combustion chamber. The slight decrease in

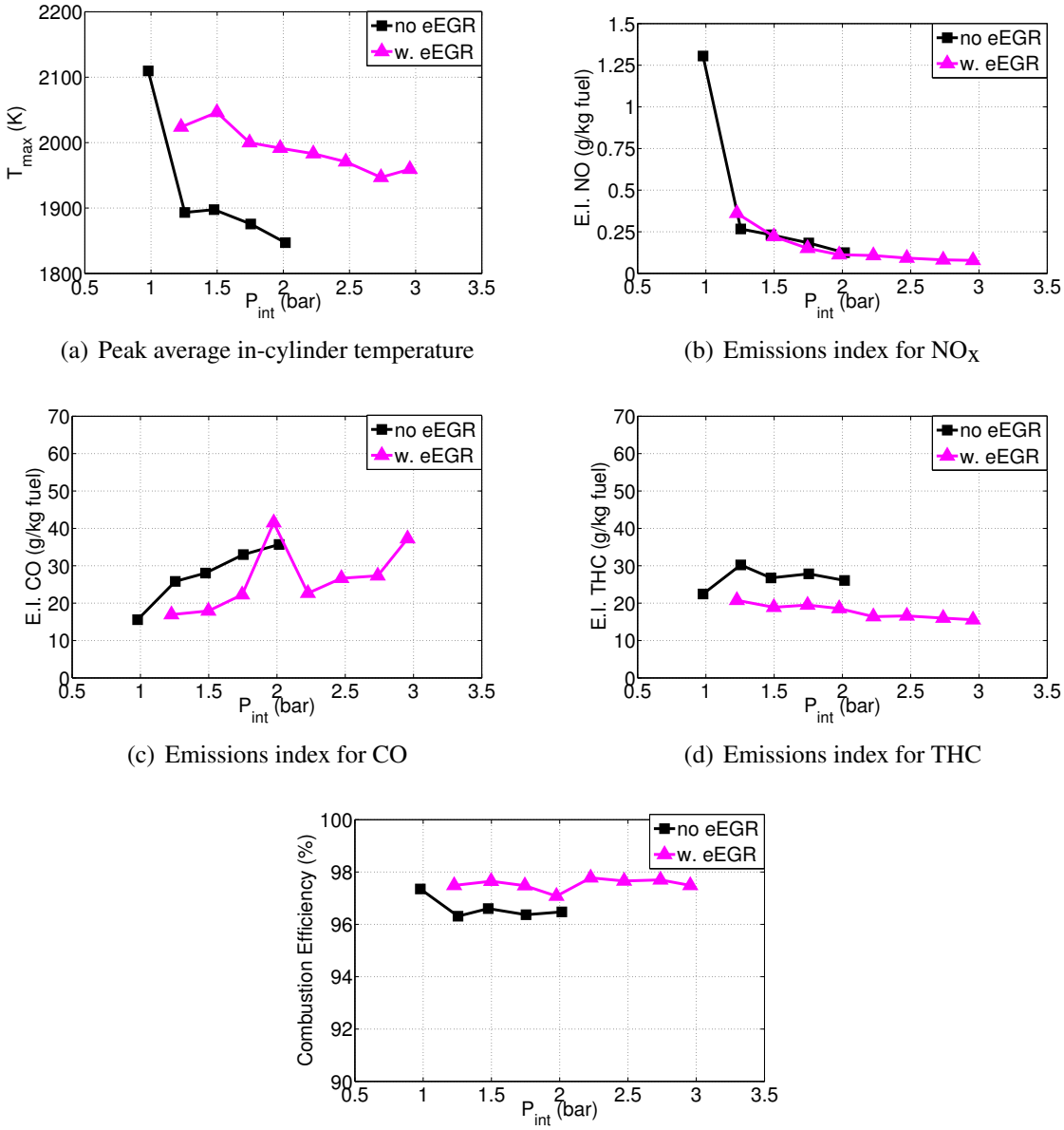

(a) Peak average in-cylinder temperature

(b) Emissions index for NO_X

(c) Emissions index for CO

(d) Emissions index for THC

(e) Combustion efficiency

Figure 3.7 Third set of results as function of intake pressure during maximum load sweeps for two engines and at two different engine speeds in case of UM NVO engine

THC could be due to smaller relative mass fraction of unburned fuel in crevice with higher P_{int} due to higher piston temperature as a result of higher $IMEP_g$. Also, fuel may already have been broken down largely, and the temperature required for oxidation is higher than for THC oxidation.

Figure 3.8 shows that there is almost no difference between eEGR and air dilute cases as far as maximum pressure rise rate, peak cylinder pressure and ringing intensity values are

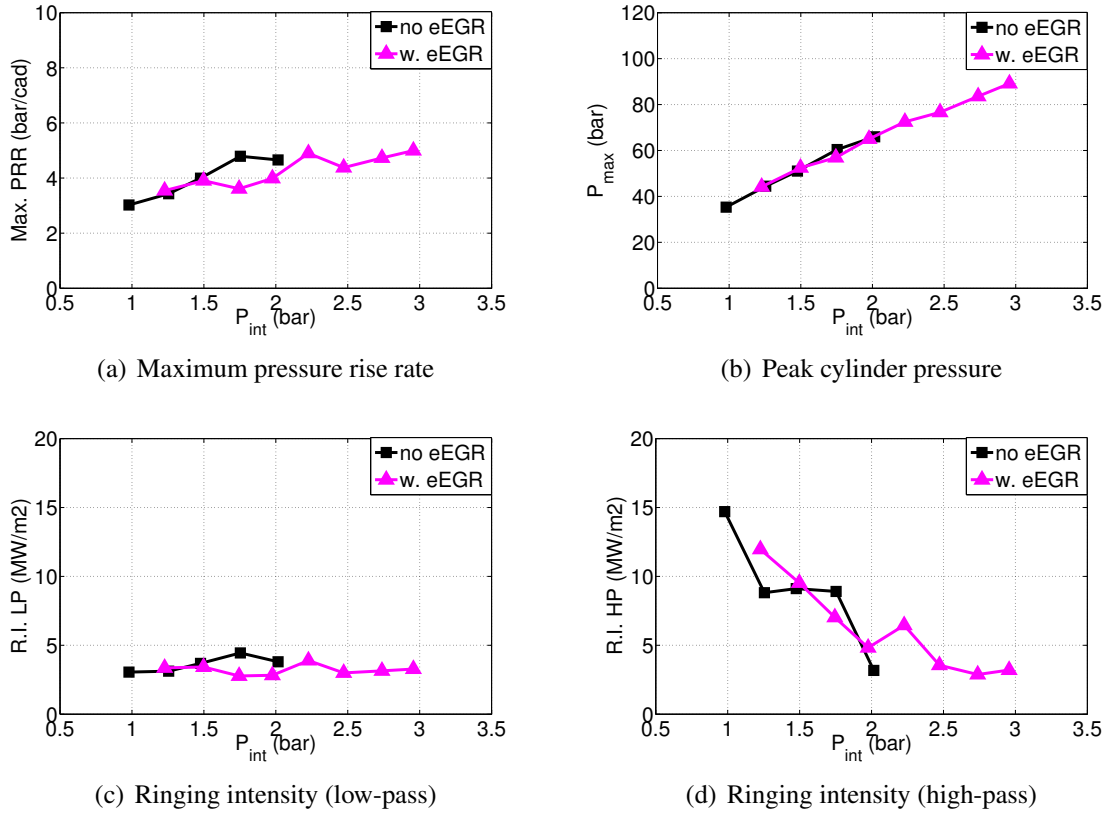

(a) Maximum pressure rise rate

(b) Peak cylinder pressure

(c) Ringing intensity (low-pass)

(d) Ringing intensity (high-pass)

Figure 3.8 Fourth set of results as function of intake pressure during maximum load sweeps for two engines and at two different engine speeds in case of UM NVO engine

concerned, which is not unexpected, as the same low-pass knock limit of $R.I._{LP}$=5 MW/m^2 was targeted in both experiments. P_{max} increases almost linearly with P_{int} and only toward higher P_{int} it drops off some, most likely due to more CA50 retard. Maximum pressure rise rate increases to a lesser extend with increasing P_{int}. Interestingly, the trend for high-pass filtered ringing intensity ($R.I._{HP}$) is very different from low-pass filtered ringing intensity ($R.I._{LP}$), especially at lower P_{int}, showing a decrease from very value at P_{int}=1.0 bar with increasing P_{int}. The significant discrepancy in R.I. values at lower P_{int}, by a factor of almost 3, between both expressions indicates that the simplified expression $R.I._{LP}$ may have some limitations under certain conditions. This will be examined and considered in more detail in chapter 5 of this thesis.

3.2.3 Results: Intake Temperature Effect

The effect of intake charge temperature, T_{int}, on maximum attainable $IMEP_g$ as a function of P_{int} is investigated in this section. Note that all three T_{int} cases considered here use

eEGR to attain a stoichiometric fuel-to-air equivalence ratio throughout the entire P_{int} sweep. Although the incoming air/eEGR mixture does not have substantially different composition, in contrast to section 3.2.2, where air is replaced by significant amounts of eEGR, the in-cylinder composition is altered to some extent as will be explored later in this section. All three cases rely on internal EGR (iEGR) and NVO as adjustment knob for combustion phasing. Experiments are performed according the procedure described in section 3.1 and the conditions listed in Table 3.1 apply to all other parameters but T_{int}, which is set constant at 40 °C, 90 °C and 120 °C for each of the three maximum load sweeps.

The controlled experimental parameters are depicted in Figure 3.9. NVO decreases as P_{int} increases compensating for the ignition promoting effect of elevated TDC pressure through lower TDC temperature. Note, that lower T_{int} requires relatively larger amounts of NVO, and that in the case of T_{int}=40 °C not even the minimum NVO value of this engine is reached. Also, for the lowest intake temperature case, T_{int} increases slightly and deviates from 40 °C as P_{int} increases due the increasingly larger eEGR portion (note that the EGR heat exchanger runs of engine coolant at 90) within the incoming charge, which raises the average temperature.

Reduced intake charge temperature clearly enables the UM NVO engine to achieve a higher maximum $IMEP_g$ value as shown in Figure 3.10. By lowering T_{int} from 120 °C to 40 °C, a 46 % increase in $IMEP_g$ from 8.0 bar to 11.7 bar can be achieved. The high load point ($IMEP_g$=11.7 bar, P_{int}=3.0 bar) for the T_{int}=40 °C case is not limited by NVO, because there is still a margin of $\sim$ 13 cad, but maximum allowable peak cylinder pressure. To ensure safety of the engine, average peak cylinder pressure, P_{max}, plus two standard deviations should not exceed 120 bar. All points during these maximum load sweeps inherently exhibit a high degree of cyclic variability, as can be seen in Figure 3.11. The average value of P_{max} is 100.5 bar and two standard deviations amount to 13.7 bar, that is to say that statistically 95 % of the cycles have a P_{max} between 86.8 bar and 114.2 bar, and 2.5 % of the cycles have a P_{max} greater than 114.2 bar and another 2.5 % have a P_{max} less than 86.8 bar. In fact, the maximum and minimum values for P_{max} are 116.4 bar and 79.4 bar respectively. It is noteworthy, that COV of P_{max}, which amounts to 6.8 %, is much more suitable to capture this high degree of variability than COV of $IMEP_g$, which only amounts to 2.8 %. From Figure 3.12, showing the histograms for the entire maximum load sweep for T_{int}=40 °C, one can see that P_{max} for the individual cycles for all P_{int} follows a Gaussian normal distribution. Note, that it is slightly skewed to the left toward lower P_{max}. Chapter 4 4 will deal with the causes and symptoms of cyclic variability in more detail.

Raising the intake charge temperature has two effects: first, it decreases the maximum amount of diluent trapped at IVC, and second, it alters the composition of the mixture at

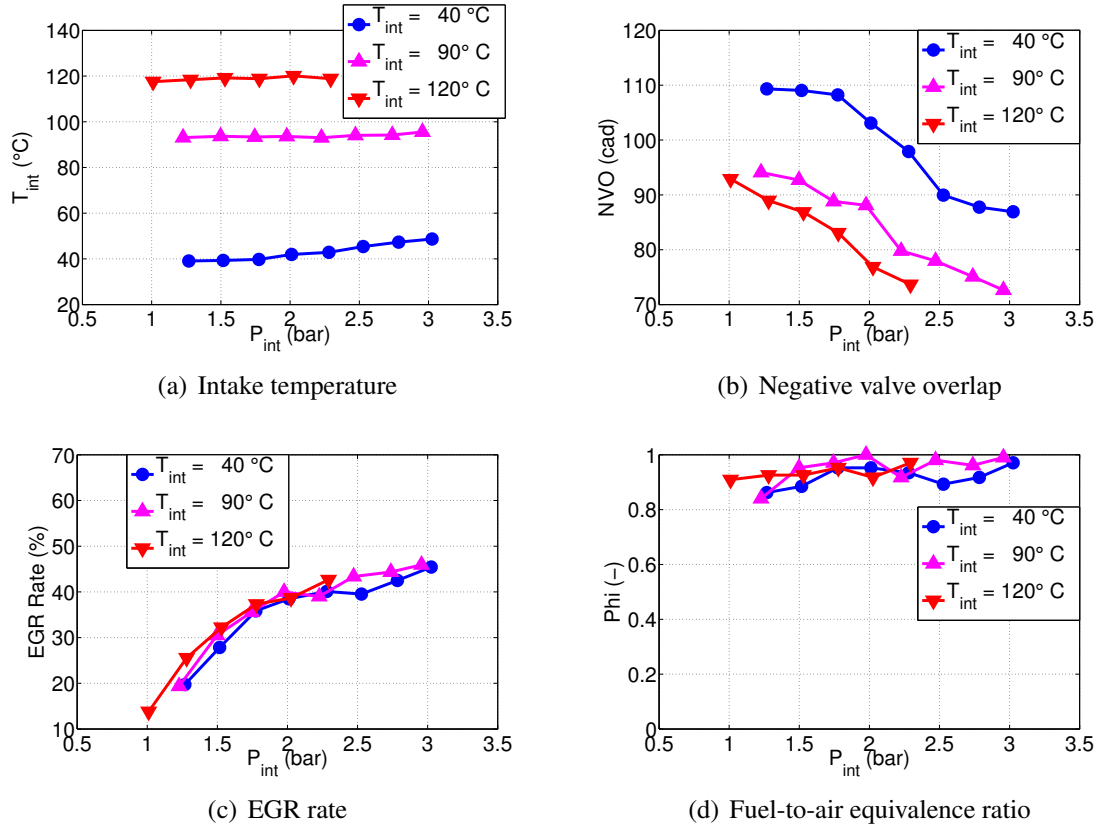

(a) Intake temperature

(b) Negative valve overlap

(c) EGR rate

(d) Fuel-to-air equivalence ratio

Figure 3.9 Boundary conditions as function of intake pressure during maximum load sweeps with different intake temperature

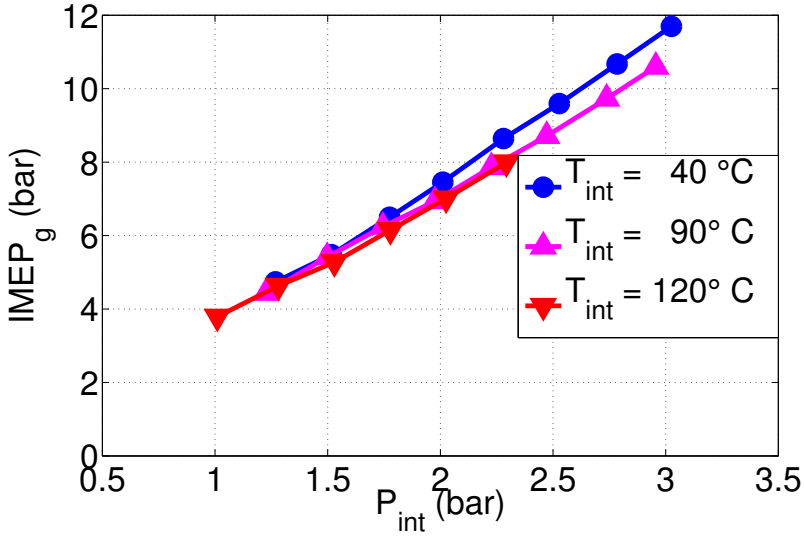

Figure 3.10 Intake temperature: effect on maximum load limit

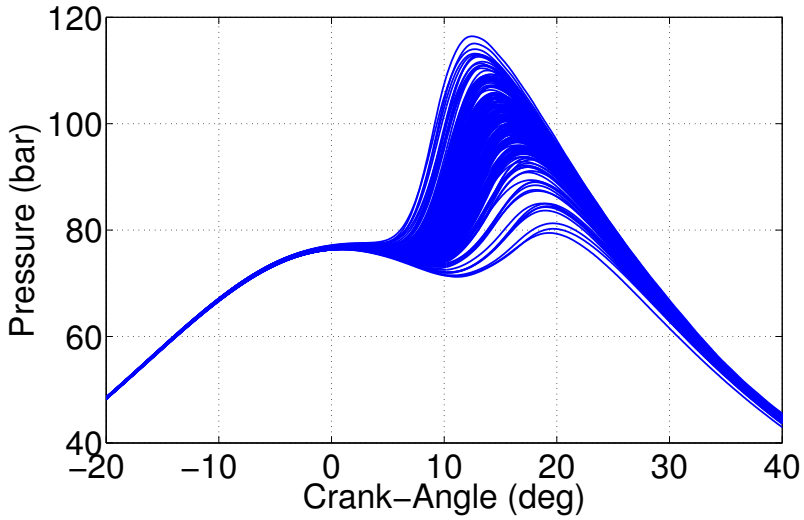

Figure 3.11 Individual low-pass-filtered cylinder pressure traces for maximum load point of maximum load sweep at T_{int}= 40 °C (P_{int}=3.0 bar, $IMEP_g$=11.7 bar)

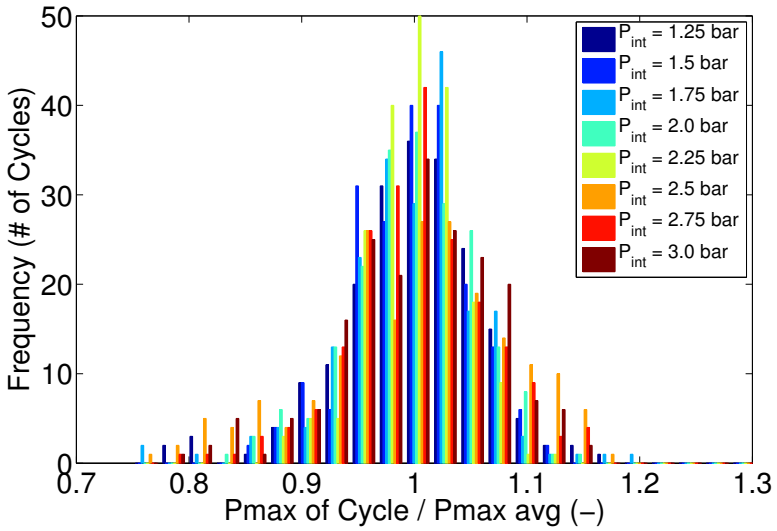

Figure 3.12 Histogram of normalized peak cylinder pressure traces for all points of maximum load sweep at T_{int}= 40 °C

IVC in terms of the ratio of eEGR versus iEGR (see Figure 3.14). Higher T_{int} means that less NVO has to be used to maintain combustion phasing, and that part of the iEGR is substituted with eEGR instead. In other words, a larger fraction of the charge is heated outside the cylinder before entering so that the amount of hot iEGR needed is reduced.

Combustion phasing trends are fairly similar to what was seen before in section 3.2.2

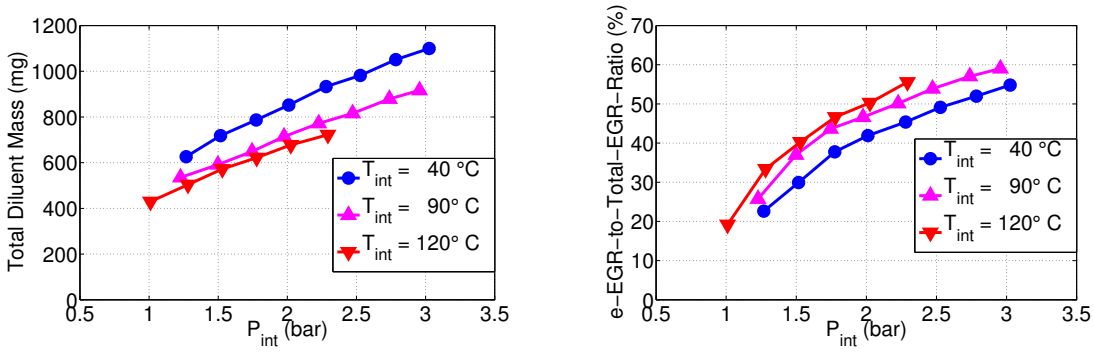

(a) Total trapped mass at IVC

(b) Ratio of eEGR to total-EGR (eEGR+iEGR)

Figure 3.13 Intake temperature: effect on total trapped mass and composition

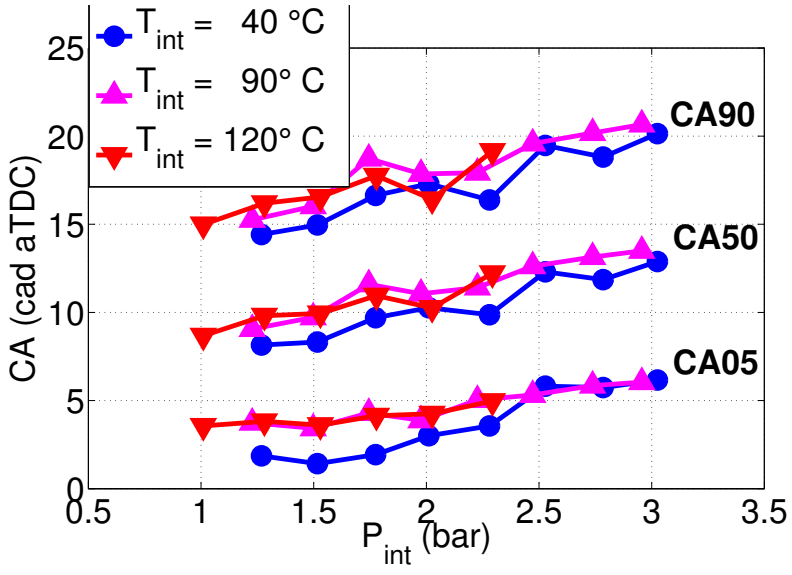

Figure 3.14 Intake temperature: effect on combustion phasing and burn duration

comparing eEGR and air dilution, that is CA50 can be further retarded as P_{int} is raised facilitating higher loads to be reached (see Figure 3.14). Only the T_{int} case of 40 °C stands out, as it seems to burn somewhat earlier and more slowly (longer CA05-50). This composition is the same for all three T_{int} cases ($\Phi \sim 1.0$), this could be due to more stratification due to less eEGR and more iEGR via NVO, but this cannot be confirmed at this point as too many other parameters are varied in the experiments i.e. CA50 is not exactly the same.

Volumetric efficiency, accounting for incoming air and eEGR, increases as P_{int} increases due to lower NVO, and also increases with increasing T_{int} due to lower NVO (see Figure 3.15). Note, though, that the reference for this volumetric efficiency is the pressure and temperature in the intake runner, so that the net effect is still that less fresh incoming

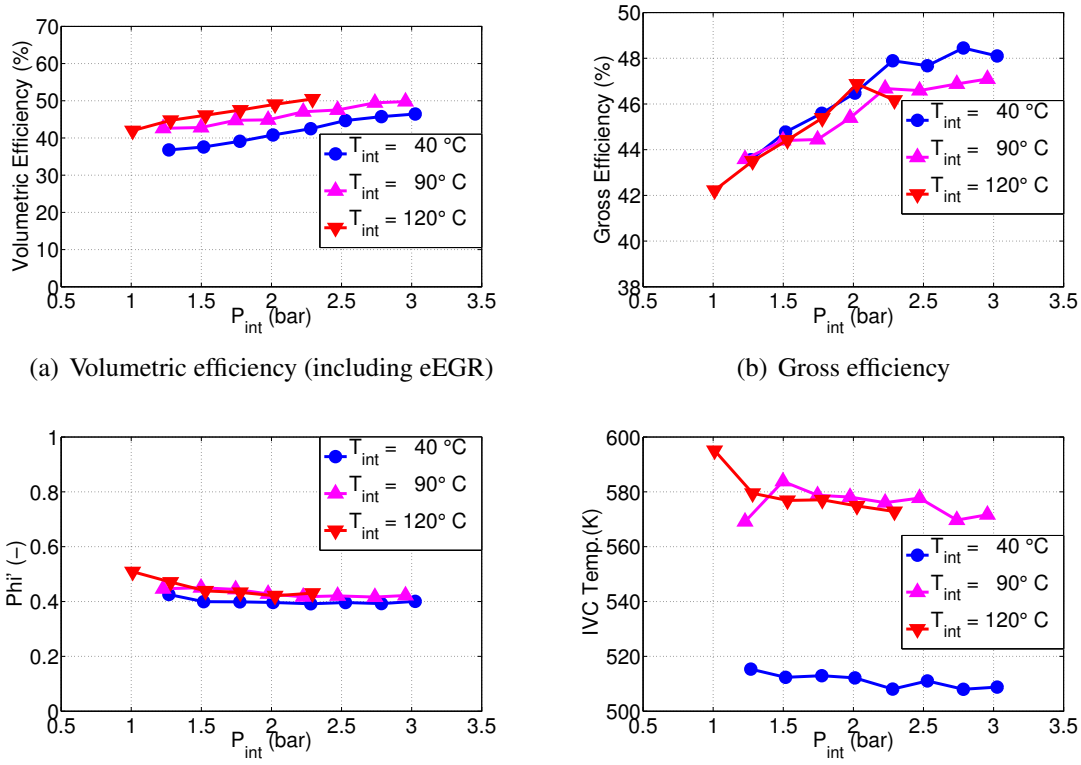

(a) Volumetric efficiency (including eEGR)

(b) Gross efficiency

(c) Fuel-to-charge equivalence ratio

(d) In-cylinder temperature at IVC

Figure 3.15 Intake temperature: effect on efficiencies, fuel-to-charge ratio, and in-cylinder temperature at intake valve closing

mass is trapped at higher T_{int} in absolute terms. Gross efficiency with increasing P_{int}, but no difference between different T_{int} can be discerned as expected because of similar composition, as shown by $\Phi' \sim$ constant.

Emissions show similar trends amongst all three T_{int} cases, that is NO_Xdecreases, CO increases and THC slightly decreases with increasing P_{int}, as seen in Figure 3.16. The increase in CO and decrease in THC seem to cancel each other out so that combustion efficiency is constant and high at $\sim$ 98 %. Reason for increasing CO is the lower peak cylinder temperature with increasing P_{int}. The higher piston temperature and smaller mass fraction of unburned fuel in the crevice with increasing load is considered the main reason for the decrease in THC. The only curious aspect is that NO_Xemissions again collapse on top of each other despite different T_{max} for the three T_{int} cases. In the previous section this could be explained by different composition and O_2availability, but they are identical here, so it may be related to thermal inhomogeneities that could be higher in case of T_{int}=40 °, where more NVO is used, compared to the case of T_{int}=120 This implies that, although average peak temperature is lower in T_{int}=40 °case, but the hottest portion that burns first

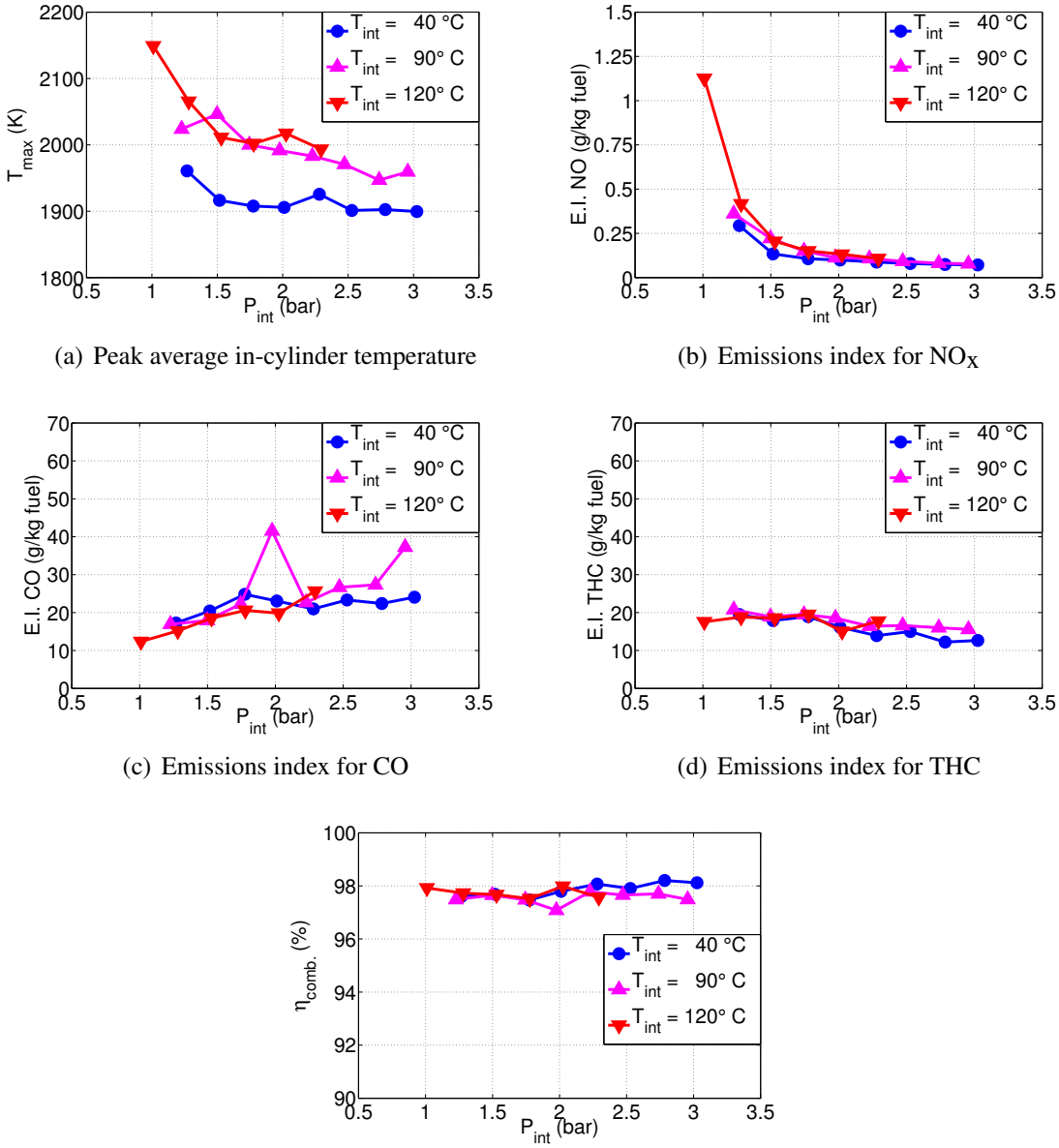

(a) Peak average in-cylinder temperature

(b) Emissions index for NO_X

(c) Emissions index for CO

(d) Emissions index for THC

(e) Combustion efficiency

Figure 3.16 Third set of results as function of intake pressure during maximum load sweeps for two engines and at two different engine speeds in case of UM NVO engine

may well be at the same temperature as the hottest portion in the case of T_{int}=120 °.

Trends for maximum pressure rise rate, peak cylinder pressure, and ringing intensity are largely similar to what was seen before in section 3.2.2, but there are some subtle differences, in particular, concerning P_{max} and the two competing R.I. values (see Figure 3.17). P_{max} do not all collapse on top of each other, instead the lowest P_{int} case shows the highest value for all P_{int}. This can be the result of higher NVO, by $\sim$ 20 cad, correspondingly

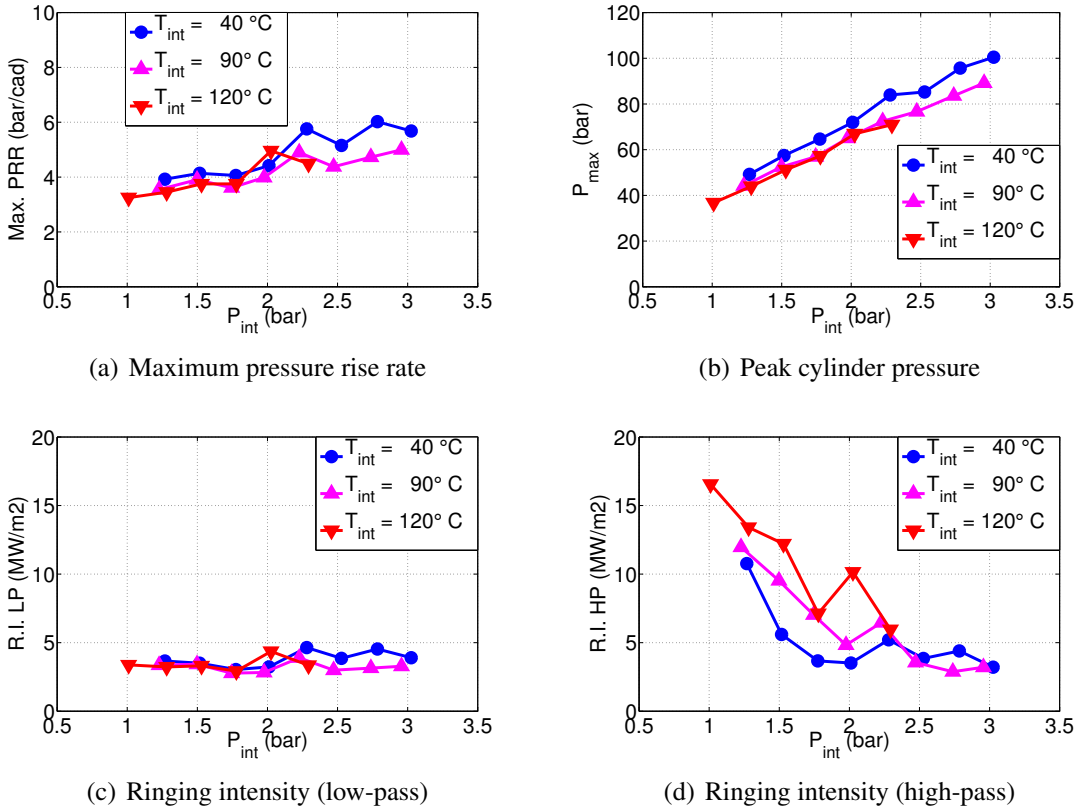

(a) Maximum pressure rise rate

(b) Peak cylinder pressure

(c) Ringing intensity (low-pass)

(d) Ringing intensity (high-pass)

Figure 3.17 Fourth set of results as function of intake pressure during maximum load sweeps for two engines and at two different engine speeds in case of UM NVO engine

later IVC timing. Note that, because of the short valve duration, NVO below 80 cad means that IVC occurs before BDC, which leads to less mass inducted and effectively lowers the compression ratio. Another explanation can be the higher charge temperature during intake process and compression and the lower total mass accompanied with higher relative heat loss and consequently reduced P_{max}. Finally, it should be pointed out that $R.I._{HP}$ is higher for higher T_{int} cases.

3.2.4 Results: Turbo-Charger Efficiency Effect

In this section, the effect of overall turbo-charger efficiency on the available operating range between knock and combustion variability limits is investigated as a function of load and intake pressure. Table 3.2 shows the important parameters held constant. For each intake pressure three loads defined by $IMEP_n$ are attempted to be attained. Intake temperature is held constant at T_{int}=40 °C and combustion phasing is adjusted via NVO from advanced to retarded. Only three points are taken that is two at the knock limit when RI_{LP} equals

Table 3.2 Experimental procedure

P_{int}	$IMEP_n$=5.0 bar	$IMEP_n$=6.5 bar	$IMEP_n$=8.0 bar
1.25	x	-	-
1.50	x	-	-
1.75	x	x	-
2.00	-	x	x
2.25	-	x	x
2.50	-	-	x

10 MW/m^2 and 5 MW/m^2 respectively and one at the combustion variability limit when COV of $IMEP_g \sim 5$ %. The low speed data acquisition system computes an approximate value of OTE in real-time based on the equation for the ideal turbo-charger efficiency. OTE is computed and kept approximately constant during the experiments and is adjusted by changing P_{exh} accordingly.

The available operating range in terms of CA50 between severely knocking (RI_{LP} equals 5 MW/m^2) and and highly unstable operation (COV of $IMEP_n \sim 5$ %) is depicted as a function of P_{int} for up to three different loads for four different OTEs, as shown in Figure 3.18, and two key observations can be made. First, for a given OTE and $IMEP_n$, the available CA50 windows becomes larger as P_{int} increases due to improved dilution, and for a given OTE and P_{int}, the available CA50 window becomes smaller as $IMEP_n$ increases due to reduced dilution. Second, for a given $IMEP_n$, the CA50 window decreases as OTE decreases and back-pressure increases due to larger amounts of RGF or iEGR trapped.

Since the trend with OTE is clear and for the purpose of simplification, from now on the focus will be one a high and low OTE case, where data for all three loads is available. Figures 3.19 and 3.20 show various key results as function of P_{int} and $IMEP_n$ for OTE=58 % and OTE=48 %. As P_{int} increases, the mixture becomes leaner and so Φ decreases. Φ', in contrast, remains approximately constant when comparing different loads, but is greater for OTE=58 % than for OTE=38 % case, because the lower OTE case requires more fuel to be injected for the same $IMEP_n$ as back-pressure (dP) and pumping work (PMEP) are significantly higher. Since the high OTE case requires more hot iEGR (RGF) because of an overall leaner mixture (lower Φ') and there is much less back-pressure available, a much higher amount of NVO is needed. The fact that PMEP is still lower for the high OTE case suggests that larger NVO is a smaller contributor to PMEP compared to dP.

From this OTE study, one can conclude that proper matching of turbo-charger to HCCI engine is crucial to avoid not only high pumping work, but also, more importantly, to be able to operate over a reasonably wide range of CA50.

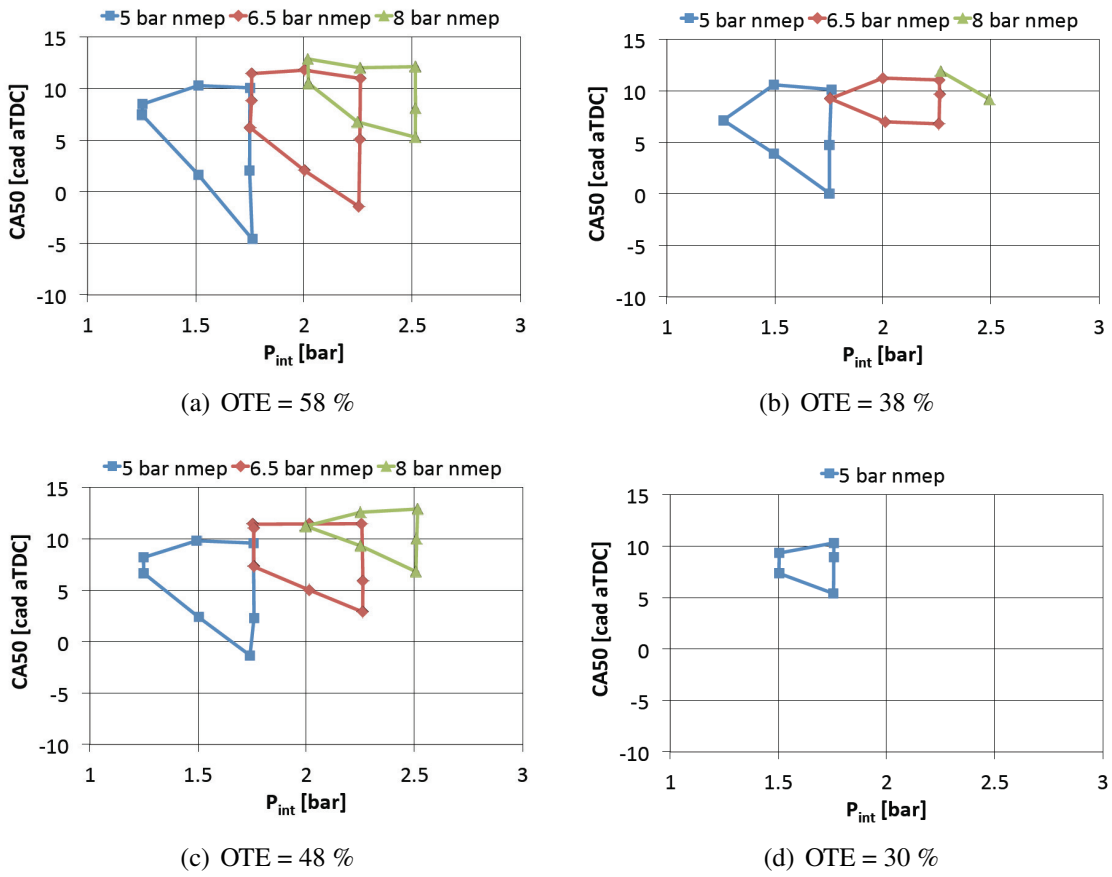

(a) OTE = 58 %

(b) OTE = 38 %

(c) OTE = 48 %

(d) OTE = 30 %

Figure 3.18 Effect of overall turbo-charger efficiency (OTE) on operating range defined by R.I.$_{LP}$=10 MW/m^2 and COV of IMEP$_g$ $\sim$ 3 % as function of intake pressure and load (IMEP$_n$)

3.2.5 Results: Engine Speed Effect

In this section, the effect of engine speed on maximum attainable IMEP$_g$ as a function of P$_{int}$ is considered. For that purpose, an additional maximum load sweep at a lower engine speed of 1200 rpm was performed with the UM NVO engine. For both engine speeds, 2000 rpm and 1200 rpm, no eEGR is added. The same procedure as described in section 3.2.1 is followed and the conditions listed in Table 3.1 are applied during the maximum load sweep experiment. For comparison and to better interpret the results of the maximum load sweep at lower engine speed (1200 rpm), experimental results from the SNL PVO engine, in particular the data set including eEGR addition at higher intake pressure is included [29].

Whereas the experimental procedure is almost identical for both maximum load sweeps with the UM NVO engine, the SNL PVO engine uses different boundary conditions, which is the result of a different strategy to control combustion phasing. The SNL PVO engine relies on T$_{int}$ and eEGR as opposed to NVO as control parameters to adjust combustion phasing. Moreover, the SNL PVO engine was operated practically without any back-pressure (dP),

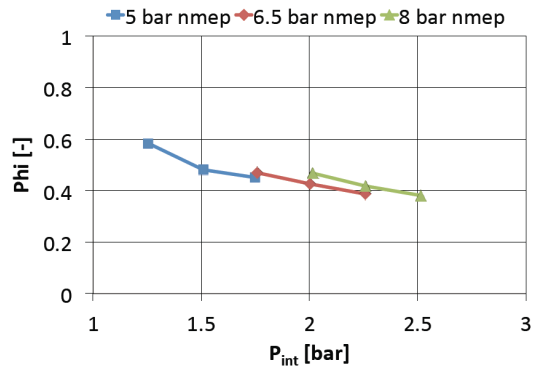

(a) Fuel-to-air equivalence ratio (OTE = 58 %)

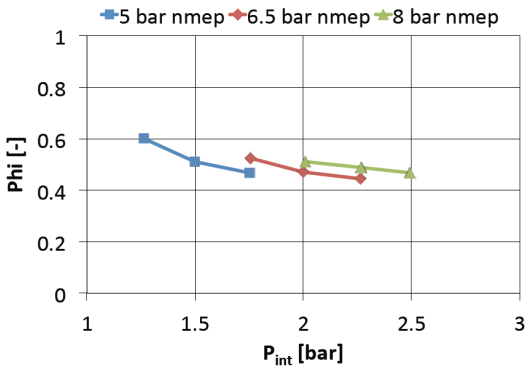

(b) Fuel-to-air equivalence ratio (OTE = 38 %)

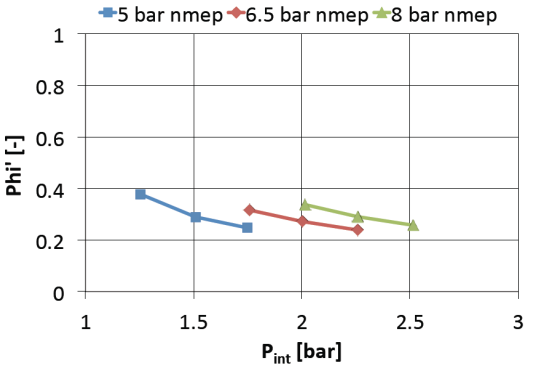

(c) Fuel-to-charge equivalence ratio (OTE = 58 %)

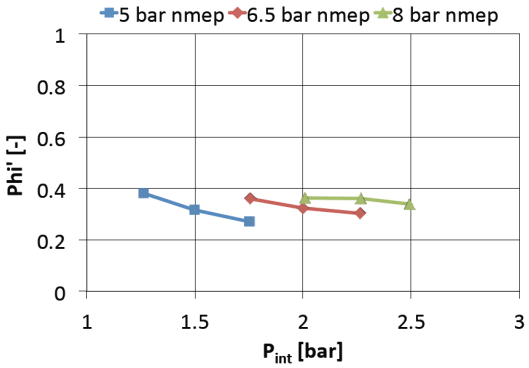

(d) Fuel-to-charge equivalence ratio (OTE = 38 %)

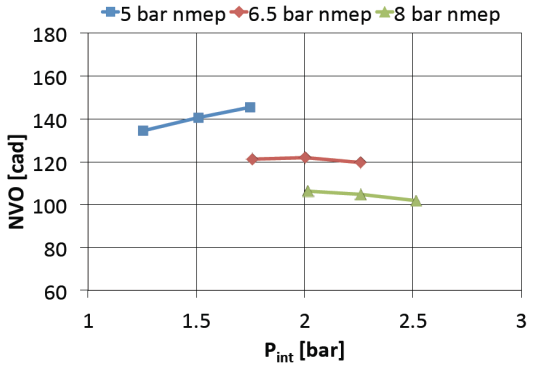

(e) Negative valve overlap (OTE = 58 %)

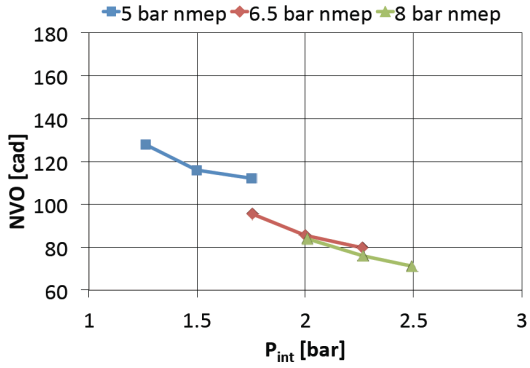

(f) Negative valve overlap (OTE = 38 %)

Figure 3.19 Comparison of various quantities for two overall turbo-charger efficiencies

as P_{exh} and P_{int} are almost identical. In contrast, the UM NVO engine was operated with dP=0.5 bar and dP=0.25 bar for the maximum load sweeps at 2000 rpm and 1200 rpm respectively. Note, though, that in case of 1200 rpm, P_{exh} had to be decreased for P_{int} greater or equal 2 bar, for the minimum NVO limit was approached and not decreasing dP at that point would have prevented reaching higher $IMEP_g$.

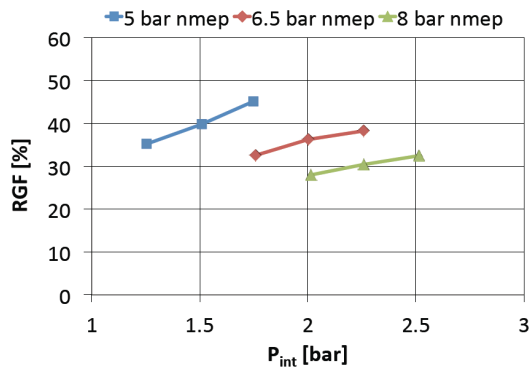

(a) Residual gas fraction (OTE = 58 %)

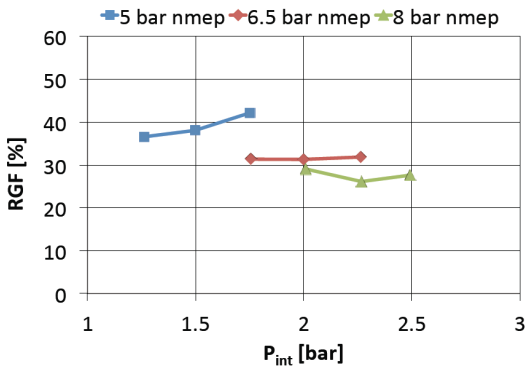

(b) Residual gas fraction (OTE = 38 %)

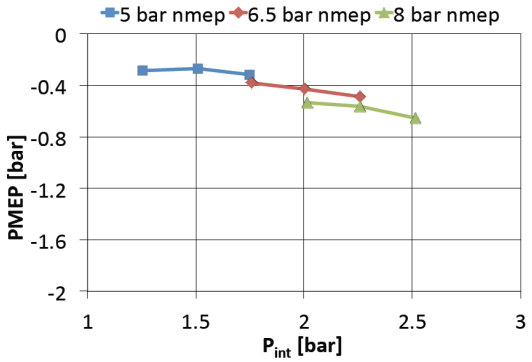

(c) Pumping work (OTE = 58 %)

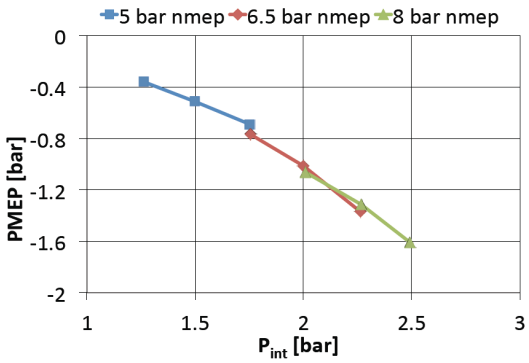

(d) Pumping work (OTE = 38 %)

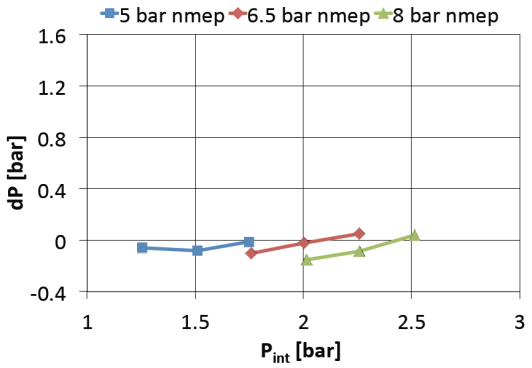

(e) Pressure differential: P_{exh} - P_{int} (OTE = 58 %)

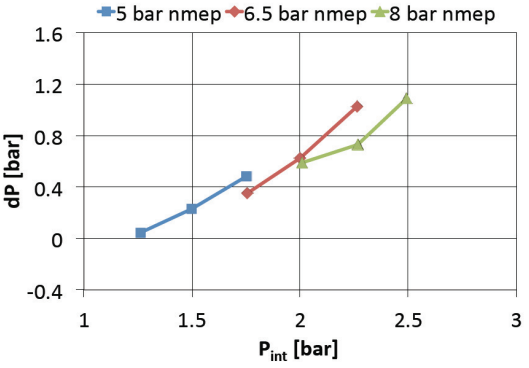

(f) Pressure differential: P_{exh} - P_{int} (OTE = 38 %)

Figure 3.20 Comparison of various quantities for two overall turbo-charger efficiencies

The maximum attainable $IMEP_g$ increases significantly i.e. by $\sim$ 1.5 bar, corresponding to a relative increase of $\sim$ 25%, when the engine speed of the UM NVO engine is lowered from 2000 rpm to 1200 rpm, as can be seen from Figure 3.22. More specifically, this almost uniform increase in $IMEP_g$ irrespective of P_{int} leads to parallel shift upward of the $IMEP_g$ curve, and as a result, the gap between the UM NVO engine at 2000 rpm and the SNL PVO engine at 1200 rpm almost appears to be closed, especially for lower P_{int}. Toward higher

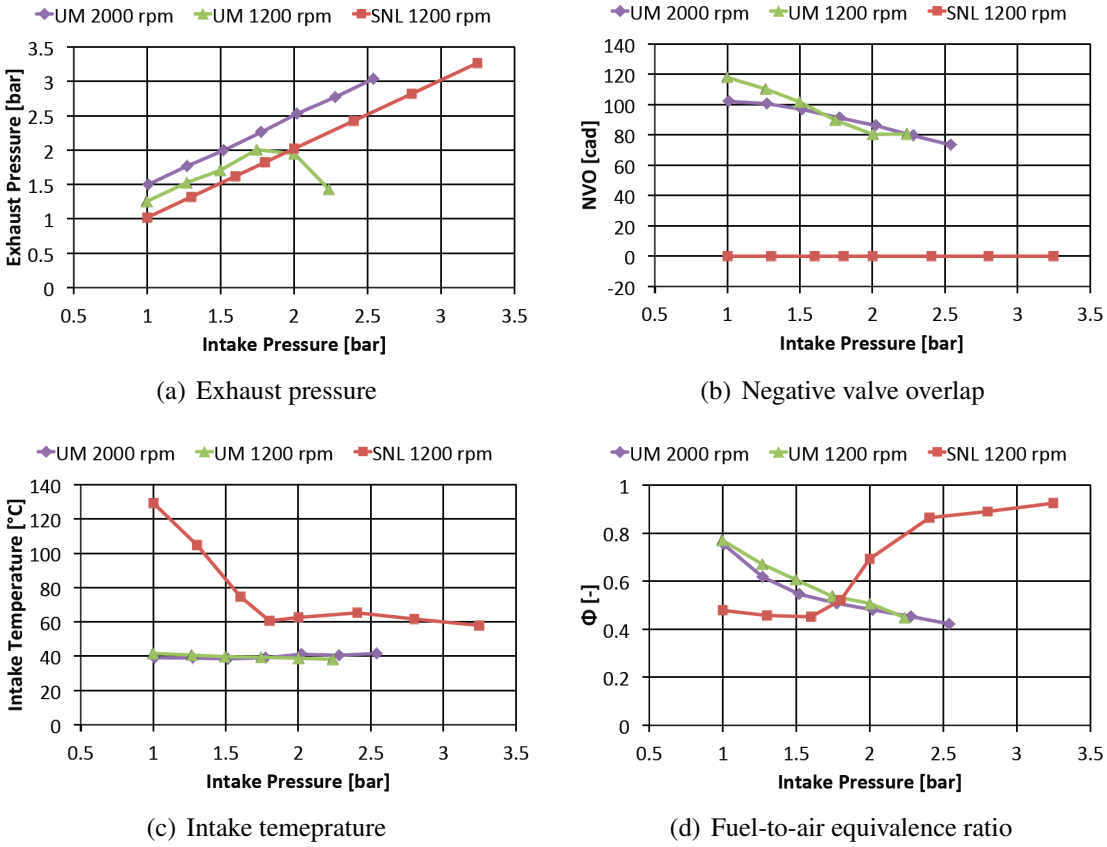

(a) Exhaust pressure

(b) Negative valve overlap

(c) Intake temeprature

(d) Fuel-to-air equivalence ratio

Figure 3.21 Boundary conditions as function of intake pressure during maximum load sweeps for two engines and at two different engine speeds in case of UM NVO engine

P_{int}, a a gradually increasing discrepancy for increasing P_{int} still exists. The substantial increase in $IMEP_g$ with lower engine speed is not related to different dP or P_{exh}, because gross quantities are compared, hence potentially different pumping work is excluded by looking at data this way.

Two mechanisms, namely increased volumetric efficiency and further possible combustion phasing retard, can be identified as key enablers facilitating maximum load extension with lower engine speed. Although the latter one is largely responsible for the increase in $IMEP_g$ ($\sim$ 75 %), and the former one to a lesser extent ($\sim$ 25 %), volumetric efficiency is considered first, because it is more straightforward to understand, followed by combustion phasing retard.

As can be seen from Figure 3.23, decreasing the engine speed from 2000 rpm to 1200 rpm yields $\sim$ 7.5% average relative increase in volumetric efficiency, which can be attributed to enhanced breathing characteristics, as a result of reduced flow friction with a lower mass flow rate (on a time base), and improved runner wave dynamics [116]. Total trapped mass

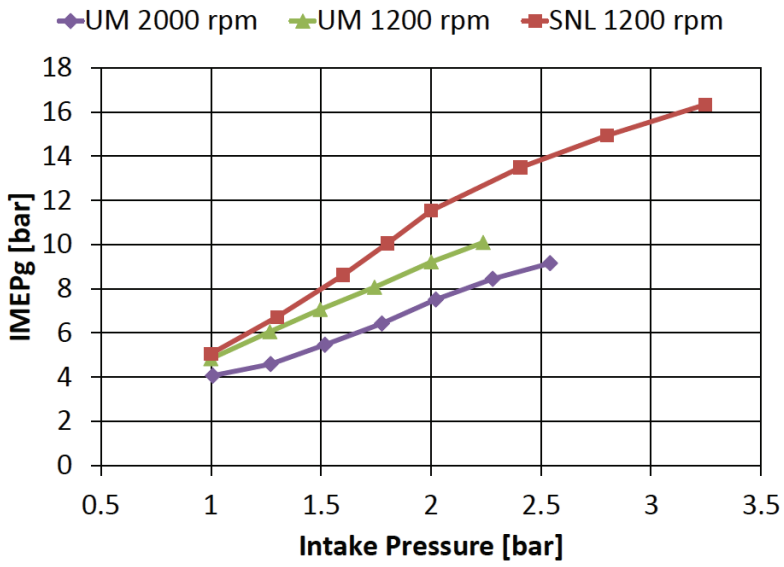

Figure 3.22 Gross indicated mean effective pressure as function of intake pressure during maximum load sweeps for two engines and at two different engine speeds in case of UM NVO engine

increases on average by $\sim 6.1\%$ for the lower engine speed, which is in good agreement with the increase in volumetric efficiency. As a result and to maintain a similar value for Φ', more fuel can be injected consequently, while still meeting knock (RI=5 MW/m^2) and combustion variability constraints (COV of IMEP$_g$=3 %). Note, though, that IMEP$_g$ increases on average by $\sim 25\%$ when decreasing engine speed, which implies that the remaining 19 % are due to further CA50 retard.

Combustion phasing (CA50) could be further retarded i.e. on average by 3.7 cad, when the engine was operated at 1200 rpm instead of 2000 rpm (see Figure 3.23). Consequently, a relatively larger amount of the bulk heat release occurs at a later point in the cycle, when the piston has already descended further and its expansion rate has increased, which leads to a decrease in maximum pressure rise rate and peak cylinder pressure in case the energy input is kept constant. For the 1200 rpm maximum load sweep, however, fueling rate and Φ' were increased in the experiment to take advantage of the additional leeway, while still meeting knock and combustion variability constraints. Burn duration (CA10-90) is up to $\sim$ 2-5 % shorter for 1200 rpm compared to 2000 rpm in case of the UM NVO engine, which is considered the primary reason enabling later CA50. If CA90 occurs too late in the cycle, in-cylinder temperature may have already decreased to such an extent that complete combustion is not possible and misfire likely to occur. Note that CA10-90 for the SNL PVO engine is even short ($\sim$ 6 cad) than for the UM NVO engine at 1200 rpm, which could be the reason, for which even later CA50 can be attained for a given P_{int} thus increasing the

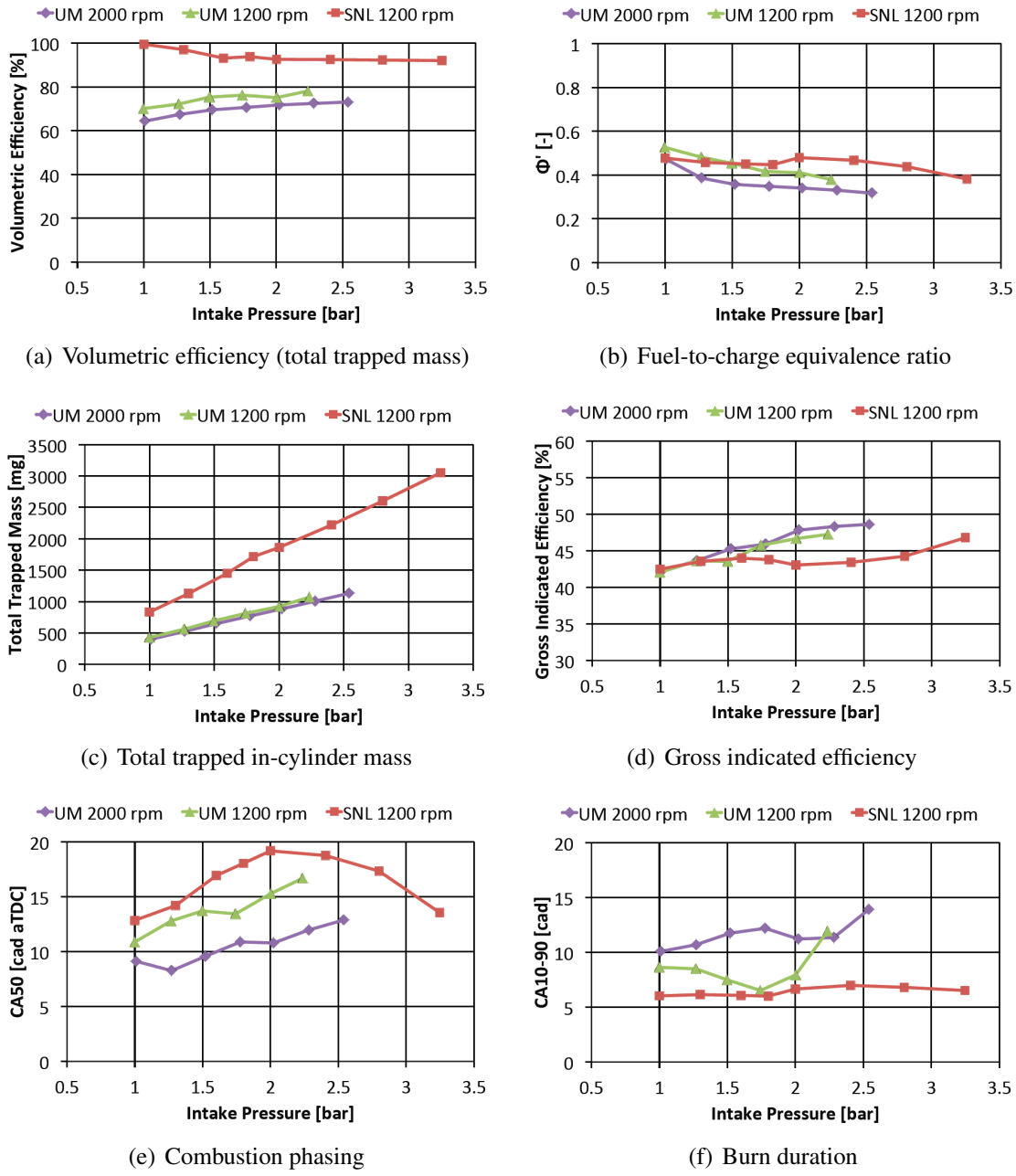

(a) Volumetric efficiency (total trapped mass)

(b) Fuel-to-charge equivalence ratio

(c) Total trapped in-cylinder mass

(d) Gross indicated efficiency

(e) Combustion phasing

(f) Burn duration

Figure 3.23 First set of results as function of intake pressure during maximum load sweeps for two engines and at two different engine speeds in case of UM NVO engine

maximum load range. Another important reason, although maybe of secondary importance, is that low temperature heat release (LTHR) is observed for high P_{int} in case of 1200 rpm.

From Figure 3.24 showing the rate of heat release (RoHR) profiles as function of P_{int} for the UM NVO engine operated at 2000 rpm and 1200 rpm, it is apparent that peak RoHR values are higher in case of the lower engine speed. By closer inspection of the close-up graphs at the bottom in the same figure, one can discern modest amounts of LTHR for P_{int}

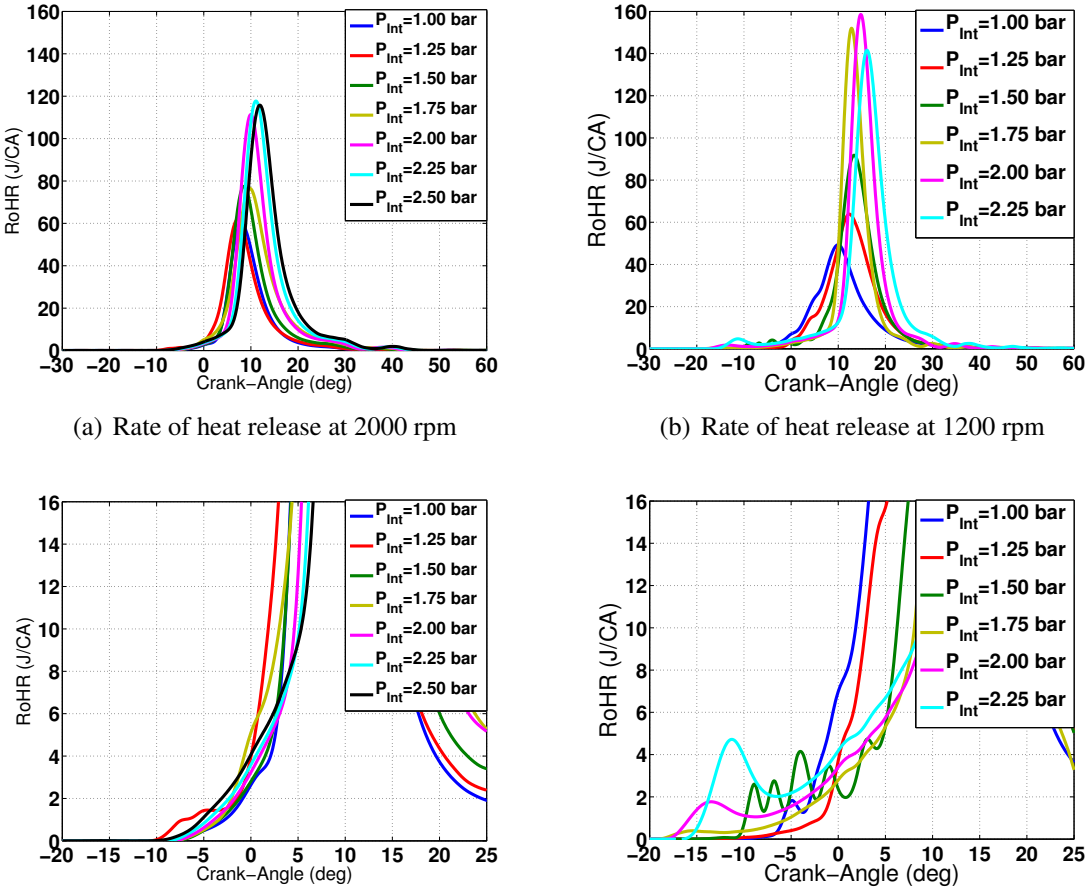

(a) Rate of heat release at 2000 rpm

(b) Rate of heat release at 1200 rpm

(c) Rate of heat release at 2000 rpm (close-up)

(d) Rate of heat release at 1200 rpm (close-up)

Figure 3.24 Second set of results: rate of heat release profiles for various intake pressures at two different engine speeds for UM NVO engine

greater than or equal to 2 bar. Although the magnitude of LTHR is fairly modest, $\sim$ 1.3 % and $\sim$ 3.2 % relative to peak RoHR for P_{int} of 2.0 and 2.25 bar respectively, it is still significant, as it may allow further CA50 retard, because some of the early heat release can partially counteract some of the in-cylinder temperature decrease due to more rapid volume expansion. No LTHR can be observed at 2000 rpm, which indicates that it is the lower engine speed of 1200 rpm in conjunction with elevated intake pressure that shifts the operating point into the low temperature combustion (LTC) regime.

One caveat with operation at lower engine speed, as seen from Figure 3.25, is that NO_Xemissions exceed the limit of 1 g/kg fuel for P_{int} less than 1.5 bar, which is a result of the peak in-cylinder temperature (T_{max}) exceeding the NO_Xformation threshold of $\sim$ 1900 K. Mainly, lower CO emissions, but also slightly lower THC emissions, lead to a modest increase in combustion efficiency for 1200 rpm. The CO decrease is most likely directly

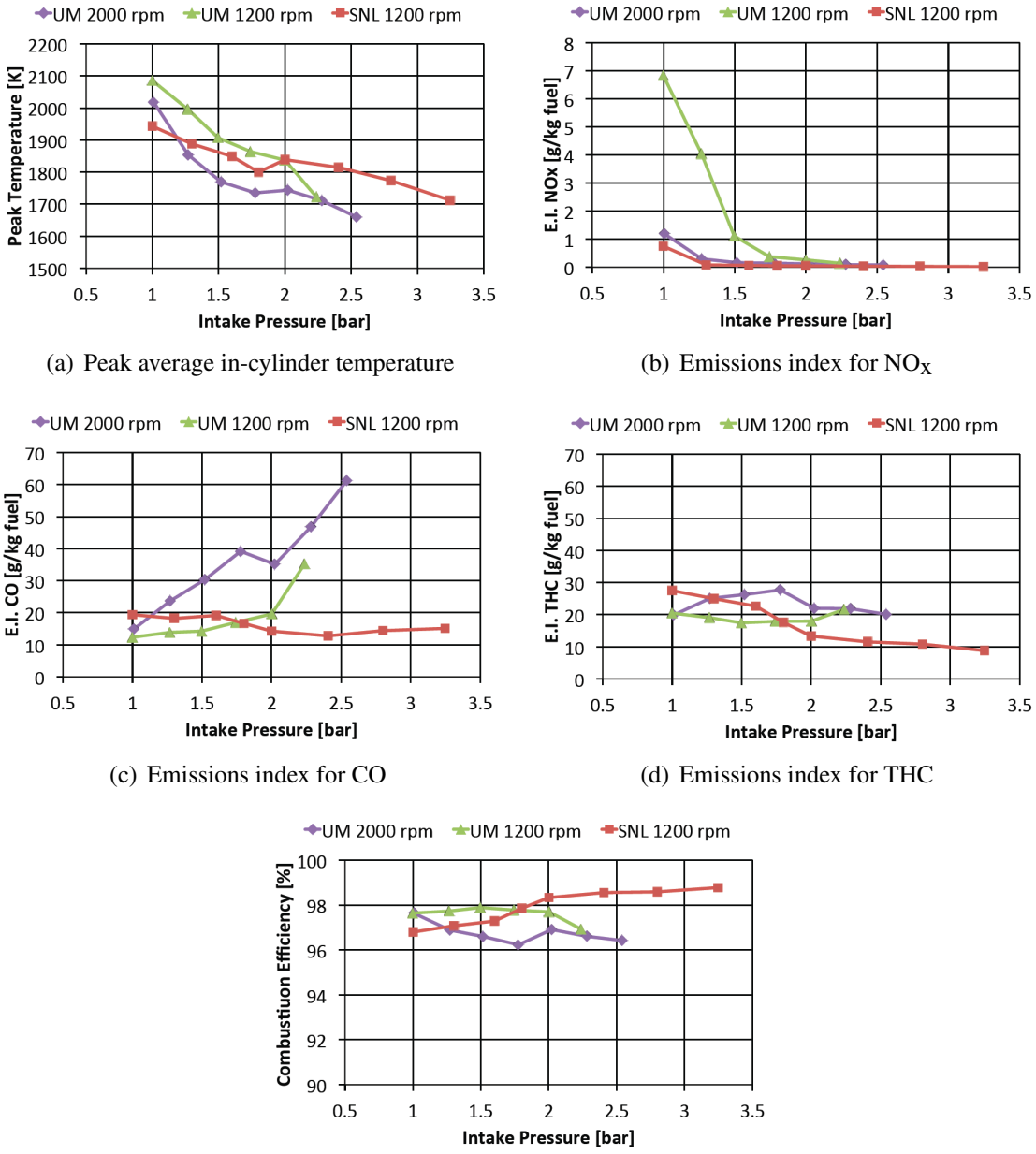

(a) Peak average in-cylinder temperature

(b) Emissions index for NO_X

(c) Emissions index for CO

(d) Emissions index for THC

(e) Combustion efficiency

Figure 3.25 Third set of results as function of intake pressure during maximum load sweeps for two engines and at two different engine speeds in case of UM NVO engine

related to higher T_{max}, which yields more complete combustion in the near-wall regions. The decrease in THC is less pronounced, which could be a consequence of the fact that most THC stems from unburned gas that does not fully convert upon outgassing from crevices due to lower in-cylinder temperature at that particular location and crank-angle degree.

As a result of higher Φ', maximum pressure rise rate (PRR_{max}) with respect to crank-

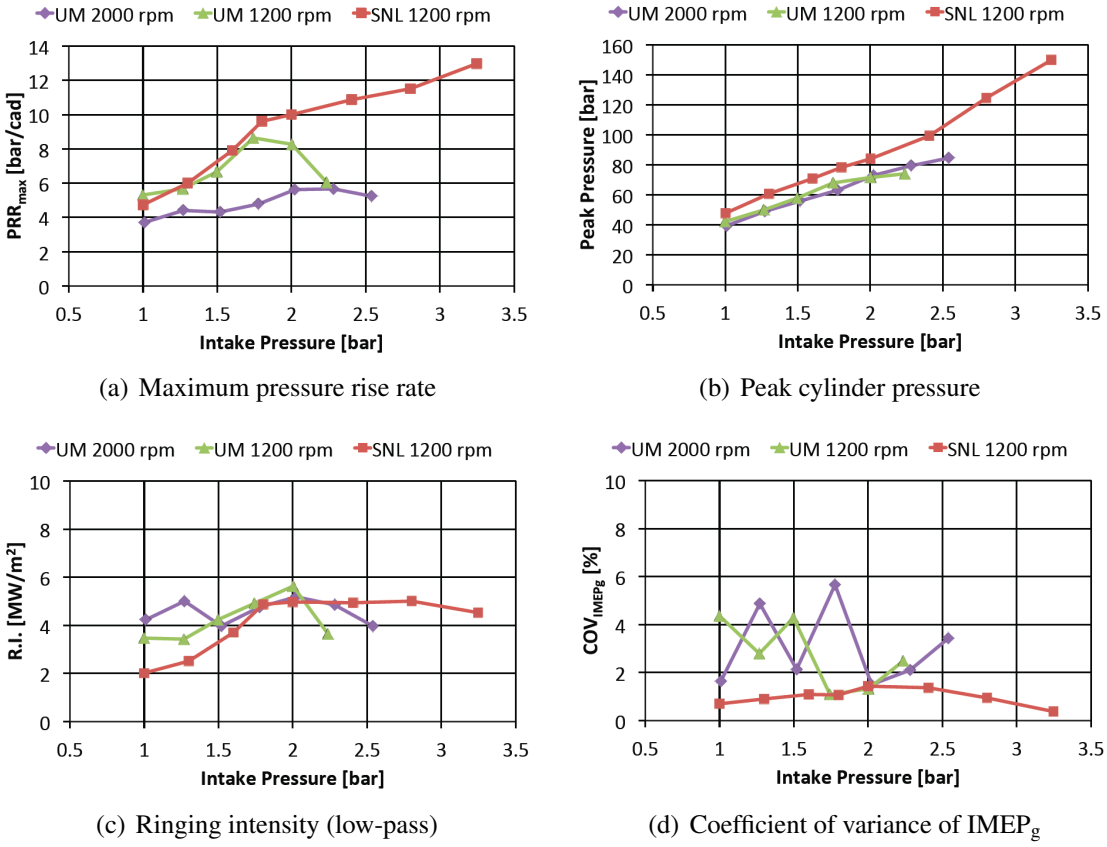

(a) Maximum pressure rise rate

(b) Peak cylinder pressure

(c) Ringing intensity (low-pass)

(d) Coefficient of variance of $IMEP_g$

Figure 3.26 Fourth set of results as function of intake pressure during maximum load sweeps for two engines and at two different engine speeds in case of UM NVO engine

angle degrees can be higher at 1200 rpm, while still meeting the knock constraint (RI= 5 MW/m^2), because RI_{LP} according to equation 2.22 $(dP/dt)_{max}$ is computed on the maximum pressure rise rate based on time and not crank-angle (see Figure 3.26). PRR_{max} decreases for P_{int} greater than 1.75 bar for the UM NVO engine at 1200 rpm, which is thought to be the results of a prolonged CA10-90 (compare Figure 3.23). P_{max} is only marginally higher for 1200 rpm compared to 2000 rpm in case of the UM NVO engine owing to a shorter CA10-90. Note that CA10-90 for the SNL PVO engine is yet shorter and manifests itself in considerably higher P_{max}. Finally, COV of $IMEP_g$ is substantially higher for the UM NVO engine for both engine speeds compared to the SNL PVO engine, that is $\sim$ 3-4 % versus $\sim$ 1 %. This significant difference in COV of $IMEP_g$ makes it more difficult to attain high $IMEP_g$ for a given maximum allowable peak cylinder pressure, $P_{cyl,max}$, because relatively speaking a larger proportion of individual cycles will have a P_{max} value much larger than the mean.

3.3 Comparison to PVO Operation: A Parametric Modeling Study

3.3.1 Motivation

From section 3.2, elaborating on the effects of various engine operating parameters on the maximum load capability of a NVO HCCI engine, it has become apparent that the maximum load limit is primarily determined by engine hardware constraints, namely cam phasing authority (min. NVO) and maximum allowable peak cylinder pressure, in conjunction with ignition delay. Since burn duration is fairly insensitive to these parameters, and for a fixed and retarded combustion phasing required to attain maximum load (CA50=10-15 cad aTDC), ignition timing inherently falls within a narrow range and is almost fixed. In comparison with another well-known boosted HCCI engine at Sandia National Laboratories (SNL), which employs a more conventional positive valve overlap (PVO) strategy with minimal RGF retention, the NVO engine used in this research at the University of Michigan (UM) shows reduced maximum load capability, when the same knock (RI=5 MW/m^2) and combustion variability constraints (COV of IMEP = 3%) are imposed (see Figure 3.27).

The key motivation for section 3.3 is to explore the reasons for these notable differences in maximum load capability, as seen in Figure 3.27, and identify which specific features or parameters, that are different between the UM NVO and SNL PVO engine, contribute most. Table 3.3 shows key parameters of both engines and their respective operating strategies. Besides different engine size, geometry and engine speed, the most notable differences between both engines are the valve strategy and combustion phasing and burn duration. The SNL PVO engine has hardly any RGF in comparison to the UM NVO engine, and is characterized by a faster burn and more retarded combustion phasing. The following subsections will shed light into these different engines and explain the difference leveraging a 1-D engine simulation tool that allows for systematic variation of all the different parameters and being fully able to capture thermodynamics and breathing. Section 3.3.2 will outline the methodology in more detail.

3.3.2 Methodology

A model of the UM single-cylinder NVO engine was built using the 1-D engine simulation software package GT Power as described in section 2.4 of the previous chapter. With the UM NVO engine as starting point, one parameter at a time was systematically varied following the sequence highlighted in Figure 3.28. First, compression ratio was raised, and second, the

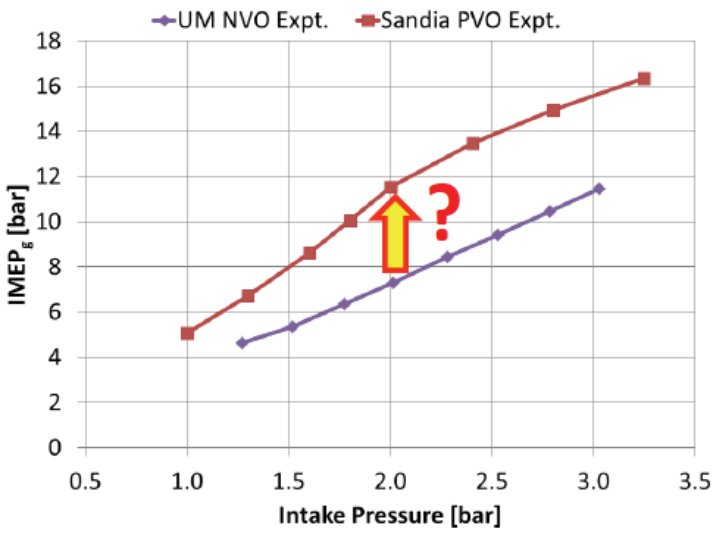

Figure 3.27 Comparison of UM NVO with SNL PVO engine: maximum attainable load vs. intake pressure (SNL data courtesy to Dec)

Table 3.3 Comparison of two fundamentally different boosted HCCI engine setups - University of Michigan NVO and Sandia National Laboratory PVO

Parameter	Unit	UM NVO Engine	SNL PVO Engine
Compression ratio	-	12.4	14.0
Displacement volume	cm^3	549	981
Engine speed	rpm	2000	1200
Valve lift	mm	4.0	10.7
Valve duration	cad	120	240
iEGR / RGF	%	25-40	~ 5
Burn duration (CA10-90)	cad	~ 16.5	~ 6.5
Intake pressure	bar	1.27-3.0	1.0-3.25
Intake temperature	K	~ 320	331-404
Mixture preparation	-	DI	PFI
Combustion phasing (CA50)	cad aTDC	8-13	13-19
Fuel-to-air ratio (Φ)	-	~ 0.9	0.48-0.92

engine size was scaled up. Whereas the former one only required changing a single-entry in the experimental setup window within GT Power, the latter one required a few more adjustments. Increasing the engine size required changing the engine geometry parameters in the corresponding object in GT Power, and in addition, scaling up the valve lifts, valve diameters and diameters of all pipe sections in intake and exhaust systems (see section **??** for details). Third, engine speed was decreased from 2000 to 1200 rpm. Fourth, combustion

phasing (CA50) and burn duration (CA10-90) of the SNL engine are imposed to replace the burn profiles imposed to replace previously imposed values of the UM NVO engine. Fifth, the valvetrain was switched from UM NVO to SNL PVO strategy, which required few adjustments to be made to SNL valve lifts to allow adequate breathing to attain correct fuel-to-charge ratio Φ'. Sixth and last, boundary conditions, including intake temperature, intake pressure, exhaust back-pressure from SNL PVO engine were imposed.

Note that all boundary conditions in the simulation for both UM NVO and SNL PVO engine, including intake temperature, intake composition, intake pressure, and exhaust back-pressure as well as fueling rate and engine speed, were imposed directly from experimental measurements. Figure 3.29 shows these boundary conditions for the starting (UM NVO engine) and end point (SNL PVO engine) of the parameter walk. Note that the SNL PVO engine requires lowering of intake temperature as intake boost pressure and IMEPg increase up to a point where it cannot be further lowered, which is when eEGR is added. The UM NVO engine is operated with increasing amounts of eEGR aiming for a close to stoichiometric mixture. Because NVO is used as combustion phasing control know, intake temperature is almost constant. Also, note that the UM NVO engine operates with noticeable back-pressure.

Burn duration was also imposed, whereby an extra step was taken, that is it was necessary to fit a Wiebe function to the experimentally measured burn profiles by matching combustion phasing (CA50) and burn duration (CA10-90). This was merely done because it is a simple approach deemed adequate enough for capturing impacts on thermal efficiency and maximum load. Note though that no constraint for knock in terms of ringing in intensity was imposed, because no predictive combustion model was used and the Wiebe fit to the actual burn profile might smear out details in the pressure trace affecting peak rate of pressure rise.

Figure 3.30 shows a comparison of simulation versus experimental results for UM NVO and SNL PVO engine. It is clear that IMEPg versus intake pressure was reasonably well predicted by the simulation for both engines, in particular for the UM NVO engine. For the SNL PVO engine trends were in agreement with the experiment. Now, that the methodology has been explained and both start and end point of the parametric study have been benchmarked and validated, the next sub-section will show results and discuss what the key enablers to higher load in case of the SNL PVO engine are, and whether or not GT Power capable of capturing the thermodynamics and breathing process is appropriate for this endeavor.

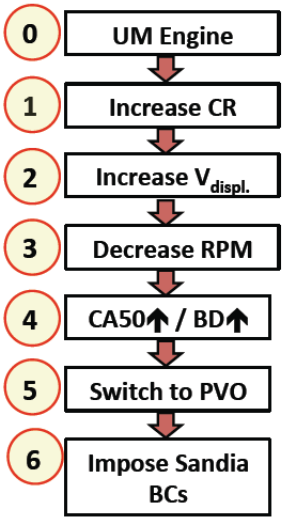

Figure 3.28 Sequence of parametric changes applied in the GT Power Model

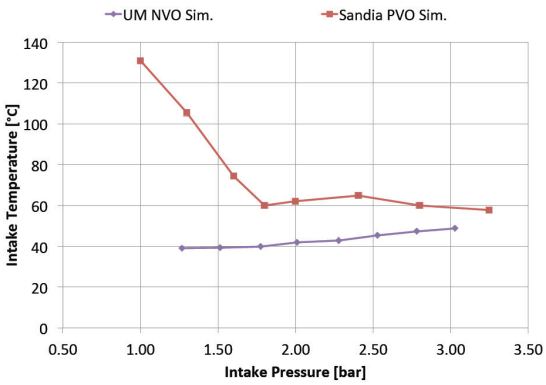

(a) Intake temperature

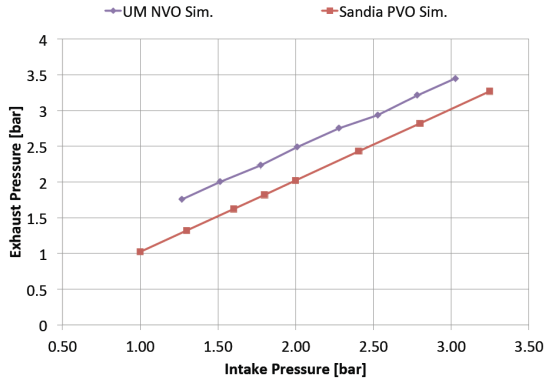

(b) Exhaust back-pressure

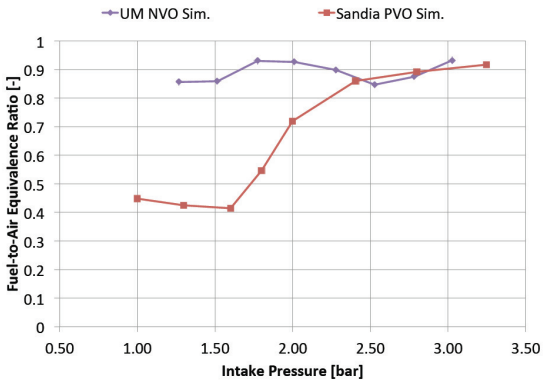

(c) Fuel-to-air equivalence ratio

Figure 3.29 Boundary conditions used for simulation

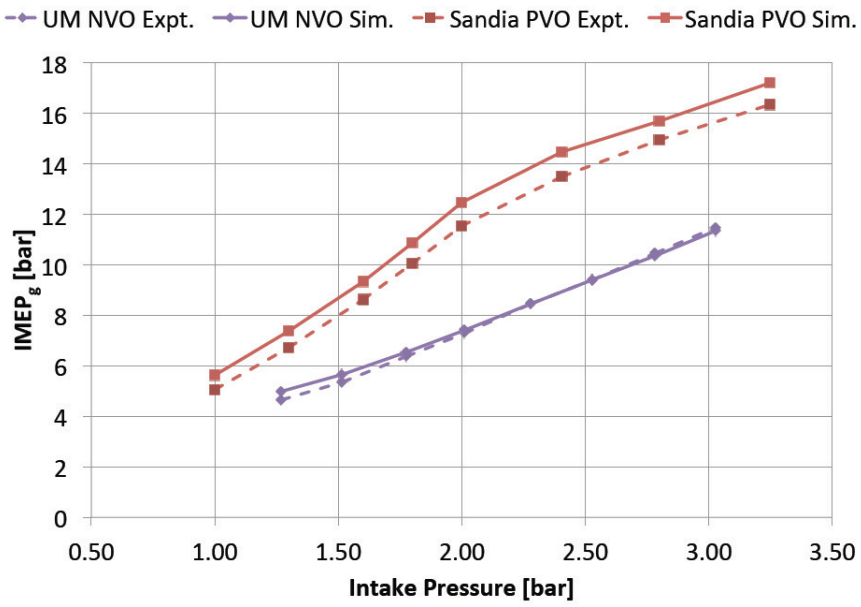

Figure 3.30 Comparison of simulation results with experimental data for both engines

3.3.3 Results

To better be able to interpret the results it is useful to look at maximum attainable load, where load is defined as gross mean indicated pressure (IMEPg), that can be extracted for a given intake pressure, and identify what are the key parameters that might affect it. According to equation (3.1), IMEPg is the amount of useful work normalized by displacement volume. Note that the last three terms in the numerator represent the heat released during combustion that is converted into mechanical work with the thermal efficiency η_{th}. Equation (3.2) shows how fuel mass and total charge mass are related through Φ', whereas equation (3.3) represents an unconventional definition of volumetric efficiency being defined as the ratio of total trapped charge mass and theoretical expected charge mass, being the product of displacement volume and density in the intake runner. Substituting equations (3.2), (3.3) and (3.4), the last one being the ideal gas law applied at intake runner conditions, into equation (3.1) yields an equation ((3.3)) that clearly shows what $\frac{IMEPg}{Pint}$ depend upon.

From (3.5) it is apparent that the first three terms largely determine the maximum IMEPg/ Pint that can be obtained. Combustion efficiency generally is fairly high (around 95-98 %) for HCCI operation and sufficiently high Tmax, and intake temperature cannot be arbitrarily chosen, but instead needs to be a certain value so that with a given valve strategy appropriate TDC temperature can be reached to get right combustion phasing. The last three terms are

constants depending on fuel and composition.

$$IMEP_g = \frac{\eta_{th} \cdot m_{fuel} \cdot \eta_{comb.} \cdot LHV_{fuel}}{V_{disp.}} \tag{3.1}$$

$$m_{fuel} = m_{charge} \cdot FA_{st.} \cdot \Phi' \tag{3.2}$$

$$\eta_{vol.} = \frac{m_{charge}}{V_{disp.} \cdot \rho_{int.}} \tag{3.3}$$

$$\rho_{int.} = \frac{P_{int.}}{R_{int.} \cdot T_{int.}} \tag{3.4}$$

$$\frac{IMEP_g}{P_{int.}} = \eta_{th} \cdot \eta_{vol.} \cdot \Phi' \cdot \eta_{comb.} \cdot \frac{1}{T_{int.}} \cdot \frac{1}{R_{int.}} \cdot FA_{st.} \cdot LHV_{fuel} \tag{3.5}$$

Figure 3.31 shows the final results of the parametric study in terms of $IMEP_g$ vs. P_{int}. Whereas lines corresponding to cases 0 through 4 are very similar with respect to max. $IMEP_g$ for same P_{int}, cases 5 and 6 that is after switching to PVO cam profile show significantly higher $IMEP_g$. Generally, the SNL PVO engine can reach a higher $IMEP_g$ and the difference becomes more pronounced at higher intake pressures. Since the trends of all lines with respect to pressure are all very similar, it is instructive to look at two intake pressures and make a detailed comparison along the parameters mentioned before i.e. thermal efficiency, volumetric efficiency etc. For this purpose intake pressures of P_{int}=1.3 and P_{int}=2.8 bar were chosen.

Figure 3.32 shows relevant plots pertinent to thermal efficiency. Increasing compression ratio (CR) yields a relative increase in thermal efficiency of $\sim 2\%$. Scaling up the engine size and lowering engine speed both have no significant effect on relative heat loss and thermal efficiency. Retarding CA50 and shortening the burn duration leads to a $\sim 1-2\%$ relative decrease in thermal efficiency, indicating that combustion phasing retard outweighs the benefits of a faster burn, because expansion work is done less effectively for this later combustion phasing. Switching from NVO to PVO operation increases thermal efficiency by $\sim 2-4\%$ relative depending on intake pressure. This can be explained largely by a significant reduction in relative heat loss by $\sim 40-50\%$. Note that although various factors seem to affect thermal efficiency, the absolute change is relatively small, at most 2-4 % relative. Since thermal efficiency is certainly not the primary enabler for higher efficiency of the SNL PVO engine, it is useful to look at other parameters.

Figure 3.33 shows results from the point of view of volumetric efficiency. Volumetric efficiency, which accounts for all trapped mass including iEGR and eEGR at IVC, shows a

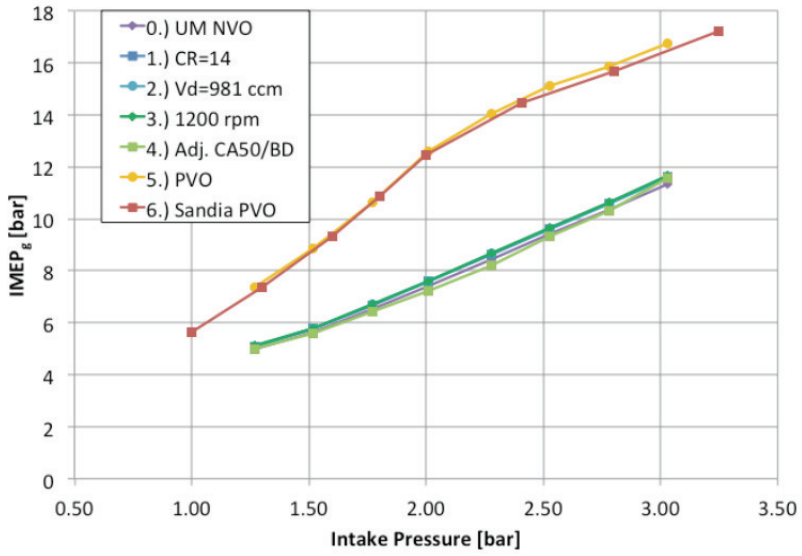

Figure 3.31 Simulation results from parameter walk

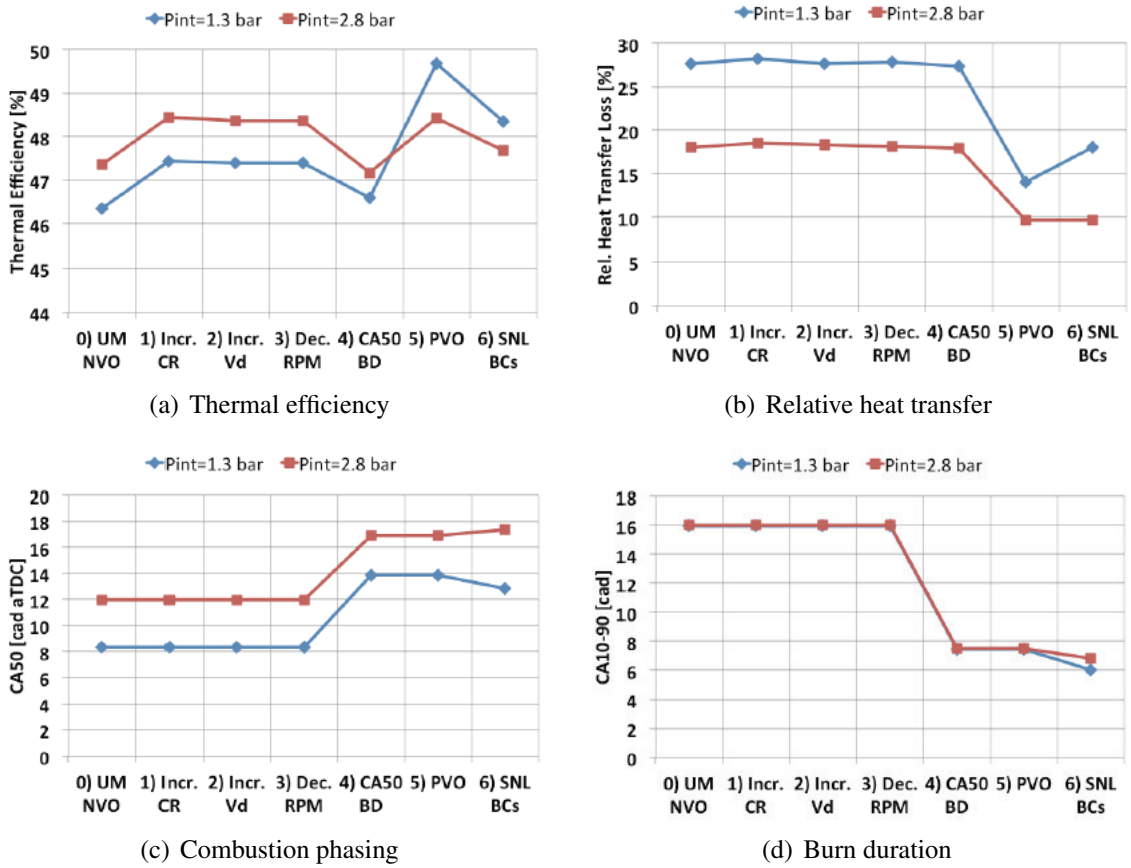

(a) Thermal efficiency

(b) Relative heat transfer

(c) Combustion phasing

(d) Burn duration

Figure 3.32 Thermal efficiency consideration: results from parameter walk for two intake pressures

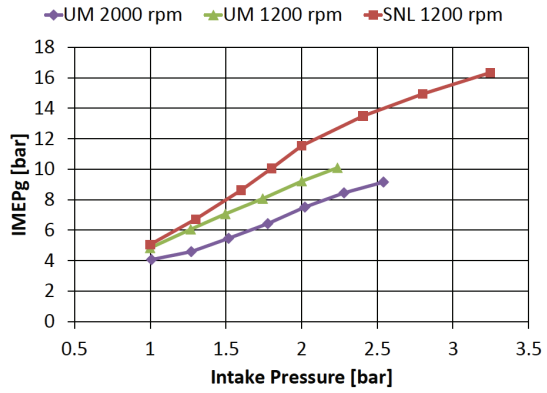

(a) Volumetric efficiency based on total trapped mass

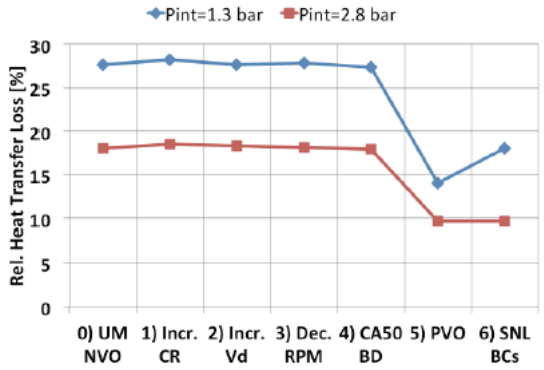

(b) Relative heat transfer

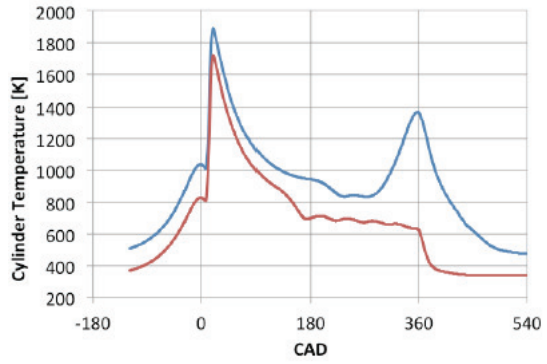

(c) In-cylinder temperature trace

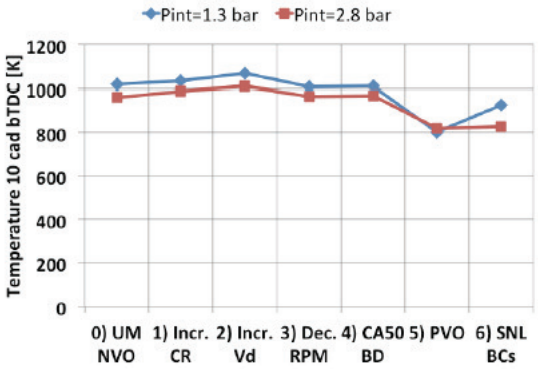

(d) In-cylinder temperature 10 cad bTDC

Figure 3.33 Volumetric efficiency consideration: results from parameter walk for two intake pressures

significant relative increase of $\sim 50\%$ when changing from NVO to PVO. Note from the in-cylinder temperature profiles (Figure 3.33 (c)) that the NVO engine (case 0) shows much higher average cylinder temperature than the PVO engine (case 7),in particular during the recompression event, which can explain the significant decrease in relative heat loss when switching from NVO to PVO. Another interesting difference is that switching from NVO to PVO (case 4 to 5) yields a $\sim 20\%$ lower in-cylinder temperature, 10 cad before TDC. This is due to ignition requirements and will be explained later, but as a consequence cylinder temperature is relatively lower during combustion in case of PVO operation.

From Figure 3.34 showing results in terms of Φ', it becomes apparent that Φ' does not change very much in most cases, with the exception when switching from NVO to PVO (cases 4 and 5), where Φ' increases modestly. Note also, that as boost pressure is an enabler for high load operation, the higher intake pressure case shows generally lower Φ' than the low intake pressure case. Looking at Figure 3.34 (b), one can see that the maximum pressure rise rate remains unchanged until combustion phasing is retarded and burn duration

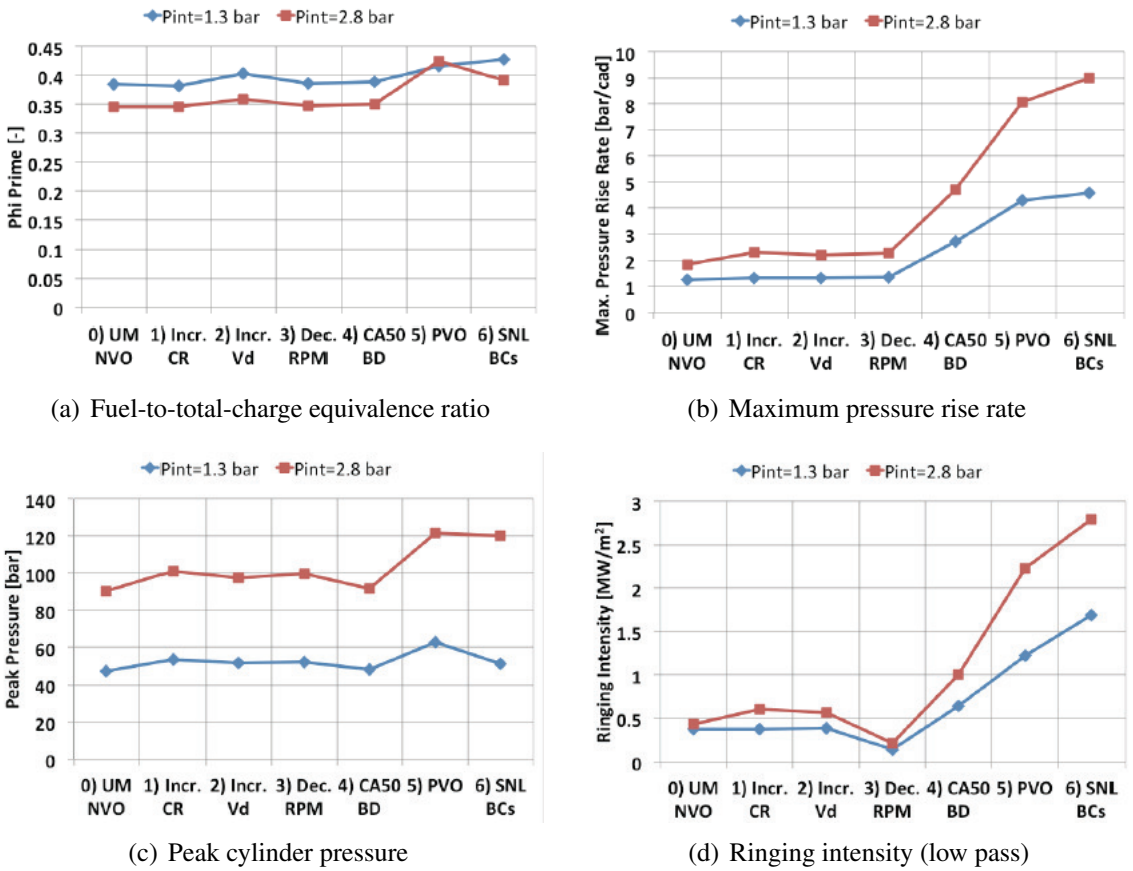

(a) Fuel-to-total-charge equivalence ratio

(b) Maximum pressure rise rate

(c) Peak cylinder pressure

(d) Ringing intensity (low pass)

Figure 3.34 Φ' consideration: results from parameter walk for two intake pressures

shortened (cases 3-4), where it rises, owing to the decrease in burn duration. When switching from NVO to PVO (cases 4 to 5), maximum pressure rise rate increases again noticeably, because Φ' is increased and more energy is released. Peak pressure increases as well for the same reason for switching valve strategy. Figure 3.34 (d) shows ringing intensity, and one can see a decrease when lowering engine speed (cases 2 to 3), which is no surprise, because it is the dP/dt enters RI calculation and a lower engine speed yields longer dt interval. The increases for changing CA50 and CA10-90 as well as switching to PVO merely reflect increases in dP/dtheta. Finally, when imposing the SNL boundary conditions (cases 5 to 6), PRRmax and RI increase still, especially for lower intake pressure, because Φ' increases.

In summary, from this parametric study in GT Power, one can determine the valve strategy i.e. switching from NVO to PVO and reducing the engine speed as two key enablers. There are several benefits associated with the switch from NVO to PVO operation. First, a much lower lower RGF content is used, hence lower IVC temperature, which yields a higher charge density at IVCn hence more diluent can be trapped. This allows more fuel to be injected to maintain a fixed Φ'. Second, there is simply less flow restriction through

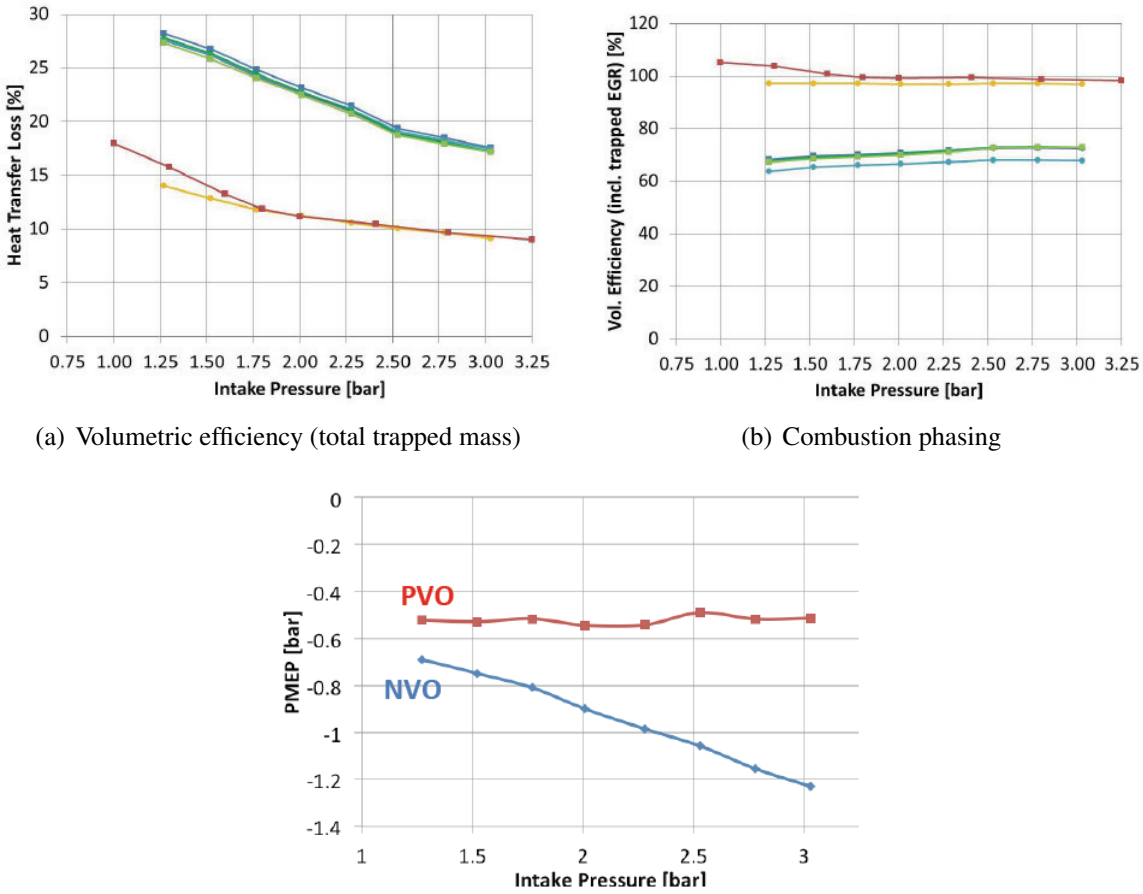

(a) Volumetric efficiency (total trapped mass)

(b) Combustion phasing

(c) Maximum attainable IMEPg

Figure 3.35 Effect of switching from NVO to PVO operation

the valves because of longer duration and larger valve lifts, so the flow will be less throttled when passing through the valves, which allows higher volumetric efficiency as well. The engine speed effect was already demonstrated in section 3.2.5 and has two components to it: a direct one and an indirect one. From the parametric study it has become apparent that burn duration alone is not a key enabler, but CA50 retard that comes with it. It is through later CA50, that allows for a decrease in ringing intensity so that more fuel can be injected to maintain fixed RI. A small additional benefit of low engine speed is increased volumetric efficiency due to improved wave dynamics in the runner. It was found that engine parameters such as compression ratio and engine size are of lesser importance.

3.4 Summary and Conclusions

3.4.1 Summary of Results and Discussion

The goal of this chapter was to explore how various engine operating parameters, including diluent (eEGR vs. air), intake temperature, overall-turbo charger efficiency (OTE) and engine speed, affect the internal thermo-physical state of the fuel-air-EGR mixture, ignition and combustion, and to quantify how the maximum load limit in terms of maximum attainable $IMEP_g$ as a function of P_{int} is affected. The relative importance of each of these was investigated, and the following order was found starting from the effect with largest impact to those with lesser impact: engine speed effect, diluent (eEGR vs. air), OTE effect, intake temperature effect. Moreover, a parametric study using GT Power was conducted in an attempt to first verify if the different maximum $IMEP_g$ between the UM NVO and SNL PVO engine can be explained with thermodynamics and breathing and second to identify key enablers and distinguish those from less important parameters.

Replacing part of the incoming air with eEGR facilitates higher load mainly because of ignition delay implications. To maintain a similar CA50 despite less O_2, a higher pressure and temperature at TDC are required, where the latter one is accomplished with more NVO. This gives more leverage regarding cam phasing authority of engine and so the minimum NVO limit is reached at a higher pressure and load respectively. The only drawback of eEGR is a slightly lower gross efficiency mainly because of mixture properties. A lower intake temperature allows for higher load for the same reasons as eEGR. Higher OTE or lower dP is not only beneficial from T/C-overall system efficiency standpoint, but also because of its positive effect on HCCI combustion, in particular a larger operating range, which is especially important for HCCI that only works for a narrow range.

High load in a NVO engine at a given intake pressure is limited by volumetric efficiency. Switching from NVO to PVO removes a breathing restriction and decreases pumping work. It also eliminates large amounts of iEGR trapped and facilitates a higher IVC charge density allowing for more fresh charge to be inducted. Lowering the engine speed from 2000 rpm to 1200 rpm not only improves volumetric efficiency, but also facilitates further CA50 retard that is augmented by LTHR at higher P_{int} and higher loads.

3.4.2 Appraisal of Results and Contributions

The results shown in this chapter indicate that intake boosting is an enabler for extending the high load limit in a NVO HCCI engine, because it facilitates later CA50 hence allows

higher fueling rates while still keeping ringing intensity in check. For a practical NVO engine, having the appropriate thermo-physical state of the fuel-air-EGR mixture around TDC is crucial to achieving auto-ignition that leads to the correct combustion phasing. The engine hardware itself ultimately poses the limiting constraint, as NVO cannot be reduced below 74 cad for the UM NVO engine and the maximum allowable peak cylinder pressure of 120 bar cannot be exceeded. The type of diluent (eEGR vs. air), intake temperature and overall-turbocharger efficiency merely affect the shape of the maximum load ($IMEP_g$ vs. P_{int}) curve, but they determine at what $IMEP_g$-P_{int}-combination a hard stop due to engine constraints is hit.

The potential of PVO relative to NVO operation has been explored thorough a parametric modeling study, starting from the UM NVO engine by successively varying individual parameters to approach the SNL PVO engine. It could be shown that the potential benefits in terms of maximum attainable $IMEP_g$ for a given P_{int} can be largely explained by thermodynamics and breathing considerations, which are adequately captured by GT Power. Since the the predictive combustion model was removed and instead burn duration for the start and end point of the parameter walk imposed, it is assumed that all parametric changes other than switching from NVO to PVO have no effect on combustion. This may not necessarily be true, but cannot be evaluated here. It is important to see burn duration not by itself but in conjunction with maximum allowable CA50 and COV. Despite shorter burn duration, the SNL PVO engine can achieve higher loads because of later CA50. It is not clear if later CA50 is the result of short burn duration and/ or much lower cyclic variability. The SNL PVO engine exhibited much lower cyclic variability (COV of $IMEP_g$), even at the stability limit, compared to the UM NVO engine, which could facilitate later CA50.

3.4.3 Shortcoming of Results and Next Steps

From the experimental and modeling results presented earlier in chapter 3, and from the discussion, summary and contributions stated in sections 3.4.1 and 3.4.2, it has become evident that that the UM NVO engine, in principle, is capable of as high a maximum load as the SNL PVO engine, provided that enough charge can be trapped and combustion phasing can be sufficiently retarded. The thermodynamic and breathing aspects have been satisfactorily understood by now, after carrying out the parameter walk between the two engines in GT Power, but it still remains unclear why the burn duration of the SNL PVO engine is significantly shorter than that of the UM NVO engine and also how it is affected by various fundamental thermo-physical variables.

Whereas the maximum load sweep experiments used for almost all experimental results

presented in section 3.2 benefited from the fact that only few data points were required to explore the maximum load limit as a function of intake pressure for a wide range of conditions, they have not been able to facilitate isolation of the effects of key thermophysical variables such as pressure, composition (O_2content), and stratification (NVO) on burn duration. At this point, it is not possible to make more conclusive statements about these effects, because P_{int}, Φ', χ_{O_2}, and NVO all have been varied at the same time. Therefore, a more controlled set of experiments is required to gain additional insight into how burn duration is affected by these. Chapter 4 will deal with this shortcoming, as a much more controlled experimental procedure is used in an attempt to to shed light on the individual effects of boost pressure and oxygen content on burn duration.

The UM NVO engine exhibits a much higher degree of combustion variability near the stability limit, which manifests itself in considerably higher values of COV of $IMEP_g$ when compared to the SNL PVO engine. Based on this observation and the fact that later CA50 is a high load enabler, it is clear that both combustion phasing limits, knock and combustion variability, together affect the maximum attainable $IMEP_g$ for a given P_{int}. Again, with the experimental approach used in this chapter, varying a myriad of parameters and operating at knock and combustion variability limits simultaneously, it is not possible to understand how these two phasing limits are affected by the aforementioned more fundamental thermophysical variables. Therefore, chapter 5 will attempt to identify how both combustion phasing limits are affected using more controlled and targeted experiments.

Chapter 4

Burn Duration: Effects of Composition and Boost Pressure

The hypothesis, that HCCI combustion is a cascade of sequential auto-ignition events, whose progression is primarily determined by temperature gradients due to thermal/ compositional stratification and to a much lesser extent by chemical kinetics, is probed in this chapter by exploring how burn duration is affected by fundamental thermo-physical parameters such as intake boost pressure and O_2 concentration. To test the hypothesis, experiments that take advantage of the high level of independent control over intake and exhaust conditions of this engine setup are performed. Combustion phasing (CA50) and negative valve overlap (NVO) are held constant, while O_2 concentration is adjusted via addition of external EGR (eEGR). The findings in this chapter motivate the need for investigating combustion phasing limits as function of these two and other thermo-physical variables in the following chapter.

4.1 Objective

This chapter addresses the most fundamental thermo-physical aspects of the three results chapters, 3, 4 and 5, with the goal of exploring if and to what extent burn duration under boosted HCCI operation is affected by intake boost pressure and O_2 concentration. In chapter 1, it has been hypothesized that HCCI combustion can be comprehended as a cascade of sequential auto-ignition events, which seems to be supported by results from recent research findings. The relevance of boost pressure in particular, as in how it could potentially affect and alter the view of the auto-ignition cascade, has not been subject of any studies in a NVO engine up to this point.

Since the beginning of research on HCCI engines, there has been the notion that combustion and especially burn duration are predominantly determined by chemical kinetics representing the view that a uniform fuel-air-EGR mixture undergoes bulk auto-ignition. Najt and Foster suggested that the completion of combustion via oxidation of CO to CO_2

is kinetically limited and proposed an expression, termed 'apparent energy release rate' or AERR, to capture bulk heat release at CA50 as a function of several engine parameters [144, 14]. Although the view of kinetics being of importance for ignition and completion of combustion in principle is correct, the conceptual model proposed implicitly assumes a perfectly homogeneous fuel-air-EGR mixture treating the mixture in the internal combustion engine like a continuously stirred chemical reactor, which is not necessarily true. Recent experimental research work by Rothamer et al. [98] and Dronniou and Dec [142] have shown that thermal and compositional inhomogeneities may have a much greater bearing on the combustion burn rates than previously thought. Recent CFD simulation work by Kodavasal investigating the effect of mixture preparation, by comparing two valve strategies, and attempting to separate contributions from thermal and compositional stratification suggested that thermal inhomogeneities are the major cause for a noticeable decrease in burn rates and that compositional inhomogeneities are less important [56]. His work also identified that different thermal properties are largely responsible for a reduced burn rate when comparing an O_2 deprived condition with an O_2 rich condition.

To date, there has not been any attempt to quantify the effect of boost pressure in conjunction with O_2 concentration under highly controlled conditions in a NVO engine. Previous work either used a conventional PVO engine or was done under naturally aspirated conditions. All NVO work reviewed looking at parametric changes lacked the degree of control to isolate the effect of pressure and O_2 from other parameters. This motivates the need for such an experiment in this thesis, as there are no results showing the dependency of burn duration on intake boost pressure in a NVO engine. If the hypothesis stated earlier was not true, increased intake boost pressure could potentially significantly alter the burn profile and may be considered as a potential control knob to manipulate combustion and keep knock in check.

4.2 Experimental Procedure

This experiment is the most controlled amongst all presented in this dissertation and takes full advantage of the high level of independent control over many engine parameters by maintaining as many parameters as possible constant and selectively varying those of interest.

For each intake boost pressure, P_{int} = 1.5 bar, 2.0 bar and 2.5 bar, increasing amounts of external EGR (eEGR) are added, which lead to a richer mixture (higher Φ). In order to maintain constant combustion phasing, CA50, intake temperature, T_{int} is increased. Φ'

Table 4.1 Experimental conditions during Φ/ eEGR sweeps at different intake boost pressures

Parameter	Value	Unit
Engine speed	2000	rpm
Fuel flow rate	10 -18	mg/cycle
Fuel pressure	100	bar
Intake pressure	1.0 - 2.5	bar
Pressure differential (P_{exh}-P_{int})	0.5	bar
Intake charge temperature	55 - 240	°C
Negative valve overlap @ 0.1 mm lift	90	cad
Coolant temperature	90	°C
Oil temperature	90	°C
Fuel injection timing	330	cad bTDC
External EGR	0 - 50	%

is kept approximately constant for each Φ/ eEGR sweep and in between different P_{int} by scaling fueling rate in proportion to P_{int}. NVO and pressure differential, dP = P_{exh} - P_{int}, are held constant at 90 cad and 0.5 bar respectively to minimize any potential bias due to thermal/ compositional stratification associated with changes in NVO/ iEGR. Table 4.1 shows experimental conditions during the Φ sweeps at three different P_{int}. From Figure 4.1, one can see that T_{int} was used as combustion phasing control knob and that EGR rate and Φ' are almost identical between all three P_{int}. The only caveat is that total trapped mass decreases as Φ increases owing to a lower IVC charge density due to the higher intake temperature. Consequently, Φ' slightly increases as Φ increases.

4.3 Experimental Results

4.3.1 Burn Duration

Crank-angle locations, where 5 %, 50 % and 90 % of the fuel mass are burned corresponding to start, mid-point, and end of combustion, are shown for different intake boost pressures as function of the fuel-to-air equivalence ratio in Figure 4.2. While combustion phasing (CA50) is held constant, burn duration (CA05-90) seems to be relatively unaffected by boost pressure and composition i.e. Φ. In particular, CA90 is virtually insensitive to both P_{int} and Φ implying that the second half of combustion is completely unaffected by these two parameters. However, start of combustion (CA05) advances moderately by $\sim$ 2 cad as

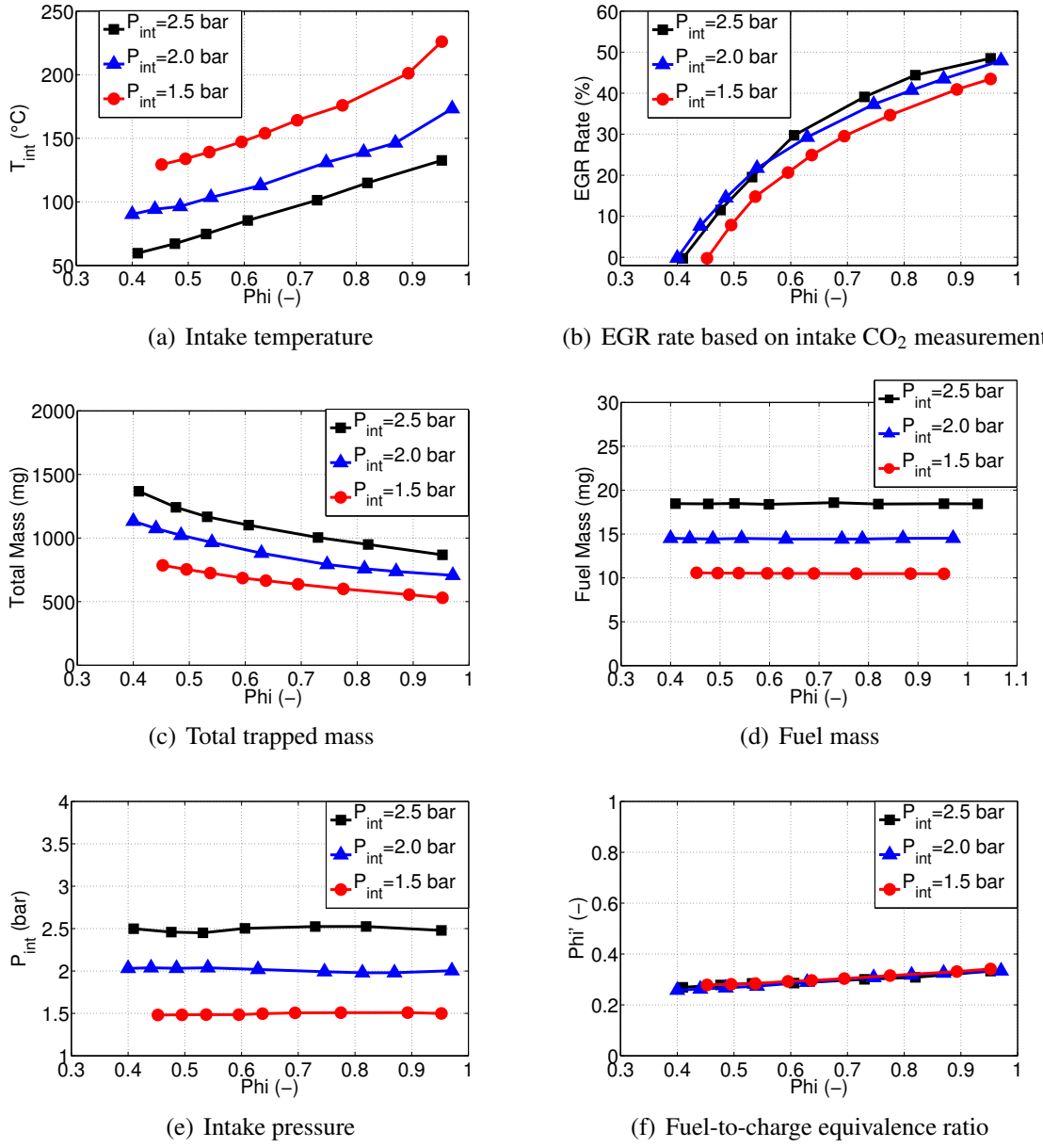

(a) Intake temperature

(b) EGR rate based on intake CO_2 measurements

(c) Total trapped mass

(d) Fuel mass

(e) Intake pressure

(f) Fuel-to-charge equivalence ratio

Figure 4.1 Boundary conditions as function of fuel-to-air equivalence ratio Φ for different intake pressures

eEGR is added and Φ increases from ~ 0.4 to ~ 0.95. Increased intake boost pressure leads to slightly later CA05 by ~ 0.5 cad when P_{int} is raised from 1.5 bar to 2.5 bar, which has only a minor effect on the first half of combustion (CA05-50). Although the composition and pressure effects are moderate and small respectively, a repetition of this particular experiment confirmed the exact same trends with respect to Φ and P_{int}.

Peak rates of heat release, $RoHR_{max}$, are clearly separated due to different fueling rates and energy inputs for the different P_{int}, but there is no clear trend with Φ. Looking at the

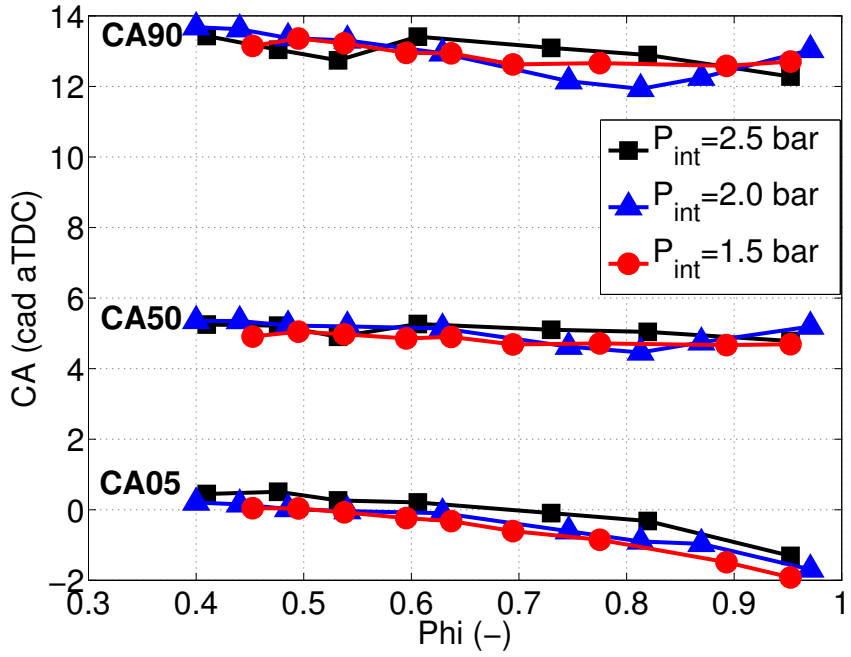

Figure 4.2 Burn profiles: crank-angles with 5 %, 50 % and 90 % mass fraction burned (CA05, CA50 and CA90) as function of fuel-to-air equivalence ratio for three intake boost pressures

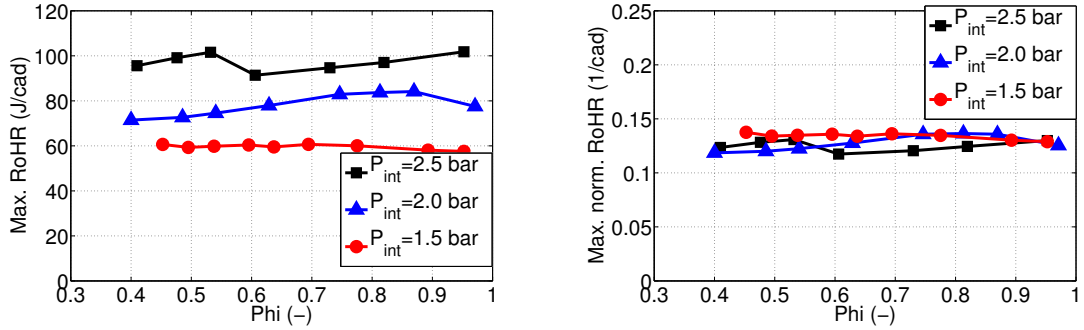

(a) Peak rate of heat release

(b) Normalized peak rate of heat release

Figure 4.3 Absolute and normalized peak rate of heat release as function of fuel-to-air equivalence ratio Φ for different intake pressures

normalized $RoHR_{max}$ no clear trends with respect to P_{int} and Φ can be identified indicating that the effects of composition and boost pressure are subtle (see Figure 4.3). Note, though, that no clear inverse relationship between CA05-90 and $RoHR_{norm.,\,max}$ can be seen.

Taking a closer look at the RoHR profiles and average in-cylinder temperature for combinations of the highest and lowest P_{int} and Φ respectively provides additional insight into the aforementioned subtle changes with composition and boost pressure. As seen in Figure 4.4, although the peak RoHR values are identical between different Φ for each P_{int}

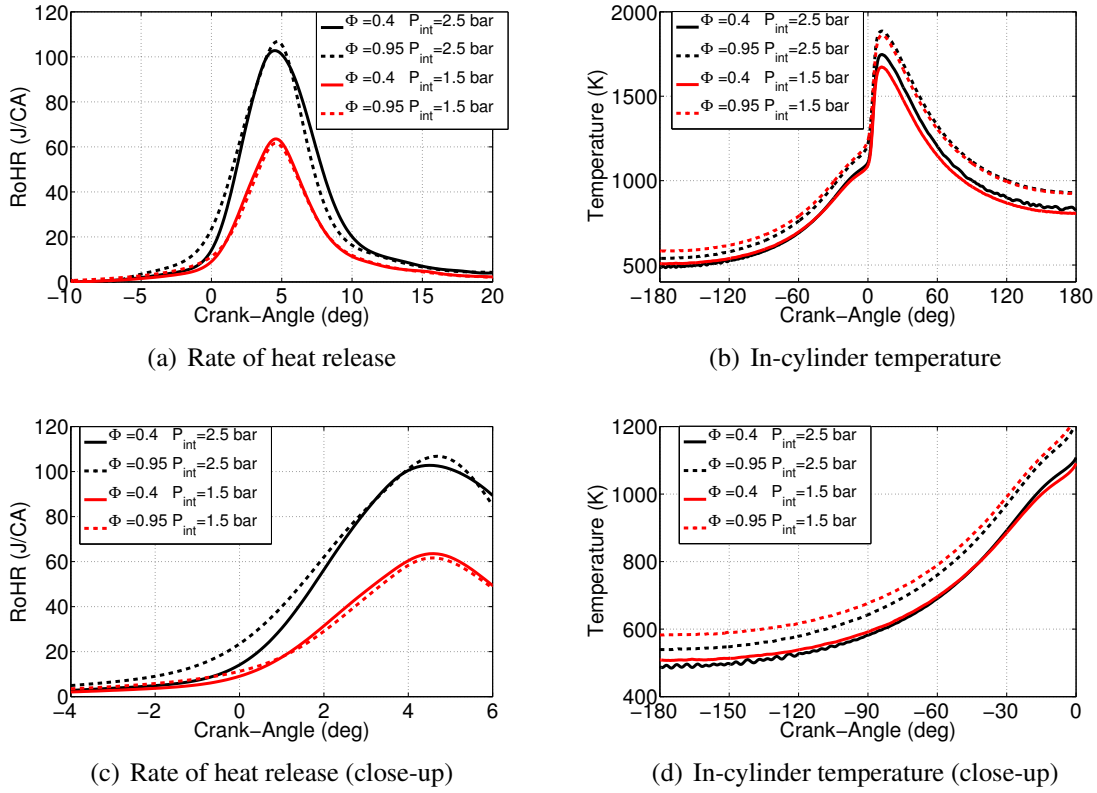

(a) Rate of heat release

(b) In-cylinder temperature

(c) Rate of heat release (close-up)

(d) In-cylinder temperature (close-up)

Figure 4.4 Rate of heat release and average in-cylinder temperature as function of crank-angle for 4 data points

and shapes at first glance look similar, closer inspection reveals that RoHR for each P_{int} with Φ=0.95 starts to increase at a relatively earlier crank-angle and the slope is less than in case of Φ=0.4. In-cylinder temperatures show a similar trend.

4.3.2 Composition Effect

There are a myriad of potential physical phenomena that can be used to explain the observed differences in CA05-90 with respect to composition including thermodynamic properties, chemical kinetics, and thermal/ compositional stratification. This section will look at each of them in an effort to justify the findings, but no definite statements can be made that is attribution to and quantification of each phenomenon is not possible. However, based on the review in Chapter 1 various aspects can be evaluated and their validity tested with this boosted data set under very controlled conditions.

Replacing part of the incoming air with eEGR thus increasing Φ from 0.4 to 0.95 leads to an increase of the isobaric specific heat capacity of the mixture, C_p, because diatomic

molecules such as O_2 and N_2 are replaced by triatomic molecules such as CO_2 and (see Figure 4.5). Triatomic molecules can store energy more easily than diatomic ones, because a larger number of vibrational and rotational modes are available owing to their structure. This thermal effect associated with different thermodynamic properties for different Φ can be considered to be the primary reason responsible for slightly longer first half of combustion (CA05-50) because of more advanced CA05 for the case of $\Phi = 0.95$ relative to the case of $\Phi = 0.4$. Therefore, the higher value of C_p for the eEGR dilute case is responsible for a slower propagation of auto-ignition throughout the fuel-air-EGR mixture in the combustion chamber due to the larger thermal inertia, which is in agreement with findings by previous workers [33, 56].

A higher in-cylinder temperature, both at intake valve closing, T_{IVC}, and 10 cad bTDC, T_{10}, in case of $\Phi = 0.95$ is required to maintain combustion phasing and to compensate for the decrease in O_2 and fits within the realm of the ignition delay expression (see Figure 4.6). Decreasing O_2 with increasing Φ certainly has an impact on ignition and could potentially also affect combustion that is the cascade of auto-ignition in a HCCI engine. For example, one could imagine that for the reduced O_2 case (Φ=0.95) there is almost no excess O_2 especially toward the end of combustion so that during the later stage of combustion RoHR would decrease indicating kinetic limitations. However, this cannot be seen from the RoHR plots in Figure 4.4 indicating that mixing is not a limitation of combustion and/ or combustion is not kinetically limited once auto-ignition has occurred. Recent computational work by Kodavasal strongly suggests that the thermal effect due to changes in thermodynamic properties, i.e. higher specific heat capacity, is relatively much more important than the kinetic effect, i.e. lower O_2 concentration [56].

Thermal stratification may also contribute to a moderately longer CA05-50 with increasing eEGR/ Φ. A more eEGR dilute mixture characterized by a higher Φ value requires a higher TDC temperature, which, based on the experimental findings by Lawler [100], should lead to more thermal stratification. A larger thermal width or wider temperature distribution due to increased heat transfer from the core to the walls, because of a higher TDC temperature, can lead to slower combustion i.e. longer CA05-50. Note that in an IC engine it is not possible to maintain fixed TDC temperature, CA50, and NVO but different composition. This would simply over-constrain the system, and in this experiment an effort was made to minimize bias due to CA50 and thermal/ compositional stratification, so TDC temperature had to be adjusted to maintain CA50 while eEGR was added, hence thermal stratification due to different TDC is unavoidable and one cannot conclusively gauge, whether the thermodynamic property or the thermal stratification effect contributes more to the moderate CA05-50 increase with increasing Φ.

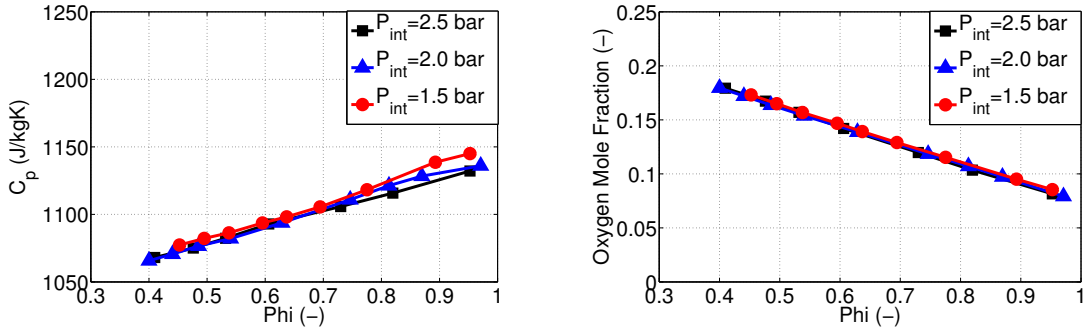

(a) Specific isobaric heat capacity

(b) In-cylinder oxygen concentration

Figure 4.5 Heat capacity and oxygen content as function of fuel-to-air equivalence ratio Φ for different intake pressures

Lastly, fuel-to-charge ratio, Φ', increases relatively by $\sim$ 10 % slightly when Φ increases from 0.4 to 0.95, because intake temperature, T_{int}, was raised to maintain constant CA50 while eEGR was increased and composition modified. Although IVC timing, intake and exhaust pressure were fixed, gas density at IVC decreases with increasing T_{int}/ Φ. This leads to lower total trapped mass and consequently higher Φ' in spite of using the same fueling rate. Higher Φ' generally implies a shorter burn duration i.e. CA05-90. This means that if the experiment was done at perfectly fixed Φ', CA05-90 could be even longer than it was, concealing the other effects to some extent, most notably due to thermodynamic properties and thermal stratification.

4.3.3 Boost Pressure Effect

Similar to composition in section 4.3.2, there are also multiple ways to explain the observed differences in CA05-90 with respect to intake boost pressure including chemical kinetics and thermal/ compositional stratification. This section will discuss each of them in an effort to justify the findings, but no conclusive statements can be made that is attribution to and quantification of each phenomenon is not possible.

Elevated intake boost pressure, P_{int}, is known to promote chemical kinetics and leads to earlier and faster ignition given everything else remains fixed. For this reason, at the same air/eEGR dilution condition (Φ), temperature needs to be lower around TDC to maintain constant CA50, because Φ' and Φ are the same. Note, however, once ignition of a certain portion of the charge has occurred, a higher P_{int} might conceivably also promote faster combustion due to chemical kinetics. But the measurement shortening of CA05-50 with increasing P_{int} seems very small ($\sim$ 0.5 cad), indicating that the effects due to kinetics

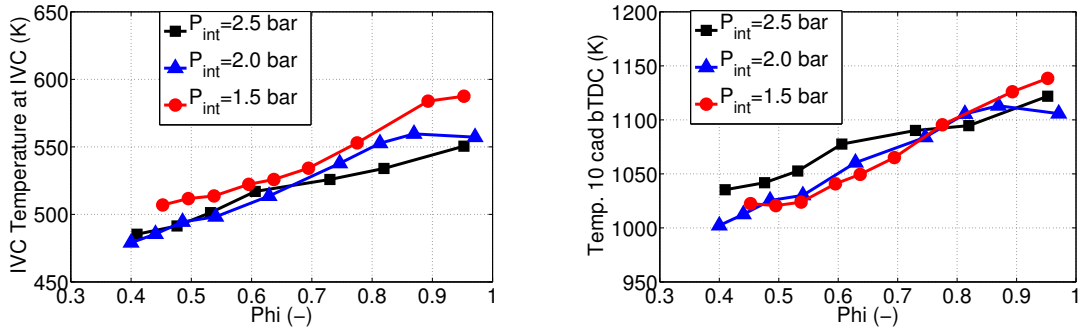

(a) In-cylinder temperature at intake valve closing

(b) In-cylinder temperature 10 cad bTDC

(c) internal EGR fraction

Figure 4.6 Average in-cylinder temperatures as function of fuel-to-air equivalence ratio Φ for different intake pressures

during the bulk part of combustion is relatively less important, compared to ignition of the first portion of the charge.

Thermal stratification could potentially also affect burn rates. The lower TDC temperature associated with higher P_{int} may imply decreased thermal stratification i.e. a more narrow temperature distribution within the combustion chamber, which could explain the minor retardation of CA05 and decrease in CA05-50 as well. Another argument employing heat transfer consideration in conjunction with thermal stratification is is the larger amount of total trapped mass in the case of P_{int}=2.5 bar. A larger amount of total trapped mass is accompanied by a lower relative heat loss. If every parameter including core gas and wall temperature, which is a hypothetical condition, was the same, a decrease in relative heat loss would imply a decrease in thermal stratification potentially leading to a shorter CA05-50. With increasing P_{int}, however, the engine load also increases because more fuel is added resulting in a larger absolute amount of heat rejected through the cylinder walls, which yields an increase in wall temperature. Although the increase in wall temperature cannot be quantified, because it was not measured, a smaller difference between core gas and wall temperature, provided core gas temperature was constant, implies less heat loss

hence a more narrow temperature distribution and thus faster burn.

Lastly, the pressure differential, $dP=P_{exh}-P_{int}$, was held constant and not scaled according to fueling rate unlike the total amount of charge was via adjusting P_{int} accordingly. As a result, internal EGR (iEGR) decreases slightly with increasing P_{int} despite NVO being held constant. Since there has not been any work done in determining whether NVO alone, dP alone or both combined to some extent affect thermal/ compositional stratification in a NVO engine, it is possible to conclusively say that the high P_{int} case with less iEGR has less thermal/ compositional stratification. But if it had less thermal/ compositional stratification, this could result in a shorter burn duration as well. It is difficult to evaluate which mechanism dominates, but since all of them, chemical kinetics, thermal stratification due to TDC temperature and thermal/ compositional stratification due to iEGR, point into the same direction, and the sum of the effect on CA05-50 is small, this implies that each of these effects is very small or almost negligible.

4.3.4 Emissions

Both peak cylinder temperature, T_{max}, and in-cylinder O_2 concentrations are important and need to be considered when evaluating the effect of P_{int} and Φ on exhaust emissions. T_{max} follows a similar trend as T_{10} with Φ for each P_{int}, which is to be expected as Φ' is the same for all three P_{int} and increases with Φ (see Figure 4.7). Emissions are evaluated with the emissions index on a relative base, accounting for tail pipe emissions normalized by the amount of fuel burned, so that differences in fueling rate and load for different P_{int} do not affect the analysis.

NO_X emissions are very low i.e. below the regulation limit of 1 g/kg fuel irrespective of P_{int} and Φ. Because of the low the relatively low load conditions chosen for this experiment i.e. relatively low Φ', T_{max} does not exceed the NO_X formation threshold ($\sim$1900 K). CO and THC emissions both decrease with increasing Φ owing to the fact that a larger portion of the charge is comprised of EGR, iEGR and eEGR, which implies that on average a larger portion of the charge has a second chance to burn and complete combustion. The net result is that combustion efficiency increases with increasing Φ/ eEGR addition for all three P_{int}. The decrease for CO with Φ is much less than for THC. CO emissions are insensitive to P_{int}, whereas THC emissions exhibit a sensitivity in that higher P_{int} leads to lower THC emissions. In the following, the trends for both CO and THC emissions are considered in more detail.

CO emissions decrease from $\sim$ 65 g/kg fuel for Φ=0.4 to $\sim$ 25 g/kg fuel for Φ=0.95, which corresponds to a decrease by a factor of $\sim$ 2.5. The total amount of EGR, that is the

burned gas retained in-cylinder via NVO strategy (iEGR) and exhaust gas fed back to the intake via an external EGR loop (eEGR), increases from $\sim$ 35 % to $\sim$ 65 % corresponding to an increase by a factor of $\sim$ 1.8, which is less than the increase in CO. The shape of the CO emissions versus Φ should follow the total EGR fraction curve inversely, but that is not the case, because the CO emissions exhibits a steeper slope at low Φ relative to the total EGR fraction line. The strong decline of CO for low Φ could be due to increasing T_{max}, while there is still a net excess of O_2 . For larger Φ, there is less O_2 available, but T_{max} is sufficiently high.

THC emissions decrease only by factor of $\sim$ 1.5 from low to high Φ depending on P_{int}. This is less than the increase in total EGR would suggest suggesting that THC is largely not only from quenching of combustion near cylinder walls but to a significant extent from crevices. This also explains the disproportionately lower than expected decrease of THC with increasing Φ, because there is always a certain amount of unburned fuel or intermediate combustion products that are not fully oxidized when outgassing irrespective of Φ. THC emissions are less by a factor of $\sim$ 1.5 for the high P_{int} case compared to the low P_{int} case for the same Φ. Part of this difference with increasing P_{int} can be attributed to a higher piston and cylinder wall temperature, due to higher load and fueling rate, effectively decreasing the density and mass fraction in the crevices. Assuming piston and crevice gas temperatures of 400 K and 500 K for P_{int}=1.5 bar and P_{int}=2.5 bar respectively only amounts to a ratio of 1.25, which is less than the observed value of 1.5. This suggests that there may be other reasons e.g. the notion that THC also results from quenching near walls hence incomplete combustion. Because the temperature required for breakdown of fuel and initial hydrocarbons is less than that required for complete oxidation of CO to CO_2 , the region where THC is prevalent due to quenching is closer to the cylinder walls.

4.3.5 Indicated Efficiencies

Gross indicated efficiency decreases irrespective of P_{int} as Φ increases owing to less advantageous thermodynamic properties i.e. lower γ, as can be seen in Figure 4.8. Increasing P_{int} also leads to an increase in gross indicated efficiency efficiency, primarily because of a decrease of relative heat loss. GT Power was used to validate both of these trends, that is with respect to Φ and P_{int}, quantitatively. While the former one could be verified entirely using the engine simulation software, only $\sim$ 50 % of the latter one could be verified and attributed to P_{int}. This implies that the heat transfer model does not fully capture the observed trends and/ or that other unknown factors may be involved.

A higher combustion efficiency with increasing Φ yields net indicated efficiency lines

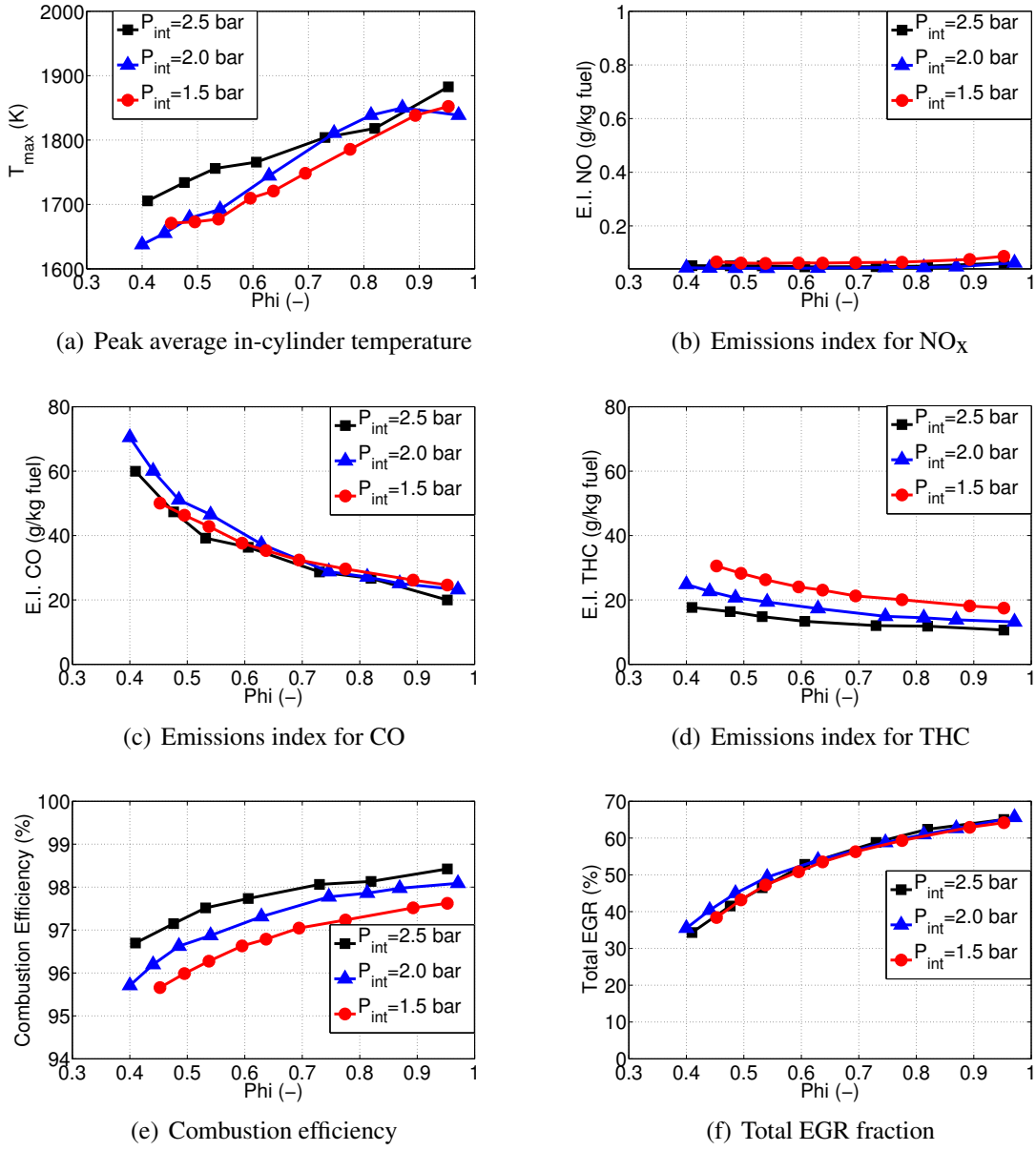

(a) Peak average in-cylinder temperature

(b) Emissions index for NO_X

(c) Emissions index for CO

(d) Emissions index for THC

(e) Combustion efficiency

(f) Total EGR fraction

Figure 4.7 Emissions indexes, peak temperature and combustion efficiency as function of fuel-to-air equivalence ratio Φ for different intake pressures

that drop off less with increasing Φ relative to the gross indicated efficiency lines. In general, high efficiency values are attained especially for high P_{int}. The results also show that eEGR does not reduce efficiency by a lot, although higher loads can be achieved. Therefore, replacing some of the incoming air with eEGR is useful in extending the high load.

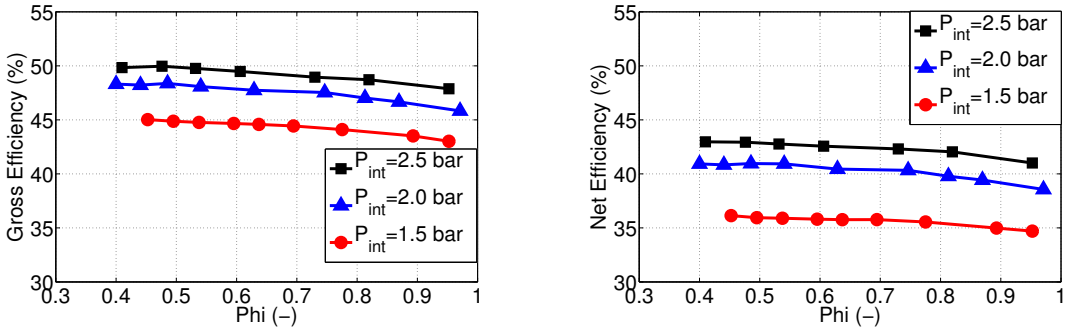

(a) Gross indicated efficiency

(b) Net indicated efficiency

Figure 4.8 Indicated efficiencies as function of fuel-to-air equivalence ratio Φ for different intake pressures

4.3.6 Knock and Combustion Stability

Maximum pressure rise rate, PRR_{max}, shows no clear trend with Φ, but PRR_{max} values are higher for increased P_{int} (see Figure 4.9). In fact, PRR_{max} values scale reasonably well with P_{int}, that is a higher P_{int} yields a higher TDC pressure, and for the same Φ', CA50 and CA10-90, a higher P_{int}/ P_{TDC} should yield a higher PRR_{max} as well. Peak cylinder pressure, P_{max}, should scale in a similar fashion, but this is not exactly the case, because the ratio of P_{max} at P_{int}=2.5 bar and P_{int}=1.5 bar is less than the ratio of P_{int} indicating that higher P_{int} may have less relative heat loss hence higher P_{max}. P_{max} decreases with increasing Φ due to the effect of thermodynamic properties i.e. larger specific heat capacity, C_P, yielding a slightly slower burn duration for all P_{int}. Low-pass ringing intensity, $R.I._{LP}$, captures and reflects effects of P_{int} and Φ on PRR_{max} and P_{max} yielding a higher $R.I._{LP}$ value for higher P_{int}, but there is no clear trend with Φ.

Lastly, combustion variability, quantified as COV of $IMEP_g$, shows no dependency on Φ / eEGR, but it is lower for higher P_{int}. There are various potential reasons for this, but at this point it can only be speculated. The higher P_{int} case has less iEGR because dP held constant and was not scaled with P_{int} and fuel mass. So, a larger amount of iEGR could potentially imply an increased level of thermal/ compositional stratification even though was kept NVO constant for all three P_{int} cases. More iEGR could imply that there is more feedback from the previous cycle affecting the following cycle.

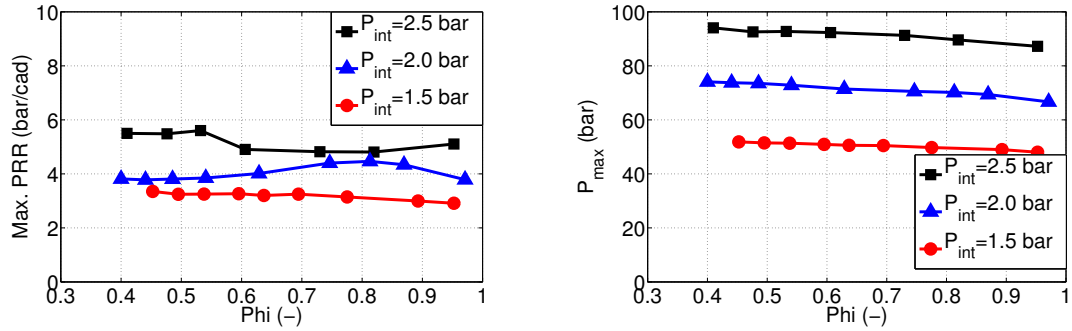

(a) Peak pressure rise rate

(b) Peak cylinder pressure

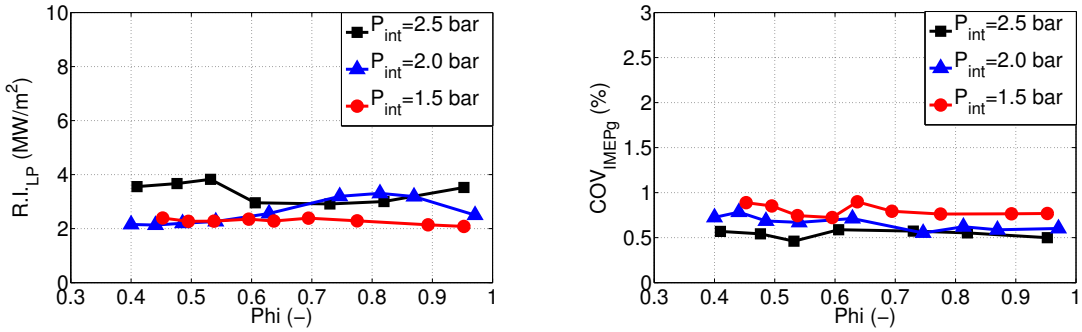

(c) Low-pass ringing intensity

(d) Coefficient of variance of IMEPg

Figure 4.9 Parameters relevant to knock limit as function of fuel-to-air equivalence ratio Φ for different intake pressures

4.4 Comparison to Phenomenological Burn Rate Model

In this section, a phenomenological combustion model suitable for advanced combustion modes including HCCI is evaluated by comparing it with experimental data. The model, recently proposed by Ortiz-Soto, predicts burn rate at CA50 based on a variety of engine and combustion parameters [145]. Making simplifications for pure HCCI combustion at a constant engine speed of 2000 rpm, the equation to calculate $\mathrm{RoHR_{CA50}}$ is given as follows

$$RoHR_{CA50} = f(CA50) \cdot \left(\frac{\phi_{F/O}}{0.5}\right)^{1.3} \cdot \left(\frac{1-X_{SCP}}{0.3}\right)^{1.67} \cdot exp\left(\frac{0.16}{T_{ign}/1100}\right) \cdot \left(\frac{P_{ign}}{50}\right)^{0.13} \cdot \left(\frac{1+f_{unmix}}{1.5}\right)^{-0.85} \tag{4.1}$$

where $\Phi_{F/O}$ is the fuel-to-oxygen equivalence ratio, X_{SCP} is the fraction of stoichiometric combustion products, T_{ign} is the in-cylinder temperature at auto-ignition, P_{ign} is the cylinder pressure at auto-ignition, and f_{unmix} is an expression capturing the level of unmixedness in the combustion chamber, which assumes a binary mixture of iEGR and fresh inducted charge comprised o air and eEGR. $f_2(CA50)$ is a function of CA50, which captures the

effect of combustion phasing on burn duration based on the piston position.

$RoHR_{CA50}$ is calculated based on equation (4.1) substituting appropriate values for the engine and combustion parameters, $\Phi_{F/O}$, X_{SCP}, T_{ign}, P_{ign}, f_{unmix}, CA50, from the experiment. T_{ign} and P_{ign} are evaluated at 10 cad bTDC, before any significant heat release has occurred, which is a simplification but sufficiently adequate. From Figure 4.10, showing the experimentally determined $\mathrm{RoHR_{max}}$ with the one predicted by the combustion model, it can be seen that the model, in general, captures the experimental trends with Φ and $\mathrm{P_{int}}$ very well. In particular, the absolute $\mathrm{RoHR_{max}}$ values for each $\mathrm{P_{int}}$ shows good agreement, and the slightly increasing trend of $\mathrm{RoHR_{max}}$ with Φ for all $\mathrm{P_{int}}$ other than 1.5 bar is adequately captured. The latter one can be attributed to both the oxygen term, $\Phi_{F/O}$, and the 'EGR' term, X_{SCP}. The former one increases, because O_2 concentration decreases while fuel mass remains constant, and is responsible for the increase in $RoHR_{CA50}$ as Φ increases. The latter one reflects the the relative amount of combustion products and the associated thermodynamic effect i.e. X_{SCP} increases with Φ thus (1-X_{SCP}) decreases, which counteracts some of the increase due to $\Phi_{F/O}$.

Based on the experimental results presented earlier in this Chapter, one could see relatively small influence of composition and boost pressure on burn duration. Although the model tested here was only calibrated against a limited set of experimental engine data under naturally aspirated conditions and complementary 3-D CFD simulation runs under boosted conditions, the comparison in this section shows reasonable agreement. The implication is that a combustion model does not need to be very complicated to capture trends. In particular, the very weak pressure dependency of $\mathrm{RoHR_{max}}$ is reflected in a very small exponent of 0.13, where a value of 0 would imply complete independence.

4.5 Summary and Conclusions

4.5.1 Summary of Results and Discussion

The goal of this chapter was to study, isolate and quantify the effect of the two fundamental thermo-physical parameters, pressure and composition, on burn duration. The relative importance of each of these was investigated by conducting experiments under very controlled conditions utilizing the high degree of freedom of the engine. Combustion phasing, CA50, overall fuel-to-charge equivalence ratio, Φ', and NVO were held constant throughout the sweeps to avoid or minimize bias from any of these parameters.

Intake boost pressure and composition were found to have a minor and moderate effect

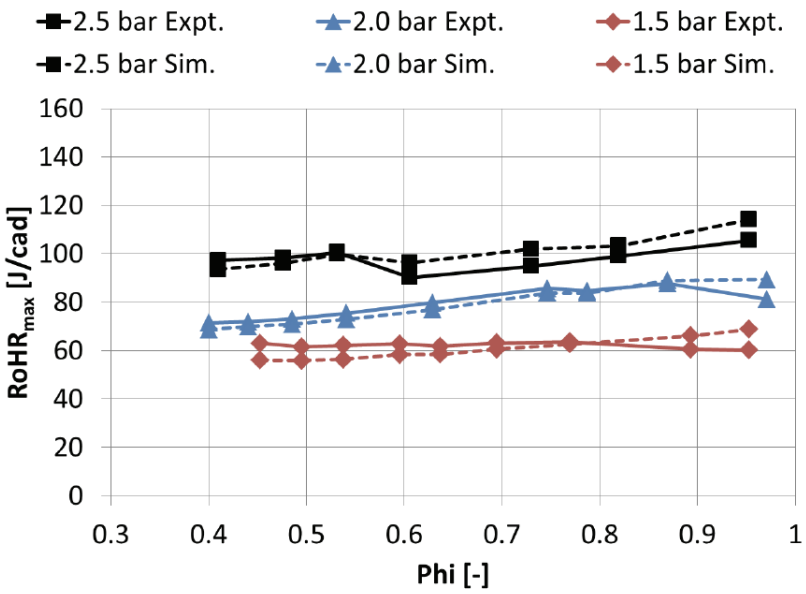

Figure 4.10 Peak rate of heat release: comparison between experiment and model as function of fuel-to-air equivalence ratio for three intake boost pressures

on burn duration respectively. Partially replacing the incoming air with eEGR thus increasing Φ yields a moderate increase in burn duration for all P_{int} i.e. $\sim$ 2 cad when Φ increases from 0.4 to 0.95. Increasing P_{int} from 1.5 bar to 2.5 bar yields a very small shortening of burn duration by $\sim$ 0.5 % irrespective of Φ. eEGR addition leads to improved combustion efficiency, especially at high P_{int}, due to decreasing CO and THC emissions. This offsets some of the decrease in gross efficiency with increasing Φ due to thermal property effects i.e. lower γ. THC emissions show some sensitivity to P_{int}, whereas CO emissions are insensitive with respect to P_{int}. Higher P_{int} leads to slightly higher ringing intensity and lower COV of $IMEP_g$ values.

This work cannot isolate and quantify the extent to which the mechanism is responsible for the increase and decrease in burn duration with Φ and P_{int} respectively. Instead, this work showed that the experimental observations are trendwise in agreement with previous works. One of the key contributions of this work is that it could be shown that intake boost pressure has no significant effect on burn duration. Most likely, the increase in burn duration with Φ is associated with corresponding changes of thermodynamic properties and thermal stratification due to different TDC temperatures and total amount of trapped masses. The experiments did not provide any evidence for O_2 concentration and chemical kinetics to impact burn duration.

4.5.2 Appraisal of Results and Contributions

The results presented in this chapter focus exclusively on combustion and burn rates. It could be shown that for stable HCCI operation burn rates in this gasoline-fueled NVO HCCI engine are relatively insensitive to composition and especially intake boost pressure. Previous findings investigating the effect of composition or eEGR addition in a PVO engine could be confirmed independently with this NVO engine. In addition, for the first time the effect of intake boost pressure was investigated independently over such a wide range in a NVO engine under highly controlled conditions, and it was shown to be of minor importance.

The experimental findings from this chapter provide additional support that, once ignition has occurred, combustion i.e. the progression of auto-ignition throughout the charge in a HCCI engine is largely determined by thermal/ compositional stratification. These findings suggest that chemical kinetics are relatively less important compared to thermodynamic properties and thermal and compositional stratification as a function of crank-angle for the bulk combustion event. As could be seen from the ignition delay expression in chapter 1, ignition and also combustion of any other charge parcel at a later point depends strongly on temperature, and less so on composition and pressure. This work provides further evidence for the hypothesis that HCCI combustion can be conceptually understood as a cascade of sequential auto-ignition events, where thermal and compositional stratification are predominant factors. The view of HCCI combustion as a perfectly mixed chemical reactor, which is kinetically limited, seems to be less suitable.

From a modeling point of view, acknowledging this auto-ignition cascade as the underlying mechanism for combustion, means that average values for fundamental thermo-physical parameters such as composition and boost pressure are less important relative to parameters adequately capturing thermal/ compositional stratification. Phenomenological combustion models do not have to be very complex, and an effort should be made to incorporate the effect of thermal and compositional inhomogeneities.

4.5.3 Shortcoming of Results and Next Steps

One of the limitations of the experiment performed is that the overall fuel-to-charge equivalence ratio, Φ', was not held perfectly constant while varying Φ, because of decreasing IVC density due to increase in T_{int}. Another caveat was that dP was not scaled with fueling rate and P_{int}, which led to slightly different amounts of iEGR trapped. It would be advisable to address especially the first shortcoming by repeating the experiment such that Φ' remains

even though Φ changes. This could be accomplished by compensating for the decrease in IVC density with slightly higher P_{int} for higher Φ data points. The third aspect could be addressed by appropriately scaling dP with fuel injection rate.

Results in chapter 4 showed that lower engine speed can lead to longer burn duration and lower TDC temperature. Combined with elevated boost pressure of 2.0 bar or above low temperature heat release (LTHR) could be observed. Realizing that low engine speed is a high load enabler, it would be very interesting to repeat the burn duration study in this chapter at lower engine speed, because LTHR could potentially result in a much larger and even non-linear effect of pressure and composition on burn duration.

The experiments conducted in this chapter were far away from both knock and combustion variability limit. Moreover, combustion phasing was held constant. Since chapter 3 provided strong evidence that both limits, but especially, the combustion variability or stability limit are crucial in determining the maximum load capability of a boosted NVO HCCI engine. Therefore, it would be very interesting to gain further insight into how the two fundamental thermo-physical parameters considered in this chapter but also others, notably NVO, because it is associated with thermal/ compositional stratification, affect the combustion phasing limits. This will be the subject of study of chapter 5.

Chapter 5

Combustion Phasing Limits: Effects of Boost Pressure, Composition and NVO

As the maximum load limit is approached, both combustion phasing limits, knock and combustion variability, occur simultaneously confining the the viable combustion phasing window to a single point. A better understanding how these limits are affected by various fundamental thermo-physical parameters, including boost pressure, composition and negative valve overlap (NVO), can be extremely valuable and provide directions for further improvements and/ or extension of the maximum load capability of a NVO HCCI engine. Chapter 3 showed that another boosted engine with positive valve overlap exhibited much lower combustion variability, which could potentially be related to the positive valve overlap strategy employed in that engine. This chapter investigates the potential effects of intake boost pressure, composition and NVO on both combustion phasing limits by means of controlled experiments. Therefore, this chapter represents an important link between chapters 3 and 4, as it combines the practical aspects of the maximum load limit with the fundamental ones, thus providing some unique contributions.

5.1 Relevance of Combustion Phasing Limits

Combustion phasing limits, that is knock and combustion variability limits for advanced and retarded combustion timing respectively, occur simultaneously at the maximum load limit in a HCCI engine. Higher fueling rates hence loads for a given intake boost pressure yield higher peak pressure rise rates, which can be attenuated by retarding combustion phasing. Later CA50 can therefore be used to keep ringing intensity in check, which is used to quantify the knock limit. Increasing P_{int} not only facilitates higher loads but also further CA50 retard. However, CA50 cannot be retarded beyond a certain point, the combustion stability limit, which can exhibit bi-modal behavior, where an overly advanced cycle follows a partial or complete misfire due to the internal feedback via hot iEGR from the previous

cycle and vice versa. Operating at the combustion variability limit could potentially be very deleterious to the engine, as structural components could easily be severely and irreversibly damaged.

Note that knock also occurs at the maximum load limit in addition to a high level of combustion variability. Having a large number of cycles with fairly advanced combustion phasing amongst the ensemble of all cycles could lead to higher than normal engine component temperatures and consequently possibly damage. Excessive ringing is known to significantly augment heat transfer, because the resulting standing pressure waves tend to break down wall boundary layers. Not only can the engine structure be damaged, but the operating condition is highly undesirable from a harshness, vibration and noise point of view. Also, from a controls point of view, it is extremely challenging or nearly impossible to properly manage and control this erratic combustion behavior near the knock limit.

Whereas chapter 3 showed that ignition requirements and engine constraints determine the practical maximum load limit of a NVO HCCI engine, and chapter 4 showed that burn duration is fairly insensitive toward changes in intake boost pressure and composition, the objective of this chapter is to shed light on how various thermo-physical parameters affect both combustion phasing limits. The role of intake boost pressure, composition and negative valve overlap (NVO) will be investigated through means of controlled experiments, where combustion phasing is varied. The following section describes the experimental procedure in more detail.

5.2 Experimental Procedure

The experiments performed in this chapter are also well controlled, because many engine parameters are held constant to facilitate isolation of the effects of various fundamental thermo-physical parameters on the combustion phasing limits. The primary goal was to sweep combustion phasing (CA50) while keeping as many thermo-physical parameters constant, so that effects and causes of individual parameters can be separated and isolated. Table 5.2 shows those engine parameters that applied to all the different experiments performed in this chapter irrespective of the individual thermo-physical parameter studied. In contrast, Table 5.2 gives an overview of parameters that vary according to the fundamental thermo-physical parameter being studied and whose isolation from others was sought.

For the study of the effect of intake boost pressure, P_{int}, in chapter 5.3, fueling rate was scaled accordingly so as to maintain approximately constant overall fuel-to-charge ratio Φ' amongst all P_{int}. As the effect of composition i.e. external EGR (eEGR) addition is

Table 5.1 Engine operating parameters applied to all experiments throughout chapter 5

Parameter	Value	Unit
Engine speed	2000	rpm
Fuel pressure	100	bar
Pressure differential (P_{exh}-P_{int})	0.5	bar
Coolant temperature	90	°C
Oil temperature	90	°C
Fuel injection timing	330	cad bTDC

Table 5.2 Specific engine operating parameters applied to experiments and separated according to the effect studied in each sub-chapter of chapter 5

Effect	Boost Pressure (Chpt. 5.3)	Composition (Chpt. 5.4)	NVO (Chpt. 5.5)	
Parameter				Unit
Intake pressure	1.5 / 2.0 / 2.5	1.5	1.5	bar
Fuel flow rate	10.5 / 14.5 / 18.5	10.5	10.5	mg/cyc.
External EGR	0	0 / 36 / 46	0 - 31 / 36 - 41	%
F/A equiv. ratio Φ	0.4	0.4 / 0.8 / 0.95	0.4 - 0.8 / 0.8 - 0.95	-
Neg. valve overlap	90	90	90 / 120	cad
F/C equiv. ratio Φ'	0.25	0.25 / 0.30 / 0.33	0.27 / 0.31	-
Intake temperature	40 - 140	110 - 240	70 - 200	°C

studied in chapter 5.4, fueling rate and P_{int} were held constant, while different external EGR rates were used (0-46 %). For the study of the effect of negative valve overlap (NVO), two sets of experiments were performed at a lower and higher NVO setting, one with lower and one with higher eEGR/ Φ. The goal was to achieve approximately constant overall fuel-to-charge ratio, Φ', amongst different NVO for comparison. Effectively, in this case, internal EGR (iEGR) is partial replaced with eEGR isolating the potential effect of thermal/ compositional owing to iEGR/ NVO.

A key aspect of all experiments in this chapter, other than in Chapter 5.5), is that combustion phasing, CA50, was varied via adjustments of intake temperature, and not NVO, to minimize any potential thermal/ compositional stratification bias due to iEGR/ NVO.

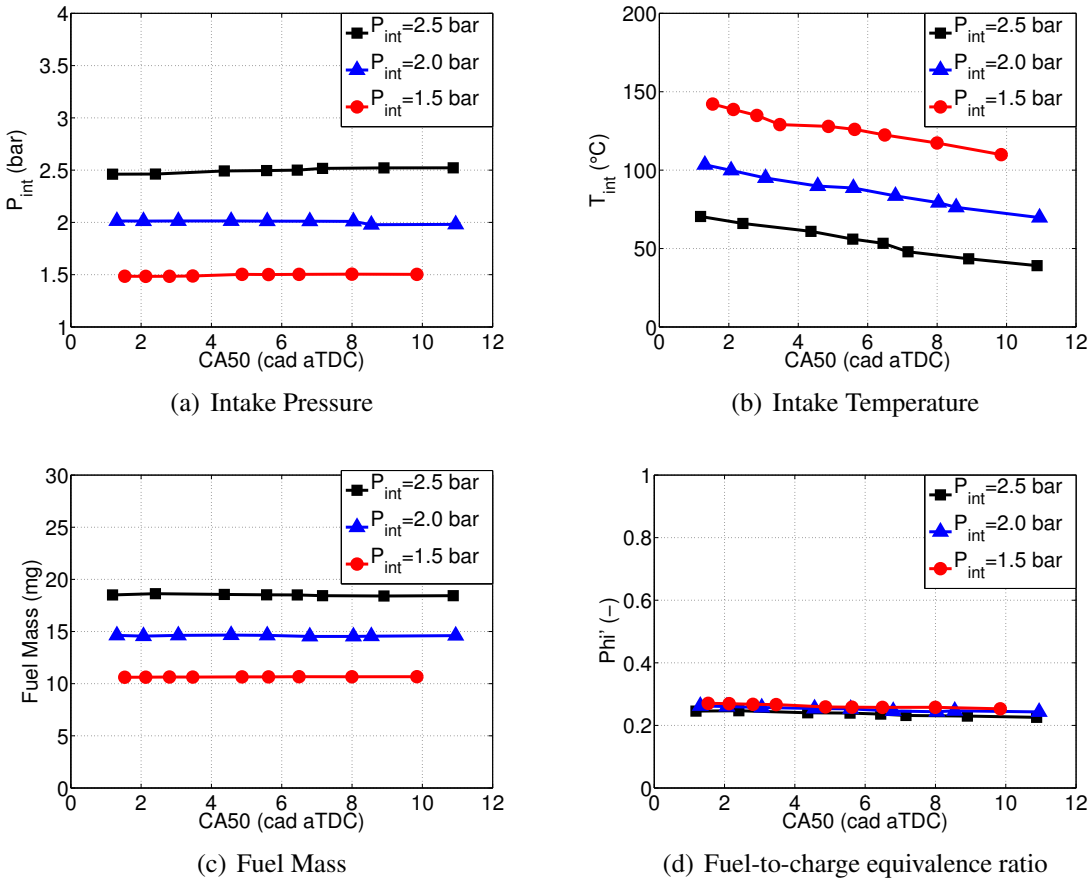

(a) Intake Pressure

(b) Intake Temperature

(c) Fuel Mass

(d) Fuel-to-charge equivalence ratio

Figure 5.1 Boundary conditions as function of CA50 for different intake pressures

5.3 Boost Pressure Effect on Combustion Phasing Limits

The experimental procedure followed for investigating the effect of intake boost pressure on both combustion phasing limits is displayed in Figure 5.1. For a given intake pressure, P_{int}, starting from a retarded operating condition at the combustion variability limit, T_{int} was gradually increased to advance CA50 from stability limit to early CA50 approaching the knock limit. Φ' was approximately constant i.e. 0.25, 0.27, and 0.29 for P_{int} of 2.5 bar, 2.0 bar, and 1.5 bar respectively. For each P_{int}, CA50 only increased slightly as CA50 was advanced owing to the higher T_{int} thus decreased IVC density.

Figure 5.2 shows results with respect to both combustion phasing limits i.e. knock and combustion variability limit. The combustion variability limit (COV of $IMEP_g$) is insensitive to P_{int}, as the curves corresponding to different P_{int} almost fall on top of each other. COV of $IMEP_g$ remains low i.e. $\sim$ 1 % for CA50=1-6 cad aTDC and it only starts to increase significantly for CA50 later than 6-8 cad aTDC. Therefore, intake boost pressure appears to have no effect on the combustion variability/ COV of $IMEP_g$ limit.

The knock limit, however, is sensitive to P_{int} irrespective of the ringing intensity metric used i.e. low-pass or high-pass. First, the focus lies on low-pass ringing intensity, and then high-pass ringing intensity is addressed. Peak cylinder pressure rise rates, PPR_{max}, increase as CA50 is advanced for all P_{int}, because the bulk part of the heat release due to combustion occurs closer to TDC and the piston is descending at lower speed. Higher Pint yields higher PPR_{max}, because a larger amount of heat is released, simply due to the fact that more fuel is injected and undergoes combustion. Peak cylinder pressure, P_{max}, scales with P_{int} and fueling rate, which also scales with P_{int}, hence it is greater for higher P_{int}. According to the ringing intensity equation for $R.I._{LP}$, PPR_{max} enters the numerator and is squared while P_{max} enters the denominator. The result is that $R.I._{LP}$ increases approximately in a linear fashion with P_{int}. Note that the effect of P_{int} is more pronounced for more advanced CA50, because the piston is closer to TDC.

The high-pass ringing intensity increases dramatically for a CA50 of 5 cad aTDC or earlier. The case with higher P_{int} exhibits significantly higher $R.I._{HP}$ compared to the case with lower P_{int}. Both ringing metrics, $R.I._{LP}$ and $R.I._{HP}$, seem to agree relatively well until a value of ~ 4 MW/m^2 is reached, beyond which $R.I._{HP}$ increases to a much larger extent than $R.I._{LP}$. Note that the high-pass ringing intensity appeared to agree more with the audible noise monitored during the experiments via an intercom.

Figure 5.3 compares the results for very advanced and slightly retarded combustion phasing with CA50=1.5 cad aTDC and CA50=5.5 cad aTDC respectively. The reason for choosing these was that the former one shows significant discrepancy between both ringing intensity metrics and the latter one there is still agreement. Note that the median cycle with respect to peak cylinder pressure is plotted.

The cylinder pressure traces for the advanced cases exhibit significant pressure oscillations, which increase with intake pressure. The maximum amplitude of the pressure oscillation for the advanced case at P_{int}=2.5 bar amounts to $\sim \pm 4$ bar. This fluctuation corresponds to $\sim \pm 4$ % relative change of e.g. in-cylinder temperature i.e. $\sim \pm 60$ K. The majority of the heat has already been released for the advanced cases around 5 cad aTDC. The frequency of the pressure oscillation, $\sim$ 5-6 kHz, corresponds to the first resonance mode. Generally, as CA50 is advanced, T_{max} increases, burn duration is shorter and more heat is released in a shorter period of time. Also, the piston is closer to TDC and its descending velocity is relatively low so that pressure rise due to heat release is not significantly attenuated.

The main reason for the existence of these larger pressure oscillations and knock for the cases with advanced CA50, especially in conjunction with high P_{int} could be that almost half of the heat release occurs before or close to TDC, which yields higher in-cylinder

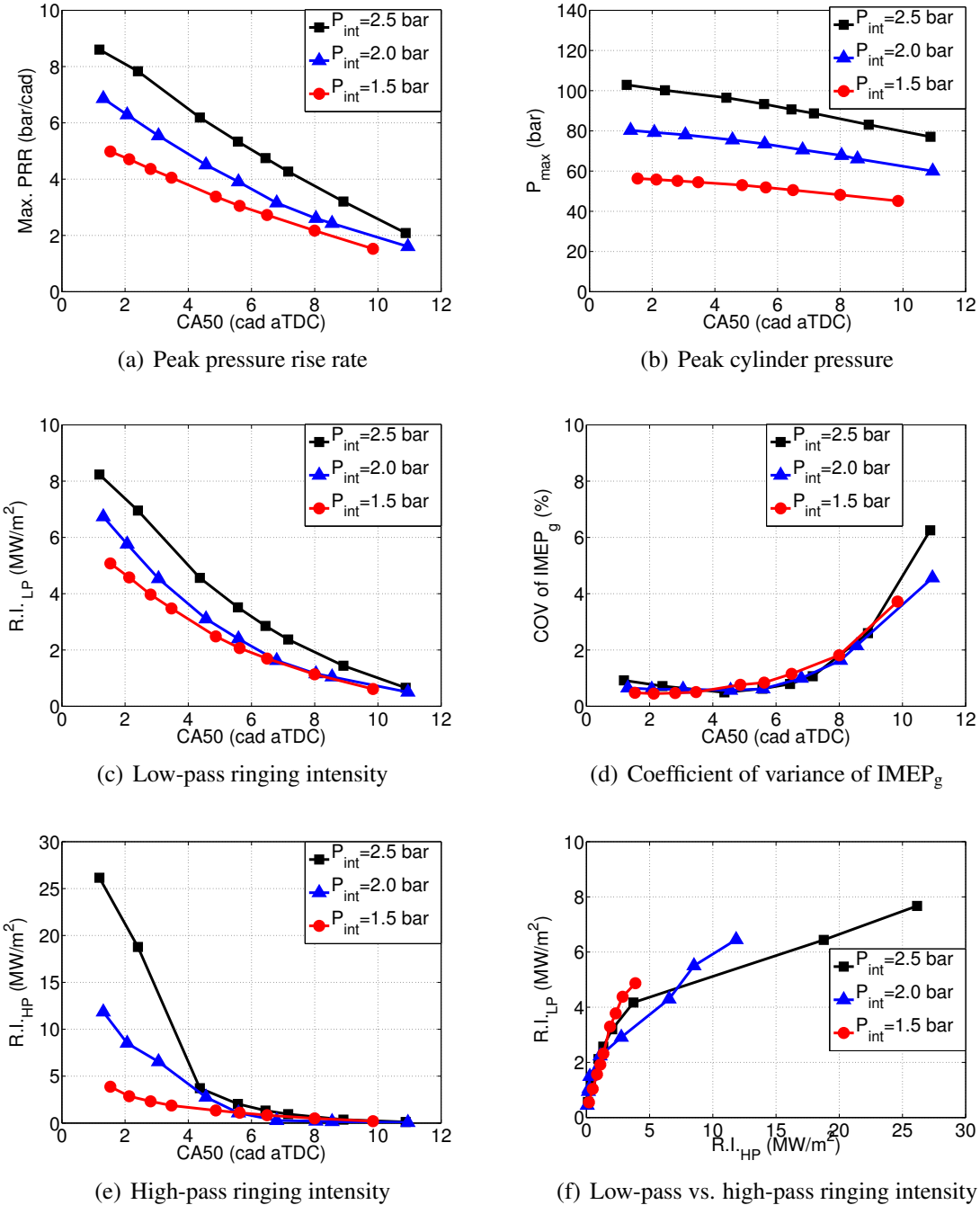

(a) Peak pressure rise rate

(b) Peak cylinder pressure

(c) Low-pass ringing intensity

(d) Coefficient of variance of $IMEP_g$

(e) High-pass ringing intensity

(f) Low-pass vs. high-pass ringing intensity

Figure 5.2 Parameters relevant to knock and combustion variability limits as function of CA50 for different intake pressures

temperature. Once auto-ignition occurs presumably in the hottest portion of the fuel-air-EGR mixture and combustion progresses, pressure waves develop and standing waves form. It is conceivable that pressure peak due to the magnitude of the oscillation can lead to an instantaneous increase of in-cylinder temperature, including the hottest portion of the charge, thus promoting faster reactions and burn rates. The pressure fluctuations may act to self-enforce and speed up the heat release. In particular, a higher boost pressure results in a larger magnitude of pressure/ temperature oscillations, even before significant heat release has occurred, which then allows more self-reinforcement and higher pressure oscillation ins turn. The relative importance and impact of these pressure waves is greatest when CA50 is advanced.

Emissions are primarily dictated by peak in-cylinder temperatures and are therefore sensitive to combustion phasing and overall fuel-to-charge ratio (see Figure 5.4). Peak in-cylinder temperature, T_{max}, is higher for the lower P_{int} case, due to slightly higher Φ', and decreases as CA50 is retarded for all P_{int} due to the fact that the piston downward motion acts to attenuate pressure/ temperate increase. NO_X emissions are higher for lower P_{int} due to higher T_{max} because of Φ', but generally below the limit of 1 g/kg fuel. CO emissions increase as CA50 is retarded, more notably for high P_{int} due to too low T_{max} to facilitate complete combustion even in the colder regions closer to the combustion chamber walls. THC emissions also increase with increasing CA50, but to a much lesser extent than CO emissions, probably because the majority of the THC stems from crevice regions and the required temperature for fuel break-down is lower than that for CO oxidation. Note that the low P_{int} case has relatively higher THC emissions compared to the high P_{int} case. Combustion efficiency is mainly the result of trends in CO and THC emissions and decreases with increasing CA50 especially when CA50 is retarded to a point that T_{max} is below 1400 K. CO emissions contribute most to the shape of the combustion efficiency lines, which is the reason why it is fairly insensitive to P_{int}.

Figure 5.5

Maximum gross indicated efficiency occurs at CA50 $\sim$ 4-6 cad aTDC as a result of a trade-off between expansion-to-compression work ratio and wall heat loss. Higher P_{int} leads to a decrease in relative heat losses, which is considered to be one of the major factors responsible for the obvious difference in gross indicated efficiency between different P_{int}. Thermodynamic properties are almost identical between the three P_{int}, hence cannot be the main reason for this difference in efficiency. Note that there is no clear trend and correlation with burn duration either.

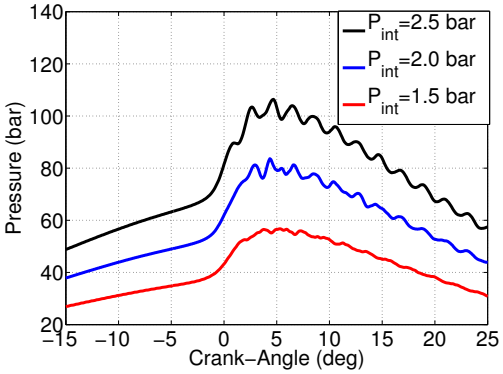

(a) Cylinder pressure (CA50=1.5 cad aTDC)

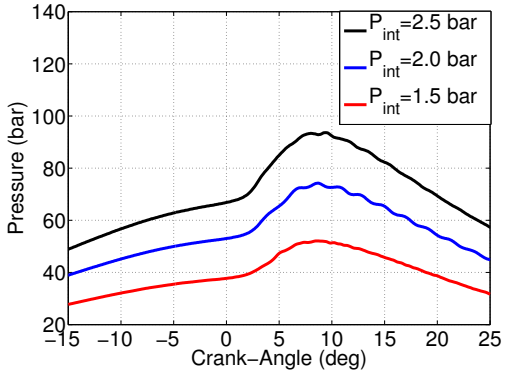

(b) Cylinder pressure (CA50=5.5 cad aTDC)

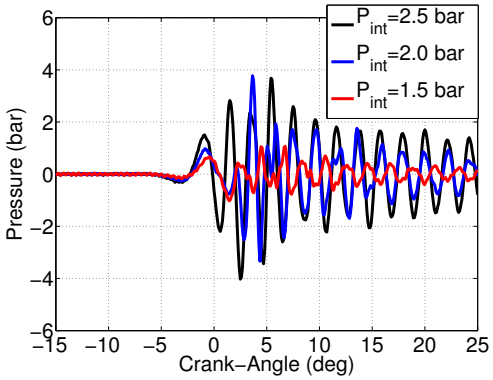

(c) dP_{cyl} (CA50=1.5 cad aTDC)

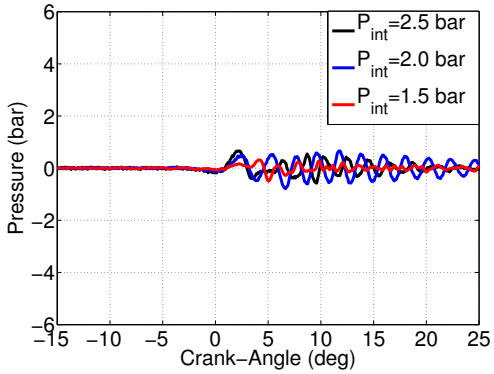

(d) dP_{cyl} (CA50=5.5 cad aTDC)

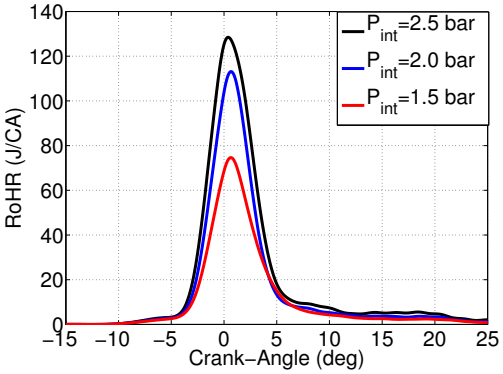

(e) Rate of heat release (CA50=1.5 cad aTDC)

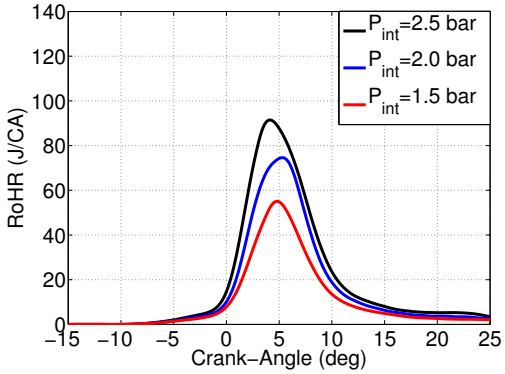

(f) Rate of heat release (CA50=5.5 cad aTDC)

Figure 5.3 Cylinder pressure, pressure difference between unfiltered and filtered cylinder pressure, and rate of heat release for early (CA50=1.5 cad aTDC) and slightly retarded (CA50=5.5 cad aTDC) combustion phasing as function of crank-angle for different intake pressures (results are based on median cycle with respect to peak cylinder pressure)

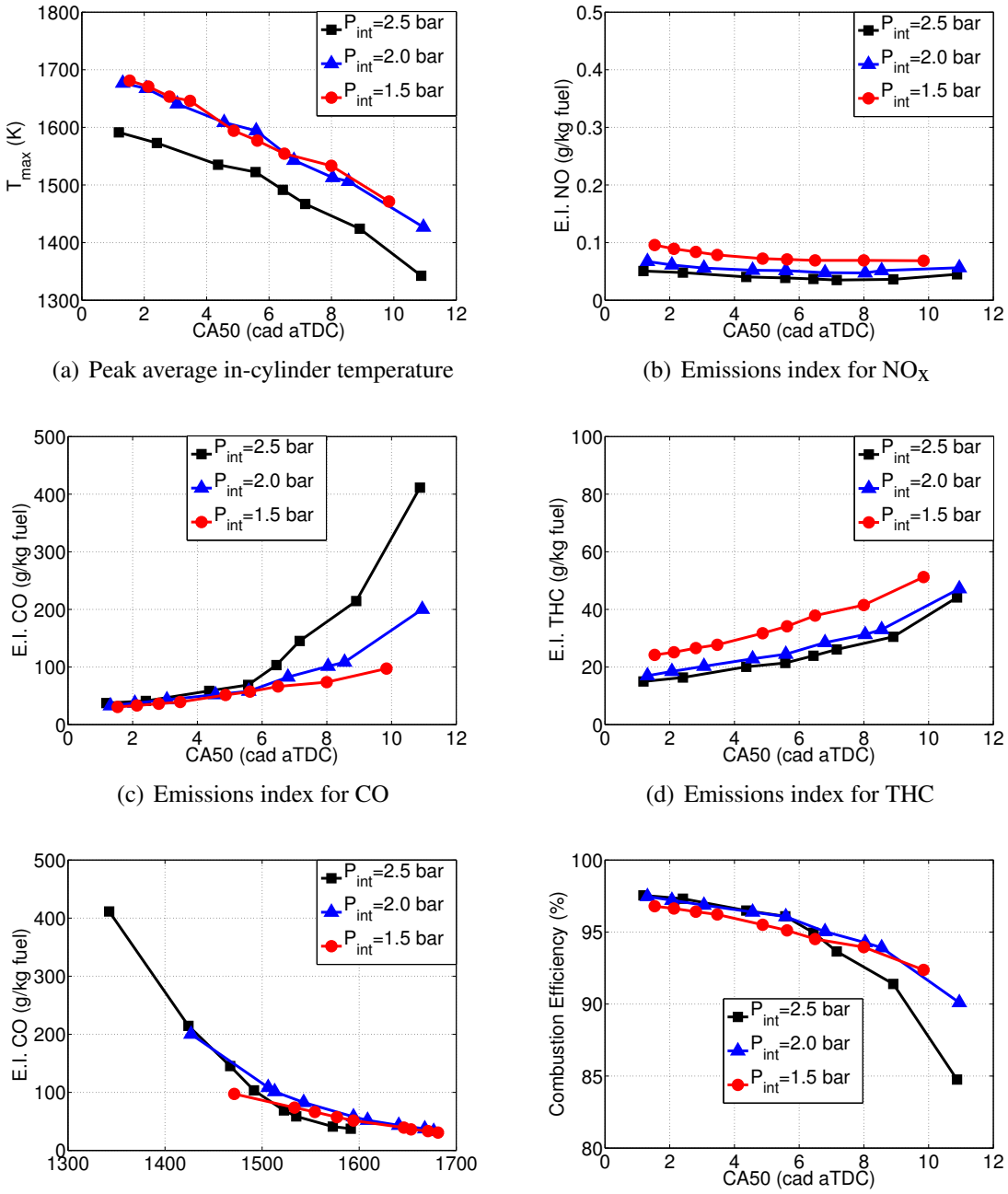

(a) Peak average in-cylinder temperature

(b) Emissions index for NO_X

(c) Emissions index for CO

(d) Emissions index for THC

(e) Emissions index for CO vs. peak temperature

(f) Combustion efficiency

Figure 5.4 Emissions indexes, peak temperature and combustion efficiency as function of combustion phasing (CA50) for different intake pressures

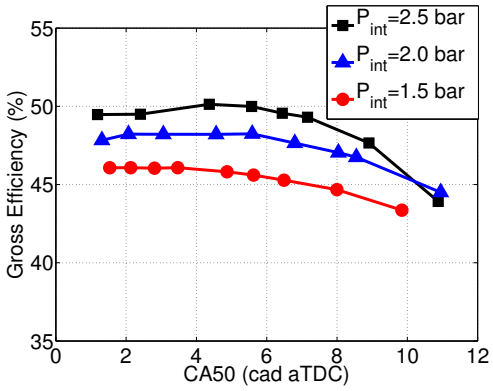

(a) Gross indicated efficiency

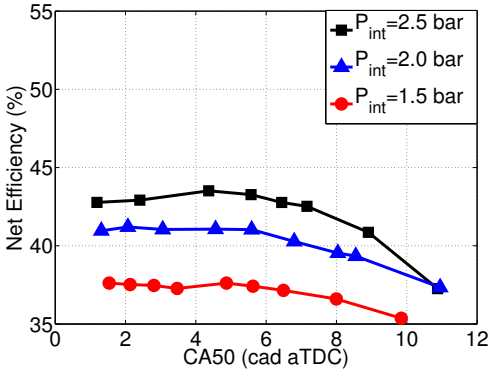

(b) Net indicated efficiency

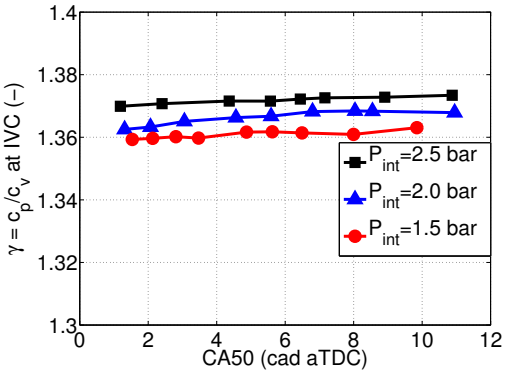

(c) Specific heat capacity γ

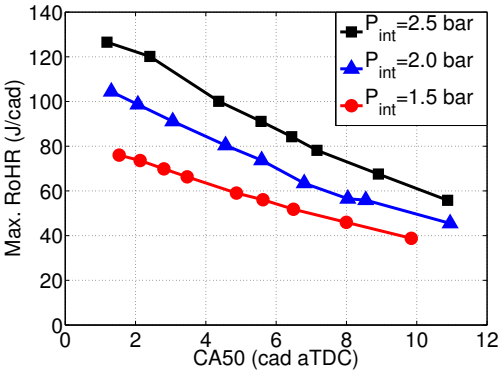

(d) Peak rate of heat release

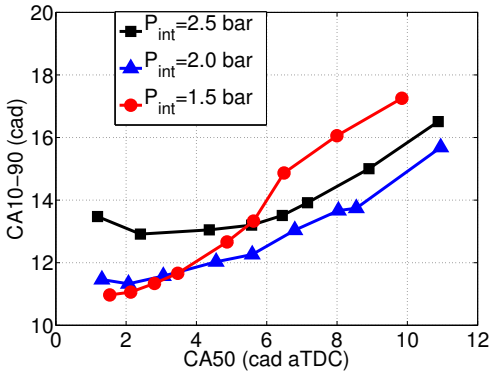

(e) Burn duration CA05-90

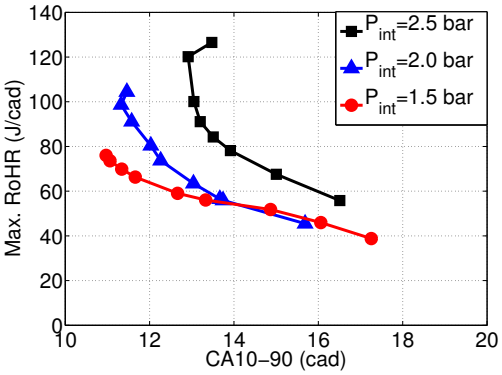

(f) Peak rate of heat release vs. CA05-90

Figure 5.5 Indicated efficiencies as function of combustion phasing (CA50) for different intake pressures

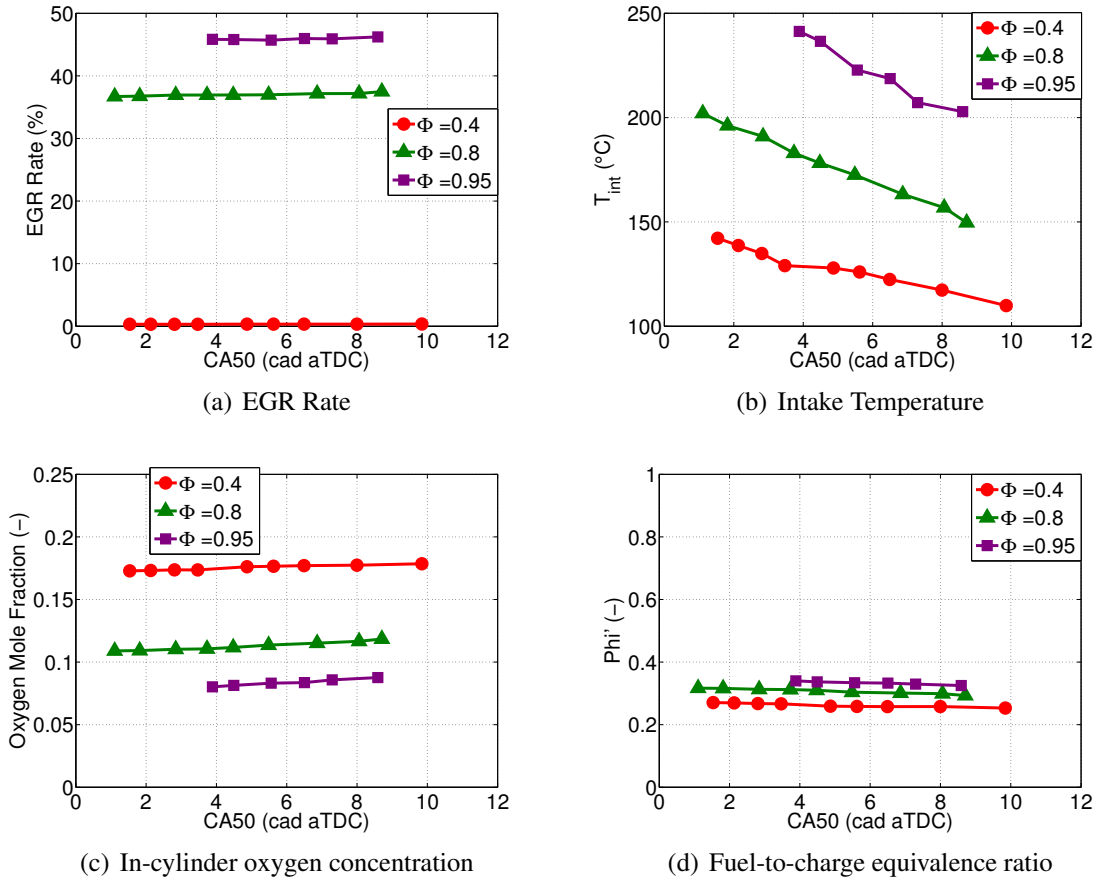

(a) EGR Rate

(b) Intake Temperature

(c) In-cylinder oxygen concentration

(d) Fuel-to-charge equivalence ratio

Figure 5.6 Boundary conditions as CA50 for different composition (amounts of eEGR)

5.4 Composition Effect on Combustion Phasing Limits

To investigate the effect of composition on the combustion phasing limits, P_{int} is held constant at 1.5 bar and different amounts of EGR are added (Φ=0.4, 0.8 and 0.95), as can be seen in Figure 5.6. Oxygen concentration decreases substantially with increasing amounts of eEGR. Φ' is relatively constant during each CA50 sweep, but is not exactly same between three different Φ cases, because of substantially different T_{int} requirements. For each P_{int}, T_{int} is gradually increased to advance CA50 from the combustion variability/ stability to the knock limit.

Figure 5.7 shows quantities related to knock and combustion variability limits. There appears to be a small dependency of the combustion variability limit, COV of $IMEP_g$, on the charge composition i.e. more eEGR addition leads to a small decrease in COV of $IMEP_g$ at fixed CA50, which translates into slightly later CA50 with eEGR when the same COV limit value is imposed. The separation of lines with different composition only becomes apparent for CA50 later than 6 cad aTDC, while there is no discernible difference for earlier CA50.

A possible explanation for the eEGR effect on COV of $IMEP_g$ could be the higher TDC temperature along with increased thermal stratification and larger specific heat capacity i.e. lower γ. The former implies slightly longer burn duration allowing for more stable combustion at same CA50, and the latter may make the mixture thermal more inert and less susceptible to fluctuations in temperature due to fluctuation in iEGR amount or different burn profiles.

On the other hand, for advanced CA50, a similar trend with eEGR for the low-pass ringing intensity can be observed i.e. higher Φ yields lower $R.I._{LP}$, hence earlier CA50 is possible if one were to impose the same fixed limiting value for $R.I._{LP}$. Both of these findings i.e. lower $R.I._{LP}$ with more eEGR and lower P_{int} are in agreement with the findings about burn duration with respect to these fundamental thermo-physical parameters in Chapter 4. Note, however, that the low-pass and high-pass ringing intensity values show opposite trends with respect to the parameter studied. While changes for both low-pass and high-pass R.I. values were in the same direction i.e. they would both increase with increasing P_{int}, adding eEGR leads to a decrease in $R.I._{LP}$, but to an increase in $R.I._{HP}$. There is only moderate agreement between both metrics as long as the R.I. value does not exceed 1.5 MW/m^2.

The high eEGR case ($\Phi = 0.95$) has visibly larger high-frequency cylinder pressure oscillations than the low eEGR case ($\Phi = 0.4$), as can be seen in Figure 5.8. Whereas the effect of lower $R.I._{LP}$ with increasing eEGR could explained by slightly slower burn duration and larger thermal inertia of the diluent, the increase in $R.I._{LP}$ with increasing eEGR is less clear. There is a chance that the first portion of the charge undergoing combustion, burns more vigorously hence creating more high pressure oscillations, because it is hotter and the mixture closer to stoichiometry.

Partially replacing air with eEGR helps to improve combustion efficiency mainly due to higher in-cylinder peak temperatures due to somewhat higher Φ' (see Figure 5.9). Later CA50 leads to lower T_{max} hence lower combustion efficiency. The increase in CO with later CA50 is more pronounced than the increase in THC owing to the fact that relatively more CO is created in quenching regions near the walls. NO_X emissions increase with eEGR addition but are well below the limit of 1 g/kg fuel, because T_{max} never exceeds 1900 K.

Gross indicated efficiency decreases with successive eEGR addition as a direct result of changes of the thermodynamic properties i.e. lower ratio of specific heat capacities, γ, with increasing Φ. Note, that gross indicated efficiency reaches its maximum value for slightly later CA50 with increasing eEGR due to a decrease in burn duration. The moderately longer burn duration for Φ=0.95 compared to Φ=0.4 manifests itself in slightly lower peak rates of heat release. Net indicated efficiency follows similar trend as gross efficiency, although lines for different eEGR/ Φ are spaced closer together.

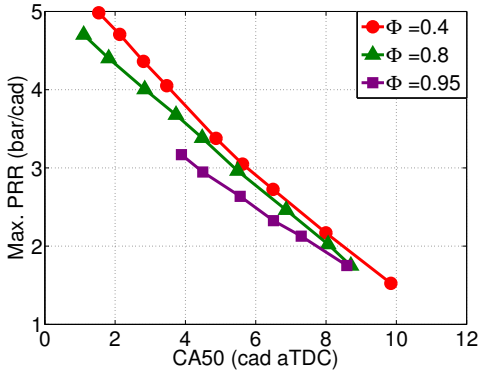

(a) Peak pressure rise rate

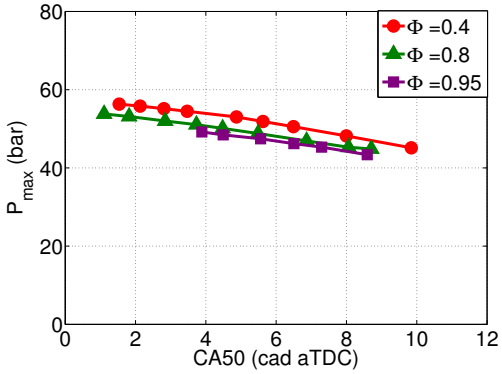

(b) Peak cylinder pressure

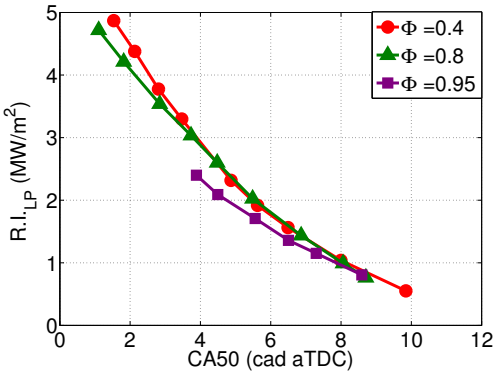

(c) Low-pass ringing intensity

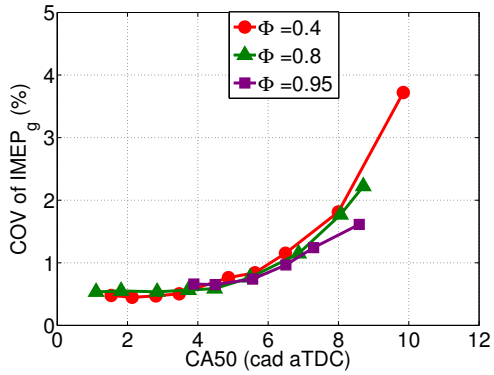

(d) Coefficient of variance of $IMEP_g$

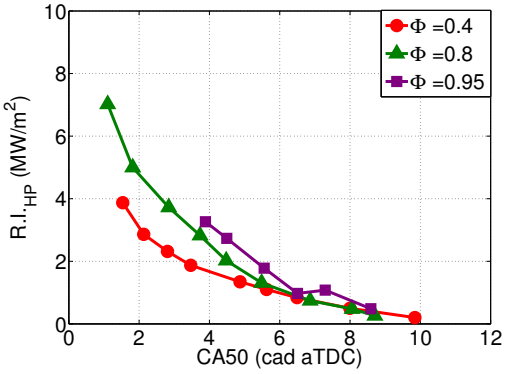

(e) High-pass ringing intensity

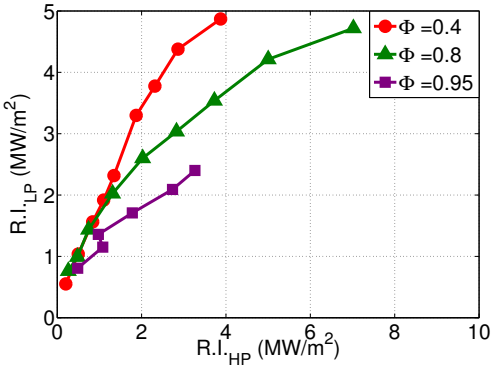

(f) Low-pass vs. high-pass ringing intensity

Figure 5.7 Parameters relevant to knock and combustion variability limits as function of CA50 for different composition (amounts of eEGR)

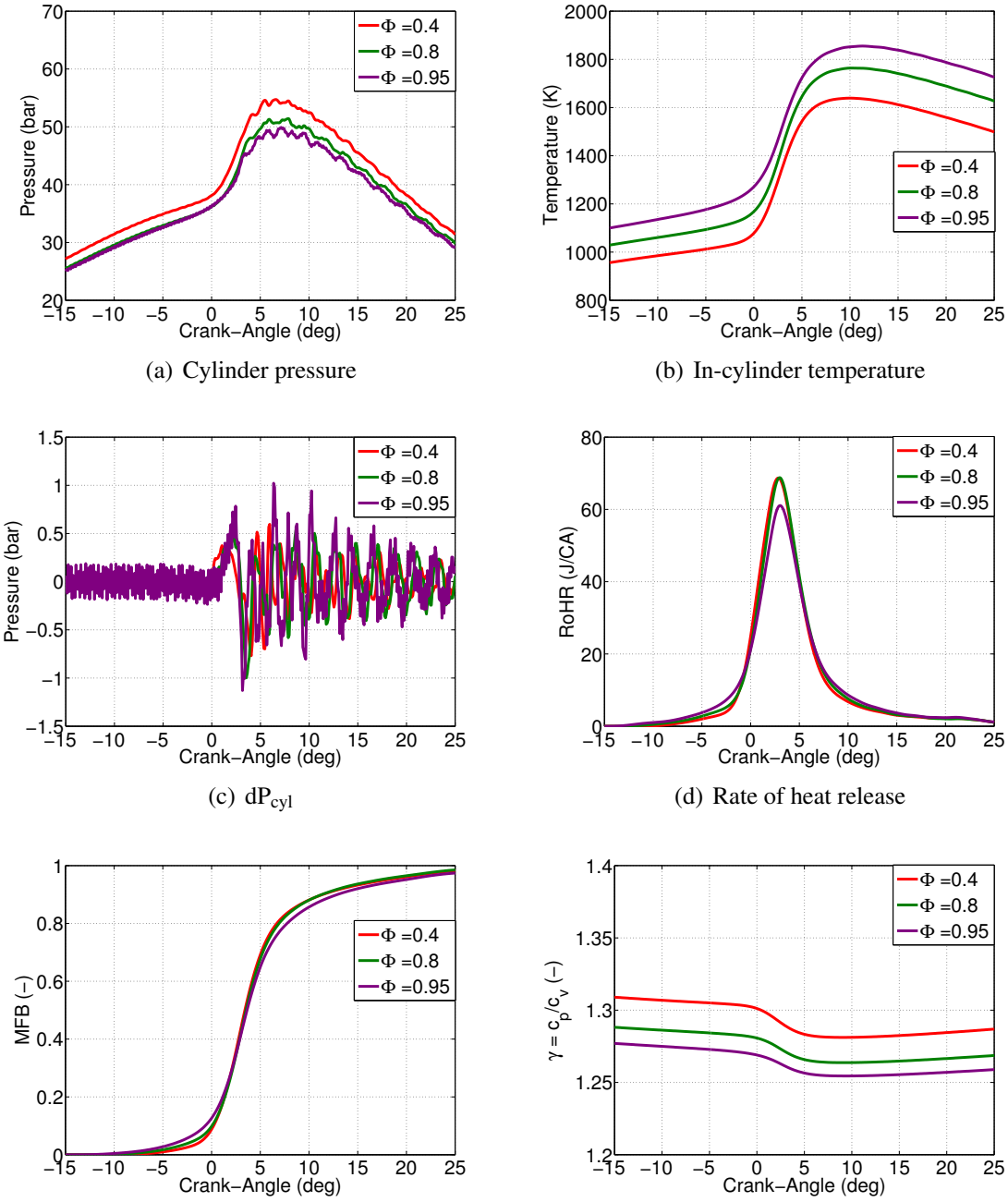

(a) Cylinder pressure

(b) In-cylinder temperature

(c) dP_{cyl}

(d) Rate of heat release

(e) Mass fraction burned

(f) Ratio of specific heat capacities

Figure 5.8 Cylinder pressure, average in-cylinder temperature, pressure difference between unfiltered and filtered cylinder pressure, rate of heat release, mass fraction burned, and ratio of specific heat capacities for early (CA50=4 cad aTDC) combustion phasing as function of crank-angle for fuel-to-air equivalence ratios (results are based on median cycle with respect to peak cylinder pressure)

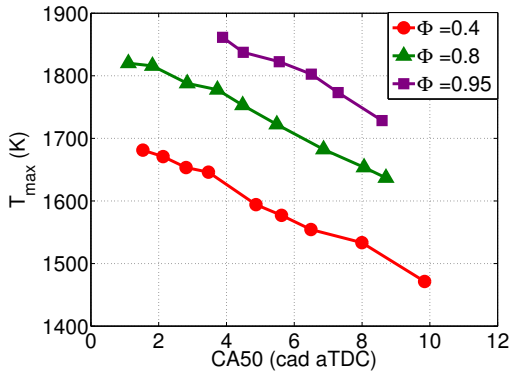

(a) Peak average in-cylinder temperature

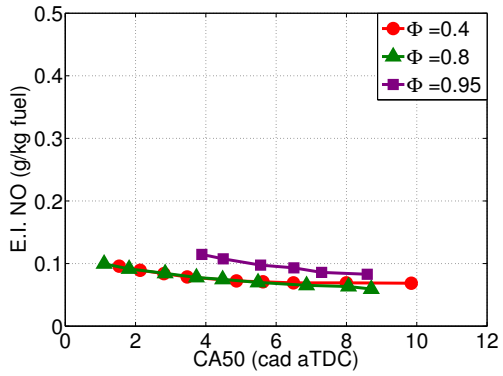

(b) Emissions index for NO_X

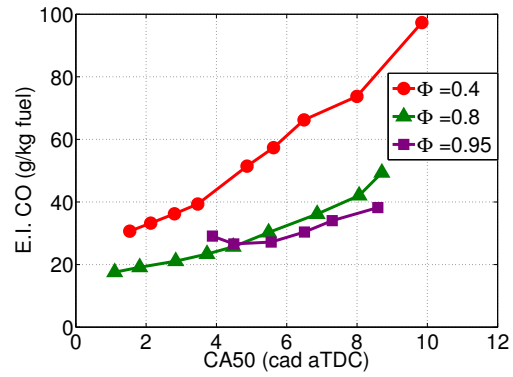

(c) Emissions index for CO

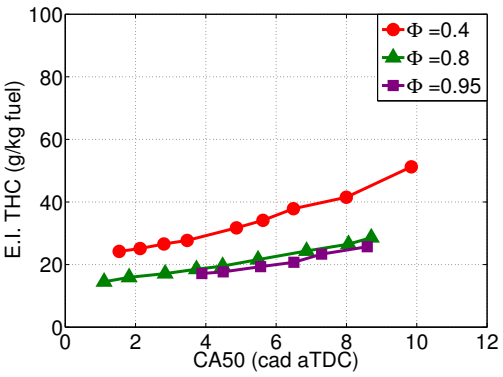

(d) Emissions index for THC

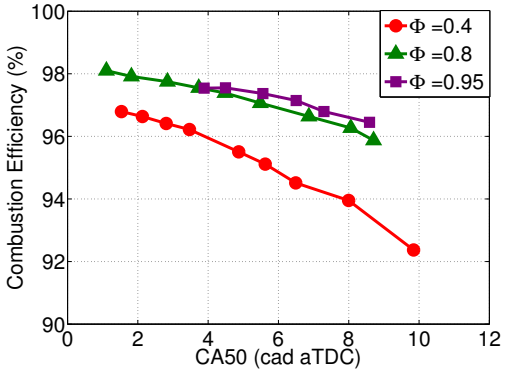

(e) Emissions index for CO vs. peak temperature

Figure 5.9 Emissions indexes, peak temperature and combustion efficiency as function of combustion phasing (CA50) for different fuel-to-air equivalence ratios

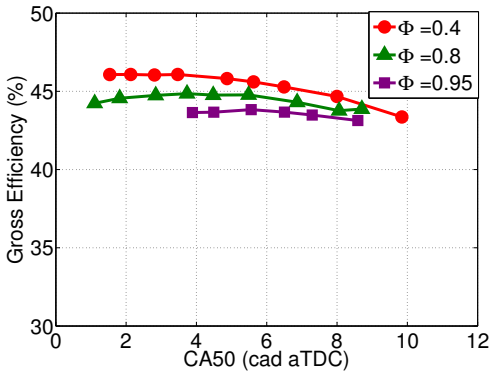

(a) Gross indicated efficiency

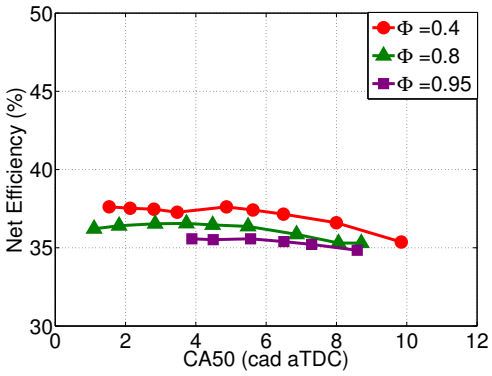

(b) Net indicated efficiency

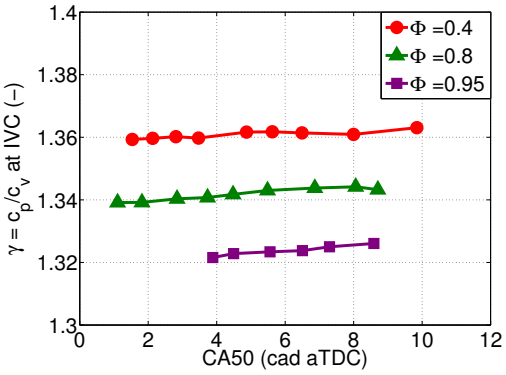

(c) Specific heat capacity γ

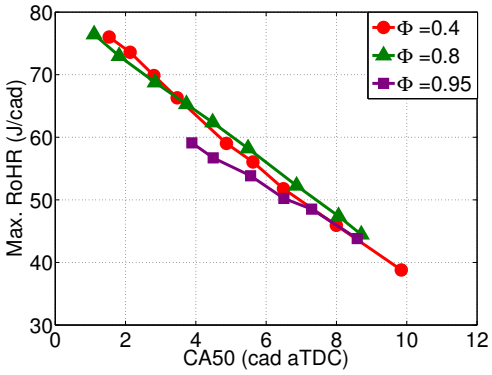

(d) Peak rate of heat release

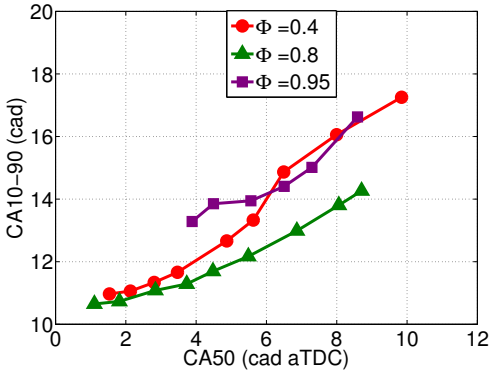

(e) Burn duration CA05-90

Figure 5.10 Indicated efficiencies as function of combustion phasing (CA50) for different fuel-to-air equivalence ratios

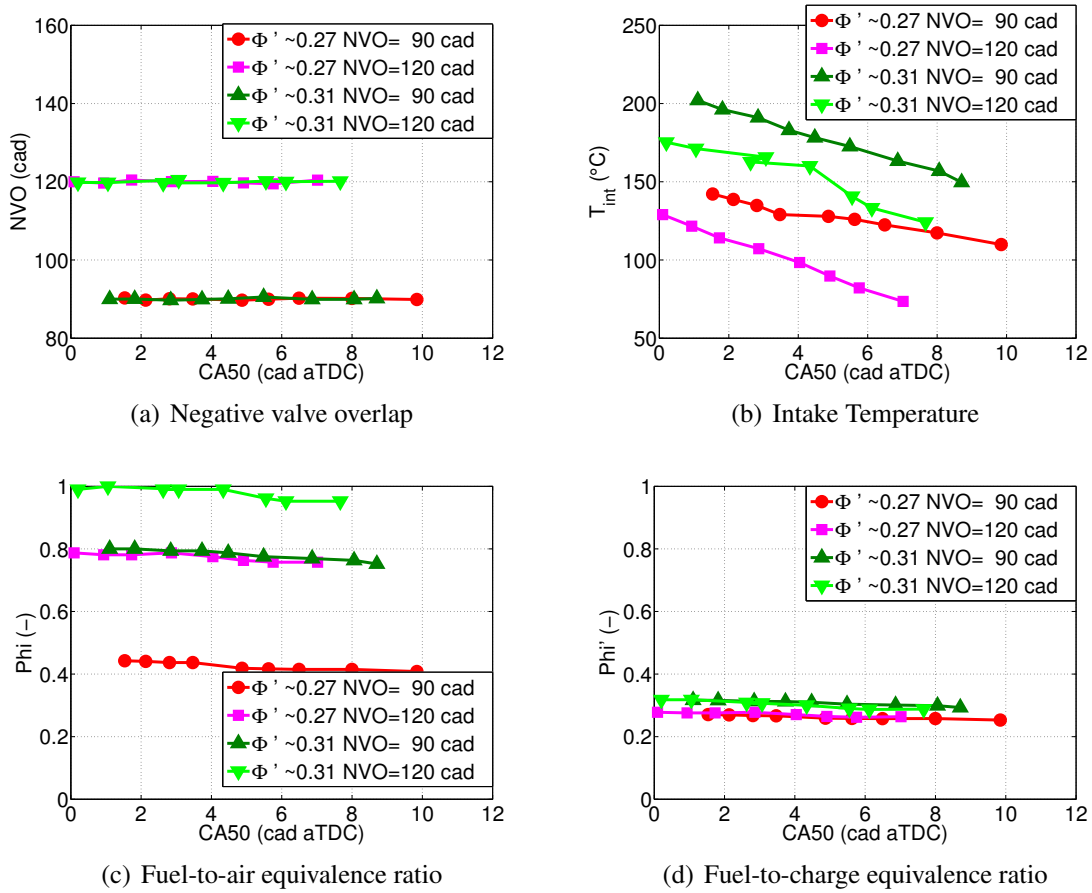

(a) Negative valve overlap

(b) Intake Temperature

(c) Fuel-to-air equivalence ratio

(d) Fuel-to-charge equivalence ratio

Figure 5.11 Boundary conditions as CA50 for different NVO and composition

5.5 NVO Effect on Combustion Phasing Limits

The effect of thermal/ compositional stratification due to iEGR/ NVO on the combustion phasing limits is investigated at constant P_{int} of 1.5 bar by partially trading eEGR with iEGR. As can be seen in Figure 5.6, combustion phasing sweeps were performed for different combinations of NVO, 90 and 120 cad, and fuel-to-charge ratio, Φ, to be able to compare different NVO and overall fuel-to-charge ratio, Φ'. For each CA50 sweep, T_{int} is gradually increased to advance CA50 from the combustion variability/ stability to the knock limit.

Knock and combustion variability limits are both affected by increasing amount of NVO although in very different ways, as can be seen in Figure 5.12. Higher NVO implies a larger amount of internally fed-back and recycled burned residual gas, which consequently leads to higher combustion variability. Therefore, if the same COV of $IMEP_g$ limit was imposed, less CA50 retard could be accomplished in case of high NVO. This is true irrespective of overall Φ'. On the other hand, higher NVO facilitates lower ringing intensity values, both $R.I._{LP}$ and $R.I._{HP}$, which allows further combustion phasing advance, if a fixed R.I. value

were to be imposed. Note, that, while eEGR addition led to a slightly wider viable CA50 operating window, increasing NVO leads to a shift of the operating window toward earlier CA50. It appears that the gain toward advanced phasing is greater than the loss on the combustion variability limit, hence adding NVO may increase to a slightly wider viable operating window that is shifted toward earlier CA50.

When comparing $R.I._{LP}$ and $R.I._{HP}$, there is again only partial agreement between both metrics over a limited range i.e. R.I. up to 3 MW/m^2 beyond which $R.I._{HP}$ increases relatively much more than $R.I._{LP}$. This corresponds to a CA50 of ~ 4 cad aTDC i.e. all cases that are more advanced suffer from some form of disagreement. The reason for lower R.I., both high-pass and low-pass, with increasing NVO is most likely directly associated with an increase in thermal/ compositional stratification owing to more iEGR. Also, note that the NVO cases with higher Φ' both show higher $R.I._{HP}$ values than the cases with lower Φ' for advanced CA50. The reason for that is most likely a larger amount of fuel for a given amount of charge hence a more vigorous heat release accompanied by a shorter burn duration.

Figure 5.13 also shows earlier beginning and slower burn rate for the lower NVO cases relative to the higher NVO cases for both Φ', which is supporting the observation that increasing NVO decreases $R.I._{LP}$. As far as $R.I._{HP}$ is concerned, the same observation holds true, but also lower Φ' leads to lower R.I. value. The reason for that could be higher in-cylinder temperature prior to combustion hence more thermal stratification and there less knock. It is difficult to make any definitive conclusions based on the nature of the experiments, but everything else was held constant.

Figure 5.14 shows low-pass and high-pass ringing intensities for each individual cycle, and one can see that there is much less variability from cycle to cycle for $R.I._{LP}$ compared to $R.I._{HP}$ data. This demonstrates that burn rates that determine pressure rise rates and peak pressures, both entering the $R.I._{LP}$ equation, are fairly stable at this advanced operating condition with CA50=2 cad aTDC. In contrast, $R.I._{HP}$ exhibits more variability due to its nature i.e. standing pressure waves are generated and measured. Note, though, that for NVO=90 cad the absolute values and variability are greater for higher Φ'. This is remarkable, since larger NVO usually implies more internal cyclic feedback and hence more variability. But this is apparently not the case for advanced CA50 and the lower peak temperature before combustion for lower NVO case thus less thermal stratification may be responsible for the variability.

Inspecting cyclic quantities at a later combustion phasing, closer to the stability limit i.e. CA50=6 cad aTDC, cyclic quantities do not offer any additional insight as to why higher NVO is responsible for slightly higher COV of $IMEP_g$ (see Figure 5.15). At this point, the

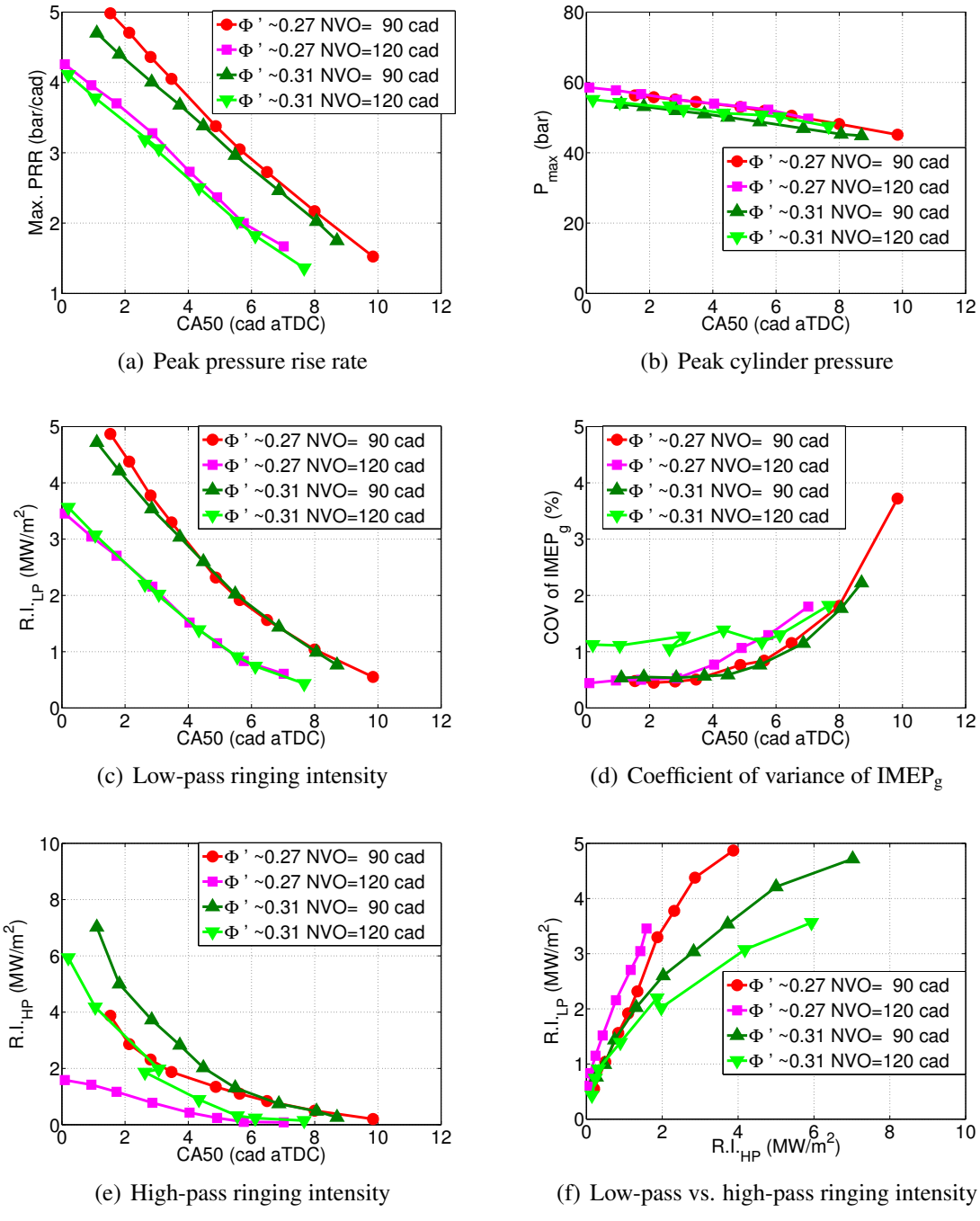

(a) Peak pressure rise rate

(b) Peak cylinder pressure

(c) Low-pass ringing intensity

(d) Coefficient of variance of $IMEP_g$

(e) High-pass ringing intensity

(f) Low-pass vs. high-pass ringing intensity

Figure 5.12 Parameters relevant to knock and combustion variability limits as function of CA50 for different NVO and composition

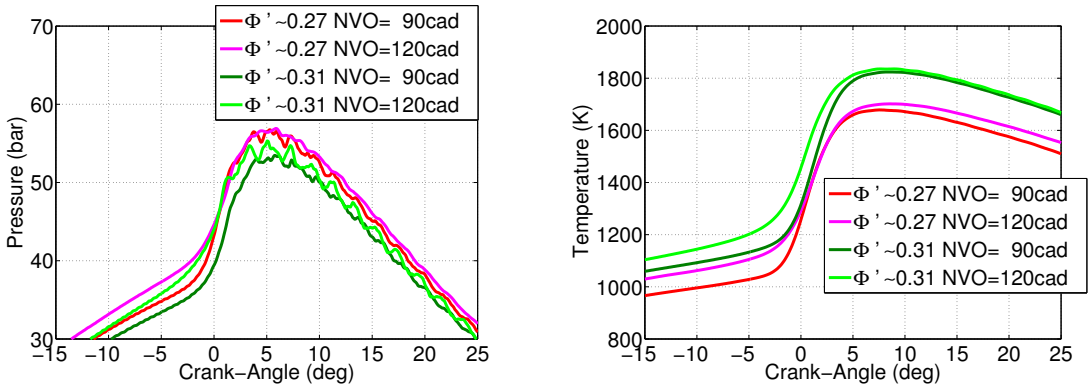

(a) Cylinder pressure

(b) In-cylinder temperature

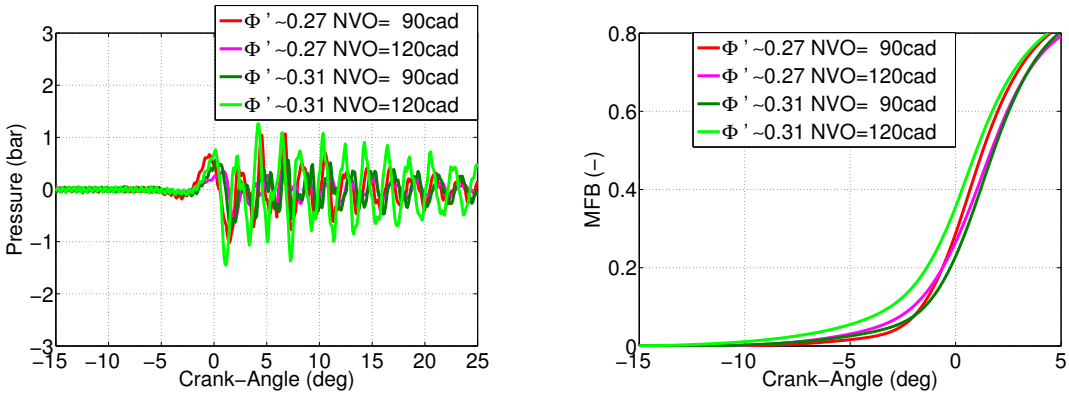

(c) dP_{cyl}

(d) Mass fraction burned

Figure 5.13 Cylinder pressure, average in-cylinder temperature, pressure difference between unfiltered and filtered cylinder pressure, and mass fraction burned for early combustion phasing (CA50=2 cad aTDC) as function of crank-angle for different NVO and fuel-to-charge equivalence ratios (results are based on median cycle with respect to peak cylinder pressure)

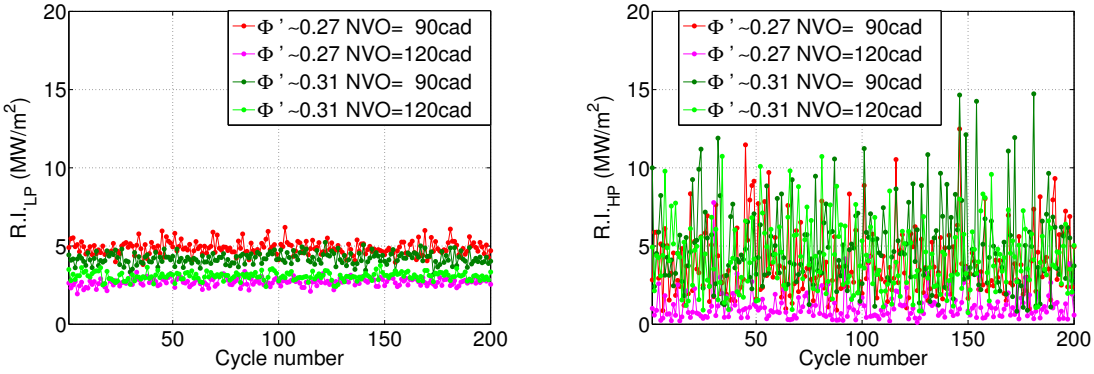

(a) Low-pass ringing intensity

(b) High-pass ringing intensity

Figure 5.14 Ringing intensities for all 200 cycles for early combustion phasing (CA50=2 cad aTDC) as function of NVO and fuel-to-charge equivalence ratio

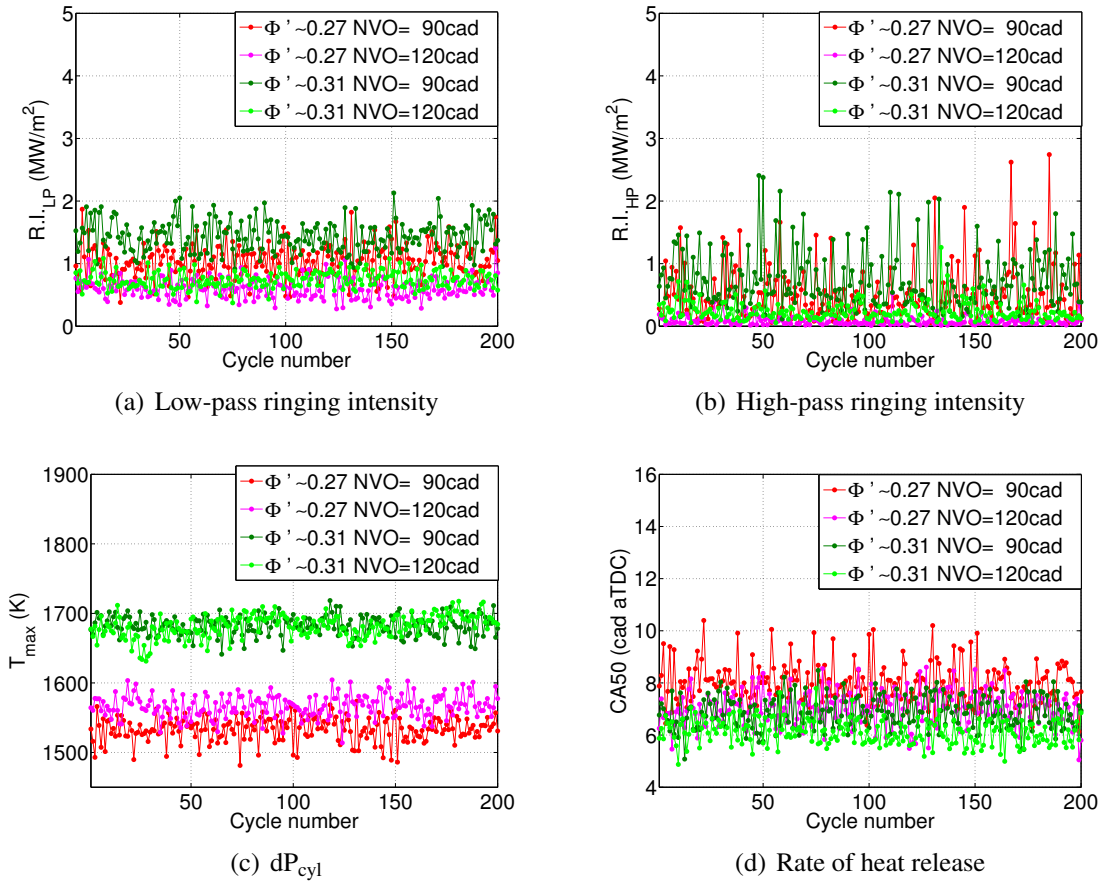

(a) Low-pass ringing intensity

(b) High-pass ringing intensity

(c) dP_{cyl}

(d) Rate of heat release

Figure 5.15 Ringing intensities, peak in-cylinder temperature, and combustion phasing for all 200 cycles for late combustion phasing (CA50=6 cad aTDC) as function of NVO and fuel-to-charge equivalence ratio

most plausible reason seems to be amore internal feedback through NVO/ iEGR.

There are not many surprises regarding emissions, as can be seen from Figure 5.16. Notice that combustion phasing and T_{max} are the key factors that determine emissions. Higher Φ' yields higher T_{max} thus more NO_X emissions. The same holds true for CO and THC emissions and combustion efficiency.

Burn duration is clearly affected by NVO i.e. higher NVO (120 cad vs. 90 cad) yields approximately to 2 cad increase in CA10-90 irrespective of CA50, as can be seen in Figure 5.17. This manifests itself also in lower values for peak RoHR for the NVO=120 cad cases, which are on average $\sim$ 15 J/cad smaller. Both burn duration and thermodynamic properties are largely responsible for difference in indicated gross and net efficiency. The highest efficiency is attained by the case combining the lowest NVO and highest Φ' value.

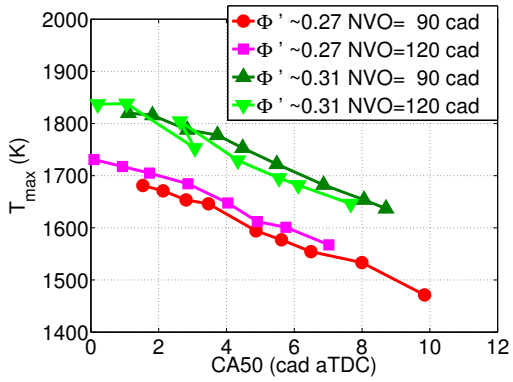

(a) Peak average in-cylinder temperature

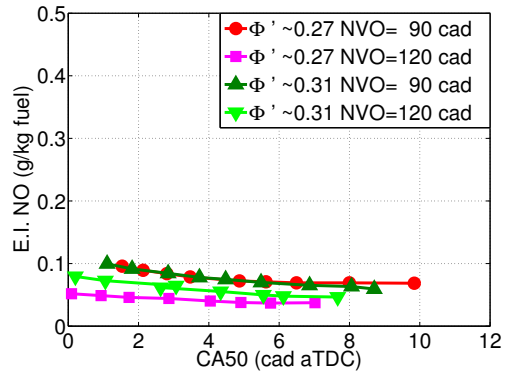

(b) Emissions index for NO_X

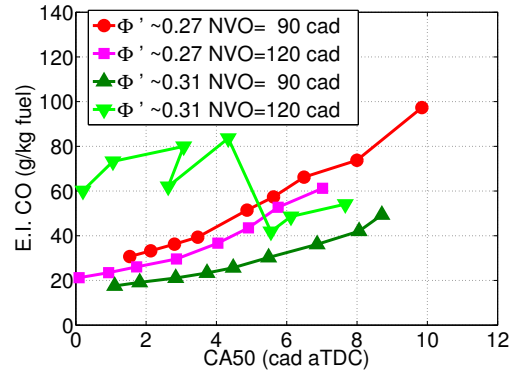

(c) Emissions index for CO

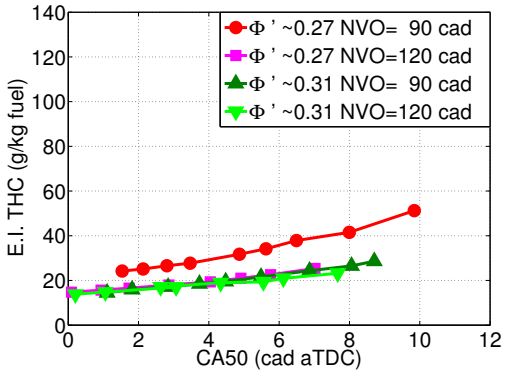

(d) Emissions index for THC

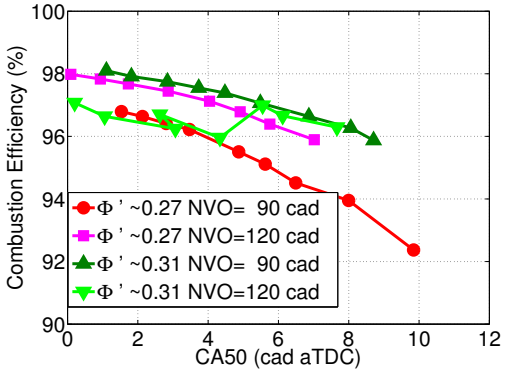

(e) Emissions index for CO vs. peak temperature

Figure 5.16 Emissions indexes, peak temperature and combustion efficiency as function of combustion phasing (CA50) for different negative valve overlap (NVO) and fuel-to-charge ratios

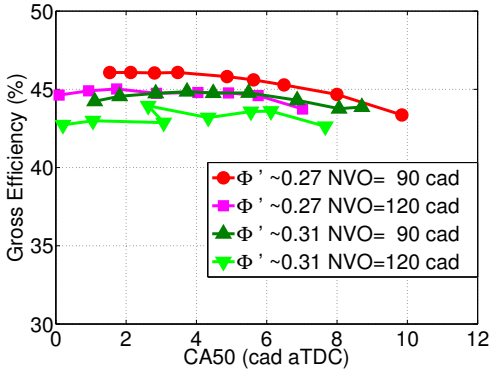

(a) Gross indicated efficiency

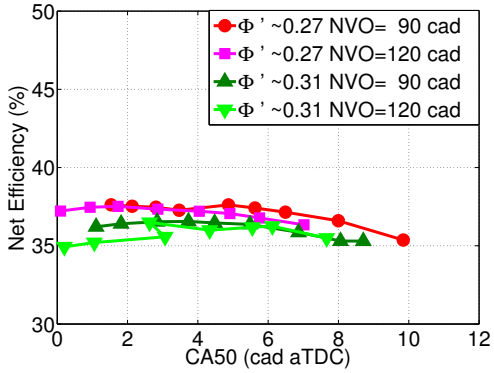

(b) Net indicated efficiency

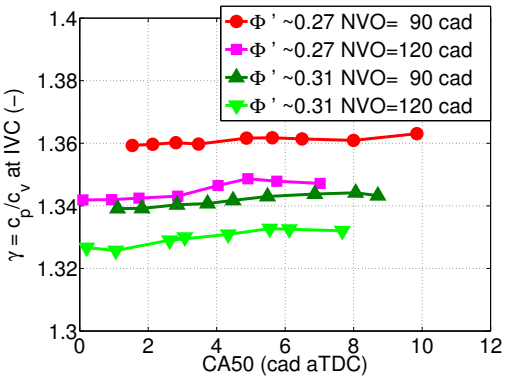

(c) Specific heat capacity γ

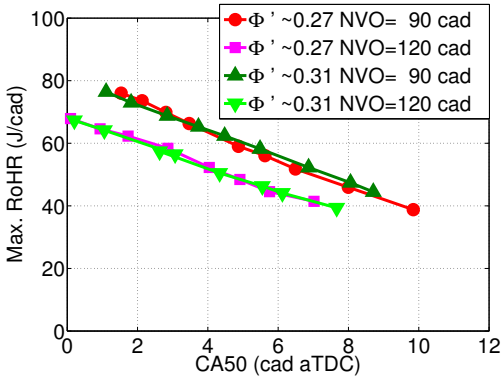

(d) Peak rate of heat release

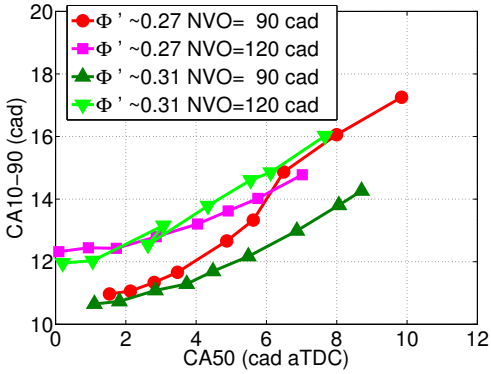

(e) Burn duration CA05-90

Figure 5.17 Indicated efficiencies as function of combustion phasing (CA50) for different fuel-to-air equivalence ratios

5.6 Summary and Conclusions

5.6.1 Summary of Results and Discussion

The goal of this chapter was to study, isolate and quantify the effect of the three fundamental thermo-physical parameters pressure, composition and stratification (via NVO) on both combustion phasing limits i.e. knock and stability limit. Experiments under controlled conditions were performed to isolate the individual effects employing a high degree of freedom engine. Combustion phasing sweeps were performed via intake temperature adjustments to focus on one effect at a time.

Boost pressure was found to have no effect on the combustion stability limit, however, it could be shown that increasing boost pressure led to an increase in ringing intensity for more advanced combustion phasing. The results are in agreement with findings from Chapter 4 and can be attributed to small changes in burn duration. Moreover, it was found that both ringing intensity metrics do not agree beyond a certain point if CA50 is sufficiently advanced and R.I. values exceed 4 MW/m^2.

Substituting part of the incoming air with eEGR was found to have beneficial effects on both the stability and knock limit. Most likely, the improved stability quantified by COV of IMEP$_g$ could be due to a higher in-cylinder temperature prior to combustion thus more thermal stratification before combustion starts, which yields a slightly longer burn and improves stability for fixed CA50. eEGR addition also was found to decrease R.I.$_{LP}$ for advanced CA50, which is in agreement with Chapter 4 and can be explained by larger thermal inertia due to thermodynamic properties. Again, above a certain threshold of only 1.5 MW/m^2, both ringing intensity metrics diverge.

Partially replacing eEGR with iEGR by increasing NVO and decreasing EGR rate was found to increase COV of IMEP$_g$ likely due to increased feedback of burned residual gas from the previous cycle via NVO valve strategy. The effect on the stability limit was relatively small and so it was difficult to quantify. As a matter of fact, more data points would have proven useful to more accurately capture the stability limit. Increasing NVO also was found to result in longer burn duration, by ~ 2 cad, which is significant. This is reflected by lower R.I.$_{LP}$.

5.6.2 Appraisal of Results and Contributions

The results presented in this chapter are a very important part of this doctoral work, as they integrate findings from previous chapters on maximum load limit and burn duration. In

general, good agreement between the results of Chapter 4 on burn rates and the findings on the knock limit in this chapter was shown. Increasing the amount of NVO used has a big effect on burn rates and can be used to extend maximum load limit, because either more advanced CA50 or higher fueling rates are feasible given the same knock constraint. Addition of eEGR was even found to be helpful in two ways that is low-pass ringing intensity decreased and also stability limit can be slightly extended.

From the results, it appears that both NVO and eEGR addition are helpful in extending the operating range of a NVO HCCI engine under the conditions studied. Boost pressure was found to have a limiting effect on the knock limit and did not show any benefit on the stability limit. However, this experiment was done at a fixed intake pressure of 1.5 bar, and the potential benefit of being able to retard combustion phasing later with higher boost pressure is not taken into account.

Another important finding of this chapter was that the two ringing intensity metrics commonly and often used interchangeably, $R.I._{HP}$ and $R.I._{LP}$, are not necessarily in agreement, especially for advanced combustion phasing, high loads and operation near knock limit. Therefore, caution should be exercised when moving from the original, and probably more appropriate, metric, $R.I._{HP}$, to the more simplistic metric, often used for modeling purposes, $R.I._{LP}$. Some potential explanations were given in terms of cycle-to-cycle statistics, but certainly more work is required to fully understand the implications.

5.6.3 Shortcoming of Results and Next Steps

This study of the combustion phasing limits suffers from a few shortcomings. For example, the NVO effect that is trading off between iEGR and eEGR was only studied over a narrow range of NVO. The fuel-to-charge ratio was also only varied within a narrow range. A major limitation of the study was that the eEGR and NVO part of the study were only carried out at a modest boost pressure of 1.5 bar. At a higher boost pressure, where more combustion phasing retard would be possible, possibly different findings could be made especially regarding the stability limit.

In this study, other parameters that could potentially affect both combustion phasing limits i.e. start of injection and pressure differential ($dP=P_{exh}-P_{exh}$) were not evaluated. However, it is quite likely that both of the parameters may have significant impact on both limits, as mixture composition and homogeneity could be dramatically altered.

Chapter 6

Conclusions, Contributions and Recommendations for Future Work

In this thesis, boosted HCCI experiments were performed under carefully controlled conditions in a NVO engine to investigate the effects of boost pressure, charge temperature and composition, and thermal/ compositional stratification on the maximum load limit. The results of the maximum load sweeps in this research were compared to results of a well instrumented HCCI engine with conventional PVO strategy reported in the literature. By means of a complementary parametric modeling study, key enablers for high load operation were identified and their effects on load extension quantified. Carefully performed experiments, holding as many operating parameters as possible constant, enabled isolation and quantification of the individual effects of boost pressure and eEGR on burn duration. This research generated an enhanced understanding of the knock and combustion variability limits and yielded new insights into what these limits depended on and how they affected the maximum load capability in a NVO HCCI engine.

This chapter summarizes important findings and conclusions from the results presented in chapters 3, 4 and 5 of this doctoral work, highlights key contributions and concludes by suggesting and discussing potential areas of interest that could be addressed in the future.

6.1 Summary and Conclusions

6.1.1 Maximum Load Limit of NVO Engine

In Chapter 3, the maximum load limit of a practical boosted HCCI NVO engine is experimentally investigated focusing on the effects of operating parameters such as diluent (eEGR vs. air), intake temperature, engine speed and overall turbocharger efficiency. The results showed that the high load and boosting limit of HCCI combustion in a NVO engine

is mainly dictated by engine hardware constraints and how various operating parameters affect ignition timing. In addition, the maximum achievable load for this NVO engine was found to be less than that obtained by previous workers on a boosted PVO engine due to less efficient breathing, less stable combustion, which limits the achievable combustion phasing retard, and lower maximum allowable peak cylinder pressure.

- Adding external EGR (eEGR) and partially replacing the incoming air with burned gas enabled higher maximum $IMEP_g$ and P_{int} to be attained. This was due to implications of composition (more eEGR) on the ignition process, requiring higher IVC temperature to maintain ignition timing, thus increasing NVO and alleviating the constraint of limited cam-phasing authority until a higher load condition. External EGR resulted in lower thermal efficiency due to lower γ, but this could be partially compensated for with higher combustion efficiency. Lowering the intake temperature had a similar effect as adding eEGR that is lowering the IVC temperature and requiring more NVO to maintain combustion phasing.
- Lowering the engine speed facilitated significantly higher achievable maximum load for all P_{int} primarily due to a shorter burn duration. A faster burn rate with respect to crank-angle degrees enabled combustion to be phased later, while still operating the engine at the stability limit. The more pronounced descending motion of the piston at a later CA50 attenuates the pressure rise rate due to heat release for a given constant fuel injection rate. Since a constant ringing intensity value was imposed, a higher $dP/d\theta$ was permissible in case of the lower engine speed yielding the same dP/dt because of lower $d\theta/dt$. Because of CA50 retardation and higher permissible peak pressure rise rate, it was possible to increase the fuel injection rate, while still keeping knock intensity in check. In addition, for P_{int} equal to or greater than 2.0 bar, low temperature heat release (LTHR) was observed at lower engine speed, which was found to enable even further combustion phasing retard and higher loads.
- Overall turbocharger efficiency (OTE) affects the maximum load limit mainly through modifying the relative amount of trapped hot internal EGR, which has implications

on the valve strategy. Higher OTE or relatively lower exhaust back-pressure enabled higher maximum $IMEP_g$ by increasing the cam phasing authority leeway because of a reduced iEGR fraction.

- A parametric modeling study using GT Power was performed comparing this NVO engine to published data from a PVO engine. The results showed that high load in the UM NVO engine for a given P_{int} was limited by low volumetric efficiency due to inadequate breathing. Hot iEGR yielded a decreased IVC density and lower and shorter valve profiles restricted gas flow through the engine and increased pumping work. Decreasing engine speed not only helped for the aforementioned reasons of later CA50 and shorter burn durations, but also because of increased volumetric efficiency and allowing higher maximum pressure rise rates, while still satisfying the knock constraint. The SNL PVO engine showed shorter burn durations than the UM NVO engine, even at the same engine speed, indicates that shorter burn duration, by itself or as a result of other yet unknown effects, is an enabler for further combustion phasing retard and higher loads.

6.1.2 Effects of Composition and Boost Pressure on Burn Duration

In chapter 4, the effects of intake boost pressure and composition on burn duration were investigated. Experiments under very controlled conditions were conducted taking full advantage of the high degree of flexibility of the engine setup. For each of the three different P_{int} ranging from 1.5 to 2.5 bar, fuel-to-charge ratio, Φ', was kept approximately constant by scaling the amount of fuel injected with P_{int}. NVO was fixed at 90 cad to minimize the potential effect of varying thermal/ compositional stratification and dP was held constant at 0.5 bar to attain similar iEGR fractions between different P_{int} cases. Combustion phasing was held constant (CA50=5 cad aTDC) to avoid any bias, because it is knowns to affect burn duration. Composition was gradually changed as intake air was replaced successively with increasing amounts of eEGR. Intake temperature was used to adjust and maintain CA50 during the sweep. These detailed studies on burn rates showed minimal effects of intake boost pressure and moderate effects of composition.

- Replacing air with eEGR (increasing Φ), thus decreasing in-cylinder O_2 concentration and increasing CO_2 and water concentration, led to a moderate increase in burn duration especially during the early stage of heat release. Peak rates of heat release did not reflect these changes, because they were neglegibly small.
- Increasing boost pressure, P_{int}, caused a minimal shortening of the burn duration, but pressure rise rates and knock were unaffected.
- Combustion efficiency increases with increasing eEGR and P_{int}. CO emissions were found to be independent of P_{int} and only varied with Φ. However, THC emissions varied not only with Φ but also with P_{int}.
- THC, most likely stemming from crevices, were found to decrease with increasing P_{int} suggesting a smaller fraction of the charge being trapped in the crevices at higher P_{int} due to higher load and piston temperature. Another possible explanation could be more post-burn-up in crevices due to steeper temperature gradients near the wall in case of higher P_{int}.

6.1.3 Effects of Boost Pressure, Composition and NVO on Combustion Phasing Limits

In chapter 5, the effects of intake boost pressure, composition (Φ) and NVO on the combustion phasing limits were investigated. Combustion phasing sweeps via intake temperature adjustments were performed to study how both of the combustion phasing limits, knock and combustion variability, depend on the aforementioned individual parameters. Because knock and combustion variability occur simultaneously at the maximum load limit, understanding the limit behavior in more detail was crucial to understanding the maximum load limit of this engine.

- The experimental results showed that external EGR (eEGR) addition, or replacing air with eEGR, yielded a wider operating window, which could lead to a higher maximum load. The results were in agreement with previous findings from Chapter 3.

- Intake boost pressure had no direct effect on either of the combustion phasing limits, which was found to be in agreement with Chapter 4.
- A higher value of negative valve overlap (NVO) increasing the amount of retained internal EGR (iEGR) had a negative effect on combustion stability, likely due to increased cycle-to-cycle feedback. Consequently, less combustion phasing retard could be achieved for the higher NVO case, therefore, reducing the potential maximum attainable load. On the other hand, NVO had a positive effect on the knock or ringing intensity limit. The knock limit could be further advanced with higher NVO, because of reduced peak pressure rise rates likely due to enhanced thermal/ compositional stratification because of a larger amount of iEGR. This would allow either advancing combustion phasing or increasing fuel injection rate thus load with higher NVO. Overall. increasing NVO shifted the viable combustion phasing window toward earlier CA50.

6.2 Contributions

Within the realm of downsizing of modern IC engines and deploying advanced combustion strategies, boosted HCCI combustion is a logical extension of naturally aspirated HCCI combustion in an attempt to leverage the benefits of HCCI operation such as increased efficiency over a wider load range. The experiments performed demonstrate a high level of control of boosted HCCI combustion in a practical NVO engine. Using a highly flexible single-cylinder research engine capable of boosted operation, the effects of a variety of engine operating parameters on combustion and performance were analyzed in terms of fundamental parameters such as intake boost pressure, charge temperature and composition (Φ), and thermal/ compositional stratification (NVO).

This current work is unique in that it combines and integrates the current work with various findings from previous works and applies them towards boosted HCCI combustion in a NVO engine to gain an enhanced understanding of the mechanisms limiting the maximum load capability. Important contributions are:

- Experimental results demonstrated that boost pressure facilitated later combustion phasing hence a higher maximum attainable load and improved efficiency due to enhanced charge dilution and more advantageous thermodynamic properties of a leaner mixture.
- The maximum achievable load in a practical NVO engine was shown to be largely determined by both ignition requirements and overall engine constraints especially cam phasing authority and maximum allowable peak cylinder pressure.
- Maximum load experiments conducted at lower engine speed revealed that a shorter burn duration in crank-angle degrees facilitating later combustion phasing was responsible for a higher maximum attainable load for a given boost pressure. Low temperature heat release (LTHR) was identified to play an additional role at highly boosted operation.
- 1-D engine simulation software was used to augment the experiments and analysis work. The difference in maximum attainable load between the NVO engine used in this research and an extensively studied PVO engine could be largely explained with thermodynamics and breathing considerations.
- Burn duration and combustion phasing need to be considered together and not independently, when evaluating the potential to extend the load limit. In particular, isolating the effect of pressure and composition on burn duration demonstrated a moderate effect of composition and minimal effect of boost pressure on burn rates,
- Both combustion phasing limits, knock and stability, were found to be very important to the maximum load limit. This work, for the first time, quantified and separated effects of various fundamental thermo-physical parameters (boost pressure, NVO/ stratification, eEGR) on these limits. Especially, the stability limit was identified to offer a lot of potential for further extending the maximum load capability, provided one could attain more stable combustion at even later combustion phasing.
- The experimental results suggested that the maximum load was more dependent on

the combustion stability and overall engine constraints than on burn rates, which were relatively insensitive to changes in pressure and other thermo-physical parameters.

6.3 Recommendations for Future Work

This doctoral thesis focused on single-cylinder NVO engine experiments to gain insight into the boosted HCCI combustion process and was augmented by a complementary 1-D engine simulation exploring the difference in maximum achievable load between this engine and another well-known PVO engine. The results were valuable and informative, and they provide direction for further experimental and computational work that can shed more light into the fundamental mechanisms limiting the maximum load capability of a NVO HCCI engine.

Future work should focus on the following aspects: (a) determine sensitivities of burn rates with respect to other operating parameters including engine speed, NVO and overall fuel-to-charge dilution ratio, (b) investigate the effects of back-pressure (OTE), injection timing, and overall fuel-to-charge dilution ratio on knock and combustion variability limits, (c) further understand why the SNL PVO engine is characterized by more stable combustion (lower COV of $IMEP_g$) and faster burn rates, (d) investigate the potential of boosted spark-assisted HCCI (SACI) for further load extension, and (e) incorporate findings into an enhanced 1-D simulation model capable of advanced boosted IC engines.

(a) Burn rates and the shape of the burn profile are directly related to maximum pressure rise rates and ringing intensity defining the knock limit. A more complete understanding of burn rate sensitivities to other quantities than intake boost pressure and composition (eEGR vs air dilution) will be helpful. Longer burn duration is desirable from a knock limit standpoint. Shorter burn duration, although by itself is disadvantageous, can yield a net benefit by enabling further combustion phasing retard. The mechanisms responsible for shorter burn duration at lower engine speed have not yet fully been explored. Therefore, conducting experiments at constant CA50 at different engine speeds and boost pressures will help isolate and quantify the effect of engine speed. Similarly, studying the impact of NVO over a wide range on burn duration for fixed

CA50 can help clarify and quantify the effect of NVO and iEGR on lengthening burn duration. Overall fuel-to-charge equivalence ratio, Φ', was not exactly constant during the experiments in Chapter3, but Φ' increased with increasing Φ, which could potentially have biased the experiment and made the burn duration increase with increasing Φ appear smaller than it actually is if Φ' was constant. A compensated Φ sweep, where either P_{int} or IVC is slightly adjusted to compensate for decreasing charge density with increasing Φ would allow a more non-biased measurement of burn duration.

(b) Although burn duration and ringing intensity are important as they affect the knock limit, combustion variability is even more important, because it determines how much CA50 retard can be achieved, which is a high load enabler. While experiments in this thesis shed light into the effects of P_{int}, NVO and eEGR on the limit, the effects of other parameters including OTE/ dP, start of injection (SOI) timing and Φ' still remain to be explored. A larger pressure differential (dP) will yield a larger iEGR fraction for the same NVO, but it is not clear if and how much dP matters in addition to NVO/ IVC alone as far as combustion variability is concerned. The injection timing is believed to potentially have a larger impact than previously suggested, because with larger dP (low OTE) there will be back-flow into the intake after IVO. Moreover, early SOI may involve fuel reforming and contribute to early formation of reactive intermediates, and late SOI may increase charge inhomogeneity. In fact, based on the SOI, there may be significant spray impingement on the piston, which could potentially dramatically effect homogeneity of the mixture hence combustion stability. Finally, Φ' may also affect stability due to its direct effect on peak and post-combustion in-cylinder temperatures affecting quenching of combustion close to walls. Low Φ' and $T_{cyl,max}$ may lead to more quenching at the walls increasing combustion variability. On the other hand, high Φ' and $T_{cyl,max}$ may initially be aiding combustion stability, beyond a certain point may cause disruption of the wall boundary layers due to increased heat transfer because of knock finally yielding less stable combustion again.

(c) The SNL PVO engine facilitates later CA50 and more stable combustion. While the GT Power model allowed quantification of individual effects and identification of key enablers, the model did not account for any combustion details and only experimentally measured burn profiles were imposed. Studying and understanding what contributes to enhanced combustion stability (much lower COV of IMEPg) is an important task to be tackled by future experiments. At this point, one can only speculate whether the largely different stability is due to the combustion chamber design and geometry properties such as displacement volume, CR, valves, piston crown design or due to fuel preparation strategy i.e. direct injection compared to port fuel-injection and SOI. In this real, PVO experiments, with very less iEGR content, could be conducted to see if and how much thermal/ compositional stratification due to iEGR/ NVO contributes to the stability limit. Previous modeling work studying the effect NVO/ PVO valve strategy and CR identified a certain favorable CR. It remains to be experimentally proven if this is correct, as the model lacked any potential influence on knock and stability limits. As a next step, in addition to assessing PVO vs. NVO strategy and different CRs, it would be useful to test the effect of piston crown topology on combustion. Instead of employing a piston with large cut-outs and squish, a pan-cake shape combustion chamber would be used with smaller surface to volume ratio at TDC, this could potentially enhance combustion stability. Although difficult to do with this engine, it may be useful to study a scaled-up engine with larger valves or replace the 4-valve head with a 2-valve head and see if bigger intake/ exhaust geometry will lead to fewer and larger eddies creating less turbulence thus allowing faster burn rates and later CA50. Lastly, the effect of LTHR could be studied in more detail to understand how much this effect is relative to lower engine speed and shorter burn duration in terms of crank-angle degrees.

(d) A logical extension of this work on boosted HCCI combustion would be to study the effect of spark-assist (SACI combustion) under boosted conditions. Combining the benefits of naturally aspirated SACI and boosting for even higher loads will be of high

practical value, whereas new insights into flame kernel development and the coupling of combustion through flame propagation and auto-ignition under high pressure conditions could be gained. Whereas multi-cylinder engines with bolted down turbocharger equipment suffer from limited degrees of freedom, in particular achieving high EGR rate is difficult, the high degree of flexibility of this single-cylinder engine will be extremely valuable in covering a wide range of conditions in terms of boost pressure and Φ'. In particular, the effect of boost pressure on the flame-portion and auto-ignition portion of the burn and the coupling of these two distinct energy release modes will be interesting. Other parameters such as composition, NVO, and engine speed on flame kernel development and auto-ignition event will be important to study and quantify.

(e) The 1-D simulation package GT Power was used to explain the difference in terms of maximum attainable load between the UM NVO engine and the SNL PVO engine, but did not account for burn duration and combustion phasing limits. Given the situation, that burn rates and both combustion phasing limits, knock and variability, have been more extensively measured under boosted conditions for the first time, it would be useful to develop and adopt an empirical model capturing the limit behavior and repeat and expand on previous system level studies. Even before a new model is developed, the current parametric study could still be improved. For example, as CA50 and CA10-90 were not studied independently, separation of these two effects could be valuable. Since burn rates were imposed, ignition was not captured adequately for the individual steps between the start and end points of the parameter walk. For example, rising CR would entail a lower intake temperature or NVO to maintain proper ignition timing. This aspect was not accounted for and a more refined study could incorporate these effects based on the ignition delay. Similarly, as eEGR is increased, intake temperature should be raised to account for that. Still, the most important aspect to attain a high fidelity combustion model is to be able to adequately capture the combustion phasing limits, in particular the stability limit.

Bibliography

[1] International Monetary Fund. "World Economic Outlook April 2013 - Hopes, Realities, Risks". Technical report, April 2013.

[2] "World Population to 2300". Technical Report ST/ESA/SER.A/236, United Nations, New York, September 2004.

[3] Obama, B. "2011 State of the Union Address". Transcript retrieved from http://www.nytimes.com/2011/01/26/us/politics/26obama-text.html?pagewanted=all, January 2011.

[4] D. Dokken. Managing the Risks of Extreme Events and Disasters to Advance Climate Change Adaption. Technical report, "Intergovernmental Panel on Climate Change", April 2012.

[5] European Commission. "Road transportation: Reducing CO2 emissions from vehicles". Transcript retrieved from http://ec.europa.eu/clima/policies/transport/vehicles/index$_e n.htm, July$2012.

[6] P. Bastani, J. B. Heywood, and C. Hope. "U.S. CAFE Standards - Potential for Meeting Light-duty Vehicle Fuel Economy Targets, 2016-2025". Technical report, MIT, 2012.

[7] W. Lerner. "The Future of Urban Mobility - Towards networked, multimodal cities of 2050". Technical report, Arthur D. Little, November 2011.

[8] N. A. Otto. "Gas Motor Engine", February 1887.

[9] C. Benz. "Vehicle with gas engine operation", January 1886.

[10] Davis, D. E. *"Thus Spake David E.: The Collected Wit and Wisdom of the Most Influential Automotive Journalist of Our Time"*. Momentum Books Ltd, Troy, Michigan, 1999.

[11] K. Epping, S. M. Aceves, R. Bechtold, and J. E. Dec. "The Potential of HCCI Combustion for High Efficiency and Low Emissions". *SAE Technical Paper 2002-01-1923*, 2002.

[12] S. Onishi, S. H. Jo, K. Shoda, P. D. Jo, and S. Kato. "Active Thermo-Atmoshpere Combustion (ATAC) - A New Combustion Process for Internal Combustion Engines". *SAE Paper 790501*, 1979.

[13] M. Noguchi, Y. Tanaka, T. Tanaka, and Y. Takeuchi. "A Study on Gasoline Engine Combustion by Observation of Intermediate Reactive Products during Combustion". *SAE Technical Paper 790840*, 1979.

[14] P. M. Najt and D. E. Foster. "Compression-Ignited Homogeneous Charge Combustion". *SAE Technical Paper 830264*, 1983.

[15] R. H. Thring. "Homogeneous-Charge Compression-Ignition (HCCI) Engines". *SAE Technical Paper 892068*, 1989.

[16] J. E. Dec. "A Conceptual Model of DI Diesel Combustion Based on Laser-Sheet Imaging". *SAE Technical Paper 970873*, 1997.

[17] A. Hultqvist, M. Christensen, B. Johansson, M. Richter, J. Nygren, J. Hult, and M. Alden. "The HCCI Combustion Process in a Single Cycle - Speed Fuel Tracer LIF and Chemiluminescence Imaging". *SAE Technical Paper 2002-01-0424*, 2002.

[18] U. Wagner, R. Anca, A. Velji, and U. Spicher. "An Experimental Study of Homogeneous Charge Compression Ignition (HCCI) with Various Compression Ratios, Intake Air Temperatures and Fuels with Port and Direct Fuel Injection". *SAE Technical Paper 2003-01-2293*, 2003.

[19] J. E. Dec, W. Hwang, and M. Sjöberg. "An Investigation of Thermal Stratification in HCCI Engines Using Chemiluminescence Imaging". *SAE Technical Paper 2006-01-1518*, 2006.

[20] B. T. Zigler, S. M. Walton, D. Assanis, E. Perez, M. S. Wooldridge, and S. T. Wooldridge. "An Imaging Study of Compression Ignition Phenomena of Iso-Octane, Indolene, and Gasoline Fuels in a Single-Cylinder Research Engine". *Journal of Engineering for Gas Turbines and Power*, 130:1–11, 2008.

[21] S. B. Fiveland and D. Assanis. "A four-stroke homogeneous charge compression ignition engine simulation for combustion and performance studies". *SAE Technical Paper 2000-01-0332*, 2000.

[22] G. Kontarakis, N. Collings, and T. Ma. "Demonstration of HCCI Using a Single Cylinder Four-Stroke SI Engine with Modified Valve Timing". *SAE Technical Paper 2000-01-2870*, 2000.

[23] N. Milovanovic, R. Chen, and J. Turner. "Influence of the Variable Valve Timing Strategy on the Control of a Homogeneous Charge Compression (HCCI) Engine". *SAE Technical Paper 2004-01-1899*, 2004.

[24] J. L. Chesa Rocafort, M. M. Andreae, W. H. Green, W. K. Cheng, and J. S. Cowart. "A Modeling Investigation into the Optimal Intake and Exhaust Valve Event Duration and Timing for a Homogeneous Charge Compression Ignition Engine". *SAE Technical Paper 2005-01-3746*, 2005.

[25] A. Babajimopoulos, D. N. Assanis, and S. B. Fiveland. "An Approach for Modeling the Effects of Gas Exchange Processes on HCCI Combustion and Its Application in Evaluating Variable Valve Timing Control Strategies". *SAE Technical Paper 2002-01-2829*, 2002.

[26] A. Babajimopoulos, G. A. Lavoie, and D. N. Assanis. "Modeling HCCI Combustion with High Levels of Residual Gas Fraction - A Comparison of Two VVA Strategies". *SAE Technical Paper 2003-01-3220*, 2003.

[27] M. Christensen, B. Johansson, P. Amnéus, and F. Mauss. "Supercharged Homogeneous Charge Compression Ignition". *SAE Technical Paper 980787*, 1998.

[28] J.-O. Olsson, P. A. Tunestål, G. Haraldsson, and B. Johansson. "A Turbo Charged Dual Fuel HCCI Engine". *SAE Technical Paper 2001-01-1896*, 2001.

[29] J. E. Dec and Y. Yang. "Boosted HCCI for High Power without Engine Knock and with Ultra-Low NO_XEmissions - using Conventional Gasoline". *SAE Technical Paper 2010-01-1086*, 2010.

[30] S. Mamalis, A. Babajimopoulos, O. Guralp, and P. Najt. "Optimal Use of Boosting Configurations and Valve Strategies for High Load HCCI - A Modeling Study". *SAE Technical Paper 2012-01-1101*, 2012.

[31] M. Sjöberg and J. E. Dec. "EGR and Intake Boost for Managing HCCI Low-Temperature Heat Release over Wide Ranges of Engine Speed". *SAE Technical Paper 2007-01-0051*, 2007.

[32] M. Sjöberg, J. E. Dec, and W. Hwang. "Thermodynamic and Chemical Effects of EGR and Its Constituents on HCCI Autoignition". *SAE Technical Paper 2007-01-0207*, 2007.

[33] J. E. Dec, M. Sjöberg, and W. Hwang. "Isolating the Effects of EGR on HCCI Heat-Release Rates and NOx Emissions". *SAE Technical Paper 2009-01-2665*, 2009.

[34] M. Sjöberg and J. E. Dec. "Effects of EGR and its constituents on HCCI autoignition of ethanol". *Proceedings of the Combustion Institute*, 33(2):3031–3038, 2011.

[35] A. Dubreuil, F. Foucher, and C. Mounaïm-Rouselle. "Effect of EGR Chemical Components and Intake Temperature on HCCI Combustion Development". *SAE Technical Paper 2006-32-0044*, 2006.

[36] M. Fathi, R. K. Saray, and M. D. Checkel. "The influence of Exhaust Gas Recirculation (EGR) on combustion and emissions of n-heptane/natural gas fueled Homogeneous Charge Compression Ignition (HCCI) engines". *Applied Energy*, 88(12):4719–4724, 2011.

[37] A. Piperel, X. Montagne, and P. Dagaut. ”HCCI Engine Combustion Control using EGR: Gas Composition Evolution and Consequences on Combustion Process”. *SAE Technical Paper 2007-24-0087*, 2007.

[38] P. Risberg, G. Kalghatgi, and H.-E. åAngstrom. ”The influence of EGR on Auto-ignition Quality of Gasoline-like Fuels in HCCI Engines”. *SAE Technical Paper 2004-01-2952*, 2004.

[39] P. G. Aleiferis, A. G. Charalambides, Y. Hardalupas, A. M. K. P. Taylor, and Y. Urata. ”Modeling and Experiments of HCCI Engine Combustion with Charge Stratification and Internal EGR”. *SAE Technical Paper 2005-01-3725*, 2005.

[40] A. P. Chialva. ”Analysis of Intake Charge Temperature and EGR Stratification Effects on HCCI Combustion”. Master’s thesis, University of Wisconsin, 2006.

[41] J. E. Dec. ”A Computational Study of the Effects of Low Fuel Loading and EGR on Heat Release Rates and Combustion Limits in HCCI Engines”. *SAE Technical Paper 2002-01-1309*, 2002.

[42] J.-O. Olsson, P. A. Tunestål, J. Ulfvik, and B. Johansson. ”The Effect of Cooled EGR on Emissions and Performance of a Turbocharged HCCI Engine”. *SAE Technical Paper 2003-01-0743*, 2003.

[43] A. Cairns and H. Blaxill. ”The Effects of Combined Internal and External Exhaust Gas Recirculation on Gasoline Controlled Auto-Ignition”. *SAE Technical Paper 2005-01-0133*, 2005.

[44] A. Cairns and H. Blaxill. ”Lean Boost and External Exhaust Gas Recirculation for High Load Controlled Auto-Ignition”. *SAE Technical Paper 2005-01-3744*, 2005.

[45] D. Yap, M. L. Wyszynski, A. Megaritis, and H. Xu. ”Applying boosting to gasoline HCCI operation with residual gas trapping”. *SAE Technical Paper 2005-01-2121*, 2005.

[46] T. Johansson, B. Johansson, P. A. Tunestål, and H. Aulin. ”HCCI Operating Range in a Turbo-charged Multi Cylinder Engine with VVT and Spray-Guided DI”. *SAE Technical Paper 2009-01-0494*, 2009.

[47] J. Hyvönen, G. Haraldsson, and B. Johansson. ”Supercharging HCCI to Extend the Operating Range in a Multi-Cylinder VCR-HCCI Engine”. *SAE Technical Paper 2003-01-3214*, 2003.

[48] S. Mamalis, V. Nair, P. Andruskiewicz, D. Assanis, A. Babajimopoulos, N. Wermuth, and P. M. Najt. ”Comparison of Different Boosting Strategies for Homogeneous Charge Compression Ignition Engines - A Modeling Study”. *SAE Technical Paper 2010-01-0571*, 2010.

[49] P. Shingne, D. Assanis, A. Babajimopoulos, P. Keller, D. Roth, and M. Becker. "Turbocharger Matching for a 4-Cylinder Gasoline HCCI Engine Using a 1D Engine Simulation". *SAE Technical Paper 2010-01-2143*, 2010.

[50] H. Ando, K. Iida, O. Nakayama, and T. Yamauchi. "Mitsubishi GDI engine - Strategies to meet the European requirements". *SAE Technical Paper 1997-29-0017*, 1997.

[51] P. Whitaker, Y. Shen, C. Spanner, H. Fuchs, A. Agarwal, and K. Byrd. "Development of the Combustion for a Flexible Fuel Turbocharged Direct Injection Engine". *SAE Technical Paper 2010-01-0585*, 2010.

[52] J. H. Lim and R. D. Reitz. "Improving high efficiency reactivity controlled compression ignition combustion with diesel and gasoline direct injection". *Proceedings of the Institution of Mechanical Engineers, Part D: Journal of Automobile Engineering*, 227(1):17–30, January 2013.

[53] Y. Li, H. Zhao, N. Brouzos, T. Ma, and B. Leach. "Effect of Injection Timing on Mixture and CAI Combustion in a GDI Engine with an Air-Assisted Injector". *SAE Technical Paper 2006-01-0206*, 2006.

[54] N. Wermuth, H. Yun, and P. Najt. "Enhancing Light Load HCCI Combustion in a Direct Injection Gasoline Engine by Fuel Reforming During Recompression". *SAE Technical Paper 2009-01-0923*, 2009.

[55] H. H. Song, A. Padmanabhan, N. B. Kaahaaina, and C. F. Edwards. "Experimental study of recompression reaction for low-load operation in direct-injection homogeneous charge compression ignition engines with n-heptane and i-octane fuels". *International Journal of Engine Research*, 10(4):215–229, 2009.

[56] J. Kodavasal. *"Effect of Charge Preparation Strategy on HCCI Combustion"*. PhD thesis, University of Michigan, 2013.

[57] A. Kulzer, A. Christ, M. Rauscher, C. Sauer, G. Würfel, and T. Blank. "Thermodynamic Analysis and Benchmark of Various Gasoline Combustion Concepts". *SAE Technical Paper 2006-01-0231*, 2006.

[58] M. Sjöberg and J. E. Dec. "An Investigation of the Relationship Between Measured Intake Temperature, BDC Temperature, and Combustion Phasing for Premixed and DI HCCI Engines". *SAE Technical Paper 2004-01-1900*, 2004.

[59] H. Zhao, J. Li, M. Tom, and N. Ladommatos. "Performance and Analysis of a 4-Stroke Multi-Cylinder Gasoline Engine with CAI Combustion". *SAE Technical Paper 2002-01-0420*, 2002.

[60] L. Koopmans and I. Denbratt. "A Four Stroke Camless Engine, Operated in Homogeneous Charge Compression Ignition Mode with Commercial Gasoline". *SAE Technical Paper 2001-01-3610*, 2001.

[61] H. Persson, M. Agrell, J.-O. Olsson, B. Johansson, and H. Ström. "The Effect of Intake Temperature on HCCI Operation Using Negative Valve Overlap". *SAE Technical Paper 2004-01-0944*, 2004.

[62] J. Allen and D. Law. "Variable Valve Actuated Controlled Auto-Ignition: Speed Load Maps and Strategic Regimes of Operation". *SAE Technical Paper 2002-01-0422*, 2002.

[63] K. Hiraya, K. Hasegawa, T. Urushihara, A; Iiyama, and T. Itoh. "A Study on Gasoline Fueled Compression Ignition Engine - A Trial of Operation Region Expansion". *SAE Technical Paper 2002-01-0416*, 2002.

[64] J. Hyvönen, G. Haraldsson, and B. Johansson. "Operating Range in a Multi Cylinder HCCI Engine Using Variable Compression Ratio". *SAE Technical Paper 2003-01-1829*, 2003.

[65] J. Hyvönen, G. Haraldsson, and B. Johansson. "Operating Conditions Using Spark Assisted HCCI Combustion During Combustion Mode transfer to SI in a Multi-Cylinder VCR-HCCI Engine". *SAE Technical Paper 2005-01-0109*, 2005.

[66] J. A. Eng. "Characterization of Pressure Waves in HCCI Combustion". *SAE Technical Paper 2002-01-2859*, 2002.

[67] J.-O. Olsson, P. A. Tunestål, B. Johansson, S. B. Fiveland, R. Agama, M. Willi, and D. Assanis. "Compression Ratio Influence on Maximum Load of a Natural Gas Fueled HCCI Engine". *SAE Technical Paper 2002-01-0111*, 2002.

[68] J. Vavra, S. V. Bohac, L. Manfosky, G. Lavoie, and D. Assanis. "Knock In Various Combustion Modes in a Gasoline-Fueled Automotive Engine". *Journal of Engineering for Gas Turbines and Power*, 134(8), 2012.

[69] A. Vressner, A. Lundin, M. Christensen, P. A. Tunestål, and B. Johansson. "Pressure Oscillations During Rapid HCCI Combustion". *SAE TechnicalPaper 2003-01-3217*, 2003.

[70] D. Dahl, M. Andersson, and I. Denbratt. "The Origin of Pressure Waves in High Load HCCI Combustion: A High-Speed Video Analysis". *Combustion Science and Technology*, 183(11):1266–1281, 2011.

[71] L. Shi, K. Deng, Y. Cui, S. Qu, and W. Hu. "Study on knocking combustion in a diesel HCCI engine with fuel injection in negative valve overlap". *Fuel*, 106(C):478–483, 2013.

[72] T. Tsurushima, E. Kunishima, Y. Asaumi, Y. Aoyagi, and Y. Enomoto. "The Effect of Knock on Heat Loss in Homogeneous Charge Compression Ignition Engines". *SAE Paper 2002-01-0108*, 2002.

[73] B. Grandin and I. Denbratt. "The Effect of Knock on Heat Transfer in SI Engines". *SAE Technical Paper 2002-01-0238*, 2002.

[74] A. Kulzer, D. Lejsek, A. Kiefer, and A. Hettinger. "Pressure Trace Analysis Methods to Analyze Combustion Features and Cyclic Variability of Different Gasoline Combustion Concepts". *SAE Technical Paper 2009-01-0501*, 2009.

[75] E. Hellström, J. Larimore, A. Stefanopoulou, J. Sterniak, and L. Jiang. "Quantifying Cyclic Variability in a Multicylinder HCCI Engine With High Residuals". *Journal of Engineering for Gas Turbines and Power*, 134(11), 2012.

[76] M. Sjöberg and J. E. Dec. "Comparing late-cycle autoignition stability for single- and two-stage ignition fuels in HCCI engines". *Proceedings of the Combustion Institute*, 31(2):2895–2902, 2007.

[77] L. Manofsky, J. Vavra, D. Assanis, and A. Babajimopoulos. "Bridging the Gap between HCCI and SI: Spark-Assisted Compression Ignition". *SAE Technical Paper 2011-01-1179*, 2011.

[78] H. Persson, R. Pfeiffer, A Hultqvist, B. Johansson, and H. Ström. "Cylinder-to-Cylinder and Cycle-to-Cycle Variations at HCCI Operation with Trapped Residuals". *SAE Technical Paper 2005-01-0130*, 2005.

[79] M. Sjöberg, J. E. Dec, A. Babajimopoulos, and D. Assanis. "Comparing Enhanced Natural Thermal Stratification Against Retarded Combustion Phasing for Smoothing of HCCI Heat-Release Rates". *SAE Technical Paper 2004-01-2994*, 2004.

[80] B. Lawler, E. Ortiz-Soto, R. Gupta, H. Peng, and Z. S. Filipi. "Hybrid Electric Vehicle Powertrain and Control Strategy Optimization to Maximize the Synergy with a Gasoline HCCI Engine". *SAE Technical Paper 2011-01-0888*, 2011.

[81] T. Aroonsrisopon, P. Werner, J. O. Waldman, V. Sohm, D. E. Foster, T. Morikawa, and M. Iida. "Expanding the HCCI Operation With the Charge Stratification". *SAE Technical Paper 2004-01-1756*, 2004.

[82] T. Urushihara, K. Yamaguchi, K. Yoshizawa, and T. Itoh. "A Study of a Gasoline-fueled Compression Ignition Engine - Expansion of HCCI Operation Range Using SI Combustion as a Trigger of Compression Ignition". *SAE Technical Paper 2005-01-0180*, 2005.

[83] L. Manofsky Olesky, J. B. Martz, G. A. Lavoie, J. Vavra, D. N. Assanis, and A. Babajimopoulos. "The effects of spark timing, unburned gas temperature, and negative valve overlap on the rates of stoichiometric spark assisted compression ignition combustion". *Applied Energy*, 105(C):407–417, 2013.

[84] J.-O. Olsson, P. Tunestål, and B. Johansson. "Boosting for High Load HCCI". *SAE Technical Paper 2004-01-0940*, 2004.

[85] P. W. Bessonette, C. H. Schleyer, K. P. Duffy, W. L. Hardy, and M. P. Liechty. "Effects of Fuel Property Changes on Heavy-Duty HCCI Combustion". *SAE Technical Paper 2007-01-0191*, 2007.

[86] E. J. Silke, W. J. Pitz, C. K. Westbrook, M. Sjöberg, and J. E. Dec. "Understanding the Chemical Effects of Increased Boost Pressure under HCCI Conditions". *SAE Technical Paper 2008-01-0019*, 2008.

[87] G. A. Lavoie, E. Ortiz-Soto, A. Babajimopoulos, J. B. Martz, and D. N. Assanis. "Thermodynamic sweet spot for high-efficiency, dilute, boosted gasoline engines". *International Journal of Engine Research*, 14(3):260–278, 2012.

[88] M. Christensen and B. Johansson. "Supercharged Homogeneous Charge Compression Ignition (HCCI) with Exhaust Gas Recirculation and Pilot Fuel". *SAE Technical Paper 2000-01-1835*, 2000.

[89] S. Saxena. *"Maximizing Power Output in Homogeneous Charge Compression Ignition (HCCI) Engines and Enabling Effective Control of Combustion Timing"*. PhD thesis, University of California, Berkeley, 2011.

[90] S. Saxena, J.-Y. Chen, and R. W. Dibble. "Maximizing Power Output in an Automotive Scale Multi-Cylinder Homogeneous Charge Compression Ignition (HCCI) Engine". *SAE Technical Paper 2011-01-0907*, 2011.

[91] D. Yap, A. Megaritis, M. L. Wyszynski, and H. Xu. "Effect of inlet valve timing on boosted gasoline HCCI with residual gas trapping". *SAE Technical Paper 2005-01-2136*, 2005.

[92] H. M. Xu, M. L. Wyszynski, A. Megaritis, D. Yap, T. Wilson, J. Qiao, S. Richardson, S. E. Golunski, and S. Peucheret. "Research on expansion of operating windows of controlled homogeneous auto-ignition engines". *International Journal of Engine Research*, 8(1):29–40, 2007.

[93] M. Martins and H. Zhao. "4-Stroke Multi-Cylinder Gasoline Engine with Controlled Auto-Ignition (CAI) Combustion: a comparison between Naturally Aspirated and Turbocharged Operation". *SAE Technical Paper 2008-36-0305*, 2008.

[94] C. B. Wildman. *"High Load Limits of the Controlled Autoignition Engine"*. PhD thesis, MIT, 2009.

[95] R. J. Scaringe, C. B. Wildman, and W. K. Cheng. "On the High Load Limit of Boosted Gasoline HCCI Engine Operating in NVO Mode". *SAE Technical Paper 2010-01-0162*, 2010.

[96] J. P. Szybist, K. D. Edwards, M. Foster, K. Confer, and W. Moore. "Characterization of Engine Control Authority on HCCI Combustion as the High Load Limit is Approached". *SAE Technical Paper 2013-01-1665*, 2013.

[97] S. Mamalis and A. Babajimopoulos. "Model-Based Estimation of Turbocharger Requirements for Boosting an HCCI Engine". *ICEF2010-35122*, 2010.

[98] D. A. Rothamer, J. A. Snyder, R. K. Hanson, R. R. Steeper, and R. P. Fitzgerald. "Simultaneous imaging of exhaust gas residuals and temperature during HCCI combustion". *Proceedings of the Combustion Institute*, 32(2):2869–2876, 2009.

[99] T. Amano, S. Morimoto, and Y. Kawabata. "Modeling of the Effect of Air/Fuel Ratio and Temperature Distribution on HCCI Engines". *SAE Technical Paper 2001-01-1024*, 2001.

[100] B. J. Lawler. *"A Methodology for Assessing Thermal Stratification in an HCCI Engine and Understanding the Impact of Engine Design and Operating Conditions"*. PhD thesis, University of Michigan, 2013.

[101] L. Manofsky Olesky, J. Vavra, D. Assanis, and A. Babajimopoulos. "Effects of Charge Preheating Methods on the Combustion Phasing Limitations of an HCCI Engine With Negative Valve Overlap". *Journal of Engineering for Gas Turbines and Power*, 134(11), 2012.

[102] J. C. Livengood and Wu, P. C. "Correlation of autoignition phenomena in internal combustion engines and rapid compression machines". *Symposium (International) on Combustion*, 5(1):347–356, 1955.

[103] M. P. Halsted, L. J. Kirsch, and C. P. Quinn. "The Autoignition of Hydrocarbon Fuels at High Temperature and Pressures - Fitting of a Mathematical Model". *Combustion and Flame*, 30:45–60, 1977.

[104] H. J. Curran, P. Gaffuri, W. J. Pitz, and C. K. Westbrook. "A Comprehensive Modeling Study of iso-Octane Oxidation". *Combustion and Flame*, 129:253–280, 2002.

[105] K. Fieweger, R. Blumenthal, and G. Adomeit. "Self-Ignition of S.I. Engine Model Fuels: A Shock Tube Investigation at High Pressure". *Combustion and Flame*, 109:599–619, April 1997.

[106] D. F. Davidson, M. A. Oehlschlaeger, J. T. Herbon, and R. K. Hanson. "Shock Tube Measurements of Iso-Octane Ignition Times and OH Concentration Time Histories". *Proceedings of the Combustion Institute*, 29:1295–1301, 2002.

[107] B. M. Gauthier, D. F. Davidson, and R. K. Hanson. "Shock tube determination of ignition delay times in full-blend and surrogate fuel mixtures". *Combustion and Flame*, 139(4):300–311, 2004.

[108] X. He, M. T. Donovan, B. T. Zigler, T. R. Palmer, S. M. Walton, M. S. Wooldridge, and A. Atreya. "An experimental and modeling study of iso-octane ignition delay times under homogeneous charge compression ignition conditions". *Combustion and Flame*, 142(3):266–275, 2005.

[109] S. S. Goldsborough. "A chemical kinetically based ignition delay correlation for iso-octane covering a wide range of conditions including the NTC region". *Combustion and Flame*, 156(6):1248–1262, 2009.

[110] E. Bumbalough. "Boosted HCCI/ SACI Engine Upgrade: Motivation, Design and Implementation". Master's thesis, University of Michigan, 2011.

[111] P. Andruskiewicz. "Design, Maintenance, and Operation of the GM Boosted HCCI Test Cell". Technical report, University of Michigan, 2009.

[112] G. J. Patterson and R. S. Davis. "Geometric and Topological Consideration to Maximize Remotely Mounted Cylinder Pressure Transducer Data Quality". *SAE Paper 2009-01-0644*, 2(1):414–420, 2009.

[113] J. Brettschneider. "Berechnung des Luftverhältnisses Lambda von Luft-Kraftstoff-Gemischen und des Einflusses von Messfehlern auf Lambda (Calculation of the air ratio lambda of air fuel mixtures and its effect on measurement errors)". *Bosch Technische Berichte*, 6, 1979.

[114] E. A. Ortiz-Soto, J. Vavra, and A. Babajimopoulos. "Assessment of Residual Mass Estimation Methods for Cylinder Pressure Heat Release Analysis of HCCI Engines With Negative Valve Overlap". *Journal of Engineering for Gas Turbines and Power*, 134(8), 2012.

[115] E. Ortiz-Soto, D. Assanis, and A. Babajimopoulos. "A comprehensive engine to drive-cycle modeling framework for the fuel economy assessment of advanced engine and combustion technologies". *International Journal of Engine Research*, 13(3):287–304, 2012.

[116] J. B. Heywood. *"Internal Combustion Engine Fundamentals"*. McGraw-Hill, New York, 1988.

[117] I. Lütkebohle. "NIST-JANAF Thermochemical Tables". `http://kinetics.nist.gov/janaf/`, 2000.

[118] A. Burcat. "Prof. Burcat's Thermodynamic Data". `http://garfield.chem.elte.hu/Burcat/burcat.html`, 2006.

[119] D. L. Stivender. "Development of a Fuel-Based Mass Emission Measurement Procedure". *SAE Technical Paper 710604*, 1971.

[120] H. J. Yun and W. Mirsky. "Schlieren-Streak Measurements of Instantaneous Exhaust Gas Velocities from a Spark-Ignition Engine". *SAE Technical Paper 741015*, 1974.

[121] R. P. Fitzgerald, R. Steeper, J. Snyder, R. Hanson, and R. Hessel. "Determination of Cycle Temperatures and Residual Gas Fraction for HCCI Negative Valve Overlap Operation". *SAE Technical Paper 2010-01-0343*, 2010.

[122] C. B. Wildman, R. J. Scaringe, and W. K. Cheng. "On the Maximum Pressure Rise Rate in Boosted HCCI Operation". *SAE Paper 2009-01-2727*, 2009.

[123] K. Chang. *"Modeling and Analysis of an HCCI Engine During Thermal Transients Using a Thermodynamic Cycle Simulation with a Coupled Wall Thermal Network"*. PhD thesis, University of Michigan, 2007.

[124] G. Woschni. "A Universally Applicable Equation for the Instantaneous Heat Transfer Coefficient in the Internal Combustion Engine". *SAE Technical Paper 670931*, 1967.

[125] J. Chang, O. Güralp, Z. Filipi, D. Assanis, T.-W. Kuo, P. Najt, and R. Rask. "New Heat Transfer Correlation for an HCCI Engine Derived from Measurements of Instantaneous Surface Heat Flux". *SAE Technical Paper 2004-01-2996*, 2004.

[126] G. Eichelberg. "Some New Investigations on Old Combustion Engine Problems". *Engineering*, 148:446–463, 1939.

[127] G. Hohenberg. "Advanced Approaches for Heat Transfer Calculations". *SAE Technical Paper 790825*, 1979.

[128] M. Bargende. *"Ein Gleichungsansatz zur Berechnung der instationären Wandwärmeverluste im Hochdruckteil von Ottomotoren"*. PhD thesis, Technische Hochschule Darmstadt, 1990.

[129] S. Hensel, F. Sarikoc, F. Schumann, H. Kubach, A. Velji, and U. Spicher. "A New Model to Describe the Heat Transfer in HCCI Gasoline Engines". *SAE Technical Paper 2009-01-0129*, 2009.

[130] S. Hensel, F. Sarikoc, F. Schumann, H. Kubach, and U. Spicher. "Investigations on the Heat Transfer in HCCI Gasoline Engines". *SAE Paper 2009-01-1804*, 2009.

[131] T. Emmrich. *"Beitrag zur Ermittlung der Wärme ubergänge in Brennräumen von Verbrennungsmotoren mit homogener und teilhomogener Energieumsetzung"*. PhD thesis, Universität Stuttgart, 2010.

[132] G. A. Lavoie, J. Martz, M. Wooldridge, and D. Assanis. "A multi-mode combustion diagram for spark assisted compression ignition". *Combustion and Flame*, 157(6):1106–1110, 2010.

[133] M. F. Russel and R. Haworth. "Combustion Noise from High Speed Direct Injection Diesel Engines". *SAE Technical Paper 850973*.

[134] AVL List GmbH. *"Evaluation of Combustion Noise from Cylinder Pressure"*, 2000. AVL Combustion Noise Meter 450 manual.

[135] S. M. Aceves, D. L. Flowers, F. Espinosa-Loza, J. Martinez-Friaz, J. E. Dec, M. Sjöberg, R. W. Dibble, and R. P. Hessel. "Spatial Analysis of Emissions Sources for HCCI Combustion at Low Loads Using a Multi-Zone Model". *SAE Technical Paper 2004-01-1910*, 2004.

[136] Inc. Gamma Technologies. `http://www.gtisoft.com`, 2013.

[137] S. Mamalis. *"Simulation and Thermodynamic Analysis of High Pressure Lean Burn Engines"*. PhD thesis, University of Michigan, 2012.

[138] A. Babajimopoulos, V. S. S. P. Challa, G. A. Lavoie, and D. N. Assanis. "Model-Based Assessment of Two Variable Cam Timing Strategies for HCCI Engines: Recompression vs. Rebreathing". *ICES2009-76103*, 2009.

[139] H. Yasar, H. S. Soyhan, H. Walmsley, B. Head, and C. Sorusbay. "Double-Wiebe function: An approach for single-zone HCCI engine modeling". *Applied Thermal Engineering*, 28(11-12):1284–1290, 2008.

[140] Figliolia, R. and Beasley D. *"Theory and Design of Mechanical Measurements"*. Wiley Inc., New York, 2000.

[141] E. Ortiz-Soto. "Enhanced Heat Release Analysis for Advanced Multi-Mode Combustion Engine Experiments". *SAE Technical Paper*, 2014. In preparation.

[142] N. Dronniou and J. Dec. "Investigating the Development of Thermal Stratification from the Near-Wall Regions to the Bulk-Gas in an HCCI Engine with Planar Imaging Thermometry". *SAE Int. J. Engines*, 5(3):2012–01–1111, August 2012.

[143] A. Babajimopoulos, G. A. Lavoie, and D. N. Assanis. "On the Role of Top Dead Center Conditions in the Combustion Phasing of Homogeneous Charge Compression Ignition Engines". *Combustion Science and Technology*, 179(9):2039–2063, 2007.

[144] P. M. Najt. "Compression-Ignited Homogeneous Charge Combustion". Master's thesis, University of Wisconsin, 1981.

[145] E. A. Ortiz-Soto. *"Combustion Modeling of Spark Assisted Compression Ignition for Experimental Analysis and Engine System Simulations"*. PhD thesis, University of Michigan, 2013.